Universidade do Minho

Escola de Engenharia

Sandra Cristina Gomes Oliveira

Polymer-Immobilized Magnetic-Responsive Biocatalysts for Food Industry

abril de 2026

Polymer-Immobilized Magnetic-Responsive Biocatalysts for Food Industry

Sandra Cristina Gomes Oliveira

UMinho | 2026

Universidade do Minho
Escola de Engenharia

Sandra Cristina Gomes Oliveira

Polymer-Immobilized Magnetic-Responsive Biocatalysts for Food Industry

Tese de Doutoramento
Programa Doutoral em Ciência e Engenharia de Polímeros e Compósitos

Trabalho efetuado sob a orientação de
Professor Doutor Zlatan Zlatev Denchev
Doutora Nadya Vasileva Dencheva

Abril de 2026

DIREITOS DE AUTOR E CONDIÇÕES DE UTILIZAÇÃO DO TRABALHO POR TERCEIROS

Este é um trabalho académico que pode ser utilizado por terceiros desde que respeitadas as regras e boas práticas internacionalmente aceites, no que concerne aos direitos de autor e direitos conexos.

Assim, o presente trabalho pode ser utilizado nos termos previstos na licença abaixo indicada.

Caso o utilizador necessite de permissão para poder fazer um uso do trabalho em condições não previstas no licenciamento indicado, deverá contactar o autor, através do RepositóriUM da Universidade do Minho.

Licença concedida aos utilizadores deste trabalho



Atribuição-Não Comercial-Sem Derivações

CC BY-NC-ND

https://creativecommons.org/licenses/by-nc-nd/4.0/

ACKNOWLEDGMENTS

I would like to express my heartfelt gratitude to everyone who contributed to this work; it could not have been completed without their support.

I would like to acknowledge the Fundação para a Ciência e a Tecnologia (FCT) for the financial support provided through doctoral scholarship 2021.07246.BD.

I sincerely thank my advisors, Prof. Dr. Zlatan Denchev and Dr. Nadya Dencheva, for the opportunity to work with them, and for the guidance, knowledge, and encouragement they have provided throughout these years.

I extend my sincere appreciation to Sogrape Vinhos S.A. for their valuable collaboration, particularly for providing enological enzymes and grape must samples, as well as for their technical support during the clarification processes.

I would like to thank the DEP technicians, particularly Eng. Maurício Malheiro, for his technical assistance.

I am grateful to all my colleagues and friends at DEP who supported me during this important journey.

I am deeply thankful to my closest friends for their friendship, love, encouragement, advice, and all the moments we have shared.

I wish to thank my parents, sister, boyfriend and all my family for their unconditional love and support, love, patience, encouragement, and advice throughout every step of this journey. I hope I have made you proud.

Thank you all for everything!

Sandra Oliveira

STATEMENT OF INTEGRITY

I hereby declare having conducted this academic work with integrity. I confirm that I have not used plagiarism or any form of undue use of information or falsification of results along the process leading to its elaboration.

I further declare that I have fully acknowledged the Code of Ethical Conduct of the University of Minho.

DECLARATION ON THE USE OF ARTIFICIAL INTELLIGENCE (AI) TOOLS

I hereby declare having acted this academic work with integrity and confirm that I have not resorted to any form of undue use of AI tools, nor to the falsification or omission of information, sources, data, results or processes in any of the stages leading to its elaboration.

I further declare that any use of AI tools was done in a transparent and responsible manner, being duly noted in the work, and that I critically verified the accuracy of the content produced with their support, assuming full responsibility for what I submit.

I further declare that I have fully acknowledged the Code of Ethical Conduct of the University of Minho, as well as the applicable standards of academic integrity and data protection.

Biocatalisadores Imobilizados em Polímeros Magneticamente Responsivos para a Indústria Alimentar

RESUMO

O objetivo desta tese de doutoramento foi desenvolver biocatalisadores com resposta magnética baseados em micropartículas de poliamida (PAMP) e pectinase para aplicações na indústria alimentar.

As PAMP (PA4, PA6, PA12 e PA6/PA12) foram sintetizadas por polimerização aniónica por abertura de anel ativada (AAROP), com e sem incorporação de ferro, originando polímeros (42–77%) com morfologias porosas e topologias superficiais diversas.

Foi desenvolvido um método de imobilização por adsorção para uma pectinase enológica comercial (PeV) em PA6 e PA6-Fe. Os biocatalisadores resultantes, PeV@PA6, apresentaram hiperativação (até 2,5 vezes maior atividade específica). Estes biocatalisadores permitiram a clarificação completa de mosto rosé e demonstraram elevada estabilidade ao longo de múltiplos ciclos. Um estudo comparativo de sete suportes de PA revelou que a estrutura do polímero e a topologia superficial influenciam significativamente a eficiência de imobilização. A maioria dos sistemas imobilizados apresentou maior eficiência catalítica do que a PeV livre. Relativamente à cinética, a PeV livre e todos os sistemas PeV@PA apresentaram efeito de inibição pelo substrato.

Estudos adicionais utilizando pectinase purificada liofilizada (PeL) e micropartículas de PA6 demonstraram que a adsorção física representa a estratégia de imobilização mais prática, superando a imobilização covalente. As análises estruturais e cinéticas mostraram que a estabilidade da PeL depende fortemente do pH (ótimo em pH 6–7). A PeL livre e todos os sistemas PeL@PA seguiram a cinética de Michaelis-Menten. Além disso, os biocatalisadores mantiveram-se ativos em condições de fermentação, sendo a glicose um inibidor e o etanol um ativador parcial.

A validação industrial em mosto branco/rosé e sumo de maçã confirmou que estes biocatalisadores preservam a cor e a composição fenólica, permitindo simultaneamente a recuperação e reutilização da enzima. Foram observadas melhorias significativas na claridade e na redução do escurecimento, demonstrando que as PAMP são suportes robustos, versáteis e reutilizáveis para a clarificação sustentável de bebidas.

Palavras-chave: biocatalisadores, imobilização enzimática, enzimas na indústria alimentar, conjugados poliamida-enzima.

Polymer-Immobilized Magnetic-Responsive Biocatalysts for Food Industry

ABSTRACT

The objective of this PhD thesis was to develop magnetic-responsive biocatalysts based on polyamide microparticles (PAMP) and pectinase for applications in the food industry.

PAMP (PA4, PA6, PA12, and PA6/PA12) were synthesized by activated anionic ring-opening polymerization (AAROP), with and without iron incorporation, yielding polymers (42–77%) with porous morphologies and diverse surface topographies.

An adsorption-based immobilization method was developed for a commercial enological pectinase (PeV) on PA6 and PA6-Fe. The resulting biocatalysts, PeV@PA6, showed hyperactivation (up to 2.5-fold higher specific activity). These biocatalysts enabled complete clarification of rosé must and demonstrated high stability over multiple cycles. A comparative study of seven PA supports revealed that polymer structure and surface topography significantly influence immobilization efficiency. Most immobilized systems exhibited higher catalytic efficiency than free PeV. Regarding kinetics, free PeV and all PeV@PA systems showed substrate inhibition.

Additional studies using purified lyophilized pectinase (PeL) and PA6 microparticles demonstrated that physical adsorption is the most practical immobilization strategy, outperforming covalent immobilization. Structural and kinetic analyses showed that PeL stability is strongly pH-dependent, with an optimum at pH 6–7. Free PeL and all PeL@PA systems followed Michaelis–Menten kinetics. In addition, the biocatalysts remained active under fermentation conditions, with glucose acting as an inhibitor and ethanol as a partial activator.

Industrial validation in white/rosé must and apple juice confirmed that these biocatalysts preserve color and phenolic composition while allowing enzyme recovery and reuse. Significant improvements in clarity and browning reduction were observed, demonstrating that PAMP are robust, versatile, and reusable supports for sustainable beverage clarification.

Keywords: biocatalysts, enzyme immobilization, enzymes in the food industry, polyamide-enzyme conjugates.

CONTENTS

DIREITOS DE AUTOR E CONDIÇÕES DE UTILIZAÇÃO DO TRABALHO POR TERCEIROS ii
ACKNOWLEDGMENTS iii
STATEMENT OF INTEGRITY iv
DECLARATION ON THE USE OF ARTIFICIAL INTELLIGENCE (AI) TOOLS v
RESUMO vi
ABSTRACT vii
Abbreviation List xiv
SYMBOLS xxv
CHAPTER 1 State of the art 1
1.1. Importance of catalysis in food industry 2
1.2. Enzymes as effective biocatalysts 3
1.2.1. Enzymes – structure and properties 3
1.2.2. Enzymes as industrial biocatalysts. Biocatalysis in food industry 7
1.2.2.1. Pectinases 12
1.2.3. Disadvantages of free enzymes as biocatalysts 14
1.3. Immobilization of enzymes and their importance 15
1.3.1. Immobilization methods 15
1.3.2. Support materials 19
1.3.2.1. Polyamides as support 21
1.4. Objectives and thesis outline 24
1.5. References 25
CHAPTER 2 Experimental methods and materials 37
2.1. Introduction 38
2.2. Materials 38
2.3. Synthesis of empty polyamide microparticles 39
2.3.1. Synthesis of polyamide 6 and 12 microparticles 39
2.3.2. Synthesis of polyamide 4 microparticles 41
2.3.3. Synthesis of hybrid polyamide microparticles with load 41
2.3.4. Designation of microparticulate samples 42
2.4. Immobilization of Pectinase 43
2.4.1. Adsorption immobilization 43

2.4.1.1. Enological pectinase 43
2.4.1.2. Lyophilized pectinase 43
2.4.2. Designation of samples obtained by physical immobilization 43
2.5. Determination of the Total Amount of Protein 44
2.6. Determination of pectinase activity 45
2.6.1. Activity assay 45
2.6.1.1. Calibration curve 45
2.6.2. Determination of immobilization efficiency and the activity recovery 46
2.6.3. Influence of ethanol on enzymatic activity 46
2.6.4. Influence of glucose on enzymatic activity 47
2.7. Kinetics parameters 47
2.7.1. Enological pectinase 47
2.7.2. Lyophilized pectinase 48
2.8. Application of Pectinase in beverage clarification 48
2.8.1. Rosé/white wine must 48
2.8.2. Apple juice 48
2.8.2.1. Production of apple juice 49
2.8.3. Pectin test 49
2.8.3.1. Rosé/white must 49
2.8.3.2. Apple juice 50
2.9. UV/Vis analyses of must and apple juice 50
2.9.1. Composition of must 50
2.9.2. Color of apple juice 51
2.10. Reusability Studies 52
2.10.1. By clarification 52
2.10.1.1. Enological pectinase 52
2.10.1.2. Lyophilized Pectinase 52
2.10.2. By activity test 52
2.11. Storage stability studies 53
2.11.1. Enological pectinase 53
2.11.2. Lyophilized Pectinase 53
2.12. Recovery and Reuse of Microparticles 53

2.13. Morphological and structural characterization 53
2.13.1. Electron microscopy 54
2.13.1.1. Optical microscopy 54
2.13.1.2. Scanning electron microscopy 54
2.13.2. Thermal characterization 54
2.13.2.1. Differential scanning calorimetry 54
2.13.2.2. Thermogravimetric analysis 55
2.13.3. Fourier Transform Infrared Spectroscopy 55
2.14. Circular Dichroism 56
2.15. UV/VIS spectroscopy 56
2.16. References 56
CHAPTER 3 Synthesis and properties of anionic polyamide pulverulent materials 60
3.1. Introduction 61
3.2. Synthesis of polyamide microparticles 61
3.3. Characterization of polyamide microparticles 63
3.3.1. Morphological studies by microscopy 63
3.3.1.1. Optical microscopy 63
3.3.1.2. SEM 64
3.3.2. Thermal properties of microparticles 68
3.3.2.1. By DSC 68
3.3.2.2. By TGA 71
3.3.2.3. FTIR studies 73
3.4. Conclusions 75
3.5. References 75
CHAPTER 4 PA6-assisted biocatalyst for wine industry: Design, optimization and application in rosé must clarification 77
4.1. Introduction 78
4.2. Quantification of the enzymes in the MP-supported complexes 79
4.3. Morphological studies by SEM 80
4.4. Activity via the DNS method 84
4.5. Kinetic studies 87
4.6. Grape must clarification 90

4.6.1. Pectin test 92
4.6.2. Color retention of must 92
4.7. Conclusions 93
4.8. References 94
CHAPTER 5 Magnetic-responsive pectinase biocatalysts based on diverse polyamides: The role of support structure and morphology in must clarification 97
5.1. Introduction 98
5.2. Determination of protein content in PeV@PA complexes 99
5.3. Characterization of polyamide microparticles 100
5.3.1. Morphological studies by SEM 100
5.3.2. FTIR spectroscopy analysis 105
5.4. Enzymatic activity of free and immobilized pectinase 106
5.5. Kinetic studies 108
5.6. Application in rosé must clarification 113
5.6.1. Pectin test 115
5.6.2. Color retention of must 115
5.7. Multiple use of PeV@PA conjugates 117
5.8. Storage stability of PeV@PA conjugates 119
5.9. Conclusions 120
5.10. References 121
CHAPTER 6 PA6-based biocatalyst: Influence of the immobilization strategy 124
6.1. Introduction 125
6.2. Enzyme immobilization 126
6.2.1. Covalent immobilization 126
6.2.2. Adsorption immobilization 127
6.3. Protein estimation 128
6.4. Determination of pectinase activity 130
6.5. Reusability of immobilized pectinase 132
6.6. Conclusions 133
6.7. References 134
CHAPTER 7 Lyophilized pectinase-based biocatalysts: Design, optimization and application for must clarification 136

7.1. Introduction 137
7.2. Protein estimation 138
7.3. Circular dichroism analysis 142
7.4. Characterization of polyamide microparticles 144
7.4.1. Morphological studies by SEM 144
7.4.2. Thermal properties of microparticles 146
7.4.2.1. By DSC 146
7.4.2.1. By TGA 150
7.5. Determination of pectinase activity and related parameters 152
7.5.1. Influence of glucose and ethanol in enzyme activity 155
7.6. Kinetic parameters 158
7.7. Application in must clarification 162
7.7.1. Pectin test 164
7.7.2. pH determination 165
7.7.3. Must color analysis 166
7.8. Reusability of immobilized pectinase 169
7.9. Storage stability 172
7.10. Conclusions 173
7.11. References 175
CHAPTER 8 PA6-based biocatalysts for enzymatic clarification of apple juice 179
8.1. Introduction 180
8.2. Juice clarification 181
8.2.1. Pectin test 184
8.2.2. pH determination 185
8.2.3. Optical properties of apple juice 185
8.3. Reuse of immobilized pectinase in consecutive clarification cycles 187
8.4. Conclusions 188
8.5. References 189
CHAPTER 9 Final conclusions and future perspectives 192
9.1. Final conclusions 193
9.1.1. Development of polyamide microparticle supports 193
9.1.2. Immobilization of pectinolytic enzymes 193

9.1.3. Catalytic performance and kinetic behavior 194
9.1.4. Stability and environmental effects 194
9.1.5. Validation of enzymatic action in real beverages 195
9.1.6. Reusability and process sustainability 195
9.1.7. Major scientific contribution 196
9.2. Future perspectives 196
APPENDIX 198
A.1. Photographic Record of Experimental Work 199
A.2. Spectroscopic 201

Abbreviation List

2PD	2-pyrrolidone
AAROP	Activated Anionic Ring-Opening Polymerization
ANS	3-amino-5-nitrosalicylic acid
AROP	Anionic Ring-Opening Polymerization
ATR	Attenuated Total Reflection
a.u.	Arbitrary units
$B.I.$	Browning index
C20	Bruggolen C20® – activator
CD	Circular dichroism spectroscopy
CLEAs	Cross-linked enzyme aggregates
CLECs	Cross-linking enzyme crystals
DEP	Department of Polymer Engineering
DSC	Differential Scanning Calorimetry
DNS	3,5-dinitrosalicylic acid
ECL	ε-caprolactam
EDX	Energy-dispersive X-ray spectroscopy
$FLAV$	Flavanols
FTIR	Fourier transform infrared spectroscopy
G.A.	D-galacturonic acid
GA	Glutaraldehyde
HCA	Hydroxycinnamic acids
IPC	Institute for Polymers and Composites
LL	ω-laurinlactam
MP	Microparticles of polyamide
NTU	Nephelometric turbidity units
PA	Polyamide
PA4	Polyamide 4
PA6	Polyamide 6
PA12	Polyamide 12
PA612	Polyamide 6-co-12
PeL	Lyophilized pectinase

PeV	Enological pectinase
PG	Endo-polygalacturonase
p/	Isoelectric point
PL	Pectin lyase
PME	Pectin methylesterase
RL	Real load
RLM	Reflected light microscopy
SEM	Scanning Electron Microscopy
SPs	Spherical cross-linked enzyme particles
TGA	Thermogravimetric Analysis
TP	Total protein
TPI	Total polyphenolic index
UV/VIS	Ultraviolet-Visible Spectroscopy

Table of figures

Figure 1.1: Example of a peptide bond. 3

Figure 1.2: Schematic representation of the four levels of protein. Adapted from [9]..... 4

Figure 1.3: Schematic representation of the formation of a functional holoenzyme. 4

Figure 1.4: Schematic diagrams for the three binding models. Adapted from [12]. 5

Figure 1.5: Activation energy: a) reaction without catalyst; b) enzyme catalyzed reaction. 6

Figure 1.6: Variety of industrial applications of enzymes. The central biocatalyst supports essential processes in sectors such as food and beverage production, pharmaceuticals, textiles, and environmental management. 7

Figure 1.7: Schematic structure of pectin (A) Linear chain. (B) Schematic model of the structure of pectin containing HG, xylogalacturonan (XG), apigalacturonan, RG-I and RG-II. Adapted from [53]. 12

Figure 1.8: Biochemical pathways for pectin degradation. (A) De-esterification of pectin by PME; (B) Hydrolytic cleavage of glycosidic bonds by PG; (C) Trans-elimination mechanism by PL resulting in an unsaturated bond. Adapted from [54]. 13

Figure 1.9: Different enzyme immobilization techniques. Adapted from [69]. 16

Figure 1.10: Classification of support materials for enzyme immobilization. 20

Figure 1.11: General chemical structures of polyamides. 22

Figure 1.12: Reaction mechanism of AROP of lactams. 23

Figure 2.1: Schematic representation of AAROP of lactams to PA microparticles. Chemical structure of the active substance of the C20 activator; of dicaprolactamato-bis-(2-methoxyethoxo)-aluminate (DL, initiator). As monomers, ECL (ε-caprolactam) or LL (ω-laurinlac)..... 40

Figure 2.2: Chemical reactions occurring during AAROP of 2-pyrrolidone (2PD) to microparticles: C20 e chemical structure of the active substance of the C20 activator; DL e chemical structure of dicaprolactamato-bis-(2-methoxyethoxo)-aluminate (initiator); 2PD (2-pyrrolidone). 41

Figure 2.3: Chemical structures of the microparticulate polyamides. 42

Figure 2.4: Apple processing stages. 49

Figure 3.1: Visual aspect of the materials prepared, from left to right: PA4, PA4-Fe, PA6, PA6-Fe, PA12, PA12-Fe and PA612. 62

Figure 3.2: Typical results from bright field transmission microscopy representing the average size and shape distributions for PA microparticles without and with load. 63

Figure 3.3: SEM micrographs of PA4 (a-d) and PA4-Fe (e-h) with different magnifications. 65

Figure 3.4: SEM images of PA4 (a) PA4-Fe (b) with EDX in the inset. 65
Figure 3.5: SEM images of PA6 (a-d) and PA-Fe (e-h) with different magnifications. 66
Figure 3.6: Selected SEM micrographs of PA12 (a-d) and PA12-Fe (e-h) with different magnifications. 67
Figure 3.7: SEM images of PA612 with different magnifications. 67
Figure 3.8: DCS traces of different polyamide samples: a) first heating scan; b) recrystallization from the melt; c) second heating scan. 68
Figure 3.9: TGA traces of MP: a) Integral weight loss curves; b) First derivative curves. 72
Figure 3.10: FTIR spectra of polyamide samples: a) PA4, PA4-Fe, PA6 and PA6-Fe; b) PA12, PA12-Fe and PA612. 73
Figure 4.1: Quantification of the pectinase immobilization: (a) UV/VIS spectra of the Viazym solutions before and after the first round of adsorption immobilization; (b) immobilization efficiency for three consecutive trials immobilization rounds at two different temperatures for PeV@PA6 and PeV@PA6-Fe pectinolytic complexes..... 80
Figure 4.2: Selected SEM micrographs of empty PA6 MPs (images a–c) and PeV@PA6 complexes (images d–f). 81
Figure 4.3: EDX results (a) empty PA6 MPs (b) PeV@PA6 complexes..... 82
Figure 4.4: SEM micrographs of (a–c) empty PA6-Fe MPs (d–f) PeV@PA6-Fe complexes and EDX results g) empty PA6-Fe MPs (h-j) PeV@PA6-Fe complexes. 83
Figure 4.5: Interaction between DNS reagent and D-galacturonic acid. 84
Figure 4.6: Activity assay of pectinolytic biocatalysts by the DNS method. (b) Standard calibration curve constructed with various concentrations of G.A. (c) Evolution of the UV/VIS absorption maxima of various concentrations of galacturonic acid treated with the DNS reagent..... 85
Figure 4.7: Comparative activity studies of free pectinolytic preparation and its MP-immobilized complexes: (a) activity in units per milliliter (U/mL) wherein 1 U is defined as the amount of enzyme required to release 1 μmol of galacturonic acid per minute under the assay conditions; (b) specific activity representing the activity in $U.mL^{-1}$ per content of pectinase in arbitrary units, a.u. The standard deviation values are obtained on the basis of three trials for each of the three samples. 86
Figure 4.8: Kinetic studies with free and immobilized pectinases: (a) general comparison of the three kinetic curves; (b) free pectinase experimental curve and its best fits with Equations (6) and

(7); (c) PeV@PA6 complex experimental curve and its best fit with Equation (7); (d) PeV@PA6-Fe complex experimental curve and its best fit with Equation (7). 87
Figure 4.9: Clarification studies with free and immobilized pectinases: (a) clarification of must containing 2.5 mg.mL^{-1} pectinase, at 23 °C; (b) clarification of must containing 2.0 mg.mL^{-1} pectinase, at 23 °C. 1 – PeV@PA6, first application; 2 –- PeV@PA6-Fe, first application; 3 – PeV@PA6, second application; 4 - PeV@PA6-Fe, second application; 5 – PeV@PA6, third application; 6 - PeV@PA6-Fe, third application. All immobilized catalysts contain 0.30 a.u. of pectinolytic enzyme, which is the amount of free enzyme employed. The dashed line indicates the level of 20 NTUs below which the must is considered completely clarified. The visual aspects of the must before and after clarification is presented in the photographs. 90
Figure 4.10: Relative activity of PeV@PA6 and PeV@PA6-Fe during 5 consecutive cycles. 91
Figure 4.11: Results of the pectin test performed on all samples. Unclarified must, must clarified with free enzyme and immobilized in PA6 and PA6-Fe. 92
Figure 4.12: Retention of must color after clarification: (a) UV/VIS absorption spectra comparison in three characteristic intervals; (b) numerical data comparison. In the last case, the error bars are calculated on the basis of three trials for every sample. 92
Figure 5.1: Quantification of the PeV immobilization: (a) UV/VIS spectra of the Viazym solutions before and after adsorption on seven different MP supports; (b) Immobilization efficiency for all PeV@PA and PeV@PA-Fe complexes. Standard deviations were calculated from three independent trials. Sample designations are shortened for better visibility. 99
Figure 5.2: Selected SEM micrographs and corresponding EDX of PA4 (images a-d) and PA4-Fe (images a-d) and Pectinase-immobilized conjugates (images e-h). 101
Figure 5.3: Morphological characterization of PA6 (images a-d), PA6-Fe (images i-j) and the PeV@PA6 (images e-h) and PeV@PA6-Fe complexes (images m-p). 102
Figure 5.4: SEM and EDX analysis of PA12 (images a-d) and PA12-Fe supports (images i-l) and respective immobilized complexes (images e-h and m-p). 103
Figure 5.5: Selected SEM images of PA612 copolymer (images a-d) and its respective immobilized complex (images e-h). 104
Figure 5.6: FTIR spectra of free and immobilized enzyme: a) PeV and PA612 supports, b) PA4 supports, c) PA6 supports, d) PA12 supports. 105

Figure 5.7: a) The standard calibration curve constructed with various concentrations of G.A. b) Evolution of the UV/VIS absorption maxima of various concentrations of galacturonic acid treated with the DNS reagent. 107
Figure 5.8: Activity of PeV@PA immobilized conjugates in comparison to free PeV, a) absolute activity. The small yellow bars show the "activity" values of the respective empty PA supports, b) specific activity per unit enzyme (free or immobilized). Sample designations are shortened for better visibility. 108
Figure 5.9: Experimental kinetic curves: (a) PeV, PeV@PA4, PeV@PA4-Fe, PeV@PA6 and PeV@PA6-Fe; (b) PeV, PeV@PA12, PeV@PA12-Fe and PeV@PA612. 109
Figure 5.10: Corresponding fits obtained using Equations (6) and (7): a) free pectinase; b) PeV@PA4, c) PeV@PA4-Fe, d) PeV@PA6, e) PeV@PA6-Fe, f) PeV@PA12, g) PeV@PA12-Fe and h) PeV@PA612. 110
Figure 5.11: Consolidated results from the kinetics studies. CE and Kk_l. The dashed lines are guides for the eye highlighting the data of the free enzyme reference. The sample designations are shortened for better visibility. 112
Figure 5.12: Clarification studies with free and immobilized pectinase preparation. a) free PeV compared to PA4 and PA6-based PeV@PA complexes; b) free PeV compared to PA12-based PeV@PA complexes. The dashed lines indicate the level of 20 NTUs, below which the must is considered completely clarified, i.e., not containing pectin. 113
Figure 5.13: Visual aspects of the rosé must during clarification with PeV@PA12 (a). b) Visual aspects of must before and after clarification. 114
Figure 5.14: Selected images from the pectin test: untreated must, must treated with free enzyme, and PA4-based complexes. 115
Figure 5.15: Color changes in treated rosé must samples: a) numerical data comparison considering the three spectral intervals at 420, 520 and 620 nm; b) corresponding UV/VIS spectra. 116
Figure 5.16: Comparison of color intensity (I) and hue (T) parameters of rosé must before and after enzymatic treatment. The sample designations are shortened for better visibility. 116
Figure 5.17: Clarification studies of rosé must over multiple reuse cycles: (a) PeV@PA4 and PeV@PA4-Fe; (b) PeV@PA6, PeV@PA6-Fe, and PeV@PA612. 117
Figure 5.18: Clarification studies of rosé must with Pec@PA12 systems in two different clarification cycles. 118

Figure 5.19: Relative activity of immobilized PeV@PA pectinolytic catalysts over eight application cycles. The red dashed line indicates 50% relative activity. The initial activity of each complex was set to 100%. 119
Figure 5.20: Storage stability of immobilized PeV@PA pectinolytic catalysts over four weeks at 4°C. Initial activity is normalized to 100% for each complex. Error bars represent the standard deviation from three independent measurements. 120
Figure 6.1: Different molecular forms of GA in an aqueous medium. Adapted from [9]. 126
Figure 6.2: Schematic representation of the covalent immobilization steps: a) acid hydrolysis of PA6/PA6-Fe MPs; b) surface activation with glutaraldehyde; c) covalent enzyme attachment. 127
Figure 6.3: Schematic representation of pectinase immobilization by physical adsorption onto PA6/PA6-Fe MPs..... 128
Figure 6.4: Quantification of the Pectinase immobilization: a) UV/VIS spectra of the pectinase solutions before and after immobilization; b) Immobilization efficiency for PeL-c-PA6 and PeL@PA6. c) Immobilization efficiency for PeL-c-PA6-Fe and PeL@PA6-Fe. Standard deviations were calculated from two independent trials. 129
Figure 6.5: Enzymatic activity of PeL-c-PA6 and PeL@PA6 conjugates compared to free PeL: a) absolute activity of PA6-based complexes; b) specific activity of PA6-based complexes; c) absolute activity of PA6-Fe-based complexes; d) specific activity of PA6-Fe-based complexes. 131
Figure 6.6: Relative activity of immobilized pectinase over four application cycles. a) PeL-c-PA6 and PeL@PA6 b) PeL-c-PA6-Fe and PeL@PA6-Fe. The red dashed line indicates 50% relative activity. The initial activity of each complex was set to 100%. 132
Figure 7.1. Quantification of the Pectinase immobilization: a) UV/VIS spectra of the pectinase solutions before and after immobilization; b) Immobilization efficiency PeL@PA6, where 0.5 corresponds to a pectinase concentration of 0.5 mg/mL and 1 corresponds to a pectinase concentration of 1 mg mL^{-1}. Standard deviations were between 0.4-0.5% and were calculated from two independent trials..... 139
Figure 7.2: Quantification of the Pectinase immobilization: a) UV/VIS spectra of the initial pectinase solutions; b) UV/VIS spectra of the pectinase solutions before and after immobilization c) Immobilization yield of PeL@PA6. Standard deviations were between 0-0.5% and were calculated from two independent trials. 140
Figure 7.3: SEM micrographs of PA6 (images a–d) and the immobilized complexes formed: PeL@PA6_pH5 (images e–h), PeL@PA6_pH6 (images i–l), PeL@PA6_pH7 (images m–p), and

PeL@PA6_pH8 (images q–t). Z1 and Z2 indicate different spots of EDX analysis – on the surface or in the pores of MPs. 145
Figure 7.4: DSC curves of PA6 and PeL@PA6 samples: a) first heating scan; b) recrystallization from the melt; c) second heating scan. The scales of y-axes in subfigures a and c are the same to enable comparison. 147
Figure 7.5: TGA curves of MP: a) Integral weight loss curves; b) First derivative curves. 150
Figure 7.6: Studies of the activity of free pectinase solution and its immobilized complexes: a) activity in units per milliliter (U/mL), where 1 U is defined as the amount of enzyme required to release 1 μmol of galacturonic acid per minute under the assay conditions; b) specific activity, representing the activity units per milligram of protein (U mL^{-1} mg^{-1}). Standard deviation values were obtained based on two independent assays for each sample. 152
Figure 7.7: Studies of the activity recovery (a) and efficiency of immobilized pectinase (b). Standard deviations were between 1-1.6% and were calculated from two independent trials. The dashed line in Figure 7.7.b indicates the level of IE = 100%. 153
Figure 7.8: Effect of glucose concentration on enzymatic activity. a) free enzyme absolute activity; b) immobilized enzyme absolute activity; c) free enzyme specific activity; d) immobilized enzyme specific activity. 156
Figure 7.9: Effect of ethanol content on enzymatic activity. a) free enzyme absolute activity; b) immobilized enzyme absolute activity; c) free enzyme specific activity; d) immobilized enzyme specific activity. 157
Figure 7.10: Selected experimental kinetic curves of free (a) and immobilized pectinases (b). Selected experimental Lineweaver-Burke plot of PeL_pH5 (c) and PeL@PA6_pH5 (d). 159
Figure 7.11: Catalytic efficiency of free and immobilized pectinases. 161
Figure 7.12: Clarification studies of white (a) and rosé must (b) with free and immobilized pectinase preparation. Images of the white (c) and rosé (d) must after clarification. 163
Figure 7.13: Pectin test results of white must samples. 164
Figure 7.14: Pectin test results of rosé must samples. 165
Figure 7.15: Analysis of must color changes after clarification. (a,c) Comparison of UV/VIS absorption spectra in three characteristic regions (420, 520, and 620 nm) for white and rosé must, respectively; (b,d) comparison of numerical color parameters for white and rosé must, respectively. 167

Figure 7.16: Reuse of immobilized enzyme in the clarification of white (a) and rosé (b) must. 170
Figure 7.17: Reuse of immobilized enzymes over five activity test cycles. Two tests were performed for each sample, with standard deviations ranging from 0 to 0.003%. 171
Figure 7.18: Storage stability profile at 4 °C of free and immobilized pectinases: a) stability over 4 weeks; b) stability over 4 months. The dashed green line corresponds to 100% activity. Standard deviation values were obtained from two independent assays for each sample and ranged between 0.002 and 0.005%..... 172
Figure 8.1: Clarification studies with free and immobilized pectinases: a) clarification of apple juice, the dashed line indicates the level of 200 NTUs below which the apple juice is considered completely clarified.; b) visual appearance of the juice before and after clarification. 182
Figure 8.2: Pectin test results of apple juice samples..... 184
Figure 8.3: UV/VIS spectrum of apple juice before and after clarification. Dashed green lines correspond to the wavelengths used to determine the clarity and browning index. 186
Figure 8.4: Reuse of immobilized enzyme in three consecutive cycles of clarification of apple juice. a) PeL@PA6_pH5 and PeL@PA6_pH6; b) PeL@PA6_pH7 and PeL@PA6_pH8..... 188
Figure A.1: Visual comparison of enzyme preparations. 199
Figure A.2: Visual comparison of PA microparticles before and after immobilization. 199
Figure A.3: DNS Method: A) Enzyme + substrate; B) Add DNS; C) 90°C water bath; D) Ice water bath. 200
Figure A.4: Visual comparison of Calibration curve (0.14 - 2.83 µmol/mL) (before and after adding DNS and heating to 90°C)..... 200
Figure A.5: Visual comparison of kinetic: A) PeV; B) PeL. 200
Figure A.6: Apple juice production (visual flowchart: A) Apples B) Sliced apples -> C) Blending -> D) Filtration/Centrifugation -> E) Raw juice)..... 201
Figure A.7: Graphs of pectinase CD at pH 6: A) free enzyme, B) supernatants after immobilization. 201
Figure A.8: Graphs of pectinase CD at pH 7: A) free enzyme, B) supernatants after immobilization. 202
Figure A.9: Graphs of pectinase CD at pH 8: A) free enzyme, B) supernatants after immobilization. 202

Table of tables

Table 1.1: Main enzymes used in the beverage industry and their industrial applications. 11

Table 1.2: Applications of pectinolytic enzymes in the clarification of fruit juices and wines. ... 14

Table 1.3: Example of immobilized enzymes in the food industry. 21

Table 1.4: Examples of pectinase immobilization on various polyamide (nylon) supports and their respective applications in beverage industry. 24

Table 2.1: Samples designation and composition of the M-samples – MPs. 42

Table 2.2: Designation of samples obtained by adsorption immobilization of enological (PeV) and lyophilized (PeL) pectinase on polyamide-based microparticles. 44

Table 3.1: PAMP sample designations, composition, and polymerization yield. 61

Table 3.2: Average values of equivalent circular diameter and sphericity of the microparticles. (Adapted from [3–5]). 64

Table 3.3: DSC data of seven types of polyamides. 69

Table 3.4: TGA analysis of polyamide microparticles. 72

Table 3.5: FTIR analysis of all polyamide microparticles samples. 74

Table 4.1: Kinetic parameters estimated for PeV, PeV@PA6 and PeV@PA6-Fe..... 89

Table 5.1: Kinetic parameters estimated for PeV and the seven PeV@PA catalytic conjugates. 111

Table 6.1: Designation of samples obtained by immobilization of lyophilized pectinase. 128

Table 7.1: Secondary structure estimation of lyophilized pectinase (PeL) before and after immobilization (SN_PeL) at different pH values. The data presented corresponds to average of all matching solutions for enhanced statistical representativeness. 143

Table 7.2: EDX results. Z1 is analysis on the surface of the microparticle and Z2 is analysis in the micropores of the microparticle. 146

Table 7.3: DSC data of PA6 MPs and PeL@PA6 samples. 147

Table 7.4: TGA analysis of polyamide microparticles. 151

Table 7.5: Activity parameters of free and immobilized lyophilized pectinase as a function of pH. 154

Table 7.6: Kinetic parameters of free and immobilized pectinase. 160

Table 7.7: pH of must after clarification time. 166

Table 7.8: Estimated white must color and composition measures after clarification with free and immobilized pectinases. Two tests were performed for each sample. 168

Table 7.9: Estimated rosé must color and composition measures after clarification with free and immobilized pectinases. Two tests were performed for each sample. 169
Table 8.1: pH of samples after enzymatic clarification. 185
Table 8.2: Results of the clarity and browning index for all juice samples. 186

SYMBOLS

LATIN SYMBOLS

°C	Gradus Celsius
A	Absorbance
B	Blue component of must
CE	Catalytic efficiency
I	Color intensity
K_m	Michaelis–Menten constant
K_i	Inhibition constant
R	Red component of must
S	Subtract
T	Temperature
	Hue
T_c	Crystallization temperature
T_g	Glass transition temperature
T_m	Melting temperature
V_{max}	Maximum reaction rate
V_{spec}	Specific activity
X_c	Degree of crystallinity
Y	Yellow component of must

GREEK SYMBOLS

ΔH_m	Melting enthalpy
λ	Wavelength
w	polymer weight fraction

CHAPTER 1

State of the art

1.1. Importance of catalysis in food industry

The production of everyday products (such as paper, food, pharmaceuticals, textiles, etc.) consumes large quantities of raw materials and energy, and generates large amounts of waste, with a negative impact on the environment and quality of life. The continuous growth of the world's population and economic development in many countries has led to increased global consumption and, consequently, greater pressure on natural resources. Production costs and the amount of raw material used are key factors considered by industries during manufacturing processes. At the same time, the environmental impact of industrial production has become an issue for both producers and consumers. As a result, industries worldwide are seeking alternative technologies that can meet the growing demand for products while consuming fewer resources and causing less environmental harm.

The use of bio-based materials and production processes from nature represents an alternative that can replace or complement conventional technologies. The use of enzymes as catalysts is one of the most promising and sustainable alternatives to conventional processing, obtaining cheaper and more environmentally friendly products [1].

A catalyst accelerates a chemical reaction by reducing the activation energy required for the conversion of reactants into products. Catalysts are not consumed during the reaction; instead, they interact with the initial reactants, facilitate their transformation into the product, which then detaches from the catalyst that remains unchanged and available for the next step of the reaction [2].

Catalysis, in its three forms—homogeneous, heterogeneous and biocatalysis—is involved in the processing of more than 80% of all manufactured products, which makes studies on this area immensely important [3].

The use of natural substances, such as enzymes or nucleic acids (RNA or ribozymes and DNAs) from biological sources or whole cells to speed up chemical reactions is called biocatalysis [4]. Biocatalysis has been used in food and beverage industry since ancient times. Nowadays its importance is constantly growing based on the emerging new biocatalytic systems and processes [1].

1.2. Enzymes as effective biocatalysts

1.2.1. Enzymes – structure and properties

Enzymes are organic molecules of protein origin that catalyze biochemical reactions without being consumed as reagents during the process [5]. They are composed of long chains of amino acids linked together by peptide bonds. Proteins are formed from 20 common amino acids, they share a basic structure: a carboxyl group (-COOH), amino group ($-NH_2$) and a variable side chain (R) connected to a central carbon atom (C_α). The R is what differentiates the twenty standard α-amino acids. The peptide bond is formed by a reaction between the carboxylic group of one amino acid and the amino group of the next (Figure 1.1) [6-9].

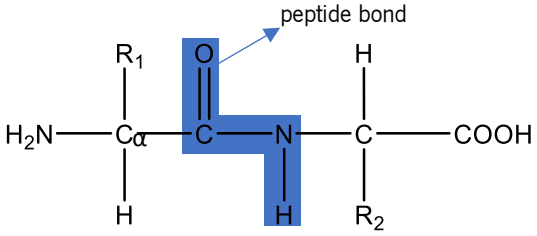


Figure 1.1: Example of a peptide bond.

The structure of the protein can be considered in four levels of organization: primary, secondary, tertiary and quaternary structure. The first level corresponds to the number and specific sequence of amino acids in the polypeptide chain. The fixed arrangement of the polypeptide backbone is the secondary structure of the polypeptide backbone, mainly α-helices, β-pleated sheets, and β-turns. They are determined by the primary sequence and stabilized predominantly by hydrogen bonds. The next level is the tertiary structure, which represents the three-dimensional folding of a protein. This structure results from the folding and bending of the protein backbone, and is stabilized by ionic bonds, hydrogen bonds and Van Der Waals forces. This level of organization is directly related to the biochemical function of the protein. Finally, the quaternary structure describes the general organization of the subunits (polypeptide chain) of the enzyme. Most enzymes are dimers, tetramers, or polymers of several polypeptide chains. The four levels of protein structure are schematically presented in Figure 1.2 [9].

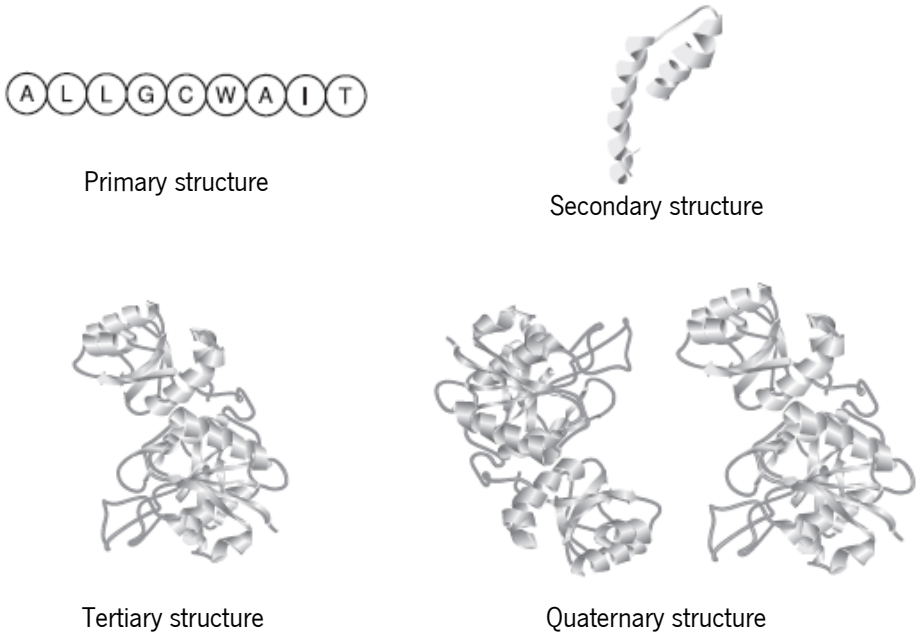


Figure 1.2: Schematic representation of the four levels of protein. Adapted from [9].

Some enzymes consist solely of protein, whereas others require a non-protein component to be catalytically active (Figure 1.3). The protein portion is referred to as the apoenzyme, while the non-protein component is known as a cofactor or a coenzyme. Cofactors are typically inorganic species, often metal ions such as iron, manganese, cobalt, copper, or zinc, whereas coenzymes are organic molecules. Together, the apoenzyme and its associated cofactor or coenzyme form the holoenzyme, which represents the active catalytic form of the enzyme [1,10].

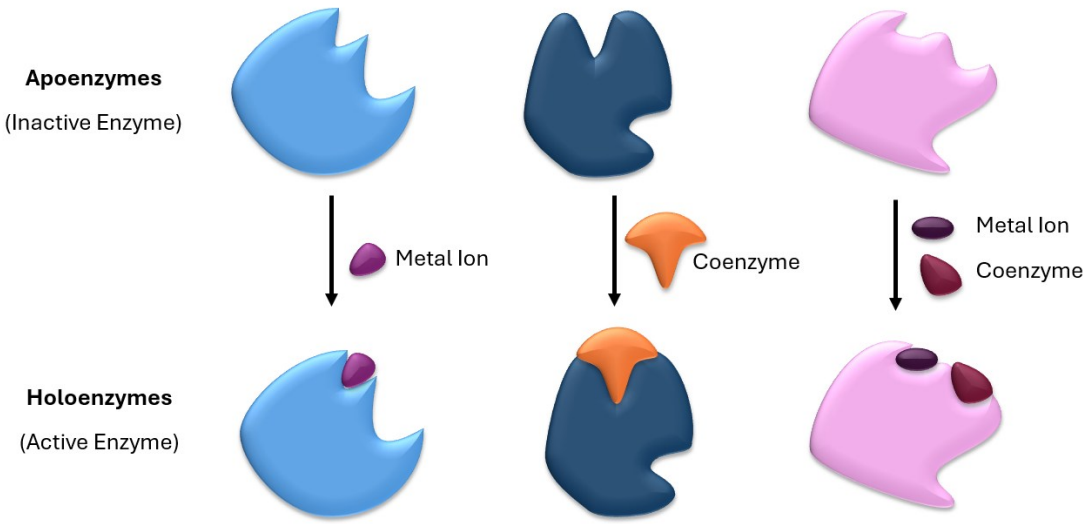


Figure 1.3: Schematic representation of the formation of a functional holoenzyme.

Enzymes catalyze reactions by converting a substrate into a product through the formation of an enzyme–substrate complex. A substrate binds to a specific region of an enzyme known as the active site, which is a small area composed of a limited number of amino acid residues, such that only one type of substrate molecule can bind to it. This highly specific interaction enables enzymes to exhibit remarkable selectivity toward their substrates and reactions [10].

Several theoretical models have been proposed to describe enzyme–substrate interactions, including the lock-and-key model, the induced-fit model, and the conformational selection model (Figure 1.4). The first theory proposed by Emil Fisher in 1890 assumes a rigid enzyme structure. This theory stated that only a key of the correct size and shape (the substrate) fits into the keyhole (the active site) of the lock (the enzyme). Subsequent studies demonstrated that enzymes are flexible molecules, leading to the induced fit model proposed by Daniel Koshland in 1958. This theory suggests that enzymes slightly change their shape to accommodate substrate binding. More recently, the conformational selection model, also known as the Monod-Wyman-Changeux (MWC) model, proposed in 1965, suggests that the unbound protein receptor fluctuates between multiple conformational states, with its occupancy probabilities determined by its relative free energies, according to the Boltzmann distribution [10-12].

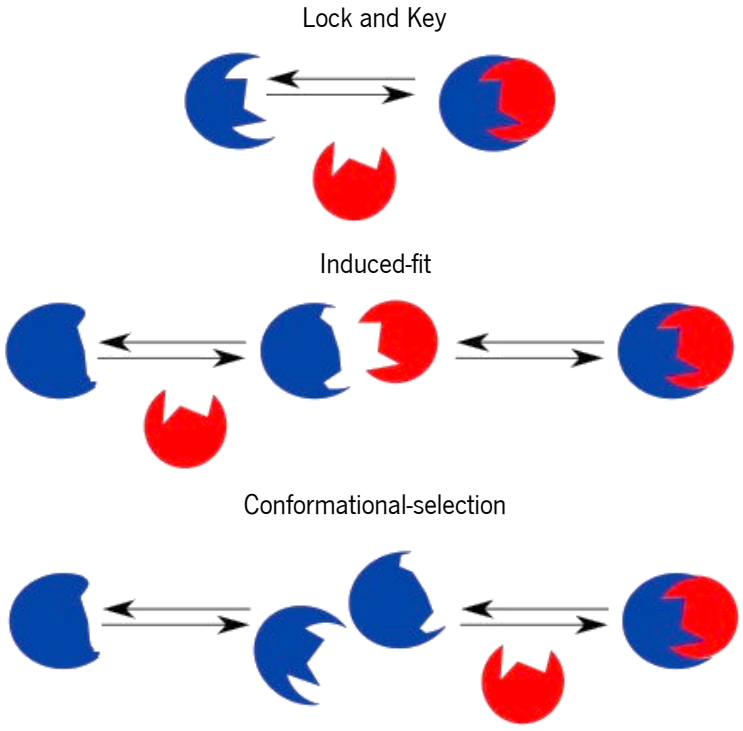


Figure 1.4: Schematic diagrams for the three binding models. Adapted from [12].

The reactions catalyzed by enzymes are highly efficient. For a chemical reaction to occur, the reactant (substrate) molecules must overcome an energy barrier associated with the transition state in order to be converted into products (Figure 1.5a). This energy barrier, known as the activation energy, is defined as the minimum amount of energy required to bring 1 mol of a substance to the transition state at a given temperature. Enzymes facilitate chemical reactions by lowering the activation energy, thereby increasing reaction rates without altering the overall thermodynamics of the process (Figure 1.5b). This kinetic effect provides an alternative reaction pathway through which reactants are converted into products under mild conditions. As a result, lower temperatures can be employed, leading to reduced energy consumption, milder material requirements, and a decrease in undesired side reactions. For optimal catalytic performance, enzymatic reactions generally require aqueous environments, moderate temperatures, and specific pH conditions [6,7,13-17].

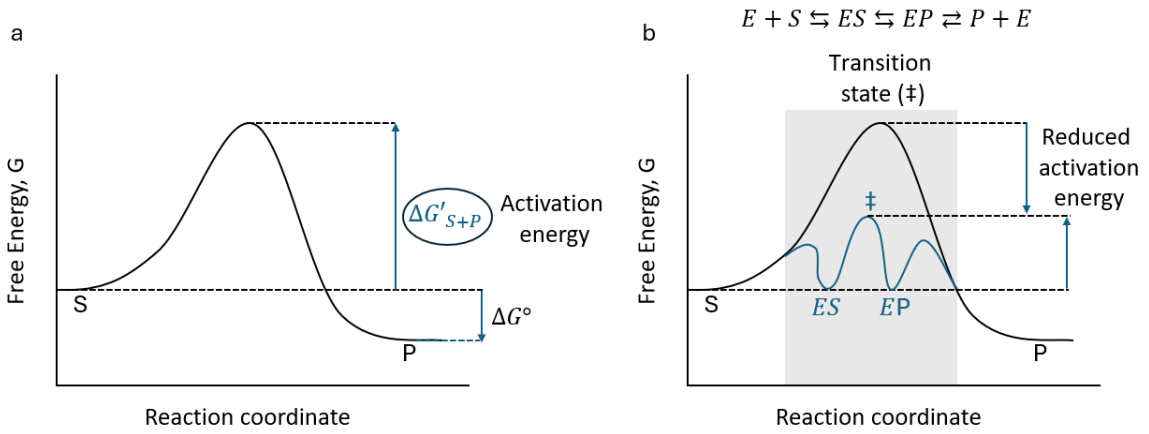


Figure 1.5: Activation energy: a) reaction without catalyst; b) enzyme catalyzed reaction.

Enzymes are classified according to the type of reaction they catalyze into six major classes: oxidoreductases, transferases, hydrolases, lyases, isomerases, and ligases. The nomenclature of enzymes typically reflects the substrate upon which the enzyme acts, as exemplified by cellulase, which catalyzes the degradation of cellulose [1].

All organisms can produce enzymes. Their ability to remain viable and perform catalytic activities even outside their native biological environment means that they can be used for industrial purposes [6,7].

1.2.2. Enzymes as industrial biocatalysts. Biocatalysis in food industry

In recent years, the application of enzymes in different industries has been steadily increasing. They play a fundamental role in a wide range of industries including food processing (baking, confectionery and cheese production), beverages (brewing, winemaking, fruit and vegetable juice production), animal feed, textiles, paper, detergents, biosensors, cosmetics, health and nutrition, wastewater treatment, biopesticide development, as well as pharmaceutical and chemical industries. This growing interest is largely driven by concerns regarding the environmental persistence, toxicity, and potential food contamination associated with conventional agrochemicals [1,6,18-20]. Some examples of enzymes used in industrial settings are shown in Figure 1.6.

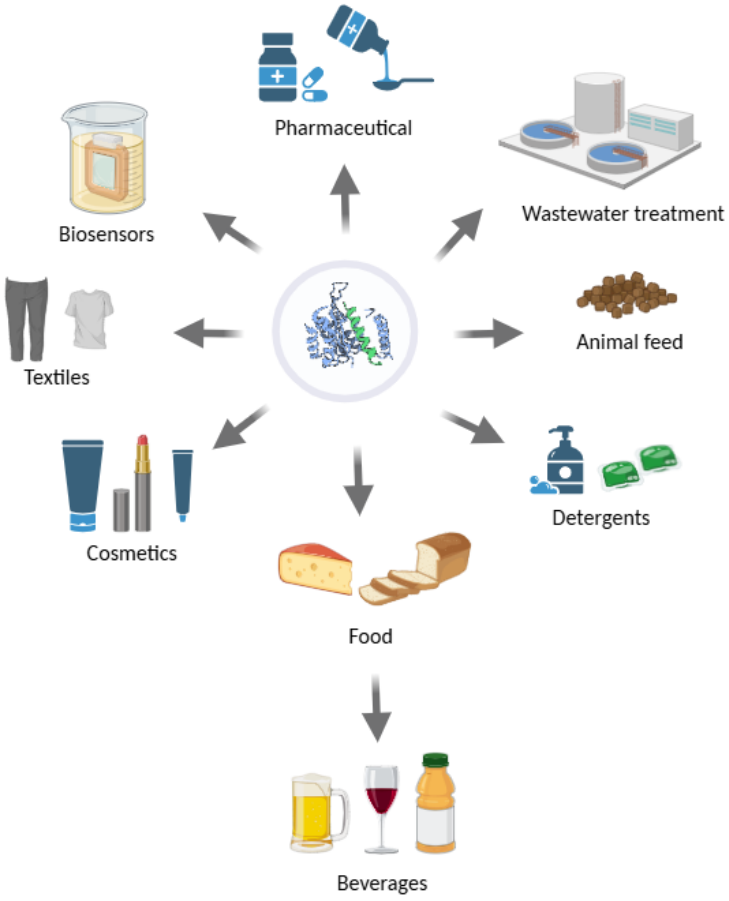


Figure 1.6: Variety of industrial applications of enzymes. The central biocatalyst supports essential processes in sectors such as food and beverage production, pharmaceuticals, textiles, and environmental management.

Most enzymes for industrial use are produced by selected and optimized microorganisms (bacteria and fungi) grown on an industrial scale under strictly controlled conditions [1,5,6].

The agro-industrial sector is a major user of enzymes, mainly due to the constant demand for foods with a long shelf life, reduced processing time, lower waste generation, and improved product quality. Enzymes contribute to transforming raw materials into final products or act as additives to modify desired properties such as flavor, texture, or processability. As a result, foods can be produced at reduced cost while ensuring higher quality and nutritional safety [5,21].

Enzymes applied to food products can be divided into two groups: endogenous and exogenous enzymes. Endogenous enzymes are naturally present in foods and can be used to change the properties of post-harvest plant products and modify animal tissues affecting color, aroma, texture, and nutritional value. However, their activity may be insufficient to catalyze all reactions required during food processing, and in some cases, they may cause nutritional or sensory deterioration. Exogenous enzymes are purposely added to foods or raw materials to induce desired changes. These enzymes can exploit specific food characteristics, replacing complex purification techniques, and enabling the detection of very small quantities of components, for example through biosensors for multiple analyte detection. They can also be used as indicators, such as catalase in milk quality assessment. The primary motivation for their application is to improve the sensory and functional characteristics of food products, ensuring appropriate appearance, taste, and texture. Enzymes used in food and beverage processing must comply with strict safety and regulatory requirements, ensuring consumer safety and product quality [5,20,22,23].

Enzymes are used at various stages of food production (e.g., clarification, stabilization). Although they may remain in the final product, they don't have a function, so they are not considered food components such as additives or thickening agents. Enzymes catalyze reactions under mild conditions, which helps preserve valuable nutrients and food components [8,16,24].

Beverages represent an important branch of the agroindustry and can be divided into two major groups: non-alcoholic beverages, such as fruit juices, and alcoholic beverages, including fermented drinks such as beer and wine. Their consumption is recommended as a source of functional compounds (vitamin C, polyphenols, and antioxidants), they are associated with health benefits such as protective effects against cancer, cardiovascular diseases, osteoporosis, and diabetes. In the beverage industry, the application of enzymes is a gainful option, which improves yields and, at the same time, reduces carbon footprint, energy consumption, and environmental pollution [25-29].

Fruit juice production began in the mid-1930s, and several production problems were encountered, such as low yield, turbidity, opaque appearance, and darkening. These issues are

mainly associated with components naturally present in fruits, such as pectins, starch, cellulose, and highly viscous proteins located in the interstitial spaces of plant cells. These components form insoluble materials, including cell fragments and partially dissolved particles, ranging in size from microparticles to larger pulp fragments [29-32]. Juice appearance is a critical factor for consumer acceptance; cloudy juices are often perceived as lower quality and lose commercial value. Several techniques, such as pressing, filtration, heating, freezing, and centrifugation, have been applied to overcome these issues. However, these methods may induce undesirable biochemical reactions, cause nutrient losses, and fail to remove fine polymers and suspended solids, ultimately affecting juice quality. The addition of enzymes during juice processing helps overcome these difficulties. Due to their high specificity and mild operating conditions, enzymes can be used to increase yield, improve the extraction of color and flavor compounds, reduce viscosity, and improve clarification, filtration, and stabilization. Consequently, nutrient losses are minimized, and high-quality juice products are obtained [20,30,33-35]. A wide variety of enzymes applied during fruit juice production, such as laccase, limoninase, naringinase, and hemicellulases (Table 1.1). A mixture of pectinases (e.g., pectinase, pectinesterase, polygalacturonase, cellulase, and pectin lyase) is also used to degrade pectic substances [26,30].

Beer is one of the oldest and most widely consumed alcoholic beverages worldwide and is produced through the fermentation of malted cereals, mainly barley, in the presence of hops, water, and yeast. Although barley malt is traditionally used, other cereals such as wheat, rye, and oats may also be employed, contributing to different sensory characteristics of the final product. Beer is composed primarily of water (approximately 93%) and is generally characterized by a relatively low alcohol content, making it a widely consumed beverage [27,36,37]. Enzymes play an important role in beer production by improving process efficiency and product quality. Enzymatic preparations such as α- and β-amylases, β-glucanases, and proteases are commonly used during brewing to promote starch hydrolysis, reduce wort viscosity, improve clarification, and enhance fermentable sugar availability. These enzymes may be applied at different stages of the brewing process, contributing to improved extraction efficiency, better filtration, and more consistent product quality, even when variations in raw materials occur [38].

Wine is one of the most widely consumed alcoholic beverages worldwide. Its quality is determined by the interaction of physicochemical parameters, such as alcohol content and residual sugars, and sensory attributes including aroma, flavor, color, and the absence of undesirable odors. These characteristics depend on intrinsic factors (e.g., grape variety) and extrinsic factors (e.g.,

winemaking techniques) [24,28]. The production of wine requires the extraction of juice from grapes followed by fermentation by yeast, during which biochemical, chemical, and physicochemical processes transform grape juice into wine [10,26]. Enzymes can be applied throughout the winemaking process and play a key role in biotransformation reactions. They are applied to improve wine clarification and filterability, releasing varietal aromas from precursor compounds and enhance the extraction of phenolic compounds. These processes are performed by enzymes originate from the grape, yeasts, and bacteria (endogenous enzymes), as well as by exogenously added commercial enzyme preparations [29,31,39]. Under winemaking conditions, endogenous enzyme activity is often insufficient or ineffective; therefore, commercial enzyme preparations are commonly applied [6,30]. Pectinases, β-glucosidases, β-glucanases, polyphenol oxidases, ureases, proteases, and lysozyme are important examples of enzymatic preparations that can be used in wine production. Pectinases, xylanases, glucanases, and proteases are used to improve clarification and filtration. These enzymes can increase the efficiency of pressing and juice extraction. By breaking down grape cell wall structures, these enzymes facilitate the release of compounds from the pulp and skins, improving aroma and color extraction. Other enzymes, such as laccases, tannases, and peroxidases, are used for wine stabilization. Overall, enzymatic treatments during winemaking improve grape maceration, color extraction, filtration, and ultimately wine quality [10,26,29,30,40]. Commercial enzyme preparations usually consist of blends of different activities, are applied at different stages of the winemaking process for several purposes including viscosity reduction, increased juice yield, enhanced color extraction, aroma release, improved clarification and filterability, and reduction of ethyl carbamate formation. These preparations exhibit higher tolerance and activity under winemaking conditions compared to endogenous enzymes [29].

Table 1.1 presents selected examples of enzymes used in beverage production and their respective applications.

Table 1.1: Main enzymes used in the beverage industry and their industrial applications.

Category	Enzymes	Application	References
Fruit juice	Pectinase	Improves yield, clarity, and filterability	[25,41]
	Amylases	Starch degradation and juice clarification	[25,42]
	Laccase	Clarification and polyphenolic stabilization	[42-44]
	Limoninase/ Naringinase	Prevention of bitterness in citrus juices	[25,45]
	Phenolases	Prevent darkening	[25]
Beer	β-glucanase	clarification and viscosity reduction	[38,46]
	Protease	Facilitation of malting and chill-haze prevention	[38]
	α and β -amylase	Starch hydrolysis into fermentable sugars	[38,42,46]
	Laccase	Oxygen removal and flavor stabilization	[42,44]
Wine	Pectinase	Flavor and color extraction; clarification and filtration	[26,47]
	β-glucosidases	Aroma enhancement through precursor release	[26,40]
	β-Glucanases	Clarification, stabilization, filtration, and maturation	[26]
	Urease	Hydrolysis of urea to prevent ethyl carbamate formation	[40,48]
	Protease	Clarification, stabilization, and filtration	[40]
	Lysozyme	Microbiological stabilization (lactic acid bacteria control)	[40]
	Xylanase	Clarification, stabilization, and filtration	[31,40]
	Laccases/Tannases and Peroxidases	Stabilization	[40]

From the literature reviewed so far, it is evident that pectinase plays a crucial role in a wide range of food-related industries, particularly in winemaking and fruit juice production. By catalyzing the hydrolysis of pectic polysaccharides in plant cell walls, pectinase facilitates juice extraction, reduces viscosity, improves clarification, and enhances filtration efficiency. In winemaking, its application is especially important for must clarification and color extraction, as well as for improving the overall stability and sensory quality of the final product. Given its broad industrial relevance and significant technological impact, pectinase merits special attention in both fundamental research and applied studies.

1.2.2.1. Pectinases

Pectinases (pectinolytic or pectic enzymes) currently represent about 20% of the global enzyme market and are among the most widely used enzymes for clarification processes [6,49]. These enzymes are a complex and diverse group involved in the degradation of pectic substances, such as pectin polysaccharides into smaller molecules, such as galacturonic acid.

Pectin is a major component of plant cell walls, acting as a reinforcing material between adjacent cells, it is responsible for the firmness and structure of plant cellulose networks. It is particularly abundant in cereals, vegetables, and fruits. Pectin is a high-molecular-weight acidic heteropolysaccharide composed mainly of *D*-galacturonic acid residues. Galacturonic acid accounts for approximately 70% of pectin, and all pectic polysaccharides contain galacturonic acid units linked through O-1 and O-4 glycosidic bonds [29,49-51]. Pectin can be categorized into four components: polygalacturonic acid, rhamnogalacturonan-I, rhamnogalacturonan-II, and xylogalacturonan. These polymers are interconnected through covalent bonds, forming a complex macromolecular network. The structural model of pectin illustrating these four components is shown in Figure 1.7 [52].

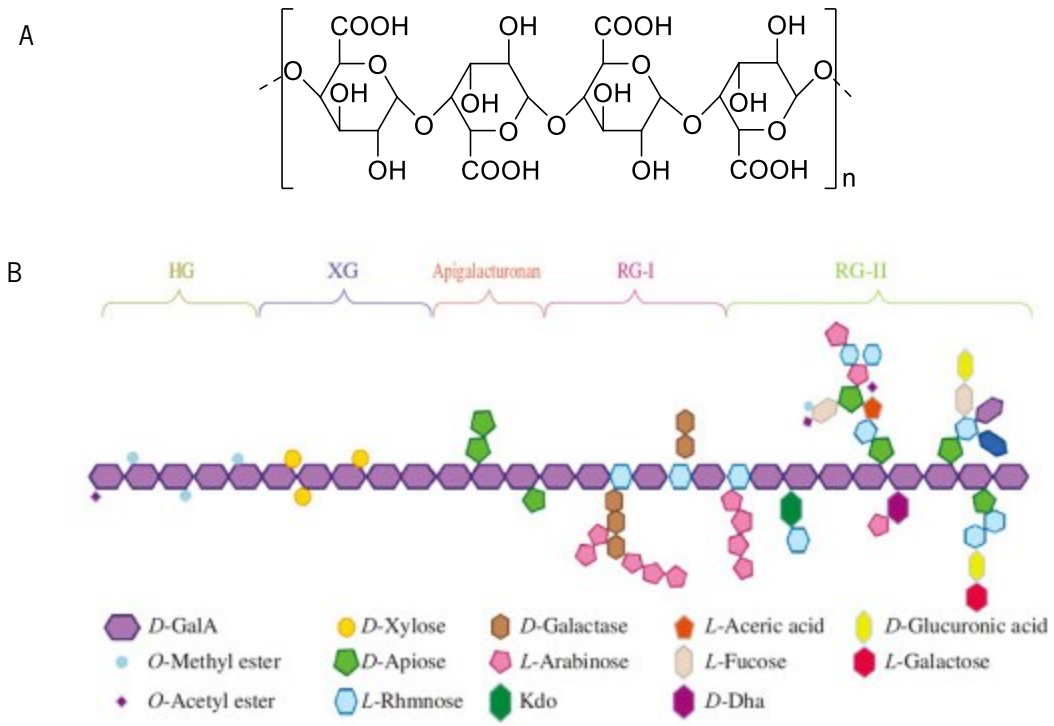


Figure 1.7: Schematic structure of pectin (A) Linear chain. (B) Schematic model of the structure of pectin containing HG, xylogalacturonan (XG), apigalacturonan, RG-I and RG-II. Adapted from [53].

Pectinases used in winemaking industry are typically derived from fungal sources, particularly species of *Aspergillus* and *Penicillium*, and are classified according to their mechanism of action. Commercial pectinase preparations usually contain several pectolytic enzyme activities such as pectin methylesterases, polygalacturonases and pectin lyases.

Pectin methylesterases (PME, E.C. 3.1.1.11) catalyze the saponification of methyl ester groups in pectic substances by removing methoxy groups from polygalacturonic acids. Some attack on the reducing end of the pectin chain, while others act on the non-reducing end, resulting in the formation of free and esterified carboxyl groups. The activity of these enzymes makes the substrate, pectin, accessible for depolymerization.

Polygalacturonases (PG, E.C. 3.2.1.15) are the most commonly found pectic enzymes and catalyze the hydrolysis of the glycosidic bonds in all chain of pectin. They operate by exo and endo mechanisms. Endo-polygalacturonases act on the homogalacturonan backbone and break it into oligogalacturonates whereas exo-polygalacturonases break down polygalacturonates to di- and monogalacturonates units.

Pectin lyases (PL, E.C. 4.2.2.10) degrades pectin polymers through β-elimination mechanism, cleaving glycosidic bond at the C-4 position while simultaneously removing hydrogen atoms at the C-5 position, thereby forming an unsaturated product containing a double bond [29,49,50,54]. Figure 1.8 shows the degradation of pectin by the different pectinases.

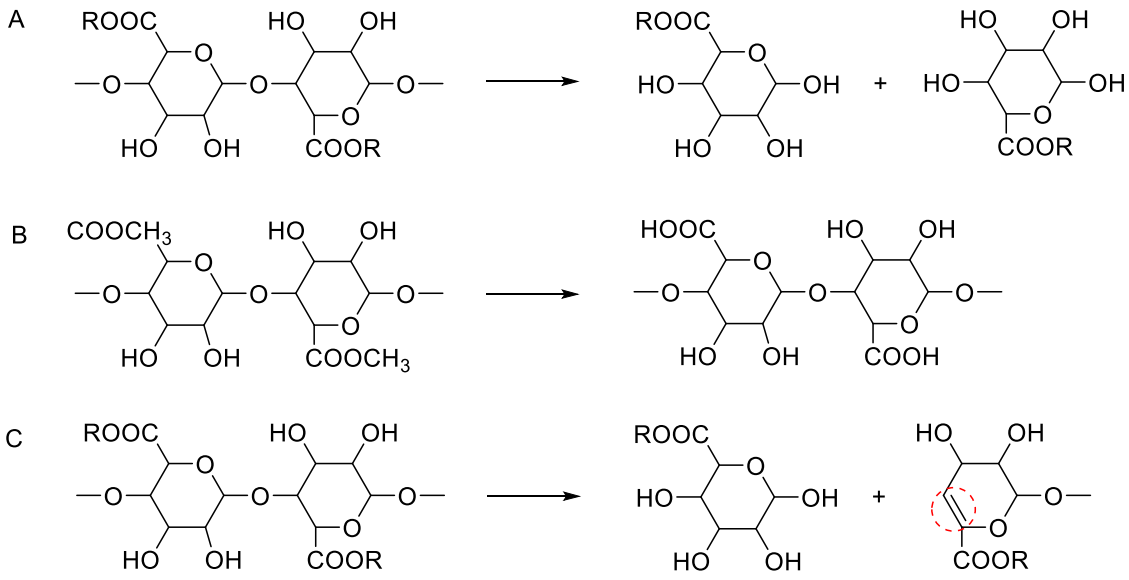


Figure 1.8: Biochemical pathways for pectin degradation. (A) De-esterification of pectin by PME; (B) Hydrolytic cleavage of glycosidic bonds by PG; (C) Trans-elimination mechanism by PL resulting in an unsaturated bond. Adapted from [54].

Several commercial enzyme formulations are available for clarification processes and mainly consist of pectin methylesterase (PME), endo-polygalacturonase (PG), pectin lyase (PL) activities, often combined with hemicellulase and cellulase activities. These enzymes are typically applied in soluble form; however, in this form they are often unable to meet industrial requirements due to their short operational stability and difficulties associated with enzyme recovery and reuse [49,55].

Table 1.2 displays the application of pectinases in juice and wine clarification.

Table 1.2: Applications of pectinolytic enzymes in the clarification of fruit juices and wines.

Application	**Enzyme Source / Type**	**Main Outcomes / Results**	**Ref.**
Fruit Juice (Pear)	Polygalacturonase from *Aspergillus niger*	Improved juice recovery and effective reduction of pectin content and viscosity.	[41]
Fruit Juice (Apple/Orange)	Pectin Lyase from Aspergillus niger, Penicillium expansum	Significant reduction in turbidity (up to 95%).	[56]
Fruit Juice (Sapodilla)	Pectinase from *Aspergillus niger*	Optimized reduction of turbidity, viscosity, and color intensity.	[57]
Grape Juice	Commercial pectinase	Continuous clarification in a packed bed reactor; achieved 87% turbidity reduction.	[58]
Wine	Enological pectinase	Maintained activity in winemaking conditions (low pH/ethanol); improved must settling.	[59]
White Grape Juice	Commercial pectinase from *Aspergillus niger*	Comparison of different enzyme brands on filtration rate and clarity.	[60]

1.2.3. Disadvantages of free enzymes as biocatalysts

As already mentioned, enzymes are biocompatible, biodegradable, and highly specific, exhibiting high catalytic activity and selectivity. As a rule, their application leads to lower energy consumption, generates biodegradable products, and results in reduced environmental impact. Moreover, enzyme-catalyzed processes typically produce fewer waste by-products due to their high specificity [16,61]. However, enzymes are proteins and therefore exhibit optimal activity only within narrow ranges of temperature and pH. Under unfavorable environmental conditions, such as

variations in temperature or pH, enzymes may undergo denaturation, leading to decreased catalytic activity or complete inactivation. In addition, enzymatic activity is influenced by substrate and enzyme concentrations, as well as by the presence of inhibitors or activators. Consequently, the use of free enzymes in industrial processes presents several limitations, the most significant being their high production cost, difficult separation from the reaction medium, limited reusability, and the possible presence of enzymatic preparation residues in the final food product, etc. [16,41,61-64].

To overcome most of these limitations and to enhance their industrial applicability, free enzymes can be attached to suitable supports through immobilization techniques [65].

1.3. Immobilization of enzymes and their importance

Immobilization is a technical process in which enzymes are fixed to or within solid supports, creating a heterogeneous immobilized enzyme system [66]. “Immobilized enzymes” have been defined as enzymes that are physically confined or located in a specific region of space, while retaining their catalytic activity and allowing for repeated and continuous use [67]. The immobilized form of enzymes mimics their natural mode in living cells, where many enzymes are associated with the cytoskeleton, membranes, or organelle structures [66]. Compared to free enzymes in solution, immobilized enzymes generally exhibit higher robustness and increased resistance to environmental changes, such as variations in pH and temperature. Furthermore, heterogeneous immobilized enzyme systems allow for easy recovery of both enzymes and products, multiple reuses of enzymes, allow continuous operation of enzymatic processes, and permit rapid interruption of reactions. These advantages significantly reduce or eliminate enzyme contamination of the final product, which is particularly important in the food and pharmaceutical industries [64]. However, immobilized enzymes often display lower catalytic activity and generally higher apparent Michaelis constants due to the reduced substrate accessibility to the active sites [64,65].

An immobilized enzyme system consists of three main components: the enzyme, the support matrix to which the enzyme is bound, and the mode of attachment between them [67].

1.3.1. Immobilization methods

The most frequently used immobilization techniques can be classified into five main groups (Figure 1.9): (a) non-covalent adsorption or deposition; (b) immobilization via ionic interactions; (c) entrapment in a polymeric gel or capsule (encapsulation); (d) covalent attachment to the support

(tethering), and (e) cross-linking of the enzyme. The choice of immobilization techniques is a crucial step in enzyme immobilization, as each enzyme differs in its structure, properties, and active-site accessibility. In general, the physicochemical characteristics of both the target enzyme and the support material dictate the selection of the most suitable immobilization strategy [19,41,64,65,68].

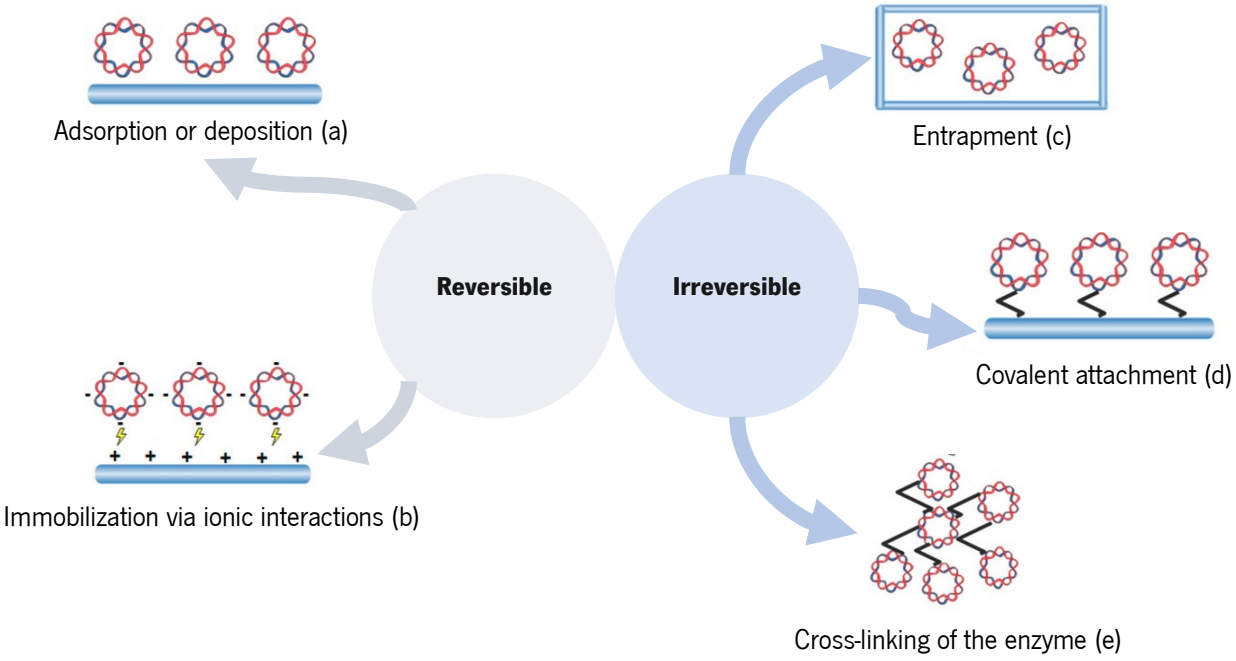


Figure 1.9: Different enzyme immobilization techniques. Adapted from [69].

Adsorption or non-covalent deposition (Figure 1.9a) is one of the simplest, easiest, and most cost-effective immobilization methods. It consists of combining the enzyme with an adsorbent support material under appropriate pH and ionic strength conditions for a specific period of time. After this period, the immobilized material, the solid support, is collected and thoroughly washed to remove any residues of free enzyme. In this process, enzymes are adsorbed onto the supports surface through weak physical interactions, such as Van der Waals forces, hydrogen bonds, and hydrophobic interactions, without the formation of chemical bonds. This method is generally non-destructive to enzymatic activity, as it does not require prior functionalization of the support or chemical modification of the enzyme. Another advantage is that the enzyme does not need to be pre-treated or chemically modified, and it is even possible to use crude enzyme preparations [19,65,68-70]. However, due to the weak nature of these interactions, variations in temperature,

pH, or ionic strength may lead to enzyme desorption or leaching, resulting in activity loss and possible contamination of the reaction medium [64,65].

Immobilization established by ionic interaction between enzymes and the support is called immobilization via ionic interactions (Figure 1.9b). In this case immobilization depends on pH, temperature, and enzyme concentration. This method is also simple and reversible, as changes in ionic strength or pH can disrupt the electrostatic interactions, often with minimal impact on enzyme conformation [64,71]. Supports used for ionic immobilization are typically charged materials, allowing protein binding through electrostatic forces. However, excessive surface charge density may lead to enzyme conformational distortion, altered kinetic behavior, or reduced catalytic efficiency [19]. The main difference between these two methods (adsorption and ionic bonding) is the strength of the interactions involved, as ionic bonds are stronger than van der Waals forces or hydrogen bonds [72].

Enzyme entrapment (Figure 1.9c) is an irreversible immobilization process based on the occlusion of the enzyme within a polymeric network or porous morphology. The support structure allows diffusion of substrates and products while retaining the enzyme within the matrix. The enzyme is not directly bound to the support surface by any physical or chemical interaction, only retained within it. Thus, the enzyme's stability can be improved, and its leaching and denaturation can be minimized. An additional advantage is the possibility of co-immobilizing multiple enzymes [19,65,72]. Entrapment generally requires the synthesis of a polymeric matrix in the presence of the enzyme. The encapsulation material can be modified to obtain an ideal microenvironment, achieving an ideal pH, adequate polarity, or amphiphilicity. The porosity and shape of the support are controlled to prevent enzyme leakage, although, due to the enzyme not binding to the support, this cannot be completely excluded. An additional disadvantage is that only small substrates/products can be used. The method requires a delicate balance between the mechanical properties of the support and its effect on enzymatic activity [19,65,66,72,73].

Covalent immobilization (Figure 1.9d) is another widely used technique. As the name indicates, it is based on the formation of covalent bonds between functional groups of the enzyme and reactive groups on the support surface. As with non-covalent adsorption, this method can be used on unmodified proteins, as it depends only on naturally occurring functional groups. The functional groups of support must be previously activated. Generally, this method involves two steps: first, activation of the support using coupling agents such as glutaraldehyde or carbodiimides; second, reaction of the activated support with nucleophilic groups on the enzyme surface. This method is

used when it is desired that the final product does not contain enzymes [1,18,19,64,65]. Covalent bonding results in strong and irreversible attachment, providing enhanced physical and chemical stability against temperature changes, denaturants, and organic solvents. It also allows control over enzyme loading [65,71,74]. A distinct disadvantage of covalent bonding, that limits its application, is that this method often leads to drastic negative changes in the conformational and catalytic properties of the enzyme. Sometimes, additional modifications to the enzyme structure are necessary to expose some functionalities suitable for covalent bonding to occur, and these changes in the reaction medium can lead to enzyme denaturation. Furthermore, some restrictions on the mobility of enzymes bound to carriers may occur, which can limit some conformational changes necessary during catalysis, resulting in decreased enzymatic activity. Moreover, the immobilized enzyme cannot be recovered without destroying its biological activity, and the immobilization procedure is generally more complex and time-consuming [18,68,69,74].

An extreme case of covalent bonding is enzyme crosslinking (Figure 1.9e) in which the enzyme itself acts as the support material. In this irreversible method, covalent bonds between enzymes occur at the functional group on the enzyme surface with bi- or multifunctional reagents such as glutaraldehyde and diisocyanate [18,65,68,75]. Cross-linking is a relatively simple technique that can yield highly stable and catalytically active biocatalysts. Due to the exclusion of support, this technique has a low production cost. It is rarely used alone and is more often combined with other immobilization strategies to enhance enzyme stability [18,19,66]. The main disadvantage of this method is that the use of bi- or multifunctional reagents can denature or structurally modify the enzyme, leading to a loss of enzymatic activity [18].

Several cross-linking-based immobilization approaches have been developed, including cross-linked enzyme aggregates (CLEAs), cross-linked enzyme crystals (CLECs), and spherical cross-linked enzyme particles (SPs). CLEAs are prepared through a single-step process involving enzyme precipitation, purification, and immobilization, typically using organic solvents as precipitants. CLECs exhibit excellent catalytic activity and operational stability; however, only crystallized enzymes with a high degree of purity can be used. SPs a more recent approach of immobilization, consists of spherical microparticles composed of enzymes crosslinked in an oily emulsion. Despite their advantages, these methods often suffer from significant activity loss, which remains their principal limitation [65,75-77].

1.3.2. Support materials

The materials used for enzyme immobilization are referred to as supports or matrices. Choosing an appropriate support is a crucial step in enzyme immobilization. An ideal support should present suitable characteristics such as adequate particle size, surface charge, surface area, tunable hydrophobic/hydrophilic properties, and sufficient stability [70]. An appropriate support must protect the enzyme against adverse reactions, be biocompatible or biodegradable, non-toxic, low-cost, and insoluble in the reaction medium, while not causing enzyme deactivation [78,79]. The properties of immobilized enzyme conjugates depend on both the enzyme and the support. Their interaction results in immobilized enzyme complexes with specific chemical, biochemical, mechanical, and kinetic properties [64]. However, certain limitations must be considered, as the matrix should not negatively affect the enzyme structure and should not disturb the enzyme more than necessary to establish stable enzyme–matrix interactions. Additionally, affinity between the functional groups of the enzyme and the support is required to allow effective binding. The carrier should expose the active sites of the catalyst, for substrate access and minimizing diffusional limitations of substrates and products [79]. The use of suitable materials, such as hydrophobic carriers for lipase immobilization, may even enhance biocatalyst activity [80].

A wide variety of materials from diverse sources can be used as supports for enzyme immobilization. These supports may be inorganic, organic, hybrid, or composite. Inorganic class mainly include silica- and metal-based materials, [81] while organic supports comprise polysaccharides, acrylic polymers, vinyl polymers, and polyamides. To improve their properties, organic and inorganic supports can be combined to form hybrid or composite materials (Figure 1.10). Supports can be fabricated in different forms, such as beads, porous particles of various sizes and shapes, membranes, and micro- or nanosized fibers [79,81,82].

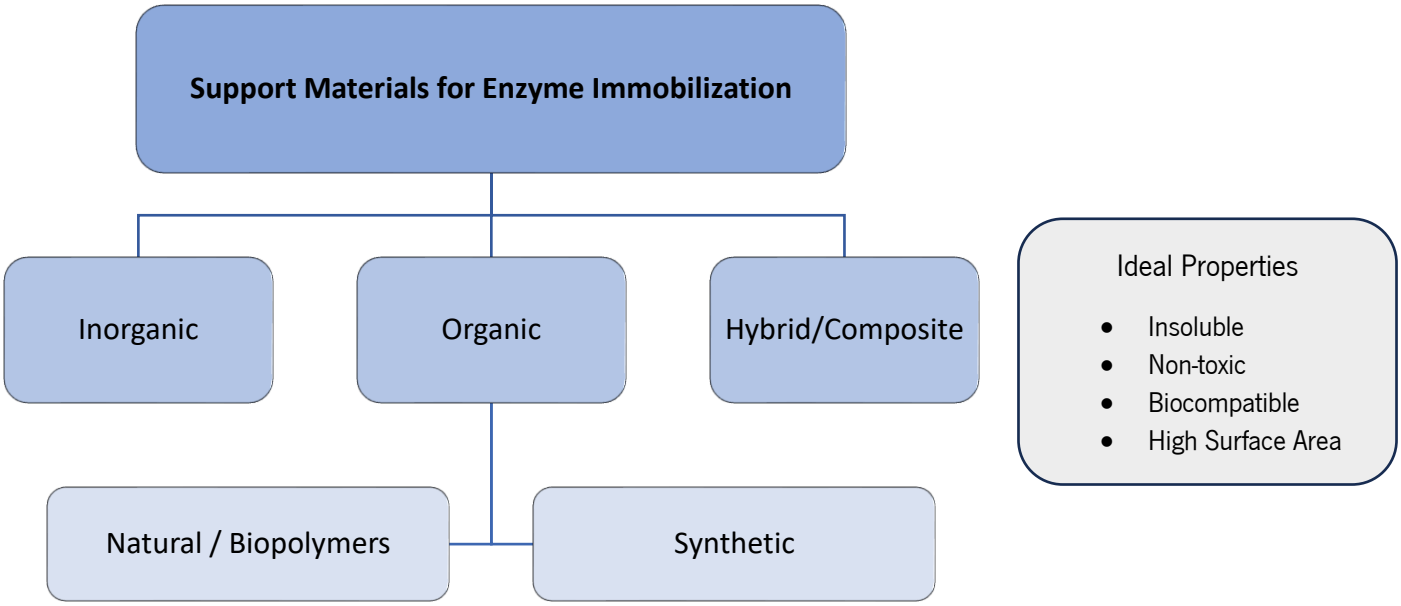


Figure 1.10: Classification of support materials for enzyme immobilization.

In recent years, the immobilization on polymeric supports has gained significant attention [46]. Polymers may be synthetic (e.g., polystyrene and polyamides) or natural biopolymers (e.g., chitosan and alginate). To obtain enzyme–polymer complexes with enhanced activity and stability, stimulus-responsive "smart" polymers may be employed as supports [79,83]. These polymers are capable of phase transitions in response to changes in their environment, including physical (temperature, pressure), chemical (pH, ionic strength), or external stimuli (magnetic or electric fields). For example, magnetic micro- or nanoparticles can be easily recovered from the reaction medium by applying an external magnetic field [84].

In summary, polymeric supports can protect immobilized enzymes without causing significant losses in catalytic activity [83]. As a result, enzyme–polymer conjugates can be reused multiple times after simple separation from the reaction medium [66,83]. Nevertheless, selecting an appropriate support material remains challenging due to its strong influence on the properties and performance of the immobilized enzyme system [79]. Furthermore, for applications in the food industry, the selection of polymeric supports must take into account chemical inertness and comply with safety standards, ensuring that the migration of monomers or residual additives into the food matrix remains below established legal limits [85,86].

Currently, supports for bioactive molecules (organic, inorganic, hybrid, or composite) are being used in food production. For example, acid ureases used to remove harmful substances from wine, such as urea and ethyl carbamate, have been covalently immobilized on graphene oxide/chitosan

spheres and successfully applied to wine production. Immobilization enabled enzyme reuse for at least ten cycles, retaining approximately 90% of the original activity after the tenth cycle, which demonstrates excellent operational stability and reusability [83,87].

Table 1.3 summarizes selected examples of immobilized enzymes applied in the food industry.

Table 1.3: Example of immobilized enzymes in the food industry.

Enzyme	Support material	Immobilization method	Food application	Ref.
Laccase	Green coconut fiber	Covalent	Juice (clarification)	[43]
Pectinases	Silylated-montmorillonite clay	Covalent		[62]
Pectinase and xylanase	Iron oxide nanoparticles	Covalent co-immobilization		[88]
Amylase, pectinase and cellulase	Calcium alginate-chitosan, chitosan, silica gel	Entrapment, covalent co-immobilization		[89]
α-acetolactate decarboxylase	Alginate/gelatin	Covalent	Beer (diacetyl prevention)	[90]
β-glucosidases	Chitosan pellets	Covalent	Wine (aroma improvement)	[91]
Ureases	Polyacrylonitrile and nylon beads	Covalent	Wine (urea degradation)	[48]
Lysozyme	Magnetic polystyrene microparticles	Covalent	Wine (Microbiological stability)	[92]
Protease	Glass beads and acrylic beads	Covalent	Wine (Protein stabilization)	[93]

1.3.2.1. Polyamides as support

Polyamides (PA), also known as nylons, are semi-crystalline polymers composed of repeating units comprising amide moieties (–C(O)-NH-). Typically, amine ($–NH_2$) and carboxylic (–COOH)

groups are located at the termini of each PA macromolecule (Figure 1.11). Amide linkages are the main structural motifs of many biological polymers, such as polypeptides (proteins), which makes synthetic polyamides close structural analogues of proteins and enzymes [94-96].

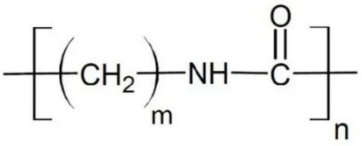


Figure 1.11: General chemical structures of polyamides.

Polyamides can be classified as natural (proteins) or synthetic. Synthetic polyamides obtained by ring-opening polymerization of lactams are designated by a single number corresponding to the number of carbon atoms separating the repeating unit from the amide functional group (e.g., PA6, PA4, PA12) [97,98]. Those that have two numbers (e.g., PA66, PA46, etc.) are prepared by high-temperature polycondensation reactions between diamines and dicarboxylic acids [95,96]. PA are inexpensive, mechanically stable, biocompatible, often biodegradable, inert in aqueous media, and can be easily processed into different forms such as films or particulate powders. These characteristics make them suitable materials for use as support in enzyme immobilization. In addition, their terminal –COOH and $–NH_2$ groups, as well as their intermediate peptide –CO–NH– groups can be used for covalent or non-covalent binding of proteins [94,96,99-103].

Recently, a new method was developed and patented at IPC-DEP for the synthesis of polyamide microparticles via activated anionic ring-opening polymerization (AAROP) of lactams in solution [104]. This technique allows the production of PA microparticles with controlled porosity, capable of incorporating a wide variety of particulate materials as payloads [105]. Further investigations at IPC-DEP demonstrated that AAROP can proceed very rapidly and, depending on the lactam used, can be conducted at temperatures between 40 and 130 °C, well below the melting point of polyamides. This process yields microparticulate powders with relatively high molecular weights between 15-35 kDa depending on the reacting lactam used [78,106].

The reaction mechanism of non-activated bulk anionic ring-opening polymerization (AROP) of lactams consists of two main steps: initiation and propagation (Figure 1.12). During initiation, the lactam monomer reacts with a strong base (the initiator), forming lactam anions, which act as the active species. These anions subsequently react with lactam molecules to form an imide dimer, which acts further as an activator of the polymerization reaction. The initiation stage is completed

by the formation of the imide dimer which then reacts with the lactam anion, followed by a rapid proton exchange with the monomer. In activated anionic ring-opening polymerization (AAROP), the imide dimer is introduced at the beginning of the process together with the lactam anion.

In the propagation step, a lactam anion reacts with the imide dimer, extending the polymer chain by one repeating unit while regenerating the lactam anion. The propagation rate depends on the concentration of monomer anion and activator, which are consequently determined by the initiator and the activator concentrations respectively [103].

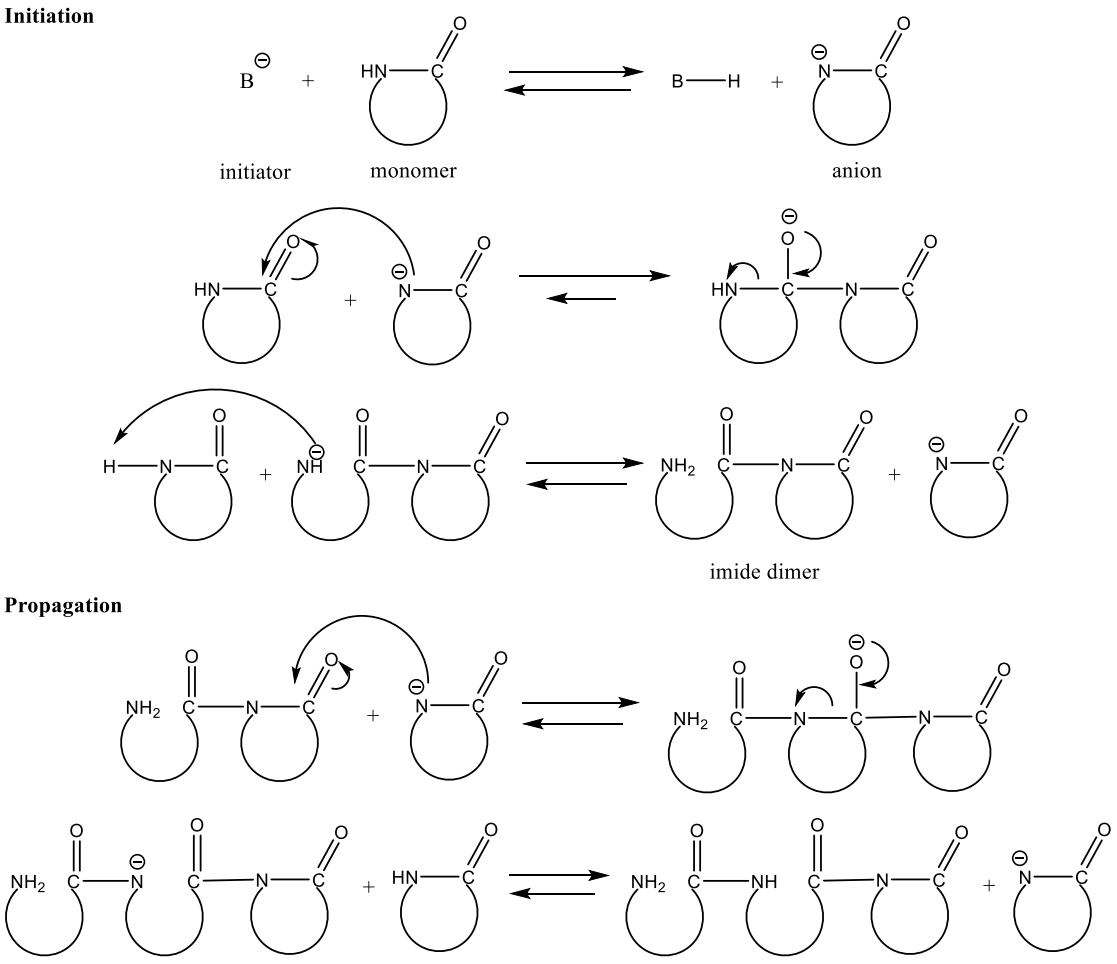


Figure 1.12: Reaction mechanism of AROP of lactams.

Researchers from IPC/DEP of the University of Minho synthesized PA6, PA4, PA12 and copolymeric magnetic microparticles [78,106,107]. PA4 and PA6 microparticles were successfully applied as supports for laccase immobilization, and the resulting conjugates were used for effluent treatment, including the discoloration of organic dyes and the deactivation of catechol compounds [78,107]. Laccase immobilized on PA6 particulate carriers was also employed in the development of an optical biosensor for catechol detection [108]. Furthermore, AAROP of γ-butyrolactam at 40

°C, using the monomer as both reactant and solvent, was applied to synthesize PA4 microparticles for molecular imprinting of bovine serum albumin [109].

It has been demonstrated by several authors that polyamide-based supports can be successfully employed in a variety of applications within the food industry (Table 1.4). These supports can host one or more immobilized enzymes, highlighting their versatility and industrial relevance. Omelková et al.[110] and Rexová-Benková et al.[111] used PA6 powders as supports for polygalacturonase covalently immobilized via glutaraldehyde binding. In this case, the activity of the immobilized enzyme decreased by approximately 50%, most likely due to steric hindrance near the enzyme's active site [111]. Ben-Othman and Rinken [112] immobilized pectinolytic enzymes on PA66 pellets and threads, reporting a 40-fold higher immobilization yield for the latter. The immobilized pectinase retained approximately 40% of its initial activity after five cycles and more than 20% after twenty consecutive cycles.

Table 1.4: Examples of pectinase immobilization on various polyamide (nylon) supports and their respective applications in beverage industry.

Enzyme	Function	Support	Food application	Ref.
Pectinases	Clarification	Nylon 6/6 pellets	Wine	[83]
Pectolytic	Clarification	Nylon membranes	Juice	[83]
Commercial pectinase	Degrading fibrous plant material and providing higher yields and clarity	Pellet and thread shaped nylon 6/6 carriers	Juice	[112]
Pectin lyase and Endocellulase	Polysaccharide liquefaction	Nylon	Juice	[113]
Polygalacturonase	Clarification	Nylon 6	Juice	[114]

Polyamides are widely used in the food industry, particularly in food packaging and technical components. According to European Union regulations governing materials intended to come into contact with food ((EC) No 1935/2004 [115] and (EU) No 10/2011 [85]), polyamides are included among the approved polymeric materials for food contact applications, provided that the established migration limits are respected.

1.4. Objectives and thesis outline

From the literature review, it became clear that enzymes play a fundamental role in the food industry. Among them, pectinases represent one of the most widely used enzyme groups, finding

application at key stages of both winemaking and fruit juice production. At the same time, it is well established that, in order to be cost-effective, stable, and reusable, enzymes (including pectinases) must be immobilized on suitable supports. Polyamide micropowders, both neat and magnetically responsive, emerge as particularly promising candidates owing to their chemical similarity to proteins, their biocompatibility, and their suitability for enzyme immobilization.

Accordingly, the main goal of this PhD thesis is to develop polyamide-based, magnetically responsive biocatalysts for application in the food industry. This goal is pursued through the following specific objectives:

1. Synthesis and characterization of polyamide pulverulent supports prepared by activated anionic ring-opening polymerization (AAROP), with and without iron incorporation, based on PA6, PA4, PA12, and copolymeric PA6/PA12 systems.
2. Design and preparation of biocatalysts by immobilizing pectinolytic enzymes—both industrial formulations and purified enzymes for fundamental studies—onto the synthesized polyamide supports.
3. Comprehensive characterization of the resulting biocatalytic systems in terms of enzymatic activity, kinetic behavior, reusability, pH and temperature dependence, and shelf stability.
4. Application and validation of the developed biocatalysts in clarification processes relevant to winemaking and fruit juice production.

To achieve Objectives 3 and 4, both model systems and real wine musts supplied by the Sogrape Vinhos Lda. winemaking company (Portugal) will be employed.

1.5. References

[1] Jegannathan, K.R.; Nielsen, P.H. Environmental assessment of enzyme use in industrial production—A literature review. *J. Clean. Prod.* **2013**, 42, 228–240. https://doi.org/10.1016/j.jclepro.2012.11.005.

[2] Haynes, A. Concepts of modern catalysis and kinetics. *Synthesis* **2005**, 2005, 851. https://doi.org/10.1055/s-2005-866709 .

[3] Catlow, C.R.A.; Davidson, M.; Hardacre, C.; Hutchings, G.J. Catalysis making the world a better place. *Philos. Trans. R. Soc. A* **2016**, 374, 20150089. https://doi.org/10.1098/rsta.2015.0089 .

[4] Paul, P.E.V.; Sangeetha, V.; Deepika, R.G. Emerging trends in the industrial production of chemical products by microorganisms. In *Recent Developments in Applied Microbiology*

and Biochemistry; Elsevier: Amsterdam, The Netherlands, **2018**; pp. 107–125. https://doi.org/10.1016/B978-0-12-816328-3.00009-X .

[5] Motta, J.F.G.; Freitas, B.C.B.; Almeida, A.F.; Martins, G.A.S.; Borges, S.V. Use of enzymes in the food industry: A review. *Food Sci. Technol.* **2023**, 43, e106222. https://doi.org/10.1590/fst.106222 .

[6] Espejo, F. Role of commercial enzymes in wine production: A critical review of recent research. *J. Food Sci. Technol.* **2021**, 58, 9–21. https://doi.org/10.1007/s13197-020-04489-0 .

[7] Meghwanshi, G.K.; Kaur, N.; Verma, S.; Dabi, N.K.; Vashishtha, A.; Charan, P.D.; et al. Enzymes for pharmaceutical and therapeutic applications. *Biotechnol. Appl. Biochem.* **2020**, 67, 586–601. https://doi.org/10.1002/bab.1919.

[8] Furlan, S.A.; Pant, H.K. General properties. In *Enzyme Technology*; Springer: New York, NY, USA, **2006**; pp. 11–35. https://doi.org/10.1007/978-0-387-35141-4_2 .

[9] Kotzia, G.A.; Platis, D.; Axarli, I.A.; Chronopoulou, E.G.; Karamitros, C.; Labrou, N.E. Biocatalysis, enzyme engineering and biotechnology. In *Food Biochemistry and Food Processing*; Wiley: Hoboken, NJ, USA, **2012**; pp. 125–166. https://doi.org/10.1002/9781118308035.ch7 .

[10] Robinson, P.K. Enzymes: Principles and biotechnological applications. *Essays Biochem.* **2015**, 59, 1–41. https://doi.org/10.1042/bse0590001.

[11] Yan, C.; Zou, X. Modeling protein flexibility in molecular docking. In *Comprehensive Medicinal Chemistry III*; Elsevier: Amsterdam, The Netherlands, **2017**; Vol. 3, pp. 319–328. https://doi.org/10.1016/B978-0-12-409547-2.12351-0 .

[12] Laddach, A.; Chung, S.S.; Fraternali, F. Prediction of protein–protein interactions: Looking through the kaleidoscope. In *Encyclopedia of Bioinformatics and Computational Biology*; Elsevier: Amsterdam, The Netherlands, **2018**; pp. 834–848. https://doi.org/10.1016/B978-0-12-809633-8.20470-6.

[13] Chapman, J.; Ismail, A.; Dinu, C. Industrial applications of enzymes: Recent advances, techniques, and outlooks. *Catalysts* **2018**, 8, 238. https://doi.org/10.3390/catal8060238.

[14] Gürsel, A.; Alkan, S.; Toppare, L.; Yağcı, Y. Immobilization of invertase and glucose oxidase in conducting H-type polysiloxane/polypyrrole block copolymers. *React. Funct. Polym.* **2003**, 57, 57–65. https://doi.org/10.1016/j.reactfunctpolym.2003.07.004.

[15] Uygun, M.; Akduman, B.; Ergönül, B.; Aktaş Uygun, D.; Akgöl, S.; Denizli, A. Immobilization of amyloglucosidase onto macroporous cryogels for continuous glucose production from starch. *J. Biomater. Sci. Polym. Ed.* **2015**, 26, 1112–1125. https://doi.org/10.1080/09205063.2015.1078928.

[16] Kuddus, M. Introduction to food enzymes. In *Enzymes in Food Biotechnology: Production, Applications, and Future Prospects*; Elsevier: Amsterdam, The Netherlands, **2018**; pp. 1–18. https://doi.org/10.1016/B978-0-12-813280-7.00001-3.

[17] Farrauto, R.J. Industrial catalysis: A practical guide. In *Handbook of Industrial Chemistry and Biotechnology*; Springer: Cham, Switzerland, **2017**; pp. 1995–2035. https://doi.org/10.1007/978-3-319-52287-6_37.

[18] Bashir, N.; Sood, M.; Bandral, J.D. Enzyme immobilization and its applications in food processing: A review. *Int. J. Chem. Stud.* **2020**, 8, 254–261. https://doi.org/10.22271/chemi.2020.v8.i2d.8779.

[19] Wahab, W.A.A. Review of research progress in immobilization and chemical modification of microbial enzymes and their application. *Microb. Cell Fact.* **2025**, 24, 167. https://doi.org/10.1186/s12934-025-02791-0.

[20] Wang, H.; Sun, Z.; Qi, Y.; Hu, Y.; Ni, Z.; Li, C. Update application of enzyme in food processing, preservation, and detection. *Food Bioeng.* **2024**, 3, 380–394. https://doi.org/10.1002/fbe2.12105.

[21] Choi, J.-M.; Han, S.-S.; Kim, H.-S. Industrial applications of enzyme biocatalysis: Current status and future aspects. *Biotechnol. Adv.* **2015**, 33, 1443–1454. https://doi.org/10.1016/j.biotechadv.2015.02.014.

[22] European Commission. Regulation (EC) No 1332/2008 of the European Parliament and of the Council of 16 December 2008 on food enzymes. *Off. J. Eur. Union* **2008**, L354, 7–15.

[23] Olempska-Beer, Z.S.; Merker, R.I.; Ditto, M.D.; DiNovi, M.J. Food-processing enzymes from recombinant microorganisms—A review. *Regul. Toxicol. Pharmacol.* **2006**, 45, 144–158. https://doi.org/10.1016/j.yrtph.2006.05.001.

[24] Moreno-Arribas, M.V.; Polo, M.C. *Wine Chemistry and Biochemistry*; Springer: New York, NY, USA, **2009**. https://doi.org/10.1007/978-0-387-74118-5.

[25] Trono, D. Recombinant enzymes in the food and pharmaceutical industries. In *Biomass, Biofuels, Biochemicals: Advances in Enzyme Technology*; Elsevier: Amsterdam, The Netherlands, **2019**, 349–387. https://doi.org/10.1016/B978-0-444-64114-4.00013-3.

[26] Bhat, M.K. Cellulases and related enzymes in biotechnology. *Biotechnol. Adv.* **2000**, 18, 355–383. https://doi.org/10.1016/S0734-9750(00)00041-0.

[27] Mignani, A.G.; Ciaccheri, L.; Mencaglia, A.A.; Ottevaere, H.; Baća, E.E.S.; Thienpont, H. Optical measurements and pattern-recognition techniques for identifying the characteristics of beer and distinguishing Belgian beers. *Sens. Actuators B Chem.* **2013**, 179, 140–149. https://doi.org/10.1016/j.snb.2012.10.029.

[28] Gutiérrez-Escobar, R.; Aliaño-González, M.J.; Cantos-Villar, E. Wine polyphenol content and its influence on wine quality and properties: A review. *Molecules* **2021**, 26, 718. https://doi.org/10.3390/molecules26030718.

[29] Cosme, F.; Inês, A.; Vilela, A. Microbial and commercial enzymes applied in the beverage production process. *Fermentation* **2023**, 9, 385. https://doi.org/10.3390/fermentation9040385.

[30] Ribeiro, D.S.; Henrique, S.M.B.; Oliveira, L.S.; Macedo, G.A.; Fleuri, L.F. Enzymes in juice processing: A review. *Int. J. Food Sci. Technol.* **2010**, 45, 635–641. https://doi.org/10.1111/j.1365-2621.2010.02177.x.

[31] Himeshi Samarasinghe, Y.A.; Hua, W.; Dong, K.; Kocherry, L.; Xu, J. Recombinant enzymes used in fruit and vegetable juice industry. In *Microbial Enzyme Technology in Food Applications*; Ray, R.C., Rosell, C.M., Eds.; CRC Press: Boca Raton, FL, USA, **2017**, 375–395. https://doi.org/10.1201/9781315368405-25.

[32] Puri, M.; Banerjee, A.; Banerjee, U.C. Optimization of process parameters for the production of naringinase by *Aspergillus niger* MTCC 1344. *Process Biochem.* **2005**, 40, 195–201. https://doi.org/10.1016/j.procbio.2003.12.009.

[33] Baumann, J.W. Application of enzymes in fruit juice technology. In *Enzymes and Food Processing*; Springer: Dordrecht, The Netherlands, **1981**, 129–147. https://doi.org/10.1007/978-94-011-6740-6_8.

[34] Hu, Y.H.; Wang, C.Y.; Chen, B.Y. Effects of high-pressure processing and thermal pasteurization on quality and microbiological safety of jabuticaba juice during cold storage. *J. Food Sci. Technol.* **2020**, 57, 3334–3344. https://doi.org/10.1007/s13197-020-04366-w.

[35] Samreen. Processing of fruit juices: Techniques, challenges, and advances. *Int. J. Adv. Biochem. Res.* **2025**, 9, 186–187. https://doi.org/10.33545/26174693.2025.v9.i1c.3437.

[36] Stewart, G.G.; Russell, I.; Anstruther, A., Eds. *Handbook of Brewing*, 3rd ed.; CRC Press: Boca Raton, FL, USA, **2017**. https://doi.org/10.1201/9781351228336.

[37] Zdaniewicz, M.; Pater, A.; Hrabia, O.; Duliński, R.; Cioch-Skoneczny, M. Tritordeum malt: An innovative raw material for beer production. *J. Cereal Sci.* **2020**, 96, 103095. https://doi.org/10.1016/j.jcs.2020.103095.

[38] Gomaa, A.M. Application of enzymes in brewing. *J. Nutr. Food Sci. Forecast* **2018**, 1, 1002. https://doi.org/10.5281/zenodo.3336203.

[39] Humbert-Goffard, A.; Saucier, C.; Moine-Ledoux, V.; Canal-Llaubères, R.-M.; Dubourdieu, D.; Glories, Y. An assay for glucanase activity in wine. *Enzyme Microb. Technol.* **2004**, 34, 537–543. https://doi.org/10.1016/j.enzmictec.2003.10.017.

[40] Minussi, R.C.; Rossi, M.; Bologna, L.; Rotilio, D.; Pastore, G.M.; Durán, N. Phenols removal in musts: Strategy for wine stabilization by laccase. *J. Mol. Catal. B Enzym.* **2007**, 45, 102–107. https://doi.org/10.1016/j.molcatb.2006.12.004.

[41] Deng, Z.; Wang, F.; Zhou, B.; Li, J.; Li, B.; Liang, H. Immobilization of pectinases into calcium alginate microspheres for fruit juice application. *Food Hydrocoll.* **2019**, 89, 691–699. https://doi.org/10.1016/j.foodhyd.2018.11.031.

[42] Raveendran, S.; Parameswaran, B.; Ummalyma, S.B.; Abraham, A.; Mathew, A.K.; Madhavan, A.; et al. Applications of microbial enzymes in food industry. *Food Technol. Biotechnol.* **2018**, 56, 16–30. https://doi.org/10.17113/ftb.56.01.18.5491.

[43] Bezerra, T.M.S.; Bassan, J.C.; Santos, V.T.O.; Ferraz, A.; Monti, R. Covalent immobilization of laccase in green coconut fiber and use in clarification of apple juice. *Process Biochem.* **2015**, 50, 417–423. https://doi.org/10.1016/j.procbio.2014.12.009.

[44] Brijwani, K.; Rigdon, A.; Vadlani, P.V. Fungal laccases: Production, function, and applications in food processing. *Enzyme Res.* **2010**, 2010, 149748. https://doi.org/10.4061/2010/149748.

[45] Ribeiro, M.H.L.; Rabaça, M. Cross-linked enzyme aggregates of naringinase: Novel biocatalysts for naringin hydrolysis. *Enzyme Res.* **2011**, 2011, 851272. https://doi.org/10.4061/2011/851272.

[46] Lalor, E.; Goode, D. Brewing with enzymes. In *Enzymes in Food Technology*, 2nd ed.; Wiley: Oxford, UK, **2009**; pp. 163–194. https://doi.org/10.1002/9781444309935.ch8.

[47] Busto, M.D.; García-Tramontín, K.E.; Ortega, N.; Perez-Mateos, M. Preparation and properties of an immobilized pectinlyase for the treatment of fruit juices. *Bioresour. Technol.* **2006**, 97, 1477–1483. https://doi.org/10.1016/j.biortech.2005.06.013.

[48] Andrich, L.; Esti, M.; Moresi, M. Urea degradation in some white wines by immobilized acid urease in a stirred bioreactor. *J. Agric. Food Chem.* **2010**, 58, 6747–6753. https://doi.org/10.1021/jf1006837.

[49] Bié, J.; Sepodes, B.; Fernandes, P.C.B.; Ribeiro, M.H.L. Enzyme immobilization and co-immobilization: Main framework, advances and some applications. *Processes* **2022**, 10, 494. https://doi.org/10.3390/pr10030494.

[50] Gummadi, S.N.; Manoj, N.; Kumar, D.S. Structural and biochemical properties of pectinases. In *Industrial Enzymes*; Springer: Dordrecht, The Netherlands, **2007**; pp. 99–115. https://doi.org/10.1007/1-4020-5377-0_7.

[51] Mohnen, D. Pectin structure and biosynthesis. *Curr. Opin. Plant Biol.* **2008**, *11*, 266–277. https://doi.org/10.1016/j.pbi.2008.03.006.

[52] Yi, L.; Cheng, L.; Yang, Q.; Shi, K.; Han, F.; Luo, W.; et al. Source, Extraction, Properties, and Multifunctional Applications of Pectin: A Short Review. *Polymers* **2024**, *16*, 2883. https://doi.org/10.3390/polym16202883.

[53] Sharma, S.; Wani, K. M.; Mujahid, S. M.; Jayan, L. S.; Rajan, S. S. Review on Pectin: Sources, Properties, Health Benefits and Its Applications in Food Industry. *J. Future Foods* **2026**, *6*, 205–219. https://doi.org/10.1016/j.jfutfo.2024.04.009.

[54] Jayani, R. S.; Saxena, S.; Gupta, R. Microbial pectinolytic enzymes: A review. *Process Biochem.* **2005**, *40*, 2931–2944. https://doi.org/10.1016/j.procbio.2005.03.026.

[55] Dutra, M. da C. P.; Carvalho, A. J. B. A.; Santos, N. C.; Freitas, S. T.; Ferreira, E. S.; Marques, A. T. B.; et al. Impact of Commercial Preparations of Pectinases on the Chemical Composition and Stability of Phenolic Compounds in Grape Juices. *J. Food Biochem.* **2025**, *2025*, 13. https://doi.org/10.1155/jfbc/2856691.

[56] Mantovani, C. F.; Geimba, M. P.; Brandelli, A. Enzymatic Clarification of Fruit Juices by Fungal Pectin Lyase. *Food Biotechnol.* **2005**, *19*, 173–181. https://doi.org/10.1080/08905430500316284.

[57] Sin, H. N.; Yusof, S.; Abdul Hamid, N. S.; Rahman, R. A. Optimization of enzymatic clarification of sapodilla juice using response surface methodology. *J. Food Eng.* **2006**, *73*, 313–319. https://doi.org/10.1016/j.jfoodeng.2005.01.031.

[58] Azimi, S. Z.; Hosseini, S. S.; Khodaiyan, F. Continuous clarification of grape juice using a packed bed bioreactor including pectinase enzyme immobilized on glass beads. *Food Biosci.* **2021**, *40*, 100877. https://doi.org/10.1016/j.fbio.2021.100877.

[59] Martín, M. C.; López, O. V.; Ciolino, A. E.; Morata, V. I.; Villar, M. A.; Ninago, M. D. Immobilization of enological pectinase in calcium alginate hydrogels: A potential biocatalyst for winemaking. *Biocatal. Agric. Biotechnol.* **2019**, *18*, 101091. https://doi.org/10.1016/j.bcab.2019.101091.

[60] Sreenath, H. K.; Santhanam, K. The use of commercial enzymes in white grape juice clarification. *J. Ferment. Bioeng.* **1992**, *73*, 241–243. https://doi.org/10.1016/0922-338X(92)90171-P.

[61] Scanlon, M. G.; Henrich, A. W.; Whitaker, J. R. Factors affecting enzyme activity in food processing. In *Proteins in Food Processing*, 2nd ed.; Elsevier, **2017**, 337–365. https://doi.org/10.1016/B978-0-08-100722-8.00014-0.

[62] Mohammadi, M.; Mokarram, R. R.; Shahvalizadeh, R.; Sarabandi, K.; Lim, L. T.; Hamishehkar, H. Immobilization and stabilization of pectinase on an activated montmorillonite support and its application in pineapple juice clarification. *Food Biosci.* **2020**, *36*, 100625. https://doi.org/10.1016/j.fbio.2020.100625.

[63] Kuo, C.-H.; Huang, C.-Y.; Shieh, C.-J.; Dong, C.-D. Enzymes and Biocatalysis. *Catalysts* **2022**, *12*, 993. https://doi.org/10.3390/catal12090993.

[64] Homaei, A. A.; Sariri, R.; Vianello, F.; Stevanato, R. Enzyme immobilization: an update. *J. Chem. Biol.* **2013**, *6*, 185–205. https://doi.org/10.1007/s12154-013-0102-9.

[65] Nguyen, H. H.; Kim, M. An Overview of Techniques in Enzyme Immobilization. *Appl. Sci. Converg. Technol.* **2017**, *26*, 157–163. https://doi.org/10.5757/ASCT.2017.26.6.157.

[66] Sheldon, R. A.; van Pelt, S. Enzyme immobilization in biocatalysis: why, what and how. *Chem. Soc. Rev.* **2013**, *42*, 6223–6235. https://doi.org/10.1039/C3CS60075K.

[67] Khan, M. R. Immobilized enzymes: a comprehensive review. *Bull. Natl. Res. Cent.* **2021**, *45*, 207. https://doi.org/10.1186/s42269-021-00649-0.

[68] Hanefeld, U.; Gardossi, L.; Magner, E. Understanding enzyme immobilisation. *Chem. Soc. Rev.* **2009**, *38*, 453–468. https://doi.org/10.1039/B711564B.

[69] Maghraby, Y. R.; El-Shabasy, R. M.; Ibrahim, A. H.; Azzazy, H. M. E.-S. Enzyme Immobilization Technologies and Industrial Applications. *ACS Omega* **2023**, *8*, 5184–5196. https://doi.org/10.1021/acsomega.2c07560.

[70] Lyu, X.; Gonzalez, R.; Horton, A.; Li, T. Immobilization of Enzymes by Polymeric Materials. *Catalysts* **2021**, *11*, 1211. https://doi.org/10.3390/catal11101211.

[71] Dwevedi, A. Basics of Enzyme Immobilization. In *Enzyme Immobilization*; Springer: Cham, **2016**; 21–44. https://doi.org/10.1007/978-3-319-41418-8_2.

[72] Rocha, J. R.; Catana, R.; Ferreira, B. S.; Cabral, J. M. S.; Fernandes, P. Design and characterization of an enzyme system for inulin hydrolysis. *Food Chem.* **2006**, *95*, 77–82. https://doi.org/10.1016/j.foodchem.2004.12.020.

[73] Nisha, S.; Arun Karthick, S.; Gobi, N. A Review on Methods, Application and Properties of Immobilized Enzyme. *Chem. Sci. Rev. Lett.* **2012**, *1*, 148–155.

[74] Brena, B.; González-Pombo, P.; Batista-Viera, F. Immobilization of Enzymes: A Literature Survey. In *Methods Mol. Biol.* **2013**, *1051*, 15–31. https://doi.org/10.1007/978-1-62703-550-7_2.

[75] Miletić, N.; Nastasović, A.; Loos, K. Immobilization of biocatalysts for enzymatic polymerizations: Possibilities, advantages, applications. *Bioresour. Technol.* **2012**, *115*, 126–135. https://doi.org/10.1016/j.biortech.2011.11.054.

[76] Brady, D.; Jordaan, J. Advances in enzyme immobilisation. *Biotechnol. Lett.* **2009**, *31*, 1639–1650. https://doi.org/10.1007/s10529-009-0076-4.

[77] Fernández-Fernández, M.; Sanromán, M. Á.; Moldes, D. Recent developments and applications of immobilized laccase. *Biotechnol. Adv.* **2013**, *31*, 1808–1825. https://doi.org/10.1016/j.biotechadv.2012.02.013.

[78] Dencheva, N.; Braz, J.; Scheibel, D.; Malfois, M.; Denchev, Z.; Gitsov, I. Polymer-Assisted Biocatalysis: Polyamide 4 Microparticles as Promising Carriers of Enzymatic Function. *Catalysts* **2020**, *10*, 767. https://doi.org/10.3390/catal10070767.

[79] Zdarta, J.; Meyer, A.; Jesionowski, T.; Pinelo, M. A General Overview of Support Materials for Enzyme Immobilization: Characteristics, Properties, Practical Utility. *Catalysts* **2018**, *8*, 92. https://doi.org/10.3390/catal8020092.

[80] Rodrigues, R. C.; Berenguer-Murcia, Á.; Fernandez-Lafuente, R. Coupling Chemical Modification and Immobilization to Improve the Catalytic Performance of Enzymes. *Adv. Synth. Catal.* **2011**, *353*, 2216–2238. https://doi.org/10.1002/adsc.201100163.

[81] Sheldon, R. A. Enzyme Immobilization: The Quest for Optimum Performance. *Adv. Synth. Catal.* **2007**, *349*, 1289–1307. https://doi.org/10.1002/adsc.200700082.

[82] Cabral, J. M.; Kennedy, J. F. Covalent and coordination immobilization of proteins. *Bioprocess Technol.* **1991**, *14*, 73–138.

[83] Shakya, A. K.; Nandakumar, K. S. An update on smart biocatalysts for industrial and biomedical applications. *J. R. Soc. Interface* **2018**, *15*, 20180062. https://doi.org/10.1098/rsif.2018.0062.

[84] Yao, T.; Feng, C.; Yan, H. Current developments and applications of smart polymers based aqueous two-phase systems. *Microchem. J.* **2024**, *204*, 111170. https://doi.org/10.1016/j.microc.2024.111170.

[85] European Commission. Commission Regulation (EU) No 10/2011 of 14 January 2011 on plastic materials and articles intended to come into contact with food. *Off. J. Eur. Union* **2011**.

[86] Arvanitoyannis, I. S.; Kotsanopoulos, K. V. Migration Phenomenon in Food Packaging. Food–Package Interactions, Mechanisms, Types of Migrants, Testing and Relative Legislation—A Review. *Food Bioprocess Technol.* **2014**, *7*, 21–36. https://doi.org/10.1007/s11947-013-1106-8.

[87] Yang, L.; Liu, X.; Zhou, N.; Tian, Y. Characteristics of refold acid urease immobilized covalently by graphene oxide-chitosan composite beads. *J. Biosci. Bioeng.* **2019**, *127*, 16–22. https://doi.org/10.1016/j.jbiosc.2018.06.012.

[88] Kharazmi, S.; Taheri-Kafrani, A. Bi-enzymatic nanobiocatalyst based on immobilization of xylanase and pectinase onto functionalized magnetic nanoparticles for efficient fruit juice clarification. *LWT* **2023**, *183*, 114914. https://doi.org/10.1016/j.lwt.2023.114914.

[89] Ozyilmaz, G.; Gunay, E. Clarification of apple, grape and pear juices by co-immobilized amylase, pectinase and cellulase. *Food Chem.* **2023**, *398*, 133900. https://doi.org/10.1016/j.foodchem.2022.133900.

[90] Costa, G. P.; Queiroz, L. B.; Manfroi, V.; Rodrigues, R. C.; Hertz, P. F. Immobilization of Alpha Acetolactate Decarboxylase in Hybrid Gelatin/Alginate Support for Application to Reduce Diacetyl Off-Flavor in Beer. *Catalysts* **2023**, *13*, 601. https://doi.org/10.3390/catal13030601.

[91] Gallifuoco, A.; Alfani, F.; Cantarella, M.; Spagna, G.; Pifferi, P. G. Immobilized β-glucosidase for the winemaking industry: study of biocatalyst operational stability in

laboratory-scale continuous reactors. *Process Biochem.* **1999**, *35*, 179–185. https://doi.org/10.1016/S0032-9592(99)00049-7.

[92] Liburdi, K.; Straniero, R.; Benucci, I.; Garzillo, A. M. V.; Esti, M. Lysozyme Immobilized on Micro-Sized Magnetic Particles: Kinetic Parameters at Wine pH. *Appl. Biochem. Biotechnol.* **2012**, *166*, 1736–1746. https://doi.org/10.1007/s12010-012-9577-z.

[93] Liburdi, K.; Benucci, I.; Esti, M. Study of Two Different Immobilized Acid Proteases for Wine Application. *Food Biotechnol.* **2010**, *24*, 282–292. https://doi.org/10.1080/08905436.2010.507158.

[94] Goldstein, L.; Freeman, A.; Sokolovsky, M. Derivatized Nylon: A New Support for the Immobilization of Enzymes. In *Enzyme Engineering*, Vol. 2; Springer: Boston, MA, **1974**, 97–104. https://doi.org/10.1007/978-1-4615-8897-9_14.

[95] Lehnert, G. Polyamides (PA). *Kunststoffe Plast Eur.* **1998**, *88*, 25–26.

[96] Jiang, Y.; Loos, K. Enzymatic Synthesis of Biobased Polyesters and Polyamides. *Polymers* **2016**, *8*, 243. https://doi.org/10.3390/polym8070243.

[97] Dubois, P; Coulembier, O; Raquez, J. M., Eds. *Handbook of Ring-Opening Polymerization*; Wiley: **2009**. https://doi.org/10.1002/9783527628407.

[98] Zeng, H.; Guan, Z. Direct Synthesis of Polyamides via Catalytic Dehydrogenation of Diols and Diamines. *J. Am. Chem. Soc.* **2011**, *133*, 1159–1161. https://doi.org/10.1021/ja106958s.

[99] Isgrove, F. H.; Williams, R. J. H.; Niven, G. W.; Andrews, A. T. Enzyme immobilization on nylon—optimization and the steps used to prevent enzyme leakage from the support. *Enzyme Microb. Technol.* **2001**, *28*, 225–232. https://doi.org/10.1016/S0141-0229(00)00312-4.

[100] Pahujani, S.; Kanwar, S. S.; Chauhan, G.; Gupta, R. Glutaraldehyde activation of polymer Nylon-6 for lipase immobilization: Enzyme characteristics and stability. *Bioresour. Technol.* **2008**, *99*, 2566–2570. https://doi.org/10.1016/j.biortech.2007.04.042.

[101] Silva, C.; Silva, C. J.; Zille, A.; Guebitz, G. M.; Cavaco-Paulo, A. Laccase immobilization on enzymatically functionalized polyamide 6,6 fibers. *Enzyme Microb. Technol.* **2007**, *41*, 867–875. https://doi.org/10.1016/j.enzmictec.2007.07.010.

[102] Song, J. E.; Kim, H. R.; Lee, S. H. Effect of enzymatic hydrolysis on developing support of polyamide woven fabric for enzyme immobilization. *Text. Res. J.* **2019**, *89*, 1345–1360. https://doi.org/10.1177/0040517518767148.

[103] Vasiliu-Oprea, C.; Dan, F. On the relation between synthesis parameters and morphology of anionic polycaproamide obtained in organic media. I. Influence of the catalytic system. *J. Appl. Polym. Sci.* **1996**, *62*, 1517–1527. https://doi.org/10.1002/(SICI)1097-4628(19961205)62:10<1517::AID-APP4>3.0.CO;2-#.

[104] Denchev, Z. Z.; Dencheva, N. V. Polyamide microcapsules and method to produce the same. *Portuguese Patent* **2015**, PT107679A.

[105] Dencheva, N.; Denchev, Z.; Lanceros-Méndez, S.; Ezquerra Sanz, T. One-Step In Situ Synthesis of Polyamide Microcapsules with Inorganic Payload and Their Transformation into Responsive Thermoplastic Composite Materials. *Macromol. Mater. Eng.* **2016**, *301*, 119–124. https://doi.org/10.1002/mame.201500194.

[106] Dencheva, N. V.; Braz, J. F. B.; Denchev, Z. Z. Synthesis and properties of neat, hybrid, and copolymeric polyamide 12 microparticles and composites on their basis. *J. Appl. Polym. Sci.* **2022**, *139*, 51784. https://doi.org/10.1002/app.51784.

[107] Dencheva, N.; Oliveira, S.; Braz, J.; Getya, D.; Malfois, M.; Denchev, Z.; et al. Magnetically Responsive PA6 Microparticles with Immobilized Laccase Show High Catalytic Efficiency in the Enzymatic Treatment of Catechol. *Catalysts* **2021**, *11*, 239. https://doi.org/10.3390/catal11020239.

[108] Cano-Raya, C.; Dencheva, N. V.; Braz, J. F.; Malfois, M.; Denchev, Z. Z. Optical biosensor for catechol determination based on laccase-immobilized anionic polyamide 6 microparticles. *J. Appl. Polym. Sci.* **2020**, *137*, 49131. https://doi.org/10.1002/app.49131.

[109] Dencheva, N. V.; Oliveira, F. D.; Braz, J. F.; Denchev, Z. Z. Bovine serum albumin-imprinted magnetic poly(2-pyrrolidone) microparticles for protein recognition. *Eur. Polym. J.* **2020**, *122*, 109375. https://doi.org/10.1016/j.eurpolymj.2019.109375.

[110] Omelková, J.; Rexová-Benková, L.; Kubánek, V.; Veruovič, B. Endopolygalacturonase immobilized on a porous poly(6-caprolactam). *Biotechnol. Lett.* **1985**, *7*, 99–104. https://doi.org/10.1007/BF01026676.

[111] Rexová-Benková, L.; Omelková, J.; Veruovič, B.; Kubánek, V. Mode of action of endopolygalacturonase immobilized by adsorption and by covalent binding via amino groups. *Biotechnol. Bioeng.* **1989**, *34*, 79–85. https://doi.org/10.1002/bit.260340111.

[112] Ben-Othman, S.; Rinken, T. Immobilization of Pectinolytic Enzymes on Nylon 6/6 Carriers. *Appl. Sci.* **2021**, *11*, 4591. https://doi.org/10.3390/app11104591.

[113] Vaillant, F.; Millan, A.; Millan, P.; Dornier, M.; Decloux, M.; Reynes, M. Co-immobilized pectinlyase and endocellulase on chitin and Nylon supports. *Process Biochem.* **2000**, *35*, 989–996. https://doi.org/10.1016/S0032-9592(00)00131-X.

[114] Shukla, S.; Saxena, S.; Thakur, J.; Gupta, R. Immobilization of polygalacturonase from *Aspergillus niger* onto glutaraldehyde activated Nylon-6 and its application in apple juice clarification. *Acta Aliment.* **2010**, *39*, 277–292. https://doi.org/10.1556/AAlim.39.2010.3.4.

[115] European Parliament and Council. Regulation (EC) No 1935/2004 of 27 October 2004 on materials and articles intended to come into contact with food. *Off. J. Eur. Union* **2021**, 4–17.

CHAPTER 2

Experimental methods and materials

2.1. Introduction

This chapter presents the materials, experimental procedures, and equipment employed in the synthesis of microparticles, as well as their use as supports for enzyme immobilization and the subsequent application in must/juice clarification. The chapter is organized into four main sections. It begins with a description of the chemical reagents, solvents, and fillers used for the synthesis of empty and loaded microparticles of polyamides 4, 6, and 12 (PA4, PA6, PA12) and the 6,12 copolymer (PA612). The subsequent section details the immobilization techniques and the pectinase enzymes used, specifically the enological preparation Viazym® Clarif Extrem and a lyophilized pectinase. Furthermore, the procedures for the enzymatic treatment of apple juice and grape must are presented. Finally, the methods for morphological and structural characterization, thermal analysis, and spectroscopic assays, together with the specific conditions employed in each case, are described.

2.2. Materials

In the activated anionic ring-opening polymerization (AAROP) of PAMP, the following materials and reagents were used:

- **Solvent:** Toluene/xylene 1:1 by volume (≥99.5% purity) were purchased from Sigma-Aldrich.
- **Monomers:** 2-pyrrolidone (2PD, purum >98%) and laurolactam (LL, purum >99%) were purchased from Sigma-Aldrich–Merck (Lisbon, Portugal). ε-caprolactam (ECL), with reduced moisture content for anionic polymerization (AP-Nylon®), was purchased from Brüggemann Chemical (Heilbronn, Germany).
- **Activator:** Difunctional hexamethylene-1,6-dicarbamoyl-caprolactam, Bruggolen C20P® (C20), was supplied by Brüggemann Chemical (Germany).
- **Initiator:** Sodium dicaprolactamo-bis-(2-methoxyethoxo)-aluminate, Dilactamate® (DL, 80% in toluene solution), was obtained from Katchem Co. (Czech Republic).
- **Payloads:** Non-insulated iron particles (Fe content >99.8%) with average diameters of 3–5 μm were kindly donated by BASF (Ludwigshafen, Germany).

For the immobilization and clarification assays, the following materials and reagents were used:

- **Enzymes:**
    - Viazym® Clarif Extrem, an enological pectinase preparation derived from *Aspergillus niger*, was sourced from Martin Vialatte (Magenta, France) and kindly

donated by Sogrape Vinhos SA (Avintes, Portugal). The preparation was stored at 4 °C until further use.

- Lyophilized pectinase (EC 3.2.1.15; CAS 9032-75-1) from *Aspergillus niger* was purchased from Thermo Scientific Chemicals (Portugal). The enzymatic preparation showed a minimum specific activity of 20.0 U/mg (dry weight). One unit (U) is defined as the amount of enzyme that liberates 1.0 μmol of galacturonic acid per minute. The powder was stored at room temperature in a dry environment until further use.

- **Must:** Industrial rosé and white musts were kindly donated by Sogrape Vinhos SA (Avintes, Portugal). The musts were stored at 4 °C, to prevent fermentation, until further use.
- **Apple juice:** Apples (green and red) for juice preparation were purchased from a local supermarket.

Pectin from citrus peel and all other chemical reagents and solvents employed in this study were of analytical grade and were purchased from Sigma-Aldrich–Merck (Lisbon, Portugal).

2.3. Synthesis of empty polyamide microparticles

2.3.1. Synthesis of polyamide 6 and 12 microparticles

The synthesis of anionic polyamide microparticles (PA6 and PA12) and their corresponding copolymer (PA612), both with and without magnetic incorporation (PA/magnetic), was performed via Activated Anionic Ring-Opening Polymerization (AAROP) in solution, using ECL (ε-caprolactam) or LL (ω-laurinlactam) as monomers. This methodology followed the procedure previously described by Dencheva et al. [1]. In this AAROP system, the activator (Bruggolen C20P®) provides the growth centers for the polymer chains, while the initiator (Dilactamate®) generates the lactamate anions required for the ring-opening step. The general reaction scheme for this polymerization process is illustrated in Figure 2.1.

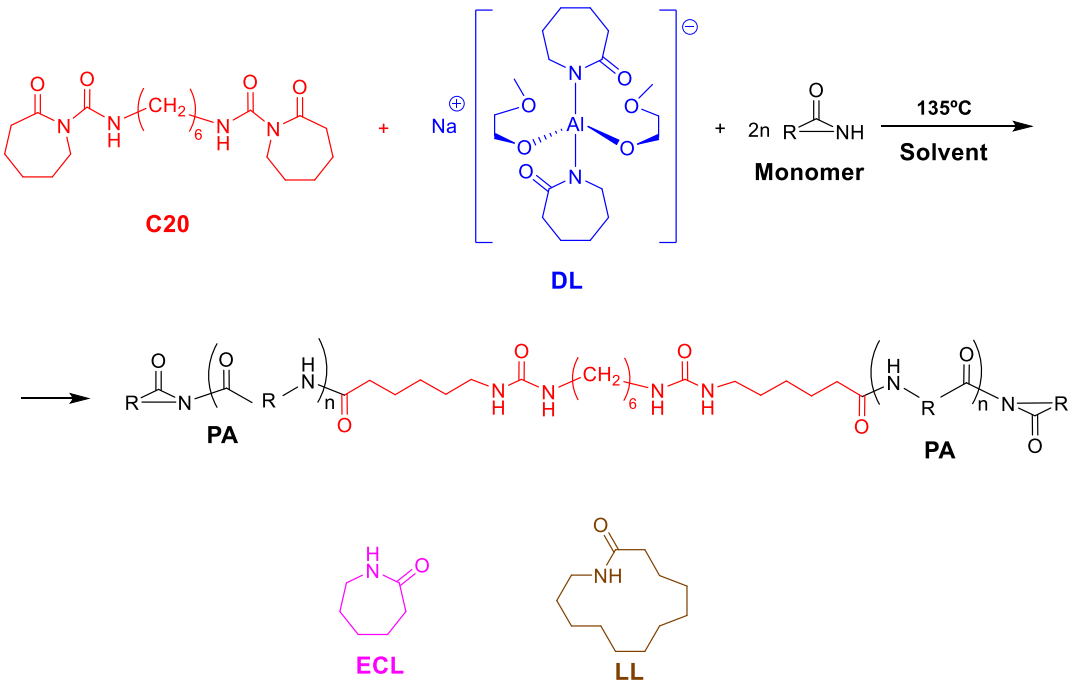


Figure 2.1: Schematic representation of AAROP of lactams to PA microparticles. Chemical structure of the active substance of the C20 activator; of dicaprolactamato-bis-(2-methoxyethoxo)-aluminate (DL, initiator). As monomers, ECL (ε-caprolactam) or LL (ω-laurinlac).

The synthesis was performed in a 250 mL three-neck glass flask fitted with a thermometer, a magnetic stirrer, attachment for azeotropic distillation with reflux condenser, and an inlet for dry nitrogen. The glass flask was placed on a heating mantle, allowing precise control of both temperature and stirring speed. The reaction started with the addition of the monomer (0.3 mol of ECL for PA6 MP, 0.2 mol of LL for PA12 MP, and a mixture of 0.1 mol CL and 0.1 mol LL for PA612 MP) to 100 mL of a mixed hydrocarbon solvent (toluene/xylene 1:1 by volume) while stirring under a nitrogen atmosphere. The reaction mixture was refluxed for 10–15 min. Then, 3.0 mol% of DL and 1.5 mol% of C20 were introduced simultaneously. The synthesis continued for 2 hours after the catalyst addition, with the temperature maintained between 125–135 °C for PA6 or around 120 °C for PA12 and PA612, and constant stirring at 800 rpm. The final MPs were obtained as a white fine powder isolated by vacuum filtration and washing with methanol to eliminate low molecular weight oligomers. The resulting microparticles were dried for 2 hours in a vacuum oven at 80°C. All MP powders were subjected to Soxhlet extraction with methanol for 4 hours to remove traces of oligomers or impurities, then dried and stored in a desiccator.

2.3.2. Synthesis of polyamide 4 microparticles

The empty anionic polyamide 4 microparticles (PA4) with or without magnetic incorporation (PA4/magnetic) was synthesized by low temperature solventless AAROP as previously described by Dencheva et al.[2]. Figure 2.2 shows the corresponding reaction scheme.

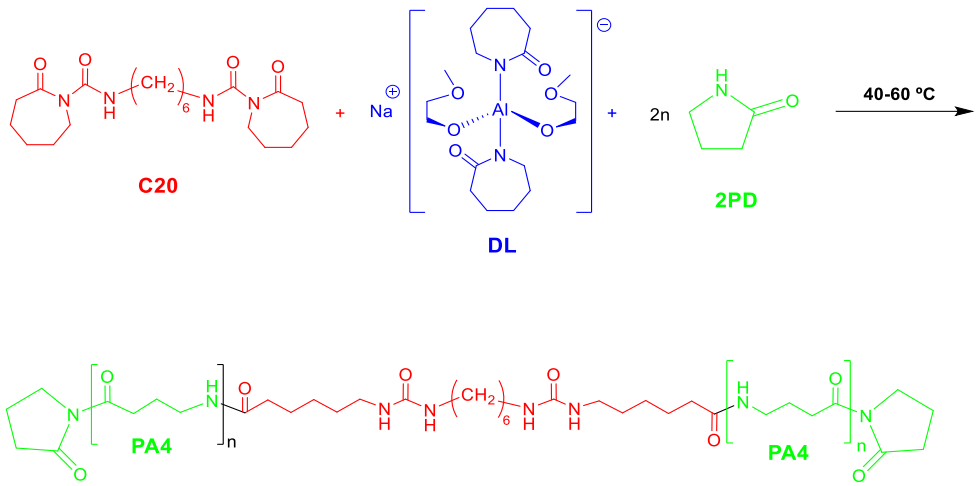


Figure 2.2: Chemical reactions occurring during AAROP of 2-pyrrolidone (2PD) to microparticles: C20 e chemical structure of the active substance of the C20 activator; DL e chemical structure of dicaprolactamato-bis-(2-methoxyethoxo)-aluminate (initiator); 2PD (2-pyrrolidone).

In a typical synthesis, 0.2 mol of 2PD and 1.5 mol % of C20 were added and stirred until the latter reagent was fully dissolved. Subsequently, 3 mol % of DL were added under nitrogen atmosphere. The temperature was gradually increased from 20°C to 40°C, and the pressure reduced to 50 mbar for 6 hours, under constant stirring. To remove the unreacted monomer, the mixture was dispersed in acetone, followed by vacuum filtration. The resulting solid was washed twice with methanol to eliminate low molecular weight oligomers, then dried in a vacuum oven at 50 °C for 1h. The PA4 MP, obtained as a fine white powder, were finally subjected to Soxhlet extraction with methanol for 4 h to ensure complete removal of residual oligomers.

2.3.3. Synthesis of hybrid polyamide microparticles with load

The microparticles with Fe content were synthesized as described in 2.2.1 (for PA6 and PA12) and 2.2.2 (for PA4).

In this case, Fe (1–3 wt.% relative to the monomer) was added to the reaction mixture, while all other polymerization, isolation, and purification steps were identical to those used for the neat MPs. The resulting microparticles were obtained as a fine gray powder.

2.3.4. Designation of microparticulate samples

Seven types of microparticle supports were synthesized, namely neat PA4, PA6, PA12 MP, iron-containing PA4-Fe, PA6-Fe, PA12-Fe MP and the copolymer PA612 MP. The designation and composition of all PAMPs are summarized in Table 2.1. The chemical structures of the synthesized polyamides are shown in Figure 2.3.

Table 2.1: Samples designation and composition of the M-samples – MPs.

Sample designation	Load, wt % [a]	Description
PA4	0	PA4 microparticles
PA4-Fe	1	PA4 containing 1 wt% Fe
PA6	0	PA6 microparticles
PA6-Fe	3	PA6 containing 3 wt% Fe
PA12	0	PA12 microparticles
PA12-Fe	2	PA6 containing 2 wt% Fe
PA612	0	PA612 microparticles

[a] Percentage based on the weight of the ECL monomer in the starting AAROP mixture.

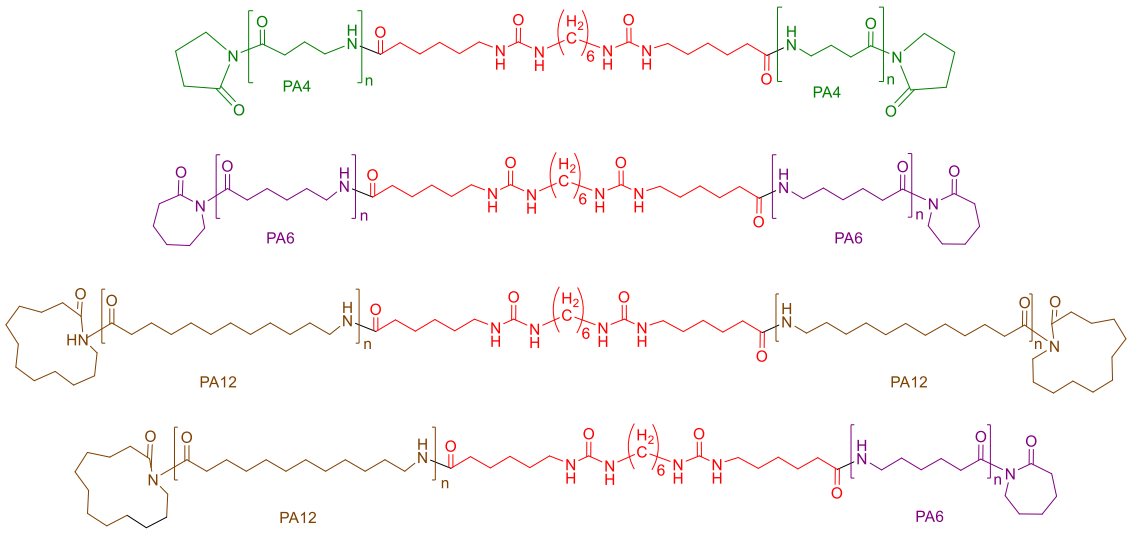


Figure 2.3: Chemical structures of the microparticulate polyamides.

2.4. Immobilization of Pectinase

2.4.1. Adsorption immobilization

2.4.1.1. Enological pectinase

The enological pectinase preparation, Viazym® Clarif Extrem (PeV), was immobilized by adsorption on the seven different microparticulate supports previously synthesized.

The enzyme was diluted tenfold in double-distilled water (H_2O) in Falcon tubes. The preparation was assumed to contain approximately 10 a.u. of protein per mL, 5 mL of the diluted solution were added to 100 mg of each PA microparticle (PA4, PA6, PA12, PA4-Fe, PA6-Fe, PA12-Fe, and PA612) in Eppendorf tubes. The mixtures were incubated at room temperature under gentle agitation in an orbital shaker for 24 h. Afterwards, the samples were centrifuged (5000 rpm, 5 min), the supernatants collected and stored at 4 °C for further analysis. The resulting PeV@PA complexes were washed twice with double-distilled water to remove unbound enzyme and stored at 4 °C until use.

2.4.1.2. Lyophilized pectinase

The lyophilized pectinase from Thermo Scientific Chemicals (PeL) were immobilized by adsorption on PA6 microparticles. A solution of PeL (0.5 mg/mL) was prepared in different media (citrate buffer pH 5 0.1M, phosphate buffer pH 6 0.1M and pH8 0.1M, and double-distilled water). For each condition, 5 mL of enzyme solution were added to 100 mg of PA6 in Eppendorf tubes. The suspensions were incubated under gentle orbital shaking at room temperature for 24 h. After centrifugation (5000 rpm, 5 min), the supernatants were collected and stored at 4 °C for analysis. The resulting PeL@PA6 complexes were washed twice with double-distilled water and stored at 4 °C until further use.

2.4.2. Designation of samples obtained by physical immobilization

The PeV and PeL were physically immobilized in different microparticulate supports previously synthesized. The designations used for the enzyme–microparticle complexes are summarized in Table 2.2.

Table 2.2: Designation of samples obtained by adsorption immobilization of enological (PeV) and lyophilized (PeL) pectinase on polyamide-based microparticles.

Sample designation	Description
PeV@PA6	enological pectinase immobilized on polyamide 6
PeV@PA6-Fe	enological pectinase immobilized on polyamide 6 containing 3 wt% Fe
PeV@PA4	enological pectinase immobilized on polyamide 4
PeV@PA4-Fe	enological pectinase immobilized on polyamide 4 containing 1 wt% Fe
PeV@PA12	enological pectinase immobilized on polyamide 12
PeV@PA12-Fe	enological pectinase immobilized on polyamide 12 containing 2 wt% Fe
PeV@PA612	enological pectinase immobilized on polyamide 612
PeV@PA[1]	general designation for polyamide microparticles loaded with enological pectinase
PeL@PA6	lyophilized pectinase immobilized on polyamide 6
PeL@PA6_pH5	lyophilized pectinase immobilized on PA6 in buffer solution at pH5
PeL@PA6_pH6	lyophilized pectinase immobilized on PA6 in buffer solution at pH6
PeL@PA6_pH7	lyophilized pectinase immobilized on PA6 in buffer solution at pH7
PeL@PA6_pH8	lyophilized pectinase immobilized on PA6 in buffer solution at pH8

[1] PeV@PA is used as a general designation when referring collectively to the complexes obtained with enological pectinase immobilized on different PA supports.

2.5. Determination of the Total Amount of Protein

After immobilization, the supernatants were analyzed by UV/VIS spectroscopy (Shimadzu model 1900i double-beam spectrophotometer 680 (Tokyo, Japan)) to determine the residual protein content and calculate the total protein (TP) incorporated into the PA microparticles (MPs), according to:

$$TP = C_0 - C_{S'} \quad (1)$$

where C_0 is the initial protein content before immobilization, and $C_{S'}$ is the protein content in the supernatant after the immobilization process. Protein concentration was determined by direct quantification of the maximum UV absorption peak at $\lambda \approx 263$ nm for PeV and $\lambda \approx 277$ nm for PeL. For this analysis, the initial solution (PeV) and the respective supernatants were diluted 10 times. This dilution was necessary to enable the clear determination of the UV/VIS absorption

maxima at 263 nm. In this study TP is considered as immobilization yield. It was assumed that 1 mL of 10-fold diluted pectinase Viazym contains 10 arbitrary units (a.u.) of protein.

2.6. Determination of pectinase activity

2.6.1. Activity assay

The activity of pectinase was determined by measuring the amount of reducing sugars released from a pectin solution using 3,5-dinitrosalicylic acid (DNS) method proposed by Miller [3]. The DNS reagent is composed of 2-hydroxy-3,5-dinitrobenzoic acid (1% w/v), potassium sodium tartrate (30% w/v) and sodium hydroxide (1% w/v). The substrate solution was prepared with citric pectin (0.25% w/v) in citrate buffer (50 mM, pH 3.8).

In a typical assay, 0.1 mL of free pectinase (PeV and PeL) or 0.020 g of wet immobilized enzyme (PeV@PA and PeL@PA6) was mixed with 0.90 mL of substrate solution and incubated at 50°C for 15 minutes. Subsequently, 1 mL of DNS solution was added to the reaction mixture, the vials were kept in water bath at 90°C for 10 minutes and then cooled in ice bath to stop the reaction. Then, the dark yellow solution was measured at 540 nm using a UV-visible spectroscopy. The blank consisted of 1 mL of DNS and 1 mL of buffer solution. The amount of reducing sugar released was quantified using the standard calibration curve for D-galacturonic acid. Enzymatic activity in units (U) was expressed as μmol of D-galacturonic acid equivalents released per minute under the assay conditions, according to the Equation (2):

$$A(U) = \frac{C}{T} \tag{2}$$

were C is the concentration of reducing sugars (μmol/mL) obtained from the calibration curve, and T is the reaction time (min).

2.6.1.1. Calibration curve

The calibration curve was prepared using D-galacturonic acid as the standard. Standard solutions in the range of 0.28–2.83 μmol/mL were prepared in citrate buffer (50 mM, pH 3.8). 1 mL of each standard was heated to 50°C and mixed with the DNS reagent under the same conditions as described in 2.5.1.

2.6.2. Determination of immobilization efficiency and the activity recovery

The activity of the supernatants was also determined using the DNS method. These results were used to calculate the immobilization efficiency and the activity recovery. The immobilization efficiency (IE, Equation 3) represents the fraction of the expected activity that was effectively retained in the immobilized form. The activity recovery (AR, Equation 4) indicates the proportion of the initial total activity preserved after immobilization. They were calculated as defined by Sheldon and van Pelt [4] and further detailed by Boudrant et al. [5].

IE was calculated as the ratio of observed immobilized activity to the theoretical activity of the bound protein, assuming unchanged specific activity, i.e.,

$$IE(\%) = \frac{SA_{imm}}{SA_{theor}} \times 100 = \frac{AR}{IY} \times 100 \quad (3)$$

wherein SA_{imm} is the observed specific activity of immobilized enzyme (U/mg); SA_{theor} is the theoretical activity of the bound enzyme (U/mg) determined as the product of the amount bound protein and the initial specific activity of the free enzyme.

AR was determined as the ratio of observed immobilized activity to the initial total enzyme activity, i.e.,

$$AR(\%) = \frac{A_{imm}}{A_0} \times 100 \quad (4)$$

wherein A_0 is the total enzymatic activity of the starting enzyme solution (U) and A_{imm} is the activity measured for the immobilized complex (U).

2.6.3. Influence of ethanol on enzymatic activity

The influence of ethanol on the activity of the free PeL or its immobilized complexes was determined by the DNS method, under the same conditions described above in 2.5.1. For this purpose, different percentages of ethanol (5, 10, and 15%) were added to both the substrate and to the blank samples. The solutions obtained after the reaction with DNS were analyzed by UV/VIS spectroscopy.

2.6.4. Influence of glucose on enzymatic activity

The activity of free and immobilized lyophilized pectinase was determined in the presence of different percentage of glucose (5, 10 and 15%). The glucose was added to the substrate solution, then 0.90 mL of this solution was added to 0.10 mL of PeL or 0.020 g of PeL@PA6 was heated to 50°C and mixed with the DNS reagent under the same conditions as the activity assay described in 2.5.1. The blank samples consisted of a solution of DNS, buffer solution and different percentage of glucose.

2.7. Kinetics parameters

2.7.1. Enological pectinase

The kinetic parameters of free pectinase and the immobilized PeV@PA complexes were determined by quantifying the release of D-galacturonic acid from pectin at various substrate concentrations (0.05–5 mg/mL) under the conditions described in Section 2.5, with a fixed incubation time of 1 min. The total amount of enzyme in the reaction mixture was kept constant. Both free and immobilized enzymes exhibited deviations from conventional Michaelis–Menten kinetics. Therefore, three kinetic models were selected based on the literature [6] to describe the experimental data: the classical Michaelis–Menten model and two substrate inhibition models, given by Equations (5)–(7):

$$V = \frac{V_{max}S}{K_m+S} \tag{5}$$

$$V = \frac{V_{max}S}{(K_m+S)(1+\frac{S}{K_i})} \tag{6}$$

$$V = V_{max}\left[\exp\left(\frac{-S}{K_i}\right) - \exp\left(\frac{-S}{K_m}\right)\right] \tag{7}$$

where V_{max} is the maximum reaction rate, K_m is the Michaelis–Menten constant, and K_i is the inhibition constant characterizing the formation of an inactive enzyme–substrate complex. The kinetic parameters (V_{max}, K_m and K_i) were estimated by nonlinear multiple regression analysis using OriginPro software (version 9.8.0.200, OriginLab Corporation, Northampton, MA, USA).

2.7.2. Lyophilized pectinase

The kinetic parameters (V_{max} and K_m) for all the pectinase preparations (PeL and PeL@PA6) were determined by applying the activity assay for different pectin concentrations ranging from 0.1 to 7 mg/mL. Michaelis–Menten curve and Lineweaver–Burk plots were constructed. The kinetic parameters were calculated from the Lineweaver-Burk equation (8) using computed linear regression calculations using OriginPro software (version 9.8.0.200, OriginLab Corporation, Northampton, MA, USA).

$$\frac{1}{V_0} = \frac{K_m}{V_{max}} \times \frac{1}{[S]} + \frac{1}{V_{max}} \quad (8)$$

2.8. Application of Pectinase in beverage clarification

2.8.1. Rosé/white wine must

Clarification of rosé must was performed at room temperature using free enological or lyophilized pectinase, as well as immobilized preparations. Clarification of white must was performed using PeL and PeL@PA. 14 mL of rosé or white must, containing 2 mg/mL pectin, were placed in Falcon tubes, where the appropriate amount of free or immobilized enzyme was added. For the enological pectinase, 10 μL of pectinase solution containing 0.13 a.u. of free or immobilized PeV was used, whereas for the lyophilized pectinase, 180 μL of PeL solution containing 0.1 mg of free pectinase (pH 5-8) or the corresponding amount of immobilized enzyme was applied. Clarification was determined by measuring turbidity using a turbidimeter. Turbidity values were expressed in nephelometric turbidity units (NTU) and recorded every 15–20 min for a total period of 3–9 h.

2.8.2. Apple juice

Fresh apple juice was prepared using four green apples and one red apple, obtained from the local supermarket. The preparation and processing steps are schematically shown in Figure 2.4.

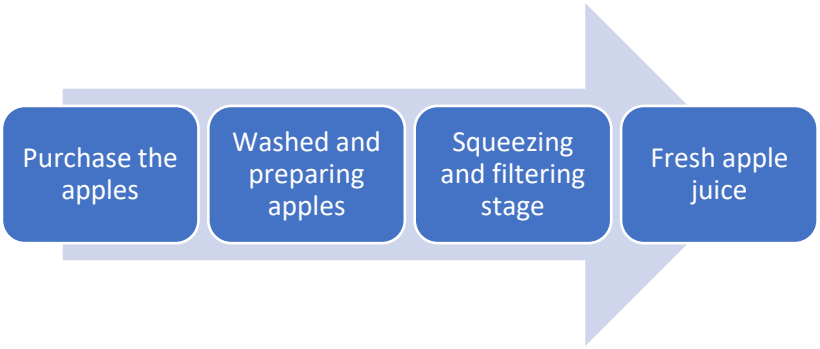


Figure 2.4: Apple processing stages.

2.8.2.1. Production of apple juice

A mixture of fresh apples (476.4 g) were washed with tap water, then the skin and seeds were removed. The fruit was cut into small cubes and homogenized using a domestic blender without the addition of water. The resulting pulp was filtered to obtain raw apple juice. To prevent enzymatic browning, 0.5% (v/v) of lemon juice was added as a natural antioxidant. The juice, obtained with an extraction yield of 69.3% (≈ 330 mL), was then centrifuged at 5000 rpm for 30 min to remove suspended solids. The supernatant was collected and stored at 4°C for the subsequent enzymatic clarification experiments.

2.8.2.2. Clarification process

Fourteen milliliters of fresh apple juice were mixed with 180 µL of pectinase solution containing 0.1 mg of free pectinase (pH 5-8) or the corresponding amount of immobilized enzyme at room temperature (23 °C ± 2 °C). The turbidity was measured every 20 minutes in NTUs min for a total period of 5 h.

2.8.3. Pectin test

2.8.3.1. Rosé/white must

After clarification, a pectin test was performed to verify whether the clarification process was complete. For this test, 5 mL of acidified alcohol (5% v/v HCl in ethanol) was added to 2.5 mL of clarified must. The mixture was gently shaken, allowed to stand for 10 min, and then visually inspected. The formation of insoluble flakes indicated the presence of residual pectin, while a clear liquid confirmed complete clarification.

2.8.3.2. Apple juice

A similar test was performed on clarified apple juice. 1 mL of juice was mixed with 1 mL of ethanol (96%), shaken vigorously, and left to stand for 1 min. If a visible residue appeared, the depectinization was incomplete; otherwise, clarification was considered complete.

2.9. UV/Vis analyses of must and apple juice

2.9.1. Composition of must

The color, browning index, hydroxycinnamic acids, polyphenolic index and flavonols of the must before and after clarification were determined by UV/VIS spectroscopy.

The color of the must was analyzed, according to the method OIV-MA-AS2-780 07B [7]. These analyses were made to evaluate any color changes resulting from enzymatic clarification. The color of the must was measured at three specific wavelengths: 420 nm (absorption of yellow), 520 nm (absorption of red) and 620 nm (absorption of blue). The baseline used was double-distilled water.

The color intensity (I), which reflects the overall amount of coloring compounds, was calculated using Equation (9). The tonality (T), also referred to as hue, which provides information on the chromatic characteristics of the must, was established by the Equation (10) by comparing the absorbance at 420 nm to that at 520 nm. The percentages of yellow (Y, Equation 11), red (R, Equation 12), and blue (B, Equation 13) colors components were derived by comparing the absorbance at 420, 520 or 620 nm, respectively [8,9]. The Browning index (BI) of musts, which measures oxidation in white and rosé wines, was directly measured at 420 nm [10].

$$I(a.u.) = A_{420} + A_{520} + A_{620} \quad (9)$$

$$T(a.u.) = {}^{A_{420}}/_{A_{520}} \quad (10)$$

$$Y(\%) = \frac{A_{420}}{I} \times 100 \quad (11)$$

$$R(\%) = \frac{A_{520}}{I} \times 100 \quad (12)$$

$$B(\%) = \frac{A_{620}}{I} \times 100 \quad (13)$$

where A_{420}, A_{520} and A_{620} represent the absorbance values at 420 nm, 520 nm, and 620 nm, respectively.

Total polyphenolic index (TPI, Equation 14), hydroxycinnamic acids (HCA, Equation 15) and flavanols ($FLAV$, Equation 16) were measured using the absorbances at 280, 320 and 365 nm, respectively, after sample dilution 1:10 with distilled water for white must [8] and 1:5 with distilled water for rose must [11].

$$TPI(a.u.) = A_{280} \times dilution\ factor \quad (14)$$

$$HCA(a.u.) = A_{320} \times diluition\ factor \quad (15)$$

$$FLAV(a.u.) = A_{362} \times diluition\ factor \quad (16)$$

where A_{280}, A_{320} and A_{362} represent the absorbance values at 280 nm, 320 nm, and 365 nm, respectively.

To evaluate whether microparticles influenced the pH of the must, the acidity was determined before and after clarification using PB-11 model pH meter.

2.9.2. Color of apple juice

Samples of apple juice before and after clarification were analyzed by UV/VIS spectroscopy, the baseline was double-distilled water. The absorbance at 420 nm was the browning index and the absorbance at 660 nm was used to determine the percentage of clarification (Clarity) of apple juice applying the Equation (17) [12].

$$Clarity(\%) = \frac{[Abs_{untreated\ sample} - Abs_{treated\ sample}]}{Abs_{untreated\ sample}} \times 100 \quad (17)$$

The pH of apple juice after and before clarification was also determined.

2.10. Reusability Studies

2.10.1. By clarification

2.10.1.1. Enological pectinase

The reusability of the PeV@PA complexes was also tested by performing three consecutive clarification cycles using 15 mL of industrial rosé must at room temperature (≈23°C). The turbidity was measured every hour until reaching levels around 20 NTUs, as described in Section 2.7.1. After each clarification cycle, the complexes were recovered by centrifugation and washed twice with 1 mL of deionized water and reused in a fresh portion of rosé must following the same procedure.

2.10.1.2. Lyophilized Pectinase

The PeL@PA6 complexes, each containing 0.1 mg of enzyme, were used for clarification of rosé/white must (15 mL) and apple juice (15 mL) in two and three consecutive cycles, respectively. Turbidity was monitored every hour for must (until ≈20 NTU) and every 30 minutes for juice (until ≈200 NTU). After each cycle, the complexes were recovered via centrifugation, washed twice with 1 mL of deionized water. Their clarification capacity was tested again under the same conditions with a fresh must/juice sample.

2.10.2. By activity test

For this study, PeV@PA or PeL@PA6 complexes (0.020 g) were incubated with 0.90 mL of citric pectin substrate (prepared as described in Section 2.5) at 50 °C for 15 minutes. After incubation, the liquid phase was separated from the immobilized complexes to terminate the reaction. Subsequently, 1 mL of DNS reagent was added to the supernatant to chemically inactivate any potential leached enzyme and stabilize the samples for storage in the dark until further processing. The complexes were then washed twice with 1 mL of deionized water to remove residual substrate before starting a new cycle. This procedure was repeated for eight cycles (PeV@PA) or five cycles (PeL@PA6). After the final cycle, all collected vials containing DNS were heated at 90 °C for 10 minutes to develop the color, cooled in ice water, and analyzed by UV/VIS spectroscopy. Residual activity was determined by comparing subsequent cycles to the first cycle (100%).

2.11. Storage stability studies

2.11.1. Enological pectinase

The free pectinase and immobilized enzyme complexes were stored in double-distilled water (H2O) at 4 °C for one month. Enzyme samples (0.1 mL of free enzyme solution and 0.020 g of PeV@PA) were withdrawn every week, and their residual activity was determined using the DNS method, as described in Section 2.5. The activity measured immediately after immobilization was taken as 100% and used as the reference value.

2.11.2. Lyophilized Pectinase

The PeL and PeL@PA6 were stored at 4 °C in the same conditions used during immobilization (pH 5, 6, 7, or 8) for up to four months. Samples were taken after 1, 2, 3, and 4 weeks, and again after 2, 3 and 4 months, and their residual activity was determined using the DNS method, as described in Section 2.5. The activity measured immediately after immobilization was taken as 100% and used as the reference value.

2.12. Recovery and Reuse of Microparticles

After the last reuse cycle, when enzymatic activity decreases, the PeV@PA6 and PeV@PA6-Fe complexes were dried in a vacuum oven at 80 °C for 72 h. Subsequently, the microparticles were transferred to 15 mL glass vials, and 5 mL of deionized water was added to each vial. The vials were placed on a hotplate, and the water was brought to a boil under constant stirring. After 1 h, the microparticles were filtered and subjected to Soxhlet extraction with ethanol for 4 h to remove the enzyme residues.

The recovered microparticles were then dried and stored in a desiccator until further use. These regenerated microparticles were reused for enzyme immobilization under the same conditions described in Section 2.3.1.1.

2.13. Morphological and structural characterization

Several characterization techniques were implemented for a detailed morphological and structural characterization of the microparticles with and without immobilized enzyme. The secondary structure of the enzyme was also determined.

2.13.1. Electron microscopy

2.13.1.1. Optical microscopy

Optical microscopy is a morphological characterization technique that allows obtaining an enlarged image of a sample, enabling the acquisition of structural and molecular information [13].

The polyamide microparticles were analyzed by reflected light microscopy (RLM), suitable for the observation of opaque samples.

In this work, the RLM study was performed in an Olympus BH-2 microscope (Olympus Corp. Japan) equipped with a Leica DFC200 (Leica Microsystems, Germany) digital camera.

All images collected were subsequently processed using the Leica Application Suite V4.4 software, which is a time-consuming process as it is semi-manual. Image processing allows individual particles to be identified and particles that appear together to be separated by drawing a separation line. The software thus provides data on the area, sphericity, and equivalent circular diameter of the particles.

All samples were observed under a microscope equipped with a 4x objective and a 1.67x eyepiece.

2.13.1.2. Scanning electron microscopy

Scanning electron microscopy (SEM) is an effective method in analysis of organic and inorganic materials, including metals and polymers, on a nanometer (nm) to micrometer (μm) scale [14]. The size and shape of all synthesized microparticles, with and without immobilized enzyme, were determined using this technique. These studies were performed in a NanoSEM-200 apparatus from FEI Nova (Hillsboro, OR, USA) using mixed secondary electron/backscattered electron in-lens detection. All the samples were observed after sputter coating with Au/Pd alloy in a 208 HR instrument from Cressington Scientific Instruments (Watford, UK) with high-resolution thickness control. SEM-EDS (scanning electron microscopy-energy-dispersive Xray spectroscopy) was also applied to provide elemental analysis.

2.13.2. Thermal characterization

2.13.2.1. Differential scanning calorimetry

DSC enables direct determination of characteristic temperatures in a polymer material, such as the melting temperature, T_m, the crystallization temperature, T_c, and the glass transition

temperature, T_g . Besides that, the degree of crystallinity, X_c , of the polymer matrix can be determined according to Equation (18):

$$X_c(\%) = \frac{\Delta H_m^i}{w.H_m^0} \quad (18)$$

where, ΔH_m^i is the registered melting enthalpy of the current sample, w is the weight fraction of the polymer present in the sample and $\mathrm{H_m^0}$ is the melting enthalpy of a 100 % crystalline sample [15].

In this work, the DSC measurements were carried out in a 200 F3 equipment of Netzsch (Selb, Germany) at a heating rate of 10 °C/min under N2 purge, temperature rate during the recrystallization step of 20 °C deg/min. The typical sample weights were in the 10-15 mg range. All the PAMP synthesized, before and after immobilization, were analyzed.

2.13.2.2. Thermogravimetric analysis

This analysis was performed to characterize PAMP with and without Fe, before and after enzyme immobilization. The TGA measurements were carried out in Q500 TGA equipment (TA Instruments, USA), heating the samples from 40 to 600°C at 10 °C/min in a N2 atmosphere. The typical sample weights were in the 10-20 mg range.

TGA was used also to determine the effective real load (RL). The RL value in PAMP was calculated according to Equation 19:

$$RL(\%) = R_f - R_{PA6} \quad (19)$$

whereR_{PA6} is the carbonized residue at 600 °C of empty PAMP and R_f represents the carbonized residue of the respective loaded PAMP measured by TGA.

2.13.3. Fourier Transform Infrared Spectroscopy

Using this method, all microparticles were analyzed, with and without magnetic incorporation, as well as all microparticles with immobilized enzymes.

The analysis started with a blank measurement to obtain the baseline. The test followed with the samples under study, obtaining spectra of the percentage of transmittance as a function of

wavelength. All tests were subject to the same measurement conditions (sample quantity, atmospheric conditions, ATR (*Attenuated Total Reflection*) coupling, and the same ATR clamping) in order to make the results comparable.

For the present study, the Jasco FT/IR 4100 equipment was used with the ATR device attached, with 64 accumulations.

2.14. Circular Dichroism

Circular dichroism (CD) spectroscopy is an optical spectroscopic method for evaluating the secondary structure of proteins. This is defined as the unequal absorption of left-handed and right-handed circularly polarized light [16].

The secondary structure of free lyophilized pectinase and supernatants of immobilization were studied by circular dichroism spectroscopy (Jasco J-1500 spectropolarimeter), using a quartz cuvette of 1 mm optical path length at room temperature (20 °C ± 1 °C). The baseline was the buffer solutions and double-distilled water (used for enzymatic immobilization, section 2.3.1.2). The spectra were recorded in the range 260–185 nm at a scan speed of 20 nm/min and bandwidth of 1 nm. The final spectra were obtained by the average of three scans for each sample. The data analysis of circular dichroism was conducted using DichroWeb (http://dichroweb.cryst.bbk.ac.uk, accessed on 21 March 2025), an online tool specialized in determining the secondary structure of proteins from circular dichroism spectra.

2.15. UV/VIS spectroscopy

Ultraviolet-Visible (UV/VIS) spectroscopy was performed using a Shimadzu model 1900i double-beam spectrophotometer (Tokyo, Japan) to analyze the solutions throughout this study. Spectra were recorded in spectral mode (absorbance) across a wavelength range of 200 to 800 nm. The measurements were carried out at room temperature (20 ± 1 °C) using quartz cuvettes with an optical path length of 10 mm. Before each analysis, a baseline was established using the respective solvent as a reference.

2.16. References

[1] Dencheva, N.; Denchev, Z.; Lanceros-Méndez, S.; Ezquerra Sanz, T. One-step in situ synthesis of polyamide microcapsules with inorganic payload and their transformation into

responsive thermoplastic composite materials. *Macromol. Mater. Eng.* **2016**, *301*, 119–124. https://doi.org/10.1002/mame.201500194.

[2] Dencheva, N.; Braz, J.; Nunes, T. G.; Oliveira, F. D.; Denchev, Z. One-pot low temperature synthesis and characterization of hybrid poly(2-pyrrolidone) microparticles suitable for protein immobilization. *Polymer* **2018**, *145*, 402–415. https://doi.org/10.1016/j.polymer.2018.04.080.

[3] Miller, G. L. Use of dinitrosalicylic acid reagent for determination of reducing sugar. *Anal. Chem.* **1959**, *31*, 426–428. https://doi.org/10.1021/ac60147a030.

[4] Sheldon, R. A.; van Pelt, S. Enzyme immobilisation in biocatalysis: Why, what and how. *Chem. Soc. Rev.* **2013**, *42*, 6223–6235. https://doi.org/10.1039/C3CS60075K.

[5] Boudrant, J.; Woodley, J. M.; Fernandez-Lafuente, R. Parameters necessary to define an immobilized enzyme preparation. *Process Biochem.* **2020**, *90*, 66–80. https://doi.org/10.1016/j.procbio.2019.11.026.

[6] Gummadi, S. N.; Panda, T. Analysis of kinetic data of pectinases with substrate inhibition. *J. Microbiol. Biotechnol.* **2003**, *13*, 332–337.

[7] International Organisation of Vine and Wine. *Compendium of International Methods of Analysis of Wines and Musts*; OIV: Paris, France, **2023**.

[8] Mangas, R.; González, M. R.; Martín, P.; Rodríguez-Nogales, J. M. Impact of glucose oxidase treatment in high sugar and pH musts on volatile composition of white wines. *LWT-Food Sci. Technol.* **2023**, *184*, 114975. https://doi.org/10.1016/j.lwt.2023.114975.

[9] Faragó, P.; Gălătuş, R.; Hintea, S.; Boşca, A. B.; Feurdean, C. N.; Ilea, A. An intra-oral optical sensor for the real-time identification and assessment of wine intake. *Sensors* **2019**, *19*, 4719. https://doi.org/10.3390/s19214719.

[10] Salacha, M. I.; Kallithraka, S.; Tzourou, I. Browning of white wines: Correlation with antioxidant characteristics, total polyphenolic composition and flavanol content. *Int. J. Food Sci. Technol.* **2008**, *43*, 1073–1077. https://doi.org/10.1111/j.1365-2621.2007.01567.x.

[11] Aleixandre-Tudo, J. L.; du Toit, W. The Role of UV-Visible Spectroscopy for Phenolic Compounds Quantification in Winemaking. In *Frontiers and New Trends in the Science of Fermented Food and Beverages*; Solís-Oviedo, L., Pech-Canul, Á., Eds.; IntechOpen: London, UK, **2019**. https://doi.org/10.5772/intechopen.79550.

[12] Berutu, C. A. M.; Fahrurrozi, F.; Meryandini, A. Pectinase production and clarification treatments of apple (Malus domestica) juice. *Ann. Bogor.* **2017**, *21*, 63–68. https://doi.org/10.14203/ann.bogor.2017.v21.n2.63-68.

[13] Murphy, D. B.; Davidson, M. W. *Fundamentals of Light Microscopy and Electronic Imaging*, 2nd ed.; Wiley-Blackwell: Hoboken, NJ, USA, **2012**. https://doi.org/10.1002/9781118382905.

[14] Mohammed, A.; Abdullah, A. Scanning Electron Microscopy (SEM): A Review. In *Proceedings of the 2018 International Conference on Hydraulics and Pneumatics (HERVEX)*, Băile Govora, Romania, 7–9 November **2018**, 77–85.

[15] Schick, C. Differential scanning calorimetry (DSC) of semicrystalline polymers. *Anal. Bioanal. Chem.* **2009**, *395*, 1589–1611. https://doi.org/10.1007/s00216-009-3169-y.

[16] Miles, A. J.; Janes, R. W.; Wallace, B. A. Tools and methods for circular dichroism spectroscopy of proteins: A tutorial review. *Chem. Soc. Rev.* **2021**, *50*, 8400–8413. https://doi.org/10.1039/d0cs00558d.

RESULTS AND DISCUSSION

CHAPTER 3

Synthesis and properties of anionic polyamide pulverulent materials

3.1. Introduction

The bibliographic research presented in Chapter 1 led to the selection of polyamide microparticles and copolymers as a support for enzyme immobilization, particularly for their potential application in the food industry.

Chapter 3 describes the *in-situ* synthesis of PA4, PA6, and PA12 microparticles (PAMP) produced with and without metallic fillers (Fe) at loadings of 1-3 wt. %, as well as the synthesis of the PA612 copolymer. The structure, morphology, and thermal properties of all synthesized PAMP were systematically evaluated, and the corresponding results are presented in this chapter. Most of these data have already been published [1].

3.2. Synthesis of polyamide microparticles

The synthesis of polyamide microparticles (PAMP), with and without magnetic load, was carried out by activated anionic ring-opening polymerization (AAROP), as described in Section 2.3 of Chapter 2. The designations of the PAMP samples produced, along with their respective polymerization yields, are presented in Table 3.1. Figure 3.1 shows the visual appearance of these materials.

Table 3.1: PAMP sample designations, composition, and polymerization yield.

Sample	Fe content [a], wt.%	Yield [b], %	Oligomers [c], wt.%
PA4	-	59.4	4.4
PA4-Fe	1.0	61.2	5.9
PA6	-	56.0	2.0
PA6Fe	3.0	58.8	2.4
PA12	-	42.0	3.2
PA12-Fe	2.0	58.5	3.4
PA612	-	77.0	2.1

a) Percentage based on the weight of the monomer in the initial AAROP mixture.
b) Relative to the monomer before polymerization.
c) After Soxhlet extraction (with methanol).



Figure 3.1: Visual aspect of the materials prepared, from left to right: PA4, PA4-Fe, PA6, PA6-Fe, PA12, PA12-Fe and PA612.

The polymerization process yielded purified polyamide microparticles with good overall yields, ranging from approximately 40 to 77% (Table 3.1). These values were determined after removing 2.0–3.5 wt.% methanol-soluble oligomers by Soxhlet extraction. The highest yield was obtained for the copolymer (PA612, 77%), whereas PA12 presented a lower yield (≈40%). PA4 and PA6 achieved yields around 60%.

According to Vasiliu-Oprea and Dan [2], the formation of PA6 microparticles during the AAROP process can be explained as follows: the growing polyamide chains bend and form viscous droplets, which represent coiled oligomer molecules. These droplets subsequently undergo macromolecular chain propagation, coalescence, and crystallization, leading to the formation of semicrystalline microparticles. In the case of the PA–Fe hybrid systems, the iron payloads are dispersed in the constantly stirred initial reaction medium; as AAROP progresses, they become entrapped within the viscous polymer and nucleate the crystallization of polyamides in PAMP. It can be assumed that the formation of PA4, PA12 (with and without Fe), and the PA612 copolymer will follow a similar path. However, as previously mentioned, the polymerization yield of PA12 was relatively low. This can be attributed to the difficulty in controlling the rapid spontaneous growth of microparticles, leading to the formation of large agglomerates instead of microparticles. To prevent this, the polymerization was intentionally stopped earlier. The high yield achieved in the PA612 copolymer system is attributed to the controlled growth and stabilization of these microparticles. The PA6-rich segments, characterized by a higher crystallization rate, act as effective nucleating agents for the PA12 blocks, thereby accelerating their crystallization. This effect induces particle precipitation, which effectively terminates anionic chain propagation. Consequently, microparticle formation in the PA612 system proceeds efficiently under elevated reaction temperatures and high stirring rates, without excessive particle coalescence and the formation of macroscopic polyamide agglomerates.

3.3. Characterization of polyamide microparticles

3.3.1. Morphological studies by microscopy

3.3.1.1. Optical microscopy

The seven types of microparticles were analyzed by optical microscopy to determine their equivalent circle diameter and sphericity. The histograms related to the size distribution of equivalent diameters and roundness are presented in Figure 3.2. Table 3.2 summarizes the data about the distribution of particles' size (maximum diameter) and shape (roundness) for all microparticles.

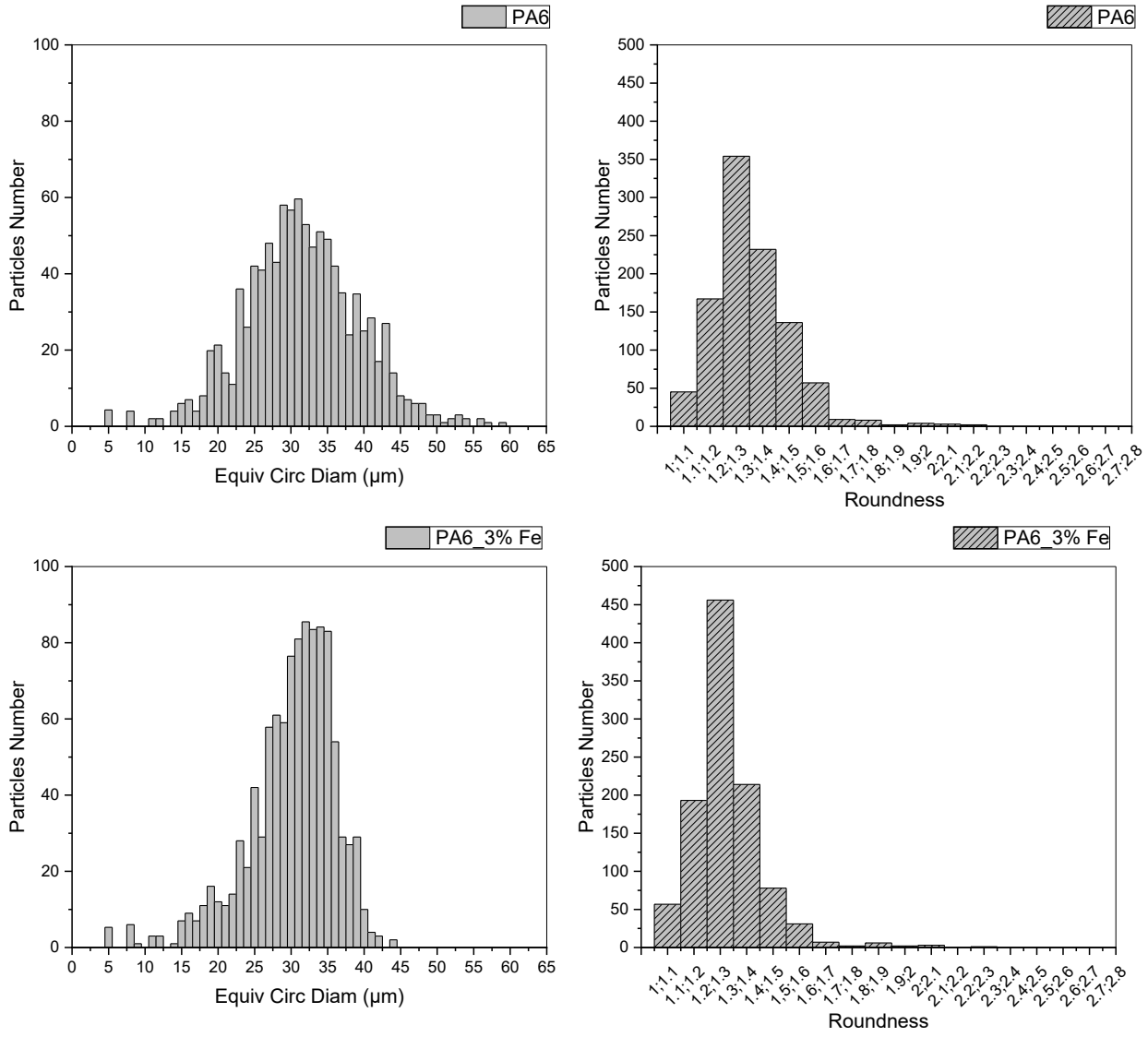


Figure 3.2: Typical results from bright field transmission microscopy representing the average size and shape distributions for PA microparticles without and with load.

Table 3.2: Average values of equivalent circular diameter and sphericity of the microparticles. (Adapted from [3–5]).

Sample	Equivalent diameter d_{max} (μm)	Average roundness d_{max}/d_{min}
PA4	10–12	1.2–1.3
PA4-Fe	10–12	1.2–1.3
PA6	30–35	1.2–1.4
PA6Fe	30–35	1.2–1.3
PA12	15–30	1.2–1.6
PA12-Fe	15–30	1.2–1.6
PA612	10–25	1.2–1.6

Analyzing the Figure 3.2 and Table 3.2 allows the conclusion that the PA4 and PA4-Fe are the smallest microparticles (d_{max}=10-12 μm), followed by the copolymer (10-25 μm). PA6 microparticles are the largest with a d_{max} of 30-35 μm. Pure and Fe-loaded PA12 have similar sizes in the range of 15–35 μm and exhibit very similar morphology.

The roundness of all samples is in the range from 1.2 to 1.6, indicating a predominantly near-spherical morphology. Neat PA4 and PA6 shows roundness varying in the 1.2-1.4 range, while PA12, PA12-Fe, and PA612 present slightly more irregular shapes (1.2–1.6), possibly due to differences in polymer crystallization behavior or viscosity during polymerization. It is also possible to state that the presence of Fe does not significantly affect particle shape or size distribution, suggesting that its incorporation occurs without disturbing droplet formation during the AAROP process.

3.3.1.2. SEM

The morphology of all synthesized PAMP samples was studied by scanning electron microscopy (SEM). This technique provides visual information on the size, shape, and surface topography of the microparticles. Figures 3.3–3.7 show the SEM images of the different PAMP.

SEM analysis showed that all microparticles have a porous structure. The PA4 and PA4-Fe MP (Figure 3.3) exhibited near-spherical morphology. The diameter of PA4 microparticles ranges from 10 to 40 μm. The presence of Fe leads to an increase in the average particle size and pore

dimensions, with PA4-Fe exhibiting a more open surface structure (Figure 3.3h) and the shape becoming less spherical.

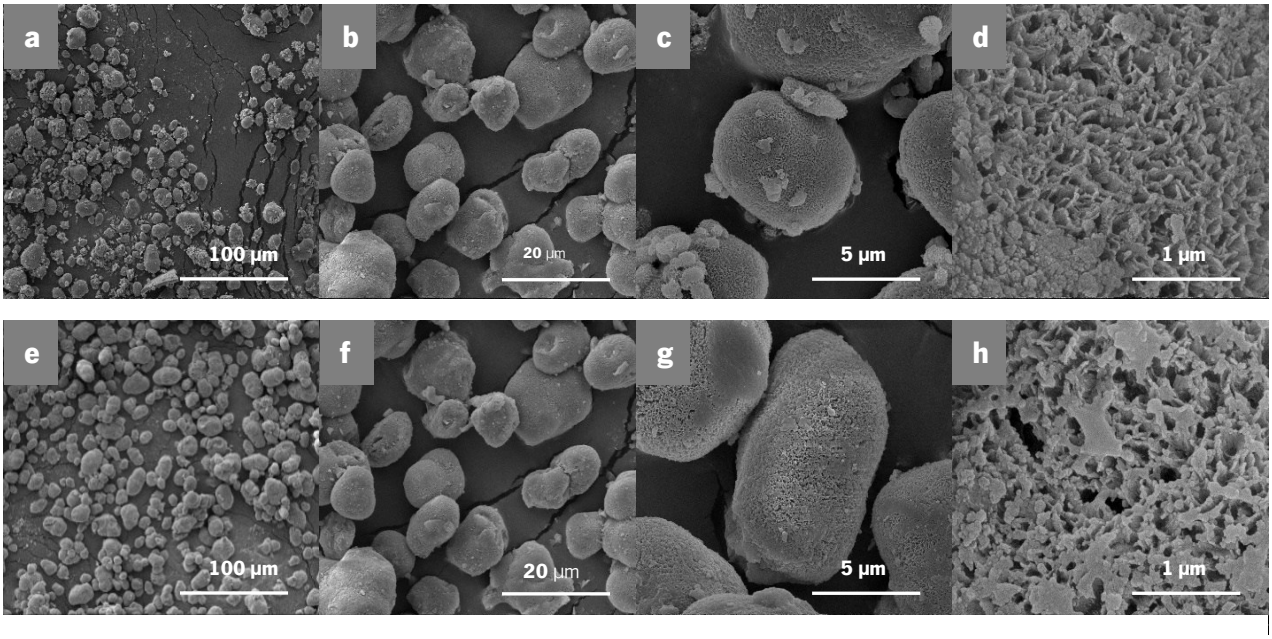


Figure 3.3: SEM micrographs of PA4 (a-d) and PA4-Fe (e-h) with different magnifications.

Energy-dispersive X-ray (EDX) analysis of the PA4 and PA4-Fe (Figure 3.4, Z3) shows that the iron is not located on the surface but rather embedded within the core of the microparticles, suggesting that Fe particles were entrapped during polymerization.

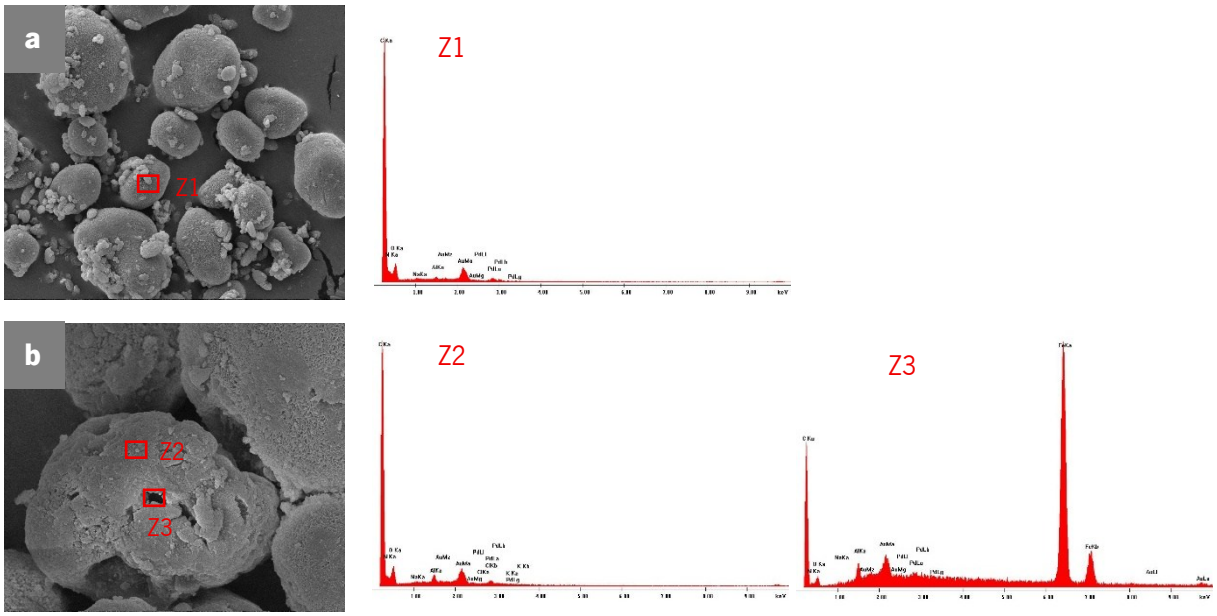


Figure 3.4: SEM images of PA4 (a) PA4-Fe (b) with EDX in the inset.

PA6 microparticles (Figure 3.5) exhibit highly porous aggregates composed of fused, irregularly shaped, nearly spherical morphologies. Their size can reach up to 150 µm, formed by the coalescence (fusion) of smaller spheres, resulting in a scaffold-like structure consisting of a 3D network of interwoven filaments ("balls of yarn") with large meshes of 300–500 µm. The magnetic PA6-Fe MPs (Figure 3.5e–h) exhibit similar morphology and porosity. Some iron-loaded MPs present elongated shapes similar to pea pods, where the Fe particles are axially aligned (Figure 3.5 f). This effect is probably due to Fe-particles magnetization caused by the magnetic stirring during the AAROP process and subsequent encapsulation by growing polyamide chains.

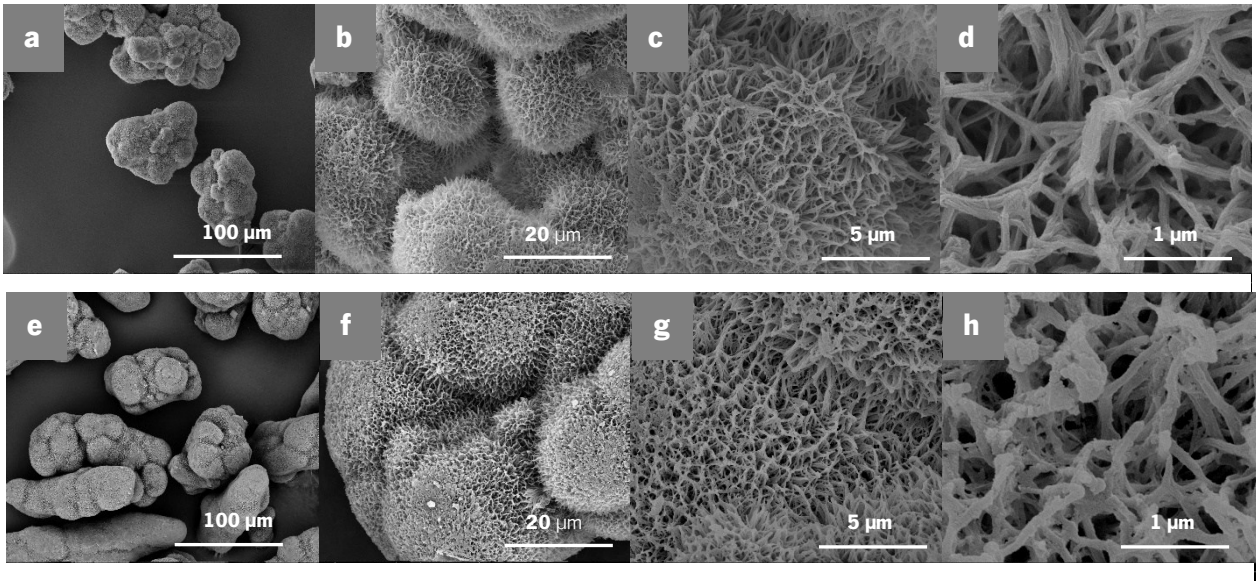


Figure 3.5: SEM images of PA6 (a-d) and PA-Fe (e-h) with different magnifications.

SEM micrographs of PA12 MPs (Figure 3.6) show irregular morphologies with both large compact aggregates (≈700 µm) and smaller particles (50–100 µm). Their surface topography exhibits a combination of solid and porous regions (similar to that of a sponge) deep channels instead of small pores. In PA12-Fe MPs (Figure 3.6e–f), the channels appear larger, while the overall particle size decreases significantly. The presence of Fe in the reaction mixture likely promotes heterogeneous nucleation of PA12, facilitating cold crystallization and resulting in better control over microparticle dimensions.

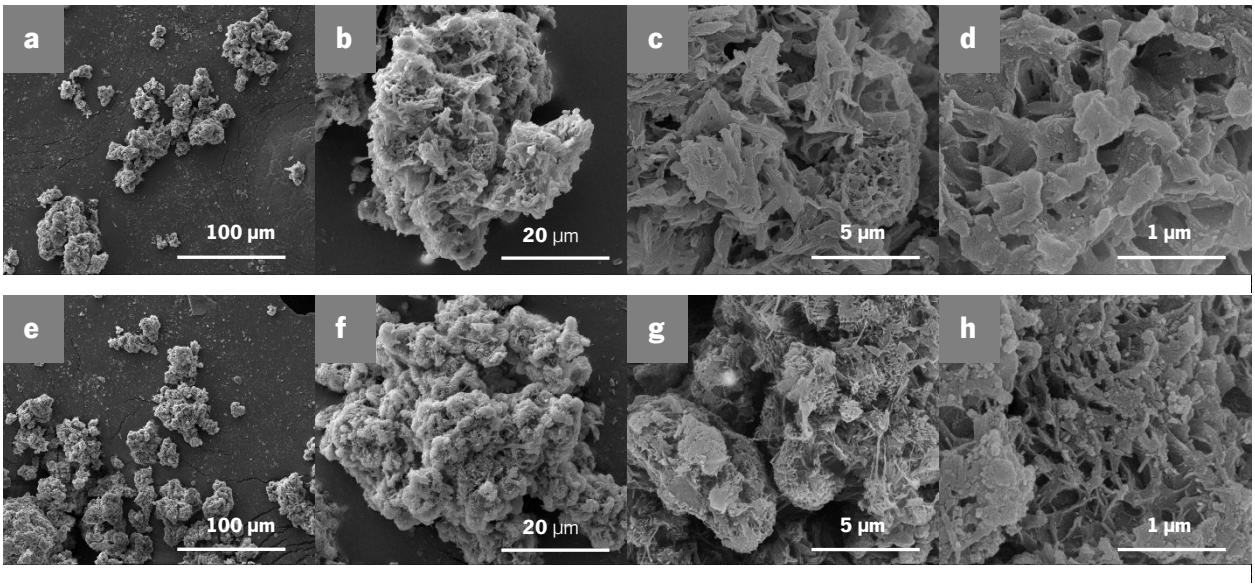


Figure 3.6: Selected SEM micrographs of PA12 (a-d) and PA12-Fe (e-h) with different magnifications.

The PA612 copolymer (Figure 3.7) consists of irregularly shaped microparticles up to 150 µm in size. Their surface topography resembles that of PA12, with a sponge-like texture composed of entangled polymer chains.

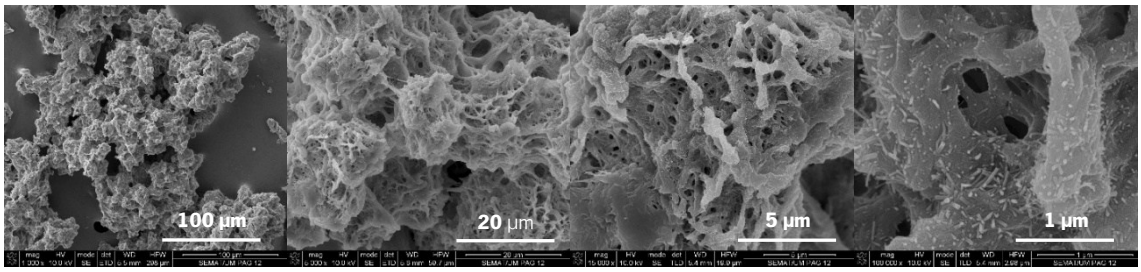


Figure 3.7: SEM images of PA612 with different magnifications.

It can be concluded at this stage that different lactam monomers, which require distinct conditions for AAROP, give rise to polyamide microparticles with diverse shapes, morphologies, and surface topologies. In other words, by appropriately selecting the lactam monomer and controlling the amount of Fe payload, it is possible to tailor the morphology of the resulting polyamide microparticles.

3.3.2. Thermal properties of microparticles

3.3.2.1. By DSC

All the samples were analyzed by differential scanning calorimetry (DSC) according to Section 2.13.2.1 of Chapter 2 to study their melting and crystallization behavior. The DSC thermograms are presented in Figure 3.8, which show the initial scan (a), followed by a cooling cycle (b) and a second heating scan (c). The main thermal parameters obtained are summarized in Table 3.3.

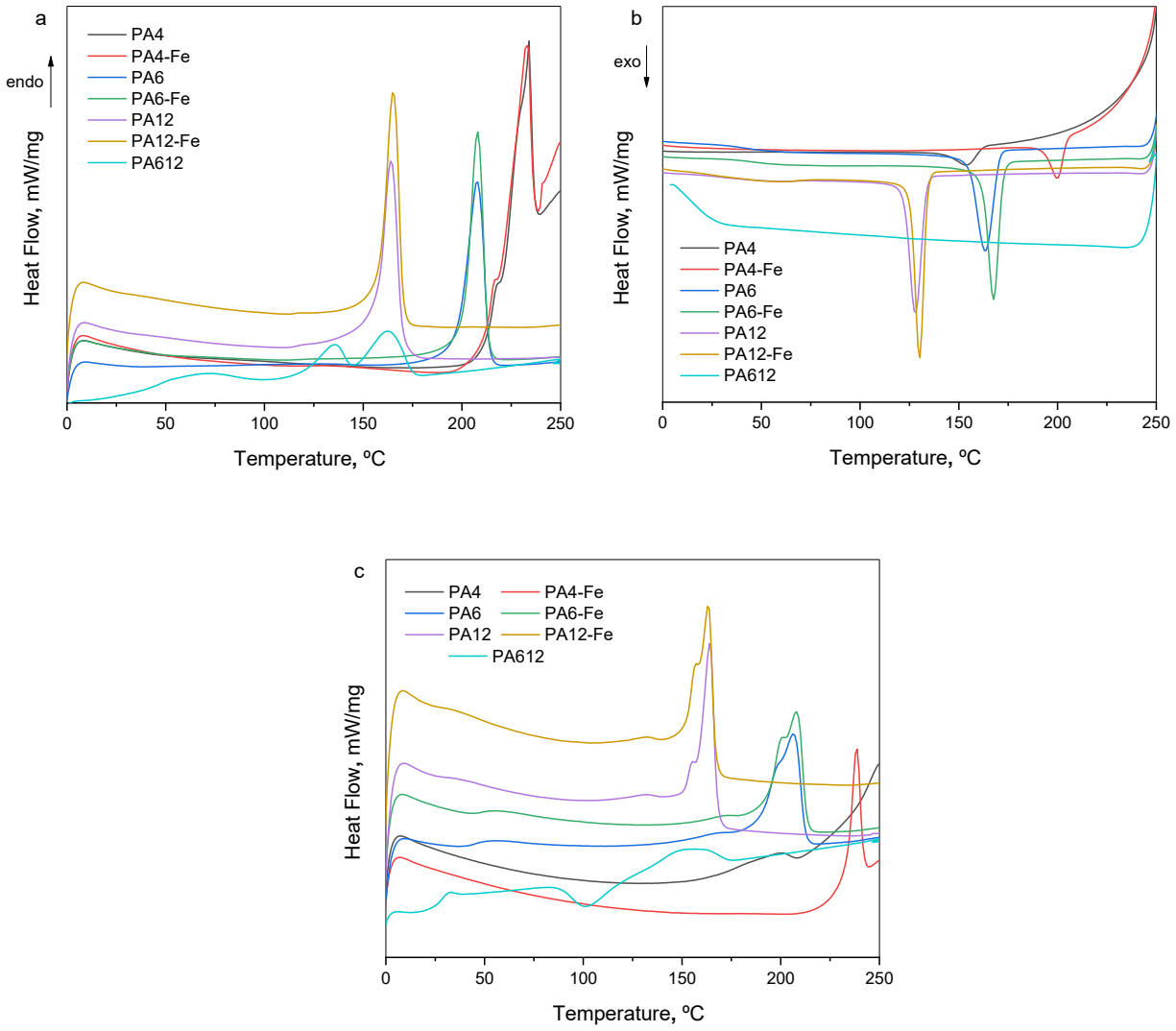


Figure 3.8: DCS traces of different polyamide samples: a) first heating scan; b) recrystallization from the melt; c) second heating scan.

Table 3.3: DSC data of seven types of polyamides.

Sample	First heating scan			Cooling scan [a]		Second heating scan			
	$T_m, °C$	$\Delta H, J/g$	$X_C, \%^{b)}$	$T_c, °C$	$-\Delta H, J/g$	$T_m, °C$	$\Delta H, J/g$	$X_C, \%^{b)}$	$T_g, °C^{d)}$
PA4	233.7	58.4	-	153.8	11.36	-	-	-	64.2
PA4-Fe	233.4	62.56	-	199.8	18.18	238.4	15.06	-	53.8
PA6	207.7	74.47	39.1	163.4	50.79	206.4	43.54	22.9	-
PA6-Fe	208.0	73.26	38.6	167.6	50.29	207.8	41.21	21.7	-
PA12	164.2	86.23	41.2	128.0	48.42	164.2	41.68	19.9	52.3
PA12-Fe	165.2	82.32	39.3	130.1	52.27	163.4	41.78	19.97	-
PA612	162.3 135.7	22.77 11.13	24.0 10.8	87.0 [c]	14.53 [c]	163.0	25.66	12.9	63.4

a) Determined after first DSC scan under fast cooling down;

b) Determined according to Eq. 19 of Chapter 2;

c) Crystallization peak obtained in the 1st heating scan;

d) Obtained in the 1st heating scan.

The first heating scan allows the investigation of the thermal properties and the degree of crystallinity of the microparticles in their as-synthesized state. All homopolymer microparticles, both neat and those containing an Fe payload, exhibit a single melting peak, located at approximately 233 °C for PA4, 207 °C for PA6, and around 164 °C for PA12. Notably, these melting temperatures are about 10–15 °C lower than those of the corresponding industrial polyamides produced by hydrolytic polymerization. It should also be emphasized that thermal degradation of PA4 begins immediately after melting, which is one of the main reasons why this polyamide has not yet found widespread industrial application, despite its chemically interesting structure, closely resembling that of polypeptides. In contrast, the PA612 copolymer microparticles exhibit two distinct melting peaks, as shown in Figure 3.8a: the first at approximately 135 °C and the second at around 160 °C. This thermal behavior suggests that, under the applied synthesis conditions, the PA612 microparticles are most likely composed of macromolecules with block copolymeric architecture, consisting of PA12- and PA6-rich segments rather than a statistically random copolymer structure. Regarding the microparticles with Fe, a slight increase (+1°C) can be observed in the case of PA6 and PA12; apparently, the melting behavior in this scan is not significantly affected by the presence of iron.

With respect to the recrystallization behavior of the PAMP (Figure 3.8b), the exothermic crystallization peaks exhibit markedly different shapes and intensities. The crystallization peak of

PA4 is small and broad, which is expected, considering that PA4 undergoes rapid thermal degradation immediately after melting. In contrast, the neat PA6 and PA12 samples display well-defined crystallization peaks at relatively high temperatures, around 163 °C and 128 °C, respectively. Notably, the PA612 copolymer microparticles exhibit a very weak and broad exothermic peak at a much lower temperature, i.e., 87 °C.

The incorporation of iron into PA4 and PA6 leads to noticeably narrower crystallization peaks, as shown in Figure 3.8b. As summarized in Table 3.3, the crystallization temperature (T_c) of the polymers ranges from 128 to 163 °C, while in the presence of iron, T_c increases by 2 to 46 °C, with the largest increase observed for PA4–Fe and the smallest for PA12–Fe. These results clearly indicate that iron acts as an efficient heteronucleating agent for the polyamide matrix, with the strongest nucleation-promoting effect observed in PA4–Fe.

Figure 3.8c presents the DSC traces obtained during the second heating scan, performed after melting and recrystallization of the PAMP samples. The thermal behavior observed in this scan differs markedly among the samples. PA4 does not exhibit a melting peak, whereas the PA612 copolymer displays both melting and crystallization events. This behavior suggests that a substantial fraction of the crystalline phase in the copolymer is formed during the second heating scan following melting. Most likely, this phenomenon is associated with transamidation reactions occurring during the first heating scan, which lead to the formation of a more statistically random copolymer architecture. This assumption is supported by the fact that the PA612 microparticles exhibit a very weak recrystallization exotherm during cooling (Figure 3.8b), while a distinct exothermic peak appears only upon reheating, at temperatures above the glass transition temperature (T_g), during the second heating ramp.

In contrast, PA6 and PA12 samples, both neat and Fe-containing, display broader melting endotherms with a pronounced low-temperature shoulder during the second heating scan. This behavior suggests the coexistence of the γ-polymorph of polyamide, characterized by a lower melting temperature, alongside the predominant α-polymorph. Importantly, the melting temperatures (Table 3.3) remain very similar to those obtained during the first heating scan, indicating that the thermal stability of the crystalline phases is not significantly affected by the heating ramp.

Another relevant comparison concerns the melting enthalpy (ΔH), which decreases during the second heating scan in almost all cases. This decrease indicates a reduction in the degree of crystallinity after the first thermal cycle, which may be attributed to incomplete recrystallization or

less efficient chain rearrangement following rapid cooling. In other words, the thermal treatment partially modifies the crystalline morphology of the microparticles. As noted previously, the first heating scan reflects the "nascent" crystalline structure of the microparticles. As discussed in Chapter 2, AAROP is carried out at temperatures well below the melting temperature (T_m) and well above the T_g of the polyamides, effectively under annealing-like conditions. These conditions promote enhanced chain mobility and a more perfect organization of the macromolecules, resulting in higher melting enthalpies and, consequently, higher degrees of crystallinity observed during the first heating ramp.

The degree of crystallinity (X_c) of PA6, PA12, and the PA612 copolymer was calculated according to Equation 19 in Chapter 2, using extrapolated melting enthalpies ΔH_m^0 of 190 J·g^{-1} for 100% crystalline PA6 [6] and 209.2 J·g^{-1} for 100% crystalline PA12 [7]. For the PA612 copolymer, equal volume fractions (V_f = 0.5) of the two polyamides were assumed. In the case of PA4, both with and without iron, crystallinity indices could not be determined because the melting endotherms are superimposed on intense degradation peaks. As shown in Table 3.3, the presence of iron does not significantly affect the crystallinity index of the polymers. PA12 exhibits a slightly higher crystallinity (≈41%) than PA6 (≈39%), while the PA612 copolymer shows the lowest X_c ($\approx 10 - 24\%$). This reduced crystallinity is consistent with its copolymeric nature, as reduced chain symmetry hinders the formation of well-ordered crystalline domains.

The T_g of the samples ranges from 52 to 65 °C. The highest T_g values are observed for PA4 and the PA612 copolymer (≈63–64 °C), indicating a more rigid molecular structure. In contrast, PA12 exhibits the lowest T_g, which is expected due to the greater flexibility of its macromolecular chains, resulting from the lower concentration of amide groups per repeat unit.

In summary, the DSC results demonstrate that all synthesized PAMP possess a semicrystalline structure. The incorporation of Fe payloads does not significantly affect the thermal or crystalline properties of the polymers, which is advantageous for the potential application of these microparticles in subsequent functional studies.

3.3.2.2. By TGA

Samples of synthesized polyamide were analyzed by TGA in order to establish the thermal stability and to determine the actual iron content. The thermogravimetric curves are presented in both integral and differential forms in Figure 3.9, and the corresponding numerical values are

summarized in Table 3.4. The determination of the real load content based on the carbonized residue at 600 °C, calculated according to Eq. 2.20 (Chapter 2), is also included in Table 3.4.

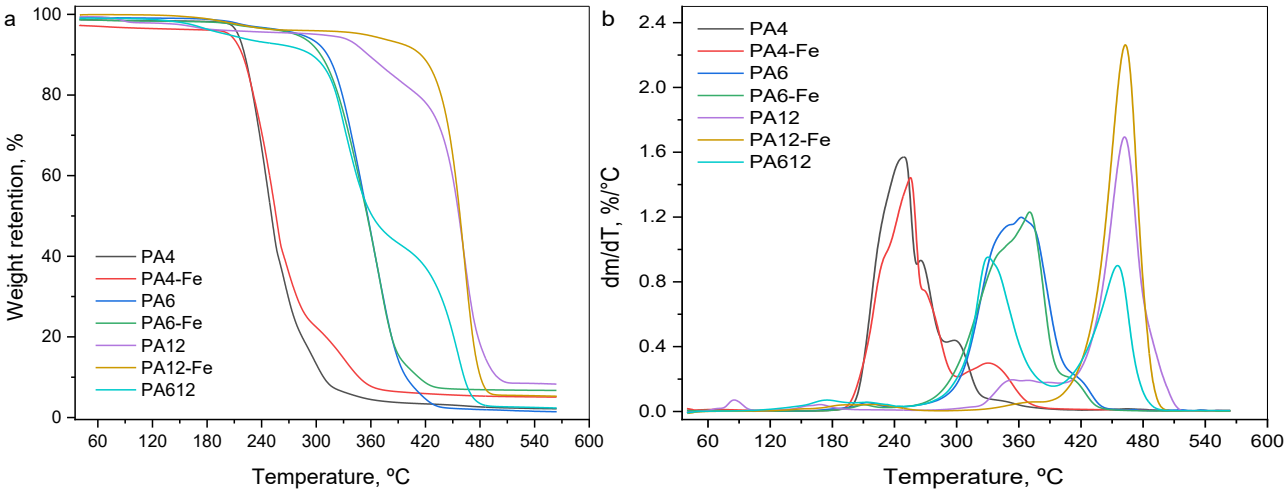


Figure 3.9: TGA traces of MP: a) Integral weight loss curves; b) First derivative curves.

Table 3.4: TGA analysis of polyamide microparticles.

Sample	Theoretical load wt. %	$T_{in}^{a)}$	$T_{max,}°C^{b)}$			$V_{max},\%°C^{c)}$			Residue at 600 °C, %	Real load, wt.%
			I	II	III	I	II	III		
PA4	-	220.9	247.7	268.4	302.8	1.6	0.9	0.4	2.2	-
PA4-Fe	1.0	223.5	255.8	265.8	334.3	1.4	0.8	0.3	5.1	2.9
PA6	-	314.8	335.4	-	-	2.8	-	-	1.5	-
PA6-Fe	3.0	319.0	370.3	-	-	1.2	-	-	6.7	5.2
PA12	-	442.3	462.0	-	-	2.3	-	-	1.7	-
PA12-Fe	2.0	440.2	462.8	-	-	2.1	-	-	7.4	6.0
PA612	-	312.3	332.3	455.5	-	0.9	0.9	-	2.4	-

a) T_{in} = Temperature of iniial degradation obtained from integral TGA curves;

b) T_{max} = Maximum degradation temperature obtained from the 1st derivative of the TGA curves;

c) Maximum degradation rate at T_{max} obtained from the first derivative of the TGA curves.

PA6 and PA12 PAMP exhibit a single major degradation event between 335 and 462 °C. For PA612 two main degradation events are observed at 332 °C and 455 °C which confirms the assumption made above that PA612 MP, as synthesized, is a block copolymer. Three main degradation events take place in the PA4 with and without Fe (i) at 247-255 °C; (ii) between 268 and 265 °C and (iii) 302-334 °C. Therefore, PA4 PAMP exhibit multi-step thermal degradation due to several competitive reactions typical of short polyamides, due to overlapping processes including

dehydration, depolymerization and chain scission, while long-chain polyamides (e.g., PA12) typically show a single major degradation step [8,9].

In general, the maximum degradation rate V_{max} (i.e., the peak of the first derivative curves in Figure 3.9 b) of microparticles containing Fe is lower than in the corresponding neat PA microparticles meaning a more gradual and less aggressive thermal degradation. As seen from Table 3.4, the initial degradation temperature (T_{in}) of the iron-containing microparticles is higher than the corresponding pure MPs. This increase indicates that iron acts as a stabilizing agent, slowing down the initial decomposition of the polymer chain.

As also mentioned in Table 3.4, the real payload content (RL) in all hybrid microparticles is higher than the theoretical value. This can be explained by two factors: (i) all Fe payload added during AAROP synthesis becomes trapped in the forming polymer matrix, and (ii) The Fe amounts are calculated based on the starting monomer. Since there is no 100% conversion of the monomer, this leads to an increased inorganic fraction in the carbonized polymer residue.

3.3.2.3. FTIR studies

Fourier transform infrared (FTIR) spectroscopy was used to study the chemical structure of the neat and hybrid polyamides. The full spectra of PA4, PA6 and PA12 with and without Fe are shown in Figure 3.10. The table below (Table 3.5) summarizes the results obtained, indicating what each band corresponds to.

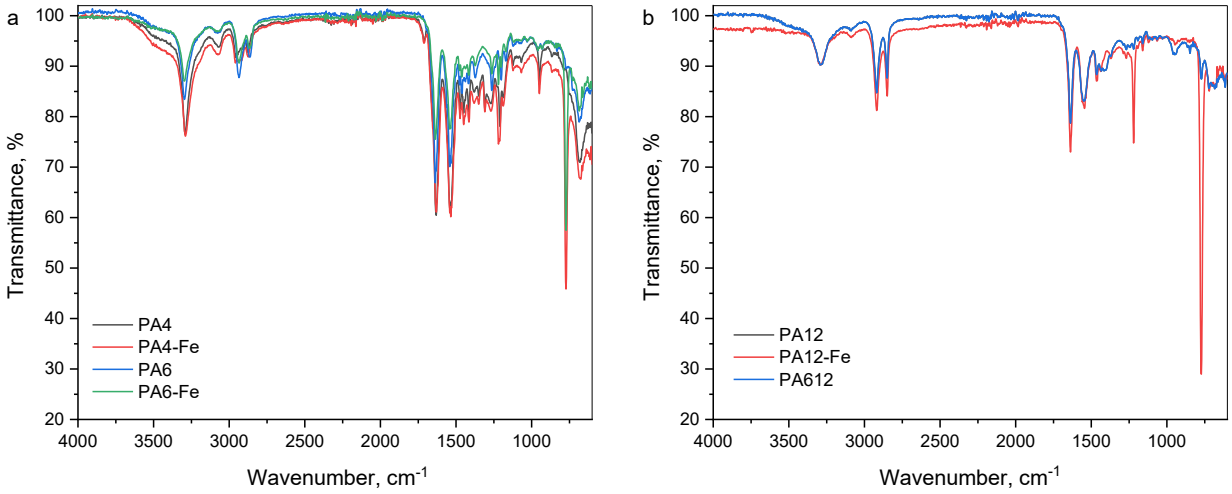


Figure 3.10: FTIR spectra of polyamide samples: a) PA4, PA4-Fe, PA6 and PA6-Fe; b) PA12, PA12-Fe and PA612.

Table 3.5: FTIR analysis of all polyamide microparticles samples.

Sample	N–H stretch (cm^{-1})	CH_2 asym. (cm^{-1})	CH_2 sym. (cm^{-1})	Amide I (C=O) (cm^{-1})	Amide II (cm^{-1})	Amide III (cm^{-1})	CH_2 rocking/wag (cm^{-1})
PA4	3289–3291	2958	—	1630–1631	1534–1535	1309	679
PA4-Fe	3291–3295	2934–2958	—	1636–1637	1541–1535	1263–1309	679–685
PA6	3295–3296	2933–2934	—	1636	1541	1219	685
PA6-Fe	3292–3295	2918–2934	2849	1637	1545–1549	1219	684–685
PA12	3288–3297	2918–2923	2849–2853	1636–1637	1541–1545	1219	682–685
PA12-Fe	3288–3297	2918–2923	2849–2853	1636–1637	1541–1545	1219	682–685
PA612	3267	—	—	1634	1539	1219	1057

All samples exhibit the characteristic vibrational bands of aliphatic polyamides, confirming that the incorporation of iron does not change the chemical backbone of the materials. Bands at 3288–3297 cm^{-1} corresponds to N–H stretching vibrations involved in hydrogen bonding, typical of secondary amide groups. The bands at 2918–2923 cm^{-1} (asymmetric CH_2 stretching) and 2849–2853 cm^{-1} (symmetric CH_2 stretching) reflect the increasing number of methylene units from PA4 to PA12. The characteristic bands of Amide I (C=O stretching) and Amide II (N–H bending and C–N stretching) are observed respectively at 1630–1637 cm^{-1} and 1535–1549 cm^{-1}. Amide III appears at 1263–1300 cm^{-1}, corresponding to C–N stretching and N–H bending. In the fingerprint area, it is possible to observe a band around 685–690 cm^{-1} that corresponds to CH_2 rocking/wagging mode, this band is almost unnoticeable in PA4 and is more intense in PA12 due to its long aliphatic sequence.

The main difference between samples with and without Fe is a slightly increased width of the Amide bands in the Fe-containing microparticles, indicating higher structural heterogeneity. No new absorption bands appear, confirming no strong coordination or chemical interaction between Fe and the polyamide functional groups.

3.4. Conclusions

Polyamide microparticles, both with and without incorporated Fe, were successfully synthesized via AAROP, with yields ranging from 42 to 77%. Structural (FTIR), morphological (optical microscopy and SEM), and thermal (DSC and TGA) characterization of the obtained microparticles demonstrated that the incorporation of iron does not significantly alter the intrinsic properties of the resulting polyamide powders. The minor differences observed namely, slightly narrower crystallization peaks in DSC and marginally higher degradation onset temperatures in TGA, suggest that Fe may act as a heteronucleating agent, providing a modest stabilizing effect against thermal degradation. Overall, these results confirm that the Fe-containing microparticles retain the essential characteristics of the corresponding pure pulverulent polyamides. Notably, Fe contents of 3–5 wt.% renders the polyamide microparticles responsive to static magnetic fields.

In general, the use of different lactam monomers, with or without the incorporation of magnetizable Fe payloads, leads to microparticles with varied shapes, morphologies, and surface topologies, which will be exploited in the subsequent stages of this study.

3.5. References

[1] Oliveira, S. C.; Araújo, S. M.; Dencheva, N. V.; Denchev, Z. Z. Polyamide microparticles with immobilized enological pectinase as efficient biocatalysts for wine clarification: The role of the polymer support. *Molecules* **2025**, *30*, 114. https://doi.org/10.3390/molecules30010114.

[2] Vasiliu-Oprea, C.; Dan, F. On the relation between synthesis parameters and morphology of anionic polycaproamide obtained in organic media. I. Influence of the $Na[O(CH_2)_2OCH_3]_2AlH_2$/isophorone diisocyanate catalytic system. *J. Appl. Polym. Sci.* **1996**, 62, 1517–1527. https://doi.org/10.1002/(SICI)1097-4628(19961205)62:10<1517::AID-APP4>3.0.CO;2-R.

[3] Dencheva, N.; Braz, J.; Nunes, T. G.; Oliveira, F. D.; Denchev, Z. One-pot low temperature synthesis and characterization of hybrid poly(2-pyrrolidone) microparticles suitable for protein immobilization. *Polymer* **2018**, *145*, 402–415. https://doi.org/10.1016/j.polymer.2018.04.080.

[4] Brêda, C.; Dencheva, N.; Lanceros-Méndez, S.; Denchev, Z. Preparation and properties of metal-containing polyamide hybrid composites via reactive microencapsulation. *J. Mater. Sci.* **2016**, *51*, 10534–10554. https://doi.org/10.1007/s10853-016-0274-0.

[5] Dencheva, N. V.; Braz, J. F. B.; Denchev, Z. Z. Synthesis and properties of neat, hybrid, and copolymeric polyamide 12 microparticles and composites on their basis. *J. Appl. Polym. Sci.* **2022**, *139*, 51784. https://doi.org/10.1002/app.51784.

[6] Dencheva, N. V.; Manso Vale, D.; Denchev, Z. Z. Dually reinforced all-polyamide laminate composites via microencapsulation strategy. *Polym. Eng. Sci.* **2017**, *57*, 806–820. https://doi.org/10.1002/pen.24456.

[7] Gogolewski, S.; Czerntawska, K.; Gastorek, M. Effect of annealing on thermal properties and crystalline structure of polyamides. Nylon 12 (polylaurolactam). *Colloid Polym. Sci.* **1980**, *258*, 1130–1136. https://doi.org/10.1007/BF01382456.

[8] Pagacz, J.; Leszczyńska, A.; Modesti, M.; Boaretti, C.; Roso, M.; Malka, I.; et al. Thermal decomposition studies of bio-resourced polyamides by thermogravimetry and evolved gas analysis. *Thermochim. Acta* **2015**, *612*, 40–48. https://doi.org/10.1016/j.tca.2015.05.003.

[9] Herrera, M.; Matuschek, G.; Kettrup, A. Main products and kinetics of the thermal degradation of polyamides. *Chemosphere* **2001**, *42*, 601–607. https://doi.org/10.1016/S0045-6535(00)00233-2.

CHAPTER 4

PA6-assisted biocatalyst for wine industry: Design, optimization and application in rosé must clarification

The characterization of the polyamide microsized powders presented in Chapter 3 showed that PA6-based materials exhibit the most favorable porosity and the largest internal surface area among the systems studied. Consequently, they provide the highest surface concentration of accessible amide groups, which are well suited for hydrogen-bond interactions with proteins. These characteristics make PA6 microparticles particularly attractive carriers for enzyme immobilization.

Therefore, this chapter focuses on the immobilization of pectinase onto PA6-based microparticles with the aim of developing an efficient biocatalyst for wine clarification. The study is carried out using a real industrial wine sample supplied by Sogrape Vinhos Lda., together with a commercial pectinase formulation Viazym® Clarif Extrem provided by the same company. The preparation, characterization, and application of the resulting biocatalytic systems are presented herein. Parts of this work have already been reported [1].

4.1. Introduction

Wine is produced through the biochemical transformation of grape juice, known as controlled alcoholic fermentation. Its production consists of four main stages [2,3]: (i) pressing and maceration, with the purpose of extracting as much grape juice as possible for must formation; (ii) alcoholic fermentation, during which the alcohol content and many other specific features of wine are formed; (iii) clarification, i.e., the reduction of turbidity to achieve a clear, visually appealing and stable wine; and (iv) aging and stabilization operations aimed at optimizing the physicochemical properties of the final product. Enzymes are necessary in various stages of wine production, and most of them originate from the grapes themselves. However, due to the continuous increase in wine production, these endogenous enzymes are often not efficient enough, nor present in sufficient quantities, to effectively catalyze the corresponding reactions. Therefore, the use of commercial enzymes during different stages of the winemaking process is a well-established practice in large-scale wine production.

Pectinases (E.C.3.2.1.15) are a heterogeneous group of enzymes used for the controlled degradation of high-molecular-weight pectic substances contained in grape cell walls, which are transferred into the must. These enzymes are essential during the clarification stage, as they are not produced by the yeasts commonly used in fermentation; consequently, they are added to the must as exogenous pectinases [3]. The main purpose of clarification is to reduce must viscosity and its insoluble fraction content, as well as to intensify the grape juice extraction and maximize yield. There is evidence that pectinases can also increase the production and retention of certain

volatile substances, thus releasing in wine more of the color- and flavor-determining compounds contained in grape skin [4], and making more effective the liberation of phenolic compounds [5].

Industrial enological pectinases are most frequently applied as free enzymes, i.e., soluble in the reaction medium. However, in this form they often fail to provide the necessary short-term operational stability and are very difficult to recover and reuse [6]. Moreover, free enzymes could be difficult to employ in continuous processes [7]. To overcome these limitations, immobilization of enzymatic catalysts can be employed. The exhaustive review by Ottone et al. [3], along with other studies [8], reports numerous examples of immobilized enzymes used at different stages of wine production. In general, immobilization of enzymes can be made on different supports (carriers), such as polymers. The immobilization leads to improved enzyme stability, the production of a final product free of biocatalysts, and, finally, the possibility of multiple uses of the same enzymatic preparation.

Based on these considerations, it was decided to immobilize enological pectinase on polyamide 6 (PA6). The main objective of this study was to perform the non-covalent immobilization of an enological pectinase (Viazym® Clarif Extrem, PeV) onto PA6 microparticles, with or without magnetic properties, obtained via AAROP. Different immobilization conditions were tested for this purpose. After immobilization, the resulting complexes were subjected to comparative activity and kinetic studies with the free enzyme and were also applied in the clarification of industrial rosé must. Their reuse was also investigated.

4.2. Quantification of the enzymes in the MP-supported complexes

The amount of non-covalently immobilized pectinolytic enzyme on the PA6-based MP supports was determined according to Equation 1 in Chapter 2, Section 2.5. UV/VIS spectroscopy was used to extract the necessary information.

Figure 4.1a compares the UV/VIS spectra of the initial Viazym stock solution (curve 1, with the highest-intensity peak) and of the remaining supernatants after removal of the MP–enzyme complexes PeV@PA6 and PeV@PA6-Fe (curves 2 and 3). The absorption band centered at $\lambda = 263$ nm is attributed to the protein moieties containing a substituted benzene ring found in the pectinases' apoenzymes, originating from tryptophan, phenylalanine or tyrosine repeat units. This direct spectroscopic method produces reliable data about the adsorption-immobilized protein with a standard deviation of 3–5%, while the indirect Bradford and bicinchoninic acid colorimetric assays for protein content result in data dispersions of up to 15%.

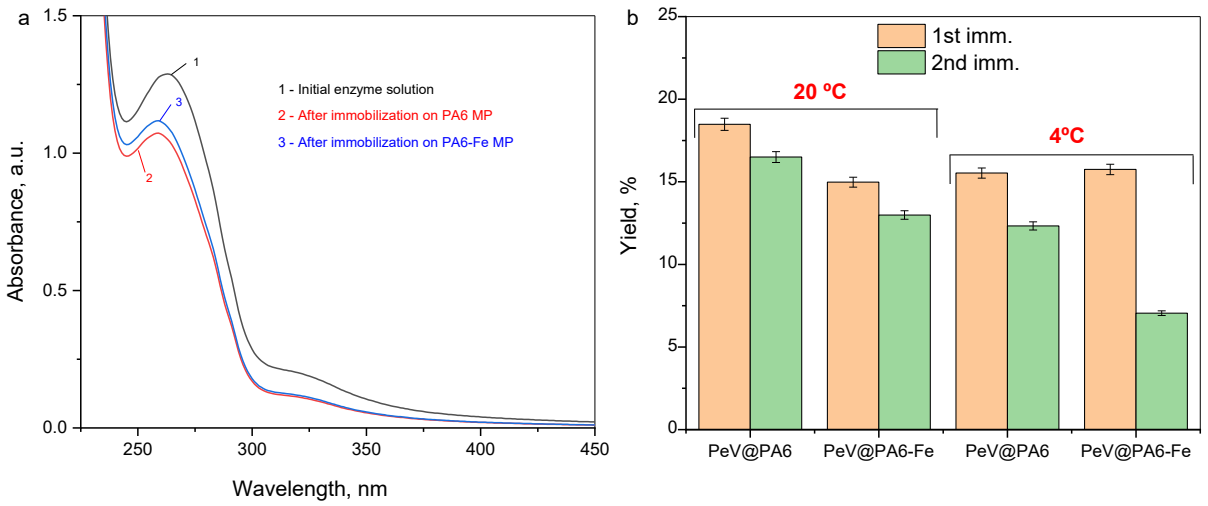


Figure 4.1: Quantification of the pectinase immobilization: (a) UV/VIS spectra of the Viazym solutions before and after the first round of adsorption immobilization; (b) immobilization efficiency for three consecutive trials immobilization rounds at two different temperatures for PeV@PA6 and PeV@PA6-Fe pectinolytic complexes.

Figure 4.1b shows the immobilization yield for the PeV@PA6 and PeV@PA6-Fe complexes, which yield is the amount of enzyme immobilized on the MP supports as a percentage of the initial enzyme concentration. To obtain the standard deviation values for each sample, three consecutive trials were made at every point. As the immobilization efficiency was relatively low (≈15–20%), it was decided to investigate whether it is possible to use the same pectinase solution repeatedly, for a new immobilization. As seen in Figure 4.1b, the enzyme solution can indeed be reused, with efficiencies in the range of 15% for each consecutive immobilization cycle. The same figure also shows that immobilization is temperature dependent. At room temperature, the immobilization process was about 5% more efficient, whereby this temperature dependence was much more pronounced in the second and each subsequent immobilization cycle.

In summary, optimal conditions were identified using the enzyme diluted 10 times, at room temperature (20–21 °C) for 24 h under agitation.

4.3. Morphological studies by SEM

The morphology and composition of PA6 and PA6-Fe MP, both neat and after pectinase immobilization, were analyzed using scanning electron microscopy (SEM) combined with energy-dispersive X-ray spectroscopy (EDX).

As observed in Figure 4.2a–c, the empty PA6 microparticles represent highly porous, scaffold-like aggregates with sizes between 100 and 200 μm. Each aggregate consists of many fused, nearly spherical particles with diameters of approximately 20 μm. At higher magnification (Figure 4.2c), the micropores appear open, with irregular form and different visible depths, most of them with sizes varying in the range between 200 and 800 nm. EDX analysis of site Z1 (Figure 4.3a) displayed only the presence of C, N and O atoms, the content of N being close to 9 wt.%.

After pectinase immobilization on the PA6 MPs (Figure 4.2d–f), the shape and size of the aggregates were generally preserved as observed at lower and medium magnifications (left column in Figure 4.2). The higher magnifications images show a marked reduction in visible microporosity, indicating that the pores were filled by the enzyme during adsorption. EDX mapping at sites Z1–Z3 (Figure 4.3b) displayed nitrogen percentages between 17 and 24 wt.%, which was accompanied by the appearance of signals characteristic of potassium and chlorine (Figure 4.3b). This is a direct proof of the adsorption deposition of the pectinases' apoenzymes in the said locations, along with ions of the respective buffer solutions.

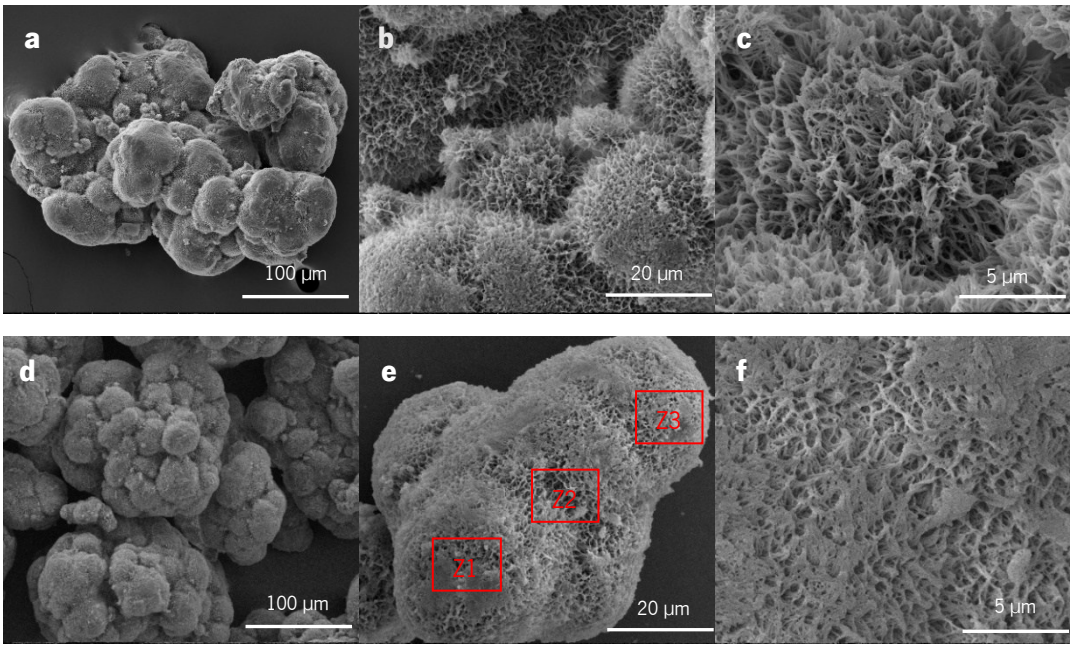


Figure 4.2: Selected SEM micrographs of empty PA6 MPs (images a–c) and PeV@PA6 complexes (images d–f).

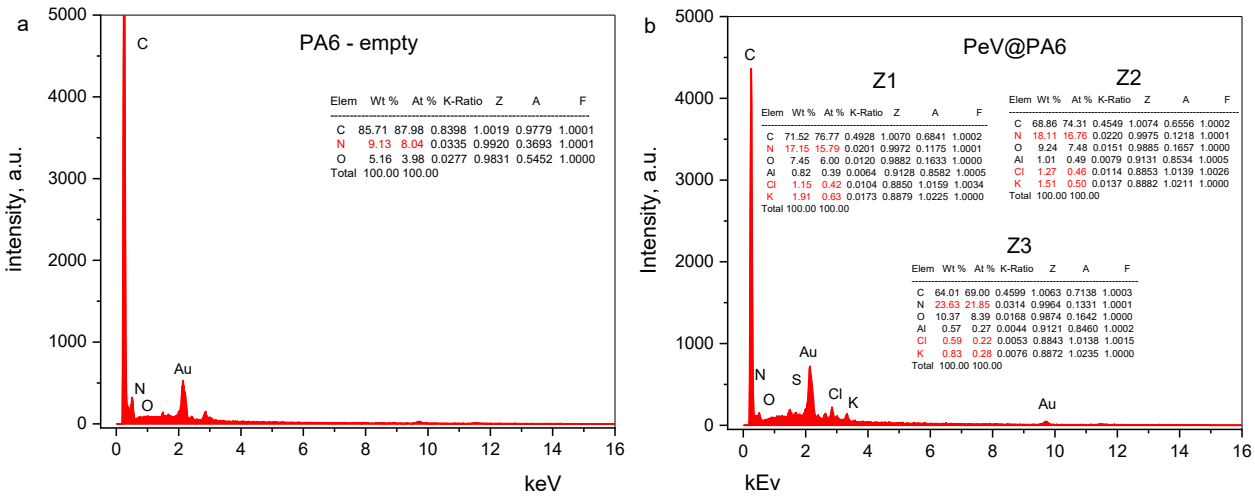


Figure 4.3: EDX results (a) empty PA6 MPs (b) PeV@PA6 complexes.

The magnetic sensitive PA6-Fe support MPs (Figure 4.4a–c) display very similar shapes and porosity of the PA6 MPs. Some particles have the form of elongated seed capsules containing several axially aligned Fe particles coated with PA6 during AAROP—likely due to magnetic alignment. EDX analysis at Z1 (Figure 4.4g) shows spectra identical to neat PA6. However, site Z2 (a crack between fused spheres) exhibits a weak but detectable K_α signal of Fe (Figure 4.4g), confirming the presence of iron within the support.

Following enzyme immobilization being the same as for PA6 (Figure 4.4d–f), the shape and size of the microparticles remain preserved. The high-magnification images reveal a reduction in surface porosity, suggesting pore filling by the enzyme. The EDX of the neat PA6-Fe MPs in site Z1 (Figure 4.4h) displayed the same emission spectra as the PA6 MPs. Mapping the chemical composition in the crack between the two fused PA6 spheres (site Z2 in Figure 4.3b) presented a weak but observable K_α line of Fe (Figure 4.4c). After pectinase immobilization, the EDX emission in sites Z1–Z3 (Figure 4.4h-j) displayed increased amounts of nitrogen in Z2 and Z3 (see Figure 4.4i–j) and the presence of K and Cl ions in all of these sites. Based on these observations, successful deposition of the pectinase can also be considered proved in the PeV@PA6-Fe complex.

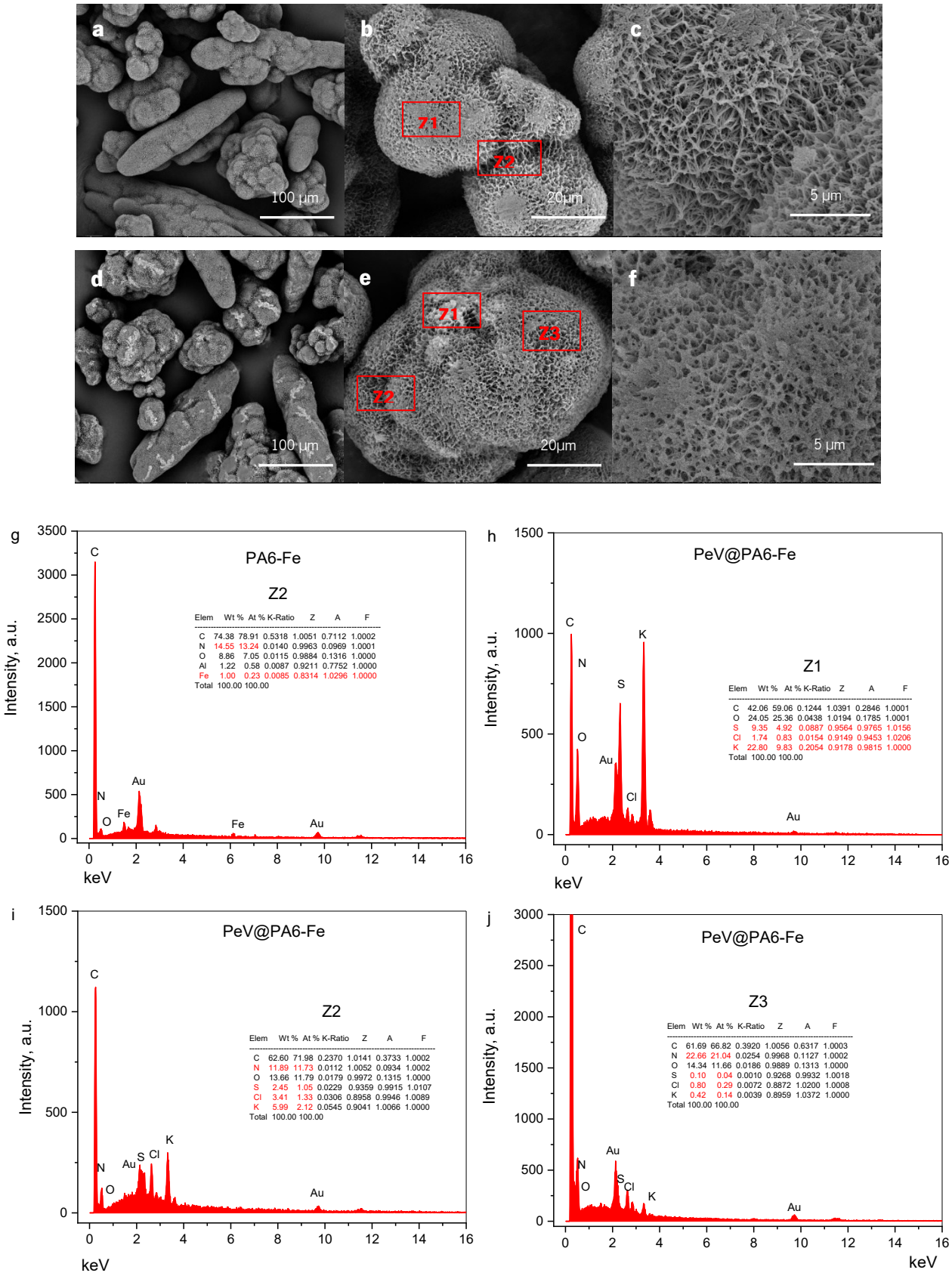


Figure 4.4: SEM micrographs of (a–c) empty PA6-Fe MPs (d–f) PeV@PA6-Fe complexes and EDX results g) empty PA6-Fe MPs (h-j) PeV@PA6-Fe complexes.

It should be noted that the non-covalent immobilization of enzymes on polyamide PAMP is accompanied by additional effects beyond the changes observed in the EDX spectra. Synchrotron WAXS and SAXS measurements of laccase@PAMP complexes have indicated that the apoenzyme protein matrix undergoes densification as a result of effective hydrogen-bond formation with the PAMP support, accompanied partial filling of its pores and channels. These phenomena are evidenced by a shift in the angular position of the diffuse WAXS peak associated with the enzyme upon immobilization, as well as by a pronounced increase in phase contrast in SAXS. The latter manifests as an abrupt increase in the intensity of the polyamide matrix periodicity peak [9-11].

4.4. Activity via the DNS method

It is well established that, under heating conditions close to 100 °C, reducing sugars; e.g., galacturonic acid (G.A.), which contains a free aldehyde group, provides a hydrogen atom to the 3,5-dinitrosalicylic acid (DNS), the DNS is reduced to 3-amino-5-nitrosalicylic acid (ANS), while the reducing end of the sugar is oxidized. This redox transformation produces a visible color change from yellow to dark orange. This chemical interaction and the color change on which the estimation of the pectinase activity is based, are presented in Figure 4.5.

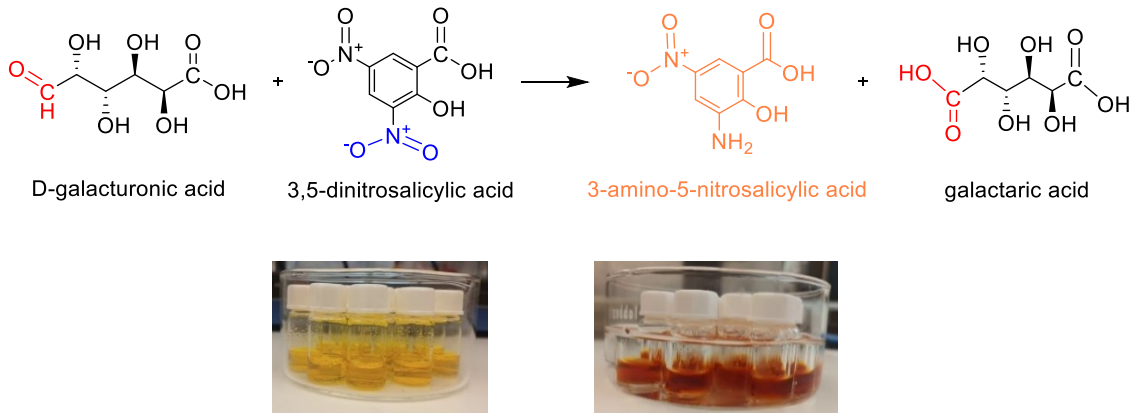


Figure 4.5: Interaction between DNS reagent and D-galacturonic acid.

In our case, both free and immobilized pectinolytic preparations depolymerize pectic polysaccharides, namely homogalacturonan, xylogalacturonan, as well as rhamnogalacturonans I and II, thus generating reducing sugar ends that participate in the DNS reaction [12].

The amount of G.A. is strictly proportional to the ANS concentration. The latter can be quantified via UV/VIS spectroscopy by the intensity of the band at λ = 540 nm. Therefore, the activity of the pectinolytic free or immobilized preparation is characterized by the concentration of ANS released per unit time. Figure 4.6a displays the evolution of the absorption at 540 nm after incubation of pectin solutions with free or immobilized Viazym preparations and subsequent treatment via the DNS method. The inset to Figure 4.6b represents the standard calibration curve constructed with various concentrations of G.A. Figure 4.6c shows the absorption spectrum of the reaction of DNS with G.A. In this figure it is possible to observe that the maximum of the experimental peak may appear near 512–515 nm at low concentrations, the characteristic absorption of ANS is resolved at 540 nm at higher concentrations. Therefore, this latter wavelength was used for quantification.

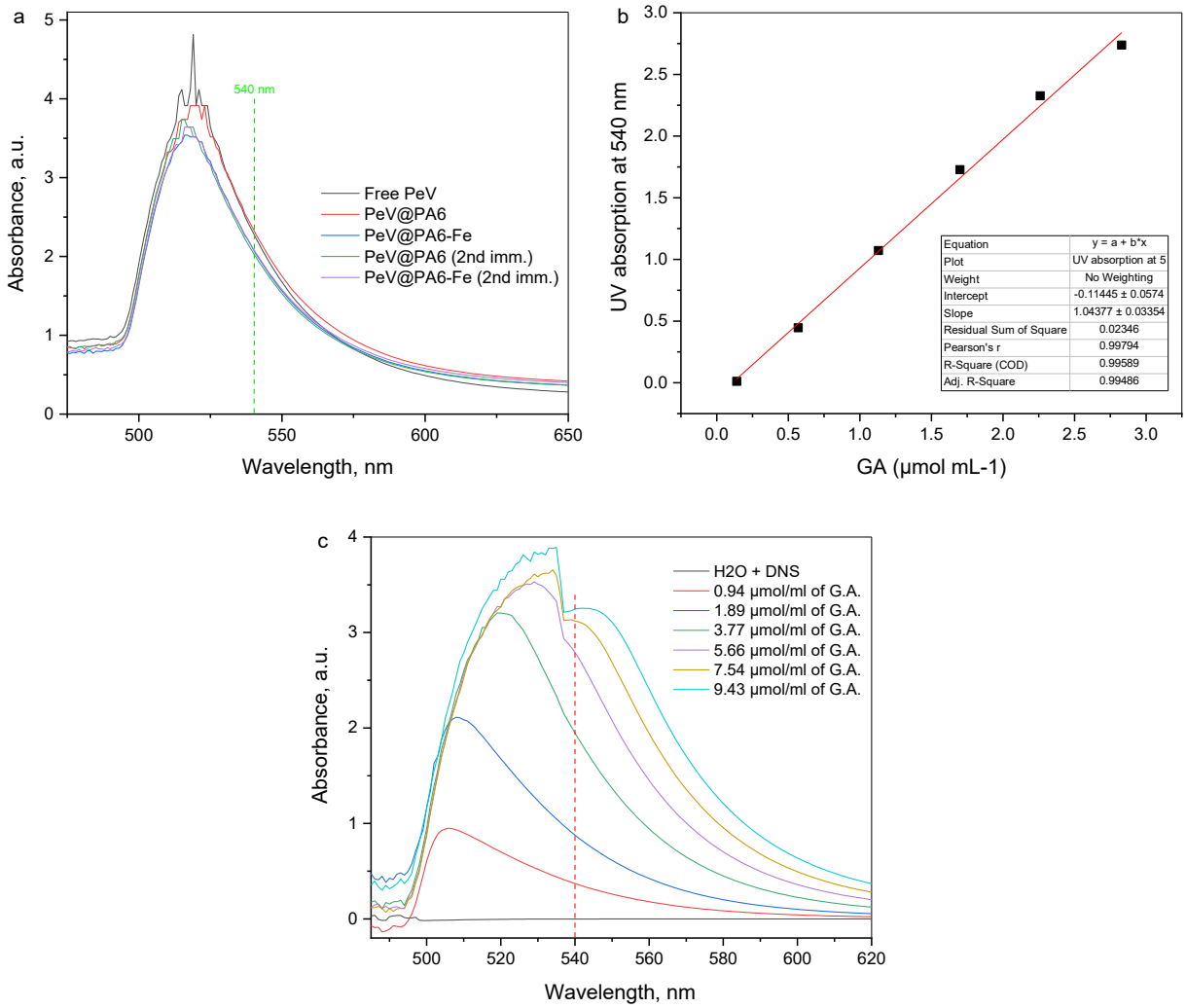


Figure 4.6: Activity assay of pectinolytic biocatalysts by the DNS method. (b) Standard calibration curve constructed with various concentrations of G.A. (c) Evolution of the UV/VIS absorption maxima of various concentrations of galacturonic acid treated with the DNS reagent.

The results of the activity tests for the free and immobilized Viazyme preparations obtained after the first and the second immobilization rounds at room temperature are presented in Figure 4.7.

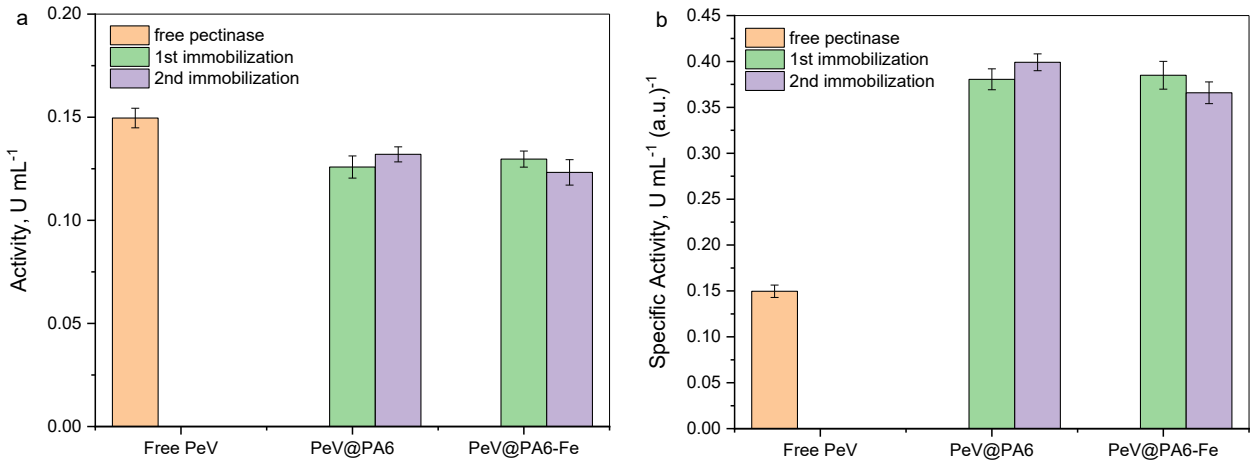


Figure 4.7: Comparative activity studies of free pectinolytic preparation and its MP-immobilized complexes: (a) activity in units per milliliter (U/mL) wherein 1 U is defined as the amount of enzyme required to release 1 μmol of galacturonic acid per minute under the assay conditions; (b) specific activity representing the activity in $U.mL^{-1}$ per content of pectinase in arbitrary units, a.u. The standard deviation values are obtained on the basis of three trials for each of the three samples.

The PeV@PA6 and PeV@PA6-Fe samples, obtained after the first and second immobilization from the same Viazym solution, are presented together for comparison, they are shown in Figure 4.7. Both PeV@PA6 and PeV@PA6-Fe display activities comparable to that of the free enzyme, with differences falling within the experimental error. This means that the same pectinase starting solution can be reused several times for immobilization on fresh microparticulate carriers without deterioration in the complex enzymatic activity.

When the activity values are normalized dividing by the protein content (Figure 4.7b), the specific activity of the immobilized complexes becomes up to 2.5-fold higher than that of the free preparation. This effect contradicts the reduced activity observed in the covalently immobilized pectinase in [13], highlighting one of the advantages of noncovalent immobilization. The notable increase in activity observed in the complexes could be attributed to a more advantageous active site configuration and/or the absence of inactivation in the former case. To shed more light on this issue, comparative kinetic studies were performed with all biocatalysts of this study.

4.5. Kinetic studies

The kinetic behavior of PeV and of the two immobilized systems, PeV@PA6 and PeV@PA6-Fe, were analyzed by plotting the dependence of the specific initial rate per unit protein (V_{spec}) against the pectin substrate concentration (S). As illustrated in Figure 4.8a, none of the catalytic systems followed the classical Michaelis–Menten kinetics, which would typically show a plateau in V_{spec} at high substrate concentrations. Instead, all curves exhibited a diminution of V_{spec} above 1 mg mL^{-1} of pectin indicating the occurrence of substrate inhibition. This inhibitory effect was most pronounced for the free enzyme.

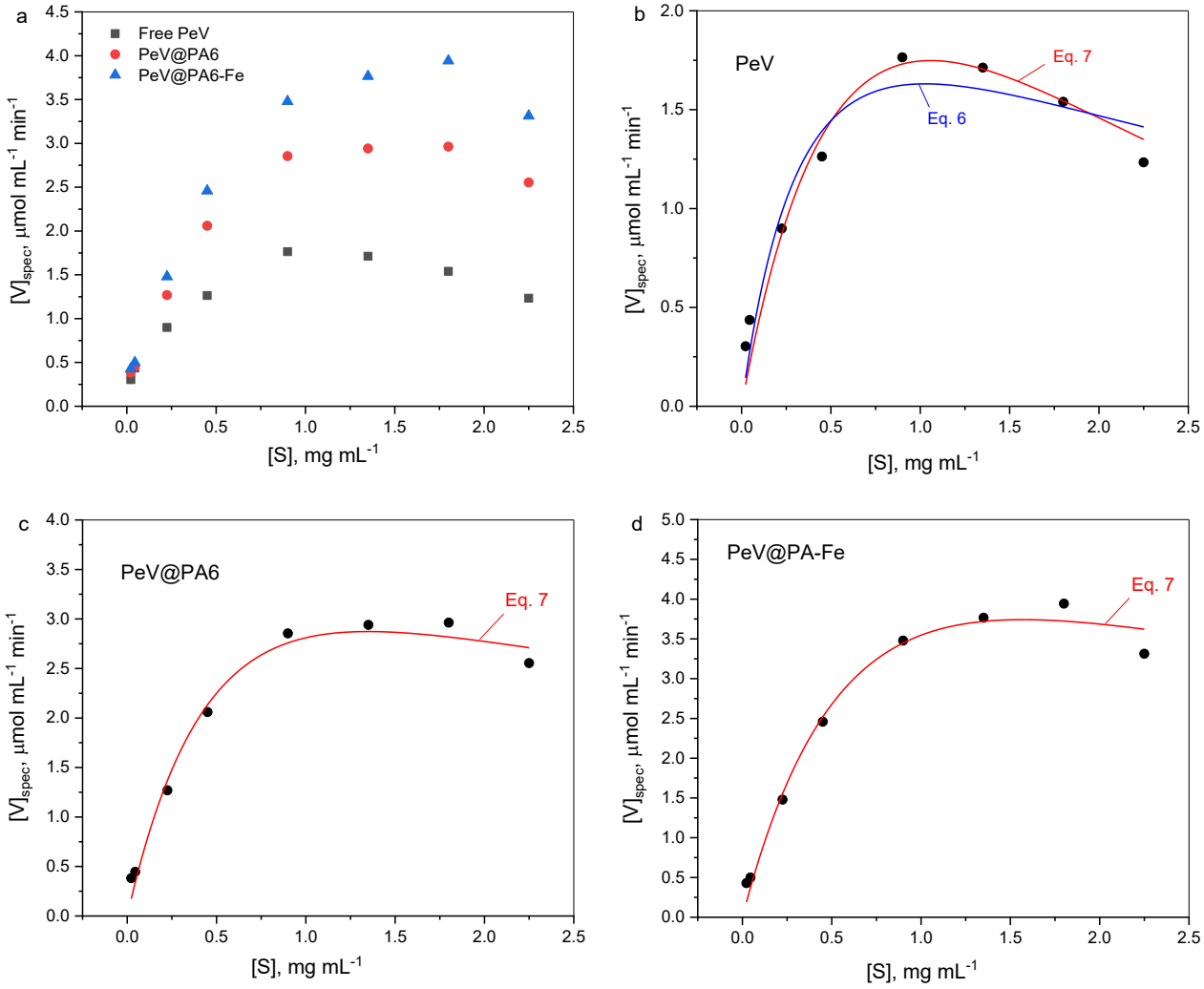


Figure 4.8: Kinetic studies with free and immobilized pectinases: (a) general comparison of the three kinetic curves; (b) free pectinase experimental curve and its best fits with Equations (6) and (7); (c) PeV@PA6 complex experimental curve and its best fit with Equation (7); (d) PeV@PA6-Fe complex experimental curve and its best fit with Equation (7).

Substrate inhibition in the pectinase-catalyzed pectin degradation was first reported by Gummadi and Panda [14]. The authors evaluated five different models of substrate inhibition and demonstrated that two of them achieve best fits reaching confidence levels of 95% (Equation 6 in Chapter 2, abbreviated as SI) and >99% (Equation 7 in Chapter 2, abbreviated as DE). Haldane's equation (Equation 6) represents a particular case of the more general formulation proposed by Yano et al. [15], which considers the formation of multiple inactive enzyme–substrate complexes (ES, ES_2, ... ES_n). Equation 6 describes inhibitory complexes involving two substrate molecules per enzyme molecule and is also valid for the SES type of inactive complexes, i.e., those with allosteric inhibition with two active sites [14,16]. In contrast, the exponential model expressed by Equation 7 reflects the empirical model proposed by Edwards [17] that combines the mechanisms of diffusion-controlled substrate supply with inhibitory substrate concentration.

To ensure that the fitting of the experimental curves of Figure 4.8a to Equations (6) and (7) resulted in physically meaningful kinetic parameters ($\mathrm{V_{max}}$, $\mathrm{K_m}$ and $\mathrm{K_i}$), the approach described by Cleland [18] for systems with substrate inhibition was adopted. Initially, the kinetic data were plotted in double-reciprocal form, i.e., $1/V_{spec}\ vs.\ 1/S$. Then, based on the linear part of the graphs the apparent Km and Vmax values were determined as in the case of Michaelis–Menten kinetics (Equation 5, Chapter 2). A preliminary estimate of the inhibitory constant Ki was then obtained using the following relationship [18]:

$$K_i(mg\ mL^{-1}) = \frac{S_{max}^2}{K_m} \tag{21}$$

wherein S_{max} is the value of S at the maximum values of V_{spec}.

These initial parameters (V_{max}, K_m and K_i) were subsequently used as starting values in the nonlinear regression routine of OriginPro, containing Equations (6) and (7) in Section 2.7 of Chapter 2 and the necessary fitting cycles were performed for each catalytic system until reaching the best adjusted R^2 coefficient.

The best fits are shown in Figures 4.8b–d, and the resulting kinetic constants are shown in Table 4.1.

Table 4.1: Kinetic parameters estimated for PeV, PeV@PA6 and PeV@PA6-Fe.

Free PeV	**Equation 5 (MM)**	**Equation 6 (SI)**	**Equation 7 (DE)**
V_{max} [$\mu mol\ mL^{-1}\ min^{-1}\ a.u.^{-1}$]	2.264	4.396 ± 0.180	3.164 ± 0.113
K_m [$mg\ mL^{-1}$]	0.342	0.659 ± 0.233	0.518 ± 0.034
K_i [$mg\ mL^{-1}$]	-	1.600 ± 0.189	2.669 ± 0.163
$Adj.R^2$	0.985*	0.930	0.977
PeV@PA6	**Equation 5 (MM)**	**Equation 6 (SI)**	**Equation 7 (DE)**
V_{max} [$\mu mol\ mL^{-1}\ min^{-1}\ a.u.^{-1}$]	3.335	-	3.520 ± 0.077
K_m [$mg\ mL^{-1}$]	0.294	-	0.419 ± 0.028
K_i [$mg\ mL^{-1}$]	-	-	8.840 ± 1.111
$Adj.R^2$	0.995*	-	0.985
PeV@PA6-Fe	**Equation 5 (MM)**	**Equation 6 (SI)**	**Equation 7 (DE)**
V_{max} [$\mu mol\ mL^{-1}\ min^{-1}\ a.u.^{-1}$]	4.256	-	4.682 ± 0.108
K_m [$mg\ mL^{-1}$]	0.341	-	0.513 ± 0.033
K_i [$mg\ mL^{-1}$]	-	-	8.975 ± 1.113
$Adj.R^2$	0.996*	-	0.985

*Note: V_{max} and K_m values in Equation 5 determined from the linear part of the double-reciprocal plot.

The free enzyme PeV kinetic data were best fitted with the double exponential empiric Equation 7, whereas the substrate inhibition expressed with Equation 6 produced an inferior fitting coefficient. This is in complete agreement with previous findings for similar systems [14]. Consequently, Equation 7 was selected to describe the immobilized PeV@PA6 and PeV@PA6-Fe systems.

The V_{max} values in Table 4.1 are the highest for the PeV@PA6-Fe, meaning that this complex is the fastest catalyst for pectin depolymerization, followed by PeV@PA6 both surpassing the free enzyme. So, it can be concluded that the immobilization of PeV produces faster catalytic complexes and that the Fe particles in PeV@PA6-Fe somehow increase this effect even more. In terms of substrate affinity related with K_m, the three systems showed similar values, however, those of the free PeV and PeV@PA6-Fe being the largest and statistically equal, followed by that of PeV@PA6. This means that the latter immobilized complex has the highest affinity to the substrate, since it requires lower concentrations to achieve half of the V_{max}. At last, inhibitory constants K_i of the PeV@PA6 and PeV@PA6-Fe systems display similar values, more than three times higher than the free PeV. This means that the immobilized systems require substantially higher substrate concentrations before inhibition occurs.

Summarizing, these results demonstrate that noncovalent immobilization of pectinase on PA6-based microparticles results in faster catalysts, with the same or slightly higher affinity to the pectin

substrate, being at the same time more difficult to inhibit. The incorporation of magnetic Fe particles further improves catalytic performance, particularly in terms of maximum reaction rate.

4.6. Grape must clarification

The next step was the application of the PeV@PA6 and PeV@PA6-Fe catalysts for the clarification of real rosé must samples containing pectin concentrations in the 2.0–2.5 mg mL^{-1} range. These values exceed the 1 mg mL^{-1} threshold above which substrate inhibition was observed in the kinetic studies (Figure 4.8). To ensure direct comparability, the amounts of immobilized pectinolytic preparation on the PA6 or PA6-Fe supports were adjusted to match the activity units of the free enzyme by appropriately selecting the mass of the polyamide–pectinase conjugate. The results of all clarification studies are presented in Figure 4.9.

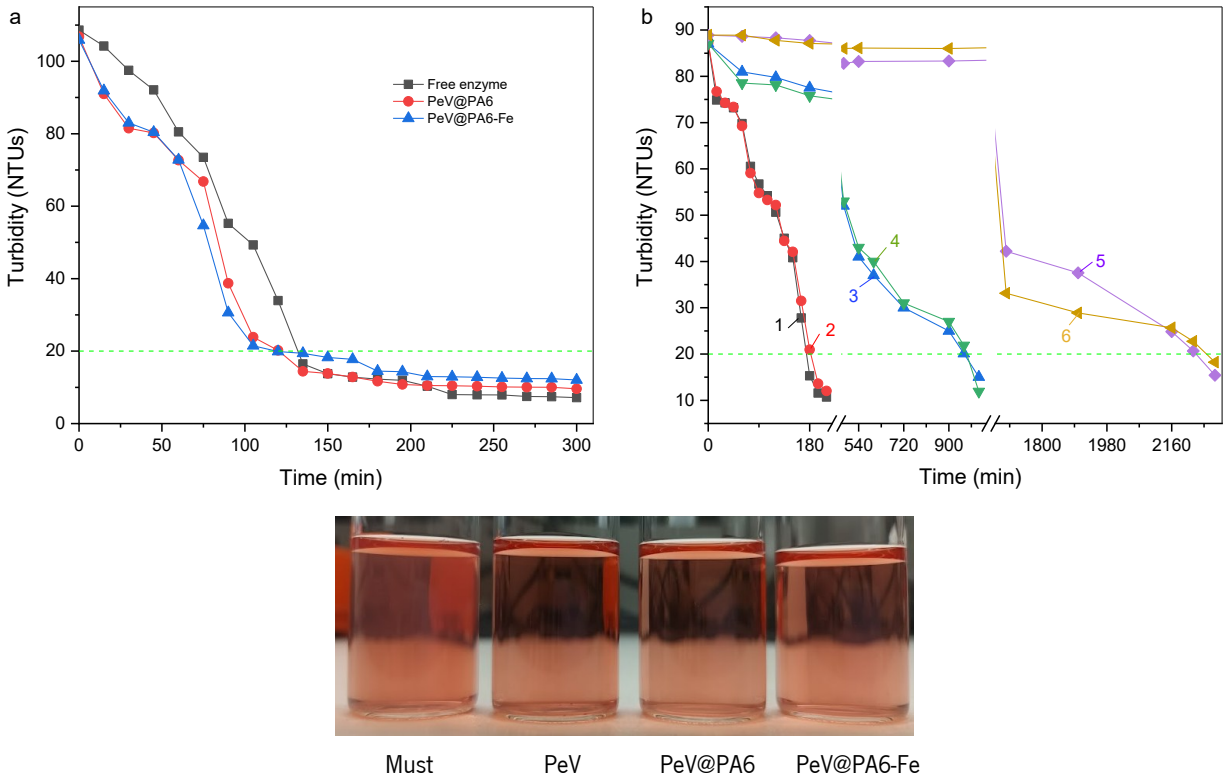


Figure 4.9: Clarification studies with free and immobilized pectinases: (a) clarification of must containing 2.5 $mg.mL^{-1}$ pectinase, at 23 °C; (b) clarification of must containing 2.0 $mg.mL^{-1}$ pectinase, at 23 °C. 1 – PeV@PA6, first application; 2 –– PeV@PA6-Fe, first application; 3 – PeV@PA6, second application; 4 - PeV@PA6-Fe, second application; 5 – PeV@PA6, third application; 6 - PeV@PA6-Fe, third application. All immobilized catalysts contain 0.30 a.u. of pectinolytic enzyme, which is the amount of free enzyme employed. The dashed line indicates the level of 20 NTUs below which the must is considered completely clarified. The visual aspects of the must before and after clarification is presented in the photographs.

Figure 4.9a shows the clarification effect at 23 ◦C of PeV@PA6 and PeV@PA6-Fe samples compared with the free enzyme. Both immobilized complexes show a distinct clarification effect 30 min after their introduction into the must, and complete clarification (turbidity < 20 NTU) was achieved in less than 120 min. The free enzyme showed a similar profile, but the same clarification effect was reached 15 min later. These results agree with the kinetic data (Table 4.1), confirming that PeV@PA6 and PeV@PA6-Fe act as slightly faster catalysts than the free enzyme.

The clarification capacity of PeV@PA6 and PeV@PA6-Fe conjugates after their first, second and third consecutive applications are presented in Figure 4.9b. During the first cycle (curves 1 (red points) and 2 (black squares)), visually clear must (turbidity < 20 NTU) was obtained after ≈3 h for both complexes. The second use of the same complexes (curve 3 (blue triangles) and 4 (green triangles)) required about 16 h to reach the same turbidity, and during the third application (curves 5 and 6) the necessary clarification time was about 36 h. The reduced clarification efficiency upon repeated use can be ascribed to the possible adsorption of byproducts produced during pectin hydrolysis onto the surface of the catalytic complex. This adsorption impedes the free transport of the substrate to the active center of the enzyme, consequently elongating the time required to achieve the desired must transparency. Nevertheless, clarification times of 16 h or even 36 h remain acceptable under industrial operating conditions.

The catalytic activity of the recycled PeV@PA6 and PeV@PA6-Fe complexes was also evaluated using the standard DNS assay over five consecutive cycles. Between the first and third cycles, the activity dropped from 100% to 60% and remained almost constant until the fifth cycle. These results are shown in Figure 4.10.

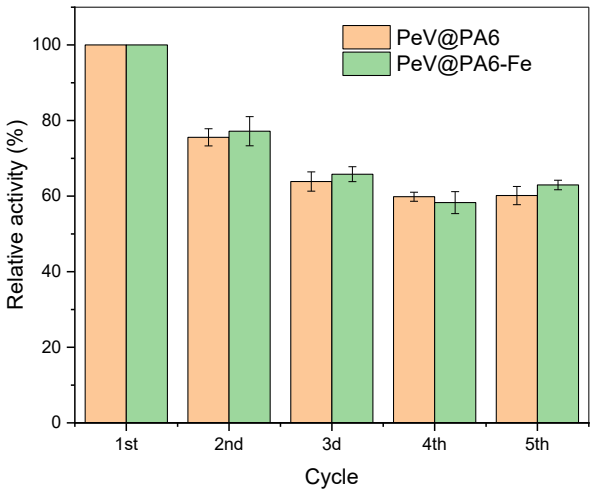


Figure 4.10: Relative activity of PeV@PA6 and PeV@PA6-Fe during 5 consecutive cycles.

4.6.1. Pectin test

At the end of the clarification and reusability studies, a residual pectin test in acidified alcohol was performed for all samples (Figure 4.11). As observed in Figure 4.11, the unclarified must sample shows some aggregates, confirming the presence of pectin, while the other samples do not show such aggregates. This finding confirms that turbidity values below 20 NTUs correspond to pectin-free must, indicating that the clarification process was complete.

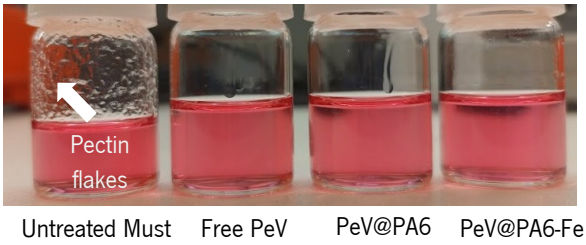


Figure 4.11: Results of the pectin test performed on all samples. Unclarified must, must clarified with free enzyme and immobilized in PA6 and PA6-Fe.

4.6.2. Color retention of must

The color of rosé and white wines is one of the most important characteristics subject to rigorous quality control. It is typically analyzed based on three bands in the UV/VIS spectrum: 420 nm (yellow component), 520 nm (red component) and 620 nm (blue component) [19,20]. Our comparative results of rosé musts treated with the free enzyme and the two immobilized conjugates are presented in Figure 4.12.

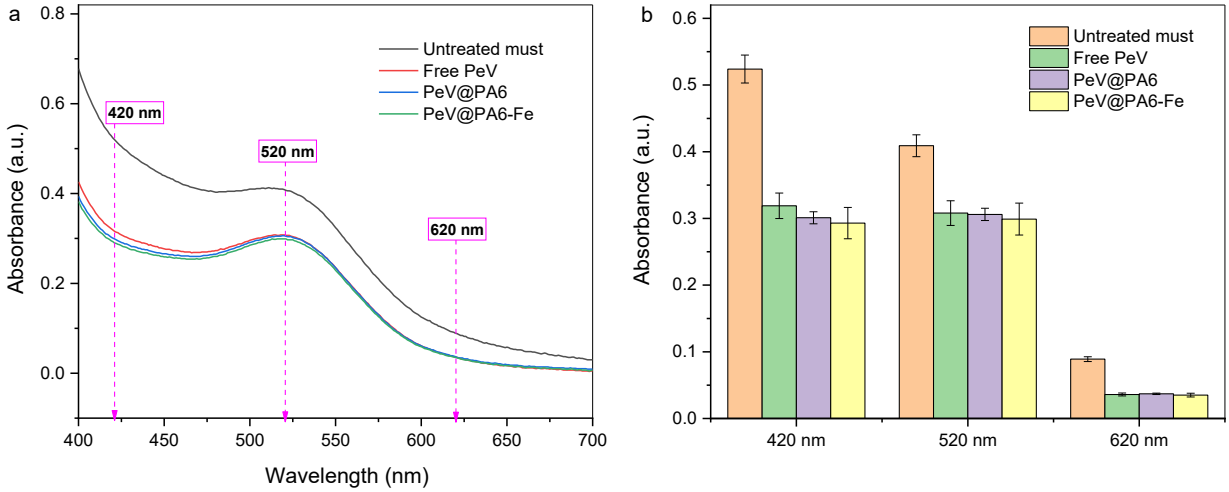


Figure 4.12: Retention of must color after clarification: (a) UV/VIS absorption spectra comparison in three characteristic intervals; (b) numerical data comparison. In the last case, the error bars are calculated on the basis of three trials for every sample.

Theoretically, the use of immobilized enzymes could induce undesirable color changes due to possible selective adsorption of wine's color components upon the microparticulate PA6 supports, which is impossible to occur with free commercial enzyme. However, the UV/VIS curves in Figure 12a and the bar graphs in Figure 12b indicate that the immobilized conjugates exhibit the same absorbances at 420 nm, 520 and 620 nm that of the commercial free pectinolytic preparation. These results demonstrate that the microparticulate polyamide supports of the PeV@PA6 and PeV@PA6-Fe conjugates do not cause any undesirable changes in the wine color, although it might have adsorbed some products of the pectin degradation, as suggested by the multiple uses of both conjugates.

The results from Figure 12 concerning the PeV@PA6-Fe also exclude any migration (i.e., leaching) of Fe or Fe ions from the immobilized complex into the must that could lead to its specific coloration. The absence of Fe leaching from enzyme-immobilized polyamide was confirmed also in an earlier work [21].

4.7. Conclusions

The immobilization of pectinase on PA6 and PA6-Fe microparticles is a simple and efficient process, carried out by incubating the supports in buffered enzyme solutions. The optimum conditions were identified as a 10-fold dilution of the enological enzyme, using 20 mg of microparticles per milliliter of enzyme solution and incubating the mixture at room temperature (20–21 °C) for 24 h under agitation. Under these conditions, two immobilization cycles were performed using the same enzyme solution, each immobilization cycle yielded approximately 15%. Through enzyme activity tests, it can be stated that the same pectinase solution could be reused for at least two consecutive immobilization circles without compromising the catalytic activity of the resulting PeV@PA6 and PeV@PA6-Fe complexes.

SEM–EDX analyses confirmed that the enzyme was successfully immobilized on the surface of the microparticles, partially filling their pores and channels.

Enzymatic activity assays demonstrated that the immobilized preparations exhibited specific activities up to 2.5 times greater than the free enzyme. Kinetic analyses confirmed that immobilization produced faster catalytic systems with a slightly higher affinity for the pectin substrate, making them more resistant to inhibition, as compared to the free enzyme.

The immobilized conjugates were subsequently applied to rosé must clarification at room temperature with the same arbitrary units of free pectinase. Complete clarification (≤20 NTU) was

achieved after 120–150 min, with the immobilized enzyme being slightly faster. Reusability studies demonstrated that both PeV@PA6 and PeV@PA6-Fe conjugates remained effective for at least three clarification cycles: approximately 3 h were required in the first cycle, 16 h in the second, and 36 h in the third. It should be noted, UV/VIS analysis showed that the polyamide microparticles did not induce any undesirable color changes in the must. The reuse of the complexes was also studied by the enzymatic activity in five consecutive cycles. It was shown that catalytic activity decreased from 100% to 60% between the first and third cycles and remained stable up to the fifth cycle.

Summarizing, immobilization commercial pectinase preparations on PA6-based microparticles results in catalytic complexes with enhanced stability and reusability. These complexes retain high enzymatic activity and do not adversely affect rosé must. Moreover, they can be reused for at least three consecutive clarification cycles, demonstrating their strong potential for practical application in enological processes.

In this context, PA6-based microparticles obtained by AAROP, both with and without incorporated Fe, represent suitable pulverulent carriers for the non-covalent immobilization of enzymes. However, the availability of anionic PA4, PA12, and copolymeric PA612 microparticles with distinct structures and morphologies provides a compelling basis for a comparative evaluation of their suitability for pectinase immobilization and subsequent wine clarification. Such broader comparative study is presented in the following chapter, using the methodology developed in the present chapter.

4.8. References

[1] Oliveira, S. C.; Dencheva, N. V.; Denchev, Z. Z. Immobilization of enological pectinase on magnetic sensitive polyamide microparticles for wine clarification. *Foods* **2024**, *13*, 420. https://doi.org/10.3390/foods13030420.

[2] Rodicio, R.; Heinisch, J. J. Carbohydrate metabolism in wine yeasts. In *Biology of Microorganisms on Grapes, in Must and in Wine*; Springer International Publishing: Cham, Switzerland, **2017**, 189–213. https://doi.org/10.1007/978-3-319-60021-5_8.

[3] Ottone, C.; Romero, O.; Aburto, C.; Illanes, A.; Wilson, L. Biocatalysis in the winemaking industry: Challenges and opportunities for immobilized enzymes. *Compr. Rev. Food Sci. Food Saf.* **2020**, *19*, 595–621. https://doi.org/10.1111/1541-4337.12538.

[4] Martín, M. C.; Morata de Ambrosini, V. I. Effect of a cold-active pectinolytic system on colour development of Malbec red wines elaborated at low temperature. *Int. J. Food Sci. Technol.* **2014**, *49*, 1893–1901. https://doi.org/10.1111/ijfs.12498.

[5] Belda, I.; Conchillo, L. B.; Ruiz, J.; Navascués, E.; Marquina, D.; Santos, A. Selection and use of pectinolytic yeasts for improving clarification and phenolic extraction in winemaking. *Int. J. Food Microbiol.* **2016**, *223*, 1–8. https://doi.org/10.1016/j.ijfoodmicro.2016.02.003.

[6] Martín, M. C.; López, O. V.; Ciolino, A. E.; Morata, V. I.; Villar, M. A.; Ninago, M. D. Immobilization of enological pectinase in calcium alginate hydrogels: A potential biocatalyst for winemaking. *Biocatal. Agric. Biotechnol.* **2019**, *18*, 101091. https://doi.org/10.1016/j.bcab.2019.101091.

[7] Benucci, I.; Lombardelli, C.; Liburdi, K.; Acciaro, G.; Zappino, M.; Esti, M. Immobilised native plant cysteine proteases: Packed-bed reactor for white wine protein stabilisation. *J. Food Sci. Technol.* **2016**, *53*, 1130–1139. https://doi.org/10.1007/s13197-015-2125-4.

[8] Barbosa, O.; Ortiz, C.; Berenguer-Murcia, Á.; Torres, R.; Rodrigues, R. C.; Fernandez-Lafuente, R. Strategies for the one-step immobilization–purification of enzymes as industrial biocatalysts. *Biotechnol. Adv.* **2015**, *33*, 435–456. https://doi.org/10.1016/j.biotechadv.2015.03.006.

[9] Dencheva, N.; Oliveira, S.; Braz, J.; Getya, D.; Malfois, M.; Denchev, Z.; Gitsov, I. Magnetically responsive PA6 microparticles with immobilized laccase show high catalytic efficiency in the enzymatic treatment of catechol. *Catalysts* **2021**, *11*, 239. https://doi.org/10.3390/catal11020239.

[10] Araújo, D.; Braz, J.; Dencheva, N. V.; Carvalho, I.; Henriques, M.; Denchev, Z. Z.; Gitsov, I. Polyamide microsized particulate polyplex carriers for the 2′-O-methylRNA EFG1 antisense oligonucleotide. *ACS Appl. Bio Mater.* **2021**, *4*, 4607–4617. https://doi.org/10.1021/acsabm.1c00334.

[11] Dencheva, N.; Braz, J.; Scheibel, D.; Malfois, M.; Denchev, Z.; Gitsov, I. Polymer-assisted biocatalysis: Polyamide 4 microparticles as promising carriers of enzymatic function. *Catalysts* **2020**, *10*, 767. https://doi.org/10.3390/catal10070767.

[12] Mohnen, D. Pectin structure and biosynthesis. *Curr. Opin. Plant Biol.* **2008**, *11*, 266–277. https://doi.org/10.1016/j.pbi.2008.03.006.

[13] Rexová-Benková, L.; Omelková, J.; Veruovič, B.; Kubánek, V. Mode of action of endopolygalacturonase immobilized by adsorption and by covalent binding via amino groups. *Biotechnol. Bioeng.* **1989**, *34*, 79–85. https://doi.org/10.1002/bit.260340111.

[14] Gummadi, S. N.; Panda, T. Analysis of kinetic data of pectinases with substrate inhibition. *J. Microbiol. Biotechnol.* **2003**, *13*, 332–337.

[15] Yano, T.; Nakahara, T.; Kamiyama, S.; Yamada, K. Kinetic studies on microbial activities in concentrated solutions: Effect of excess sugars on oxygen uptake rate. *Agric. Biol. Chem.* **1966**, *30*, 42–48. https://doi.org/10.1271/bbb1961.30.42.

[16] Webb, J. L. *Enzyme and Metabolic Inhibitors*; Academic Press: New York, NY, USA, **1963**. https://doi.org/10.5962/bhl.title.7320.

[17] Edwards, V. H. The influence of high substrate concentrations on microbial kinetics. *Biotechnol. Bioeng.* **1970**, *12*, 679–712. https://doi.org/10.1002/bit.260120504.

[18] Buxbaum, E. Enzyme kinetics and mechanism. In *Fundamentals of Protein Structure and Function*; Springer International Publishing: Cham, Switzerland, **2015**; 111–140. https://doi.org/10.1007/978-3-319-19920-7_5.

[19] International Organization of Vine and Wine (OIV). *Compendium of International Methods of Wine and Must Analysis—Chromatic Characteristics*; OIV: Paris, France, **2022**. Available online: https://www.oiv.int (accessed on 25 May 2023).

[20] Faragó, P.; Gălătuş, R.; Hintea, S.; Boşca, A. B.; Feurdean, C. N.; Ilea, A. An intra-oral optical sensor for the real-time identification and assessment of wine intake. *Sensors* **2019**, *19*, 4719. https://doi.org/10.3390/s19214719.

[21] Dencheva, N.; Braz, J.; Nunes, T. G.; Oliveira, F. D.; Denchev, Z. One-pot low temperature synthesis and characterization of hybrid poly(2-pyrrolidone) microparticles suitable for protein immobilization. *Polymer* **2018**, *145*, 402–415. https://doi.org/10.1016/j.polymer.2018.04.080.

CHAPTER 5

Magnetic-responsive pectinase biocatalysts based on diverse polyamides: The role of support structure and morphology in must clarification

As demonstrated in the previous chapter, porous PA6 microparticles can be synthesized via AAROP of ε-caprolactam and successfully applied as supports for the non-covalent immobilization of enological pectinases, yielding biocatalytic complexes suitable for rosé must clarification. Nevertheless, other polyamides obtainable in the form of microstructured powders by AAROP, such as PA4 and PA12 homopolymers and the PA612 copolymer, may also represent viable alternatives for enzyme immobilization.

Accordingly, this chapter focuses on the immobilization of pectinase onto PA4 and PA12 microparticles, as well as onto PA612 copolymeric supports, with the aim of developing efficient biocatalysts for wine clarification. The experimental work was carried out using industrial wine must and commercial pectinase preparations, both kindly provided by Sogrape Vinhos, Lda. Most of the results presented in this chapter have already been published [1].

5.1. Introduction

Pectinases are essential enzymes for must clarification, but their use in free form is often limited by low stability and the inability to recover the catalyst [2]. To overcome these limitations, immobilization on solid supports has been extensively explored [3]. Among various materials, polyamides (PA) have gained special attention as they are considered the closest synthetic analogues to the protein matrix of enzymes. PA can be synthesized via ring-opening polymerization or polycondensation in various forms, including powders and microparticles [4-10]. These polymers share structural features such as terminal amine ($–NH_2$) and carboxylic (–COOH) groups linked by aliphatic methylene segments ($–CH_2–$). The number of methylene groups between adjacent amide functionalities defines the type of polyamide (e.g., PA4 contains four methylene units), resulting in materials with distinct amide group densities, hydrophilicity, crystallinity, and surface properties [11-13]. These structural differences are expected to influence enzyme–support interactions.

While Chapter 4 focused on the development and characterization of PA6-based pectinase conjugates for wine clarification using a specific, well-defined methodology, this chapter extends the study to PA4, PA12, and the PA612 copolymer polyamide microparticles (PA MPs), with and without magnetic susceptibility. These PA MPs were synthesized via AAROP and used for the non-covalent immobilization of pectinase. Following morphological characterization, their enzymatic activity and kinetics were evaluated in rosé must clarification. By comparing these systems with free pectinase (PeV) and PeV@PA6, the influence of methylene chain length and support

morphology on pectinolytic performance is accessed, which allowed the identification of the complexes with the greatest potential for industrial application.

5.2. Determination of protein content in PeV@PA complexes

Before evaluating catalytic performance, it was essential to quantify the protein loading on the different polyamide microparticle supports (PeV@PA). The amount of non-covalently immobilized pectinolytic enzymes on all PA MPs (PA4, PA6, PA12, and PA612) was determined using a direct ultraviolet-visible spectroscopy (UV/VIS) method at λ = 263 nm as described in Chapter 2, Section 2.5. This wavelength corresponds to the absorption of aromatic amino acid residues, such as tryptophan and tyrosine, present in the pectinase protein structure. As previously justified, this method provides reliable quantitative data for protein adsorption, with standard deviations between 3–5%, in contrast to indirect assays such as Bradford or BCA, which often exhibit higher variability (up to 15%).

The results of the immobilization process, including the spectral changes observed in the supernatants and the calculated immobilization yields are presented in Figure 5.1.

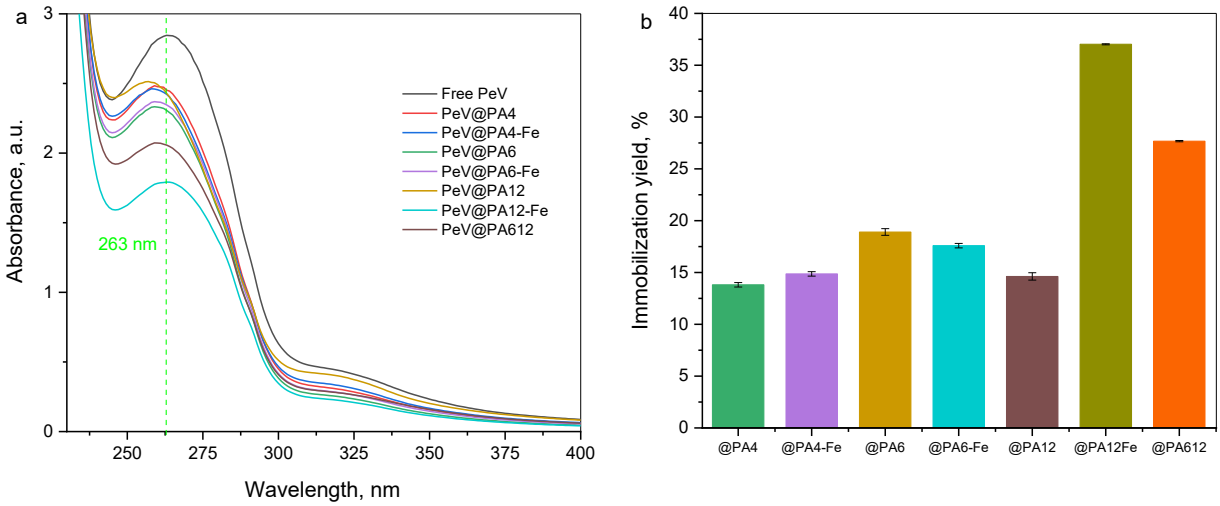


Figure 5.1: Quantification of the PeV immobilization: (a) UV/VIS spectra of the Viazym solutions before and after adsorption on seven different MP supports; (b) Immobilization efficiency for all PeV@PA and PeV@PA-Fe complexes. Standard deviations were calculated from three independent trials. Sample designations are shortened for better visibility.

Immobilization yields varied significantly, ranging from 13% to 38% (Figure 5.1b), depending on the polyamide support and the presence of iron particles. PA4-based complexes exhibited the lowest yields (13–15%), while PA6-based systems showed slightly higher values (16–18%). A

marked increase in immobilization efficiency was observed for PA12 supports, rising from 15% for the pure polymer to 38% for the PA12–Fe complex. The PA612 copolymer presented the second-highest yield (28%). These results indicate that the nature of the polyamide support plays a key role in enzyme immobilization efficiency. Two main factors can explain the effect of the support on immobilization: (i) the hydrogen bond density between the PeV apoenzyme protein matrix and the polyamide support, (ii) the surface topology and accessible surface area of the support. The results are correlated with the SEM and FTIR observations discussed in previous sections. PA12-based supports consist of the largest microparticles with large and deep surface channels; the incorporation of Fe reduces particle size while increasing channel density, thereby providing a greater effective surface area for enzyme adsorption. In contrast, PA6 exhibits a scaffold-like structure composed of a 3D network of interlaced filaments, with iron fully encapsulated within the microparticles. No matter that PA4 presents a high density of potential hydrogen bonding sites, its smaller particle size and more limited surface accessibility result in lower immobilization efficiency. These observations suggest that surface topology and accessible surface area have a greater influence on enzyme immobilization efficiency than hydrogen bonding density alone.

5.3. Characterization of polyamide microparticles

5.3.1. Morphological studies by SEM

The morphology of all polyamide microparticles, with and without immobilized enological pectinase, was investigated by scanning electron microscopy (SEM) combined with energy-dispersive X-ray Spectroscopy (EDX). Selected representative micrographs are presented in Figures 5.2–5.5.

Figure 5.1 and 5.2 displays the micrographs of PA4 and PA4–Fe and the corresponding complexes. PA4 and PA4–Fe exhibit predominantly near-spherical morphologies (Figures 5.2a and 5.2i). PA4–Fe MPs display larger surface pores compared to PA4 MPs (Figures 5.2b and 5.2j). EDX analysis (Figures 5.2, Z5 site and 5.2, Z6 site) indicates that iron particles are located deeper within the polymer matrix. The characteristic Kα and Kβ peaks of Fe at approximately 6.4 keV and 7.2 keV were detected when the electron beam interacted with surface fissures, suggesting partial exposure of the encapsulated magnetic particles. Immobilization of PeV does not significantly alter the overall morphology of PA4 and PA4–Fe MPs (Figures 5.2c and 5.2k). However, enzyme immobilization leads to partial filling of surface pores, markedly modifying the surface topology of the PeV@PA4 complexes (Figures 5.2d and 52j).

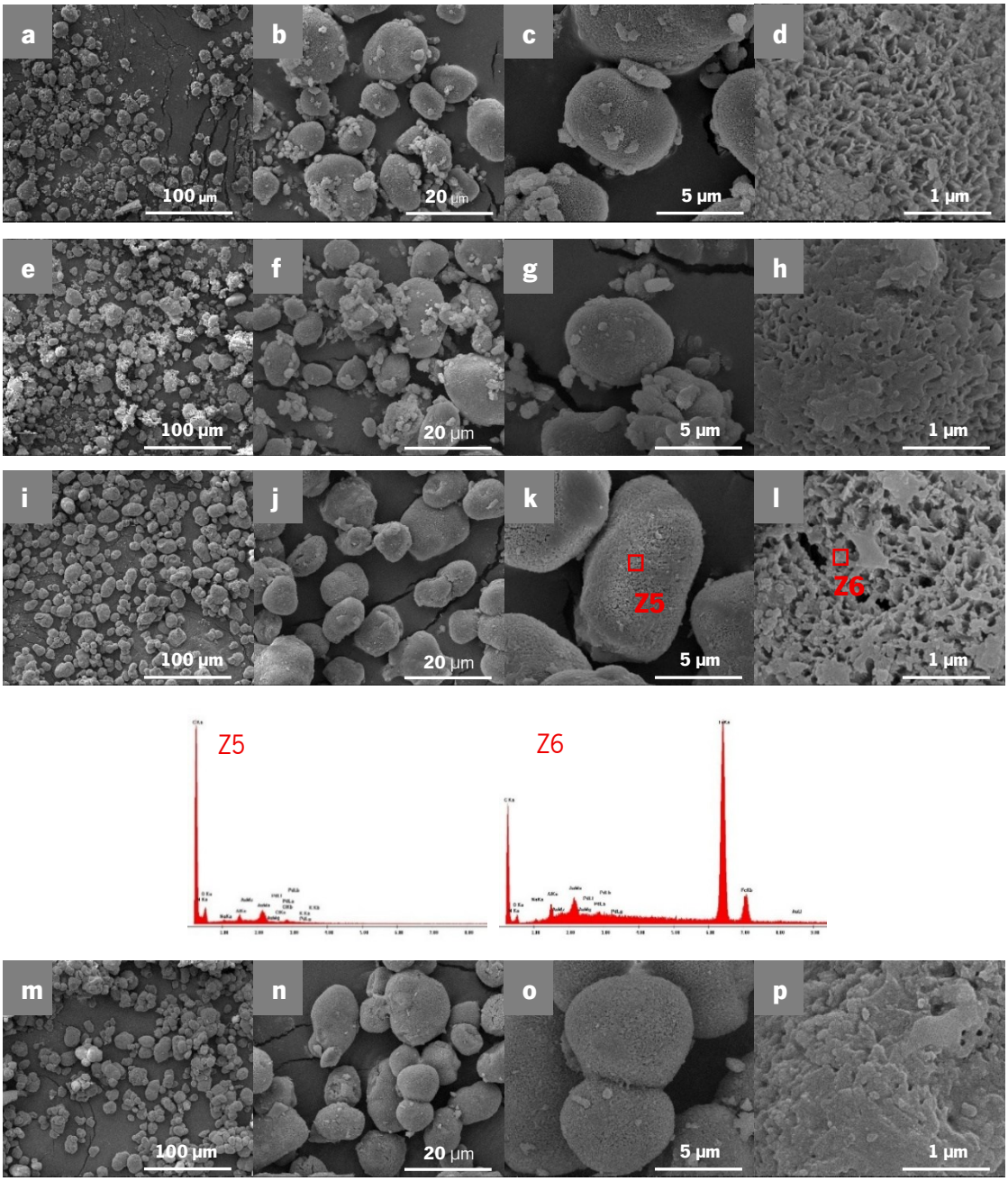


Figure 5.2: Selected SEM micrographs and corresponding EDX of PA4 (images a-d) and PA4-Fe (images a-d) and Pectinase-immobilized conjugates (images e-h).

As observed in the next Figure 5.3a, PA6 MP is composed of aggregates of irregular shape formed by smaller fused spheres resulting in a scaffold-like structure composed of a 3D network of interlaced filaments (like balls of yarn). The incorporation of Fe (PA6–Fe, Figure 5.3) induces morphological changes in some particles, which exhibit elongated, pea-pod-like structures. This morphology is likely caused by magnetic attraction between iron particles followed by encapsulation during AAROP. EDX analysis did not detect Fe at the particle surface, suggesting complete encapsulation or effective shielding of the magnetic cores within the polymer matrix. Similar to

PA4, enzyme immobilization does not significantly affect the overall size or shape of PA6 MPs. However, unlike PA4, the enzyme predominantly adheres to the polymer filaments without obstructing the three-dimensional network, preserving the open porous structure.

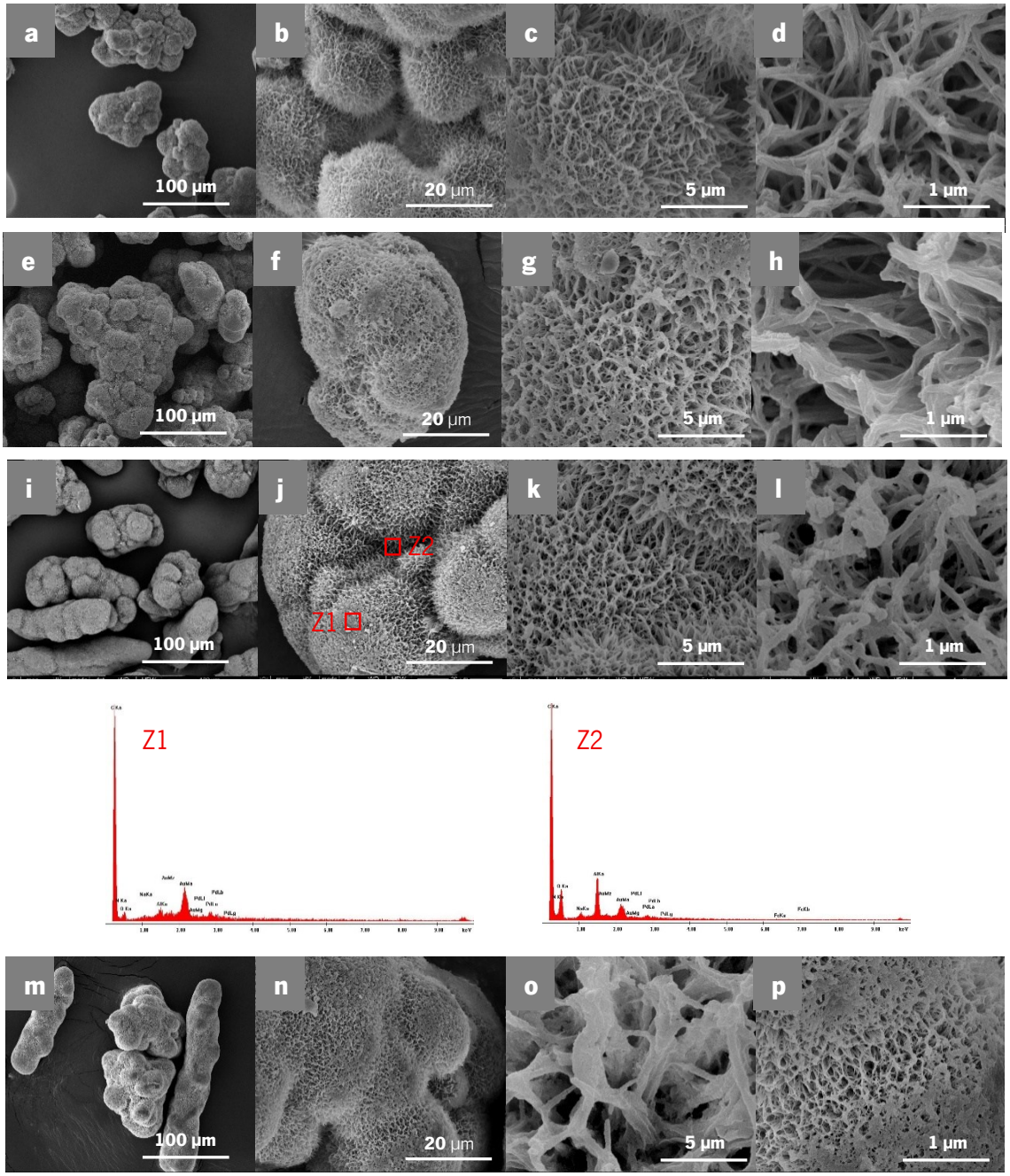


Figure 5.3: Morphological characterization of PA6 (images a-d), PA6-Fe (images i-j) and the PeV@PA6 (images e-h) and PeV@PA6-Fe complexes (images m-p).

PA12 MPs are characterized by massive, irregularly shaped particles lacking spherical symmetry (Figure 5.4a). Their surface exhibits a sponge-like morphology with large, deep channels

rather than pores (Figure 5.4d). The inclusion of Fe results in a decrease in particle size and an increase in surface channel density (Figures 5.4i and 5.4j). In this case, small Fe particles are detectable at or slightly beneath the particle surface, as confirmed by EDX analysis (Figures 5.4K and 5.4Z2). SEM images (Figures 5.4e–h and 5.4m–p) indicate that enzyme immobilization does not significantly alter the overall morphology; smaller surface pores are filled by the enzyme, while larger channels remain accessible.

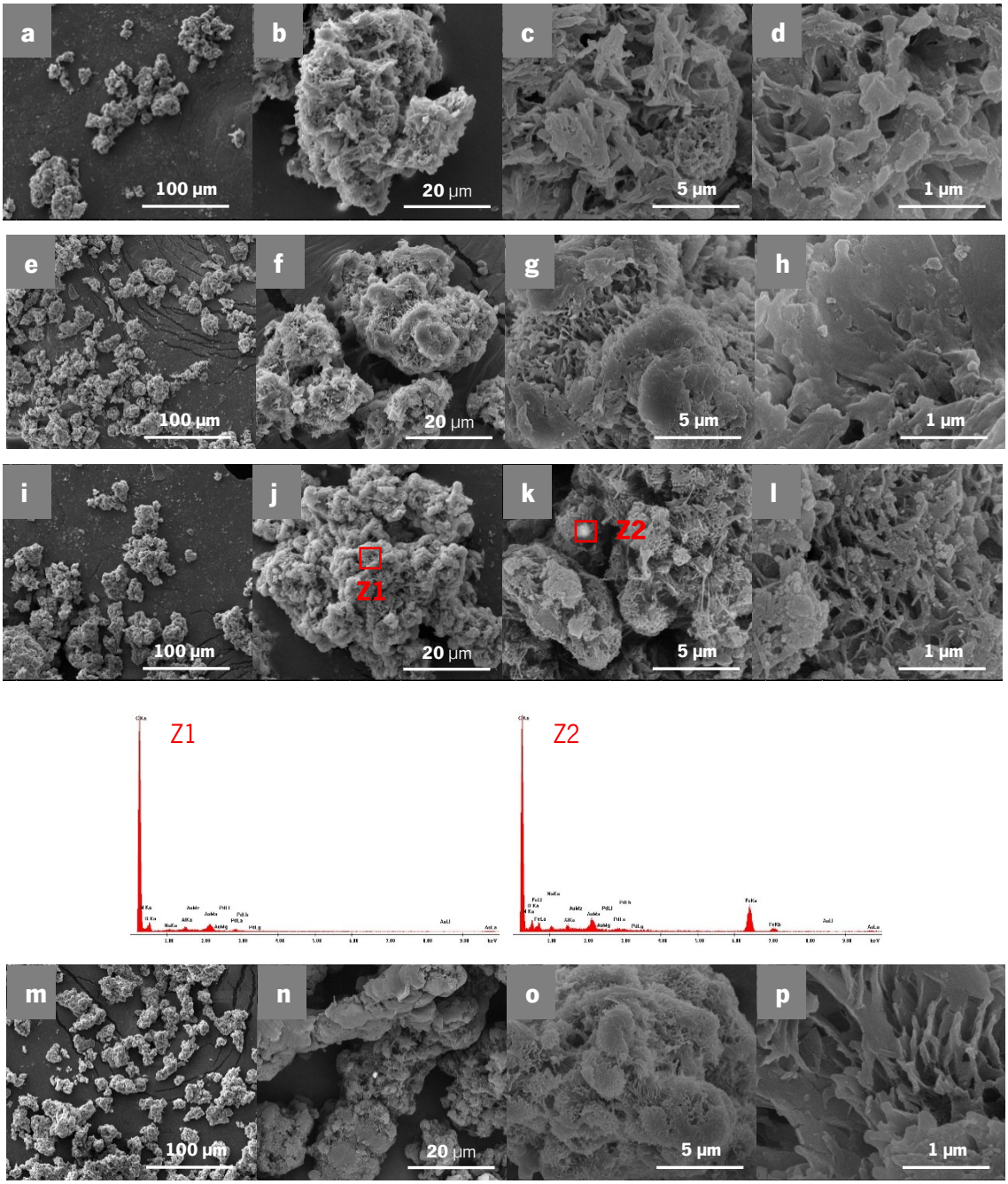


Figure 5.4: SEM and EDX analysis of PA12 (images a-d) and PA12-Fe supports (images i-l) and respective immobilized complexes (images e-h and m-p).

The morphology of PA612 copolymer MPs is similar to that of PA12, displaying irregular shapes and a sponge-like surface topography (Figures 5.5a–d). After enzyme immobilization, the particle morphology is preserved, while the enzyme appears to cover most surface channels and pores (Figure 5.5h).

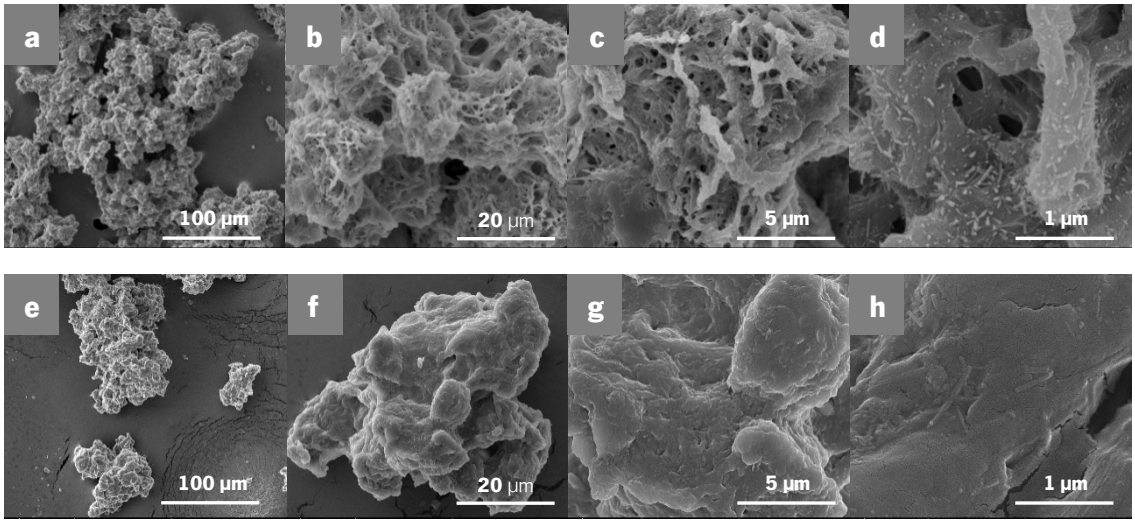


Figure 5.5: Selected SEM images of PA612 copolymer (images a-d) and its respective immobilized complex (images e-h).

This morphological analysis allows several important conclusions. EDX results confirm that the AAROP process effectively encapsulates magnetic cores within polyamide matrices, with polymer coating thickness varying depending on the polyamide type. In PA12, iron is detectable at or near the surface, whereas in PA4 it is mainly exposed through surface fissures. In contrast, Fe was not detected on the surface of PA6 MPs, indicating more effective encapsulation. These differences in metal accessibility may influence the magnetic responsiveness and the whole set of properties of the resulting complexes. Additionally, it is well-known that surface morphology and pore architecture play a crucial role in enzyme immobilization and potential catalytic performance. The 3D network of PA6 provides a high surface area for enzyme adhesion without causing total blockage of the pores, which may facilitate substrate transport during catalysis. In contrast, in PA4 and PA612 systems, enzyme-induced pore filling may lead to increased diffusional limitations compared to PA6, where the porous network remains largely unobstructed.

5.3.2. FTIR spectroscopy analysis

The PA-based supports and their respective immobilized complexes were analyzed by Fourier transform infrared (FTIR) spectroscopy. This analysis was carried out to confirm enzyme immobilization through the hydrogen bonds formed between the apoenzyme and the amide groups of supports. The obtained spectra are presented in Figure 5.6.

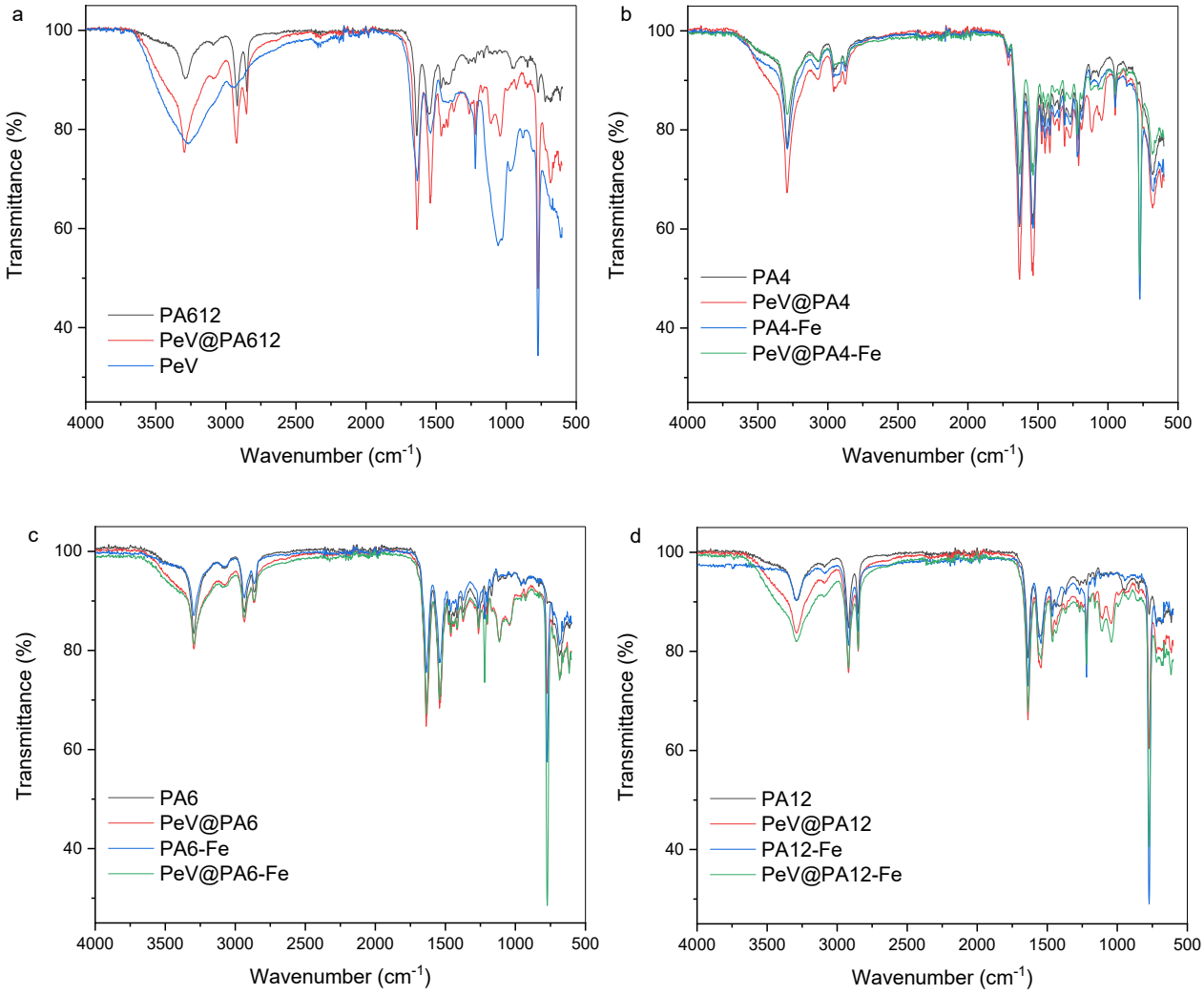


Figure 5.6: FTIR spectra of free and immobilized enzyme: a) PeV and PA612 supports, b) PA4 supports, c) PA6 supports, d) PA12 supports.

All PA microparticles exhibited similar spectra, displaying characteristic bands. Specifically, the bands around 3300 cm^{-1}, corresponding to N–H stretching vibrations, typical of secondary amide groups, involved in hydrogen bonding. Amide I (C=O stretching) and Amide II (N–H bending and C–N stretching) are also observed at 1630–1637 cm^{-1} and 1535–1549 cm^{-1} (respectively). The

spectrum of the PeV confirms that its protein matrix is a structural analog of synthetic polyamides showing similar Amide I and Amide II peaks, exhibiting a broad peak centered at 3250 cm^{-1}. A typical band at 1050 cm^{-1} is also present, this band is characteristic of the enzyme's structure. It is clearly visible in the PeV@PA spectra but absent in the neat supports. The presence of this band, and the increased intensity of the shoulder for associated –NH– and $–NH_2$ groups suggests hydrogen bond formation between the enzyme's amide groups and those of the PA MPs supports, confirming successful immobilization and suggests the formation of an extensive hydrogen-bonding network between the enzyme and the PA supports. Regarding the influence of Fe, the main difference observed is a slight increase in the width of the amide bands in the iron-containing microparticles. That is, microparticles with metallic charge have greater structural heterogeneity in the polymer matrix. No new absorption bands appear, confirming the absence of strong coordination or chemical interaction between Fe and the functional groups of the polyamide. It can be stated that the iron particles are physically encapsulated or incorporated into the PA matrix without altering its fundamental chemical structure.

5.4. Enzymatic activity of free and immobilized pectinase

As described in Chapter 4, the 3,5-dinitrosalicylic acid (DNS) method proposed by Miller was used to determine the activity of both free and immobilized enzymes [14]. In this method, galacturonic acid (G.A.), which contains an aldehyde group, donates a hydrogen atom to the DNS reagent (2-hydroxy-3,5-dinitrobenzoic acid), converting it into 3-amino-5-nitrosalicylic acid (3,5-ANS) while G.A. is oxidized. This redox reaction leads to a color change of the reaction mixture, which constitutes the basis for the UV/VIS spectrophotometric determination of pectinase activity. For the application of this method, a calibration curve using different G.A. concentrations was constructed (Figure 5.7c). Figure 5.7b shows the UV/VIS absorption maxima corresponding to increasing concentrations of galacturonic acid treated with the DNS reagent.

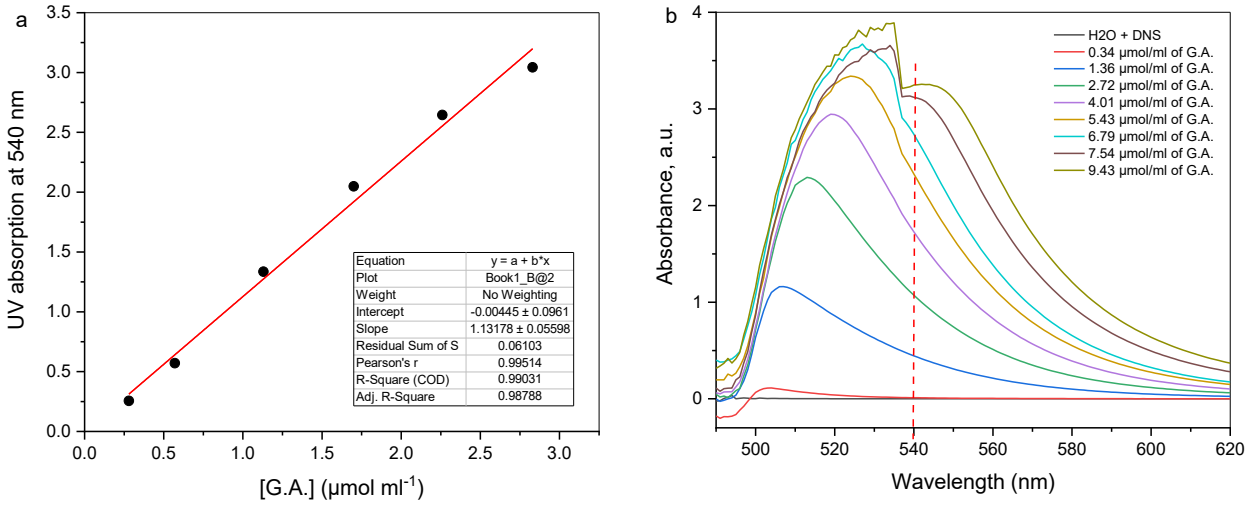


Figure 5.7: a) The standard calibration curve constructed with various concentrations of G.A. b) Evolution of the UV/VIS absorption maxima of various concentrations of galacturonic acid treated with the DNS reagent.

From the next Figure 5.8a, it can be observed that the absolute activity of the immobilized enzyme (PeV@PA) is not statistically different among the tested supports and is approximately half of that of the free enzyme. The figure also includes yellow columns corresponding to the DNS reaction performed with the PA MP supports without PeV immobilization. These values clearly fall within the experimental margin of error, confirming that microparticulate supports without enzyme do not exhibit pectinolytic activity. Figure 5.8b presents the specific activities, which normalize enzyme performance relative to the protein content of each conjugate. Remarkably, the immobilized systems exhibit specific activities comparable to that of the free enzyme (PeV@PA12-Fe) or significantly higher, reaching increases of approximately 2.5-fold for PeV@PA4 and 3.5-fold for PeV@PA12. These results suggest that adsorption onto polyamide microparticles may induce a more favorable active-site conformation and/or protect the enzyme from rapid denaturation in the reaction medium. This behavior contrasts with the activity losses frequently reported for covalently immobilized enzymes [5], highlighting the preservation of enzyme structural integrity through non-covalent interactions.

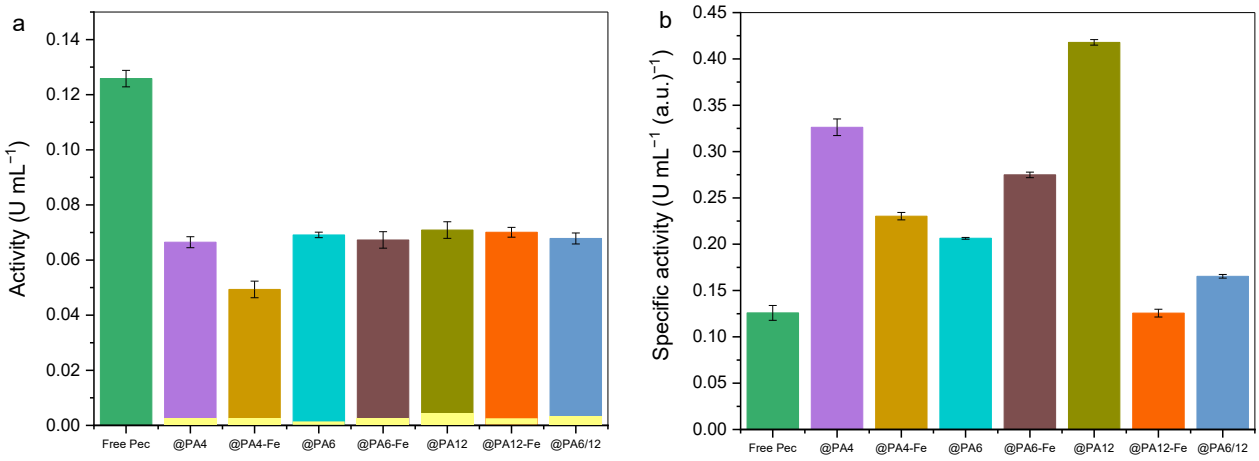


Figure 5.8: Activity of PeV@PA immobilized conjugates in comparison to free PeV, a) absolute activity. The small yellow bars show the "activity" values of the respective empty PA supports, b) specific activity per unit enzyme (free or immobilized). Sample designations are shortened for better visibility.

The observed increase in activity of adsorption-immobilized pectinolytic preparations compared to the free enzyme may therefore be attributed to improved catalytic accessibility and/or reduced inactivation. To further investigate and validate these activity results, comparative kinetic studies were conducted for all biocatalysts examined in this work.

5.5. Kinetic studies

The kinetic parameters of PeV and PeV@PA complexes were determined by quantifying the release of D-galacturonic acid from pectin at substrate concentrations ranging from 0.0225 to 2.25 mg mL^{-1} using the DNS method. This analysis was done by plotting the specific activity per unit protein (V) against pectin substrate concentration (S), graphically represented in Figure 5.9.

The main parameters describing enzymatic kinetics are the maximum specific catalytic activity (V_{max}) and the Michaelis–Menten constant (K_m). V_{max} represents the maximum reaction rate of the enzymatic system, while K_m reflects the substrate affinity, with lower K_m values indicating higher affinity.

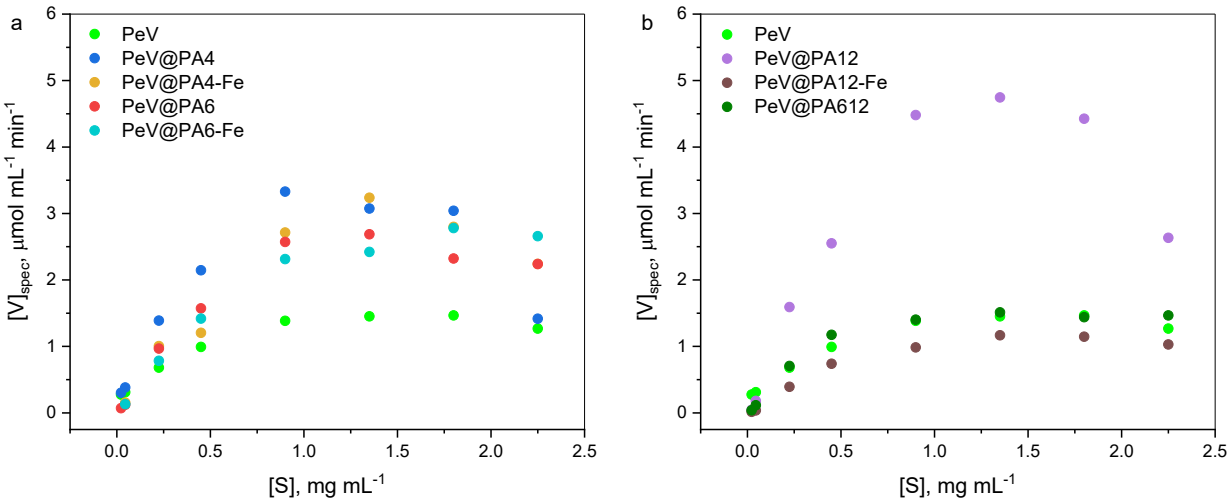


Figure 5.9: Experimental kinetic curves: (a) PeV, PeV@PA4, PeV@PA4-Fe, PeV@PA6 and PeV@PA6-Fe; (b) PeV, PeV@PA12, PeV@PA12-Fe and PeV@PA612.

Figure 5.10 shows that neither the free enzyme nor the immobilized complexes follow Michaelis-Menten kinetics behavior, as no saturation of V_{spec} was observed at high substrate concentrations. Instead, a decrease in activity occurred with increasing pectin concentration, indicating substrate inhibition. This phenomenon has previously been reported for free pectinase systems by Gummadi and Panda [15], who demonstrated that such behavior can be adequately described using two substrate inhibition models: (i) Equation 6 (Chapter 2, abbreviated as SI), which provides a 95% confidence fit, and (ii) the empirical Equation 7 (Chapter 2, abbreviated as DE), which yields confidence levels above 99%. In addition to $\mathrm{V_{max}}$ and $\mathrm{K_m}$, both models incorporate the inhibition constant $\mathrm{K_i}$, which reflects the affinity between the enzyme and the inhibitory form of the substrate. Lower $\mathrm{K_i}$ values indicate stronger inhibition occurring at lower substrate concentrations, conversely, a higher $\mathrm{K_i}$ suggests that significant inhibition only occurs at high substrate concentrations. This constant was determined by Equation 21 (Chapter 4).

To ensure that fitting the experimental curves to Equations 6 and 7 will render $\mathrm{V_{max}}$, $\mathrm{K_m}$ and $\mathrm{K_i}$ values with meaningful physical interpretation and reliable statistics, the procedure of Cleland for a single inhibitory substrate was followed [16]. Initially, kinetic data were plotted in double-reciprocal form $(1/\mathrm{V_{max}}$ vs. $1/\mathrm{S})$, and the linear portions of the plots were used to estimate the apparent V_{max} and K_m values, as in standard Michaelis-Menten kinetics (Equation 5, Chapter 2, abbreviated as MM). The best fits for the most representative biocatalysts are presented in Figure 5.10, with the corresponding $\mathrm{V_{max}}$, $\mathrm{K_m}$and $\mathrm{K_i}$ for all systems listed in Table 5.1.

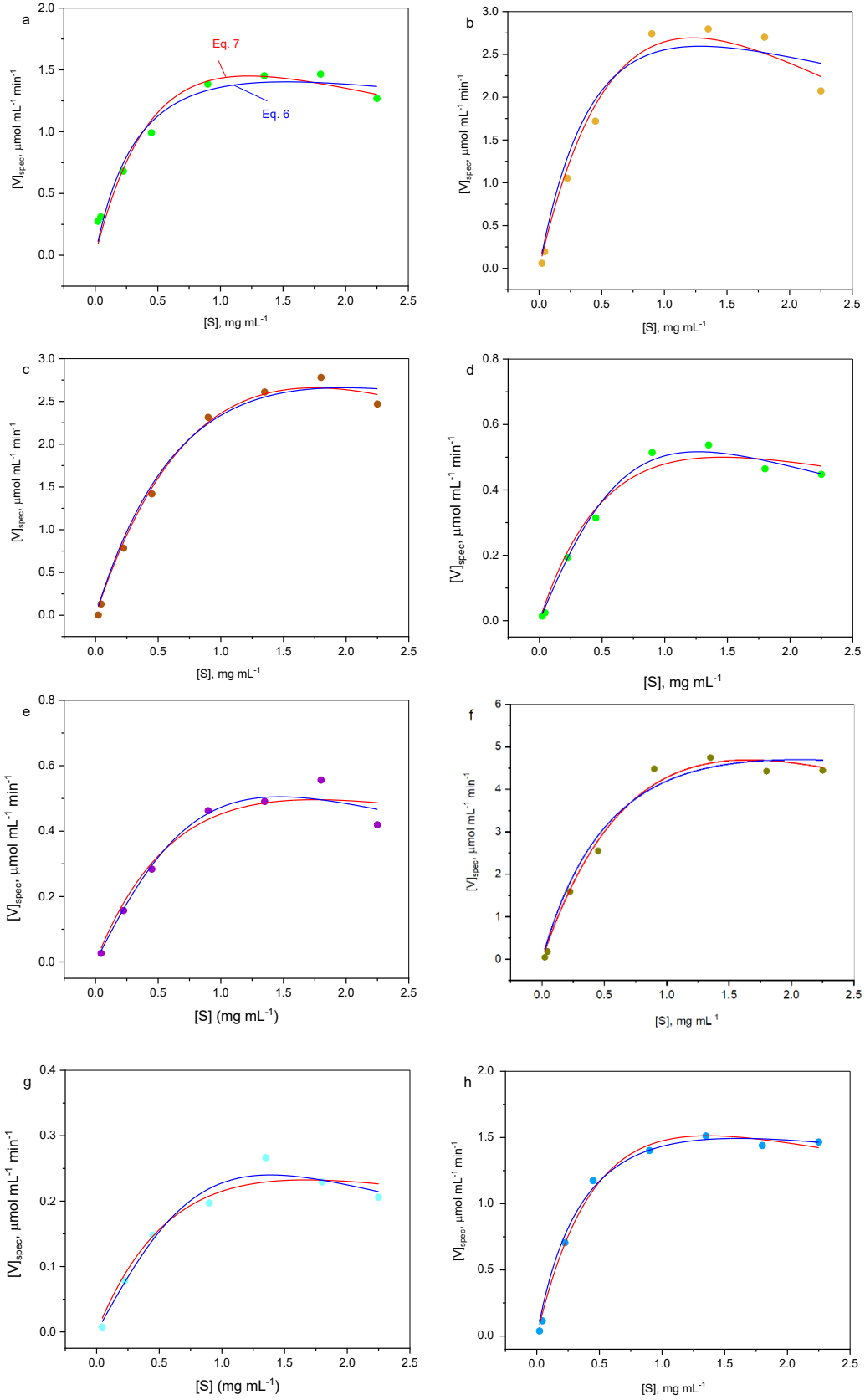


Figure 5.10: Corresponding fits obtained using Equations (6) and (7): a) free pectinase; b) PeV@PA4, c) PeV@PA4-Fe, d) PeV@PA6, e) PeV@PA6-Fe, f) PeV@PA12, g) PeV@PA12-Fe and h) PeV@PA612.

Table 5.1: Kinetic parameters estimated for PeV and the seven PeV@PA catalytic conjugates.

Biocatalyst	Parameters	Equation 5 (MM)	Equation 6 (SI)	Equation 7 (DE)
Free PeV	V_{max}	1.956 ± 0.024	2.182 ± 0.071	1.933 ± 0.001
	K_m	0.423 ± 0.009	0.423 ± 0.043	0.446 ± 0.041
	K_i	≈ 3.0**	5.520 ± 0.850	5.656 ± 0.687
	Adj, R^2	0.995*	0.958	**0.997**
PeV@PA4	V_{max}	5.672 ± 0.020	9.364 ± 0.014	5.592 ± 0.101
	K_m	0.752 ± 0.010	1.444 ± 0.035	0.720 ± 0.020
	K_i	2.5 - 3.0	1.920 ± 0.060	4.838 ± 0.304
	Adj, R^2	0.989*	0.965	**0.994**
PeV@PA4-Fe	V_{max}	4.193 ± 0.027	5.387 ± 0.015	5.981 ± 0.164
	K_m	0.662 ± 0.012	0.695 ± 0.012	0.684 ± 0.027
	K_i	2.0 - 3.0	2.390 ± 0.025	2.536 ± 0.100
	Adj, R^2	0.977*	**0.981**	**0.985**
PeV@PA6	V_{max}	4.669 ± 0.020	5.568 ± 0.005	7.679 ± 0.170
	K_m	0.863 ± 0.009	0.887 ± 0.002	0.868 ± 0.050
	K_i	≈ 2.5	2.359 ± 0.021	2.236 ± 0.131
	Adj, R^2	0.995*	0.988	**0.995**
PeV@PA6-Fe	V_{max}	5.100 ± 0.020	6.136 ± 0.003	6.133 ± 0.644
	K_m	1.222 ± 0.008	1.297 ± 0.002	0.995 ± 0.020
	K_i	≈ 2.5 – 3.0	3.035 ± 0.060	3.491 ± 0.554
	Adj, R^2	0.995*	**0.998**	0.984
PeV@PA12	V_{max}	8.666 ± 0.019	8.335 ± 0.016	8.408 ± 0.196
	K_m	1.010 ± 0.007	0.869 ± 0.032	0.799± 0.030
	K_i	≈ 2.5	5.323 ± 0.066	4.354 ± 0.226
	Adj, R^2	0.988*	**0.990**	**0.990**
Pev@PA12-Fe	V_{max}	1.872 ± 0.070	2.217 ± 0.040	2.395 ± 0.040
	K_m	0.820 ± 0.020	0.855 ± 0.030	0.821 ± 0.019
	K_i	≈ 2.5	3.737 ± 0.021	3.308 ± 0.167
	Adj, R^2	0.976*	**0.993**	**0.994**
PeV@PA6-12	V_{max}	1.931 ± 0.043	2.254 ± 0.020	1.924 ± 0.020
	K_m	0.372 ± 0.022	0.454 ± 0.010	0.448 ± 0.020
	K_i	≈ 5.0	5.708 ± 0.083	7.516 ± 0.539
	Adj, R^2	0.966*	**0.990**	**0.993**

[a] Estimations for V_{max} (µmol mL^{-1} min^{-1}) and K_m (mg mL^{-1}) from the linear part of the double reciprocal Lineweaver-Burk plot (Equation 8, Section 2.7). K_i (mg mL^{-1}), estimation from Equation 21. The final V_{max}, K_m and K_i are determined after fitting of the estimates to Equation 6 and 7.

To identify the model that best describes the experimental data, the coefficient of determination (R^2) was evaluated. Equation 7 provided the best fit for the PeV, PeV@PA4, and PeV@PA6, suggesting that these biocatalysts exhibit a combination of diffusion-controlled substrate supply and substrate inhibition effects. In contrast, Equation 6, which does not account for diffusion limitations, provides more suitable fit for PeV@PA6-Fe. For the remaining complexes, both models yielded comparable fits, producing similar V_{max}, K_m and K_i values. These differences are likely

related to variations in particle morphology and support structure. As shown in Table 5.1, the PeV@PA612 conjugate (Ki = 7.5) is notably more resistant to inhibition compared to the free PeV reference (Ki =5.7). On the other end of the range, the PeV@PA4-Fe and PeV@PA6 conjugates are more easily inhibited, with Ki values ranging from 2.2 to 2.6. The Ki values for the remaining samples fluctuate between 3.5 and 4.8, which is close to but still below the value for the free enzyme.

The catalytic efficiency (CE) of these systems can also be obtained using the following equation:

$$CE = \frac{V_{max}}{K_m} \quad [22]$$

Catalytic efficiency reflects enzymatic performance, with higher values indicating high catalytic efficiency combined with strong substrate affinity. Figure 5.11 presents the CE and Ki values for all biocatalysts.

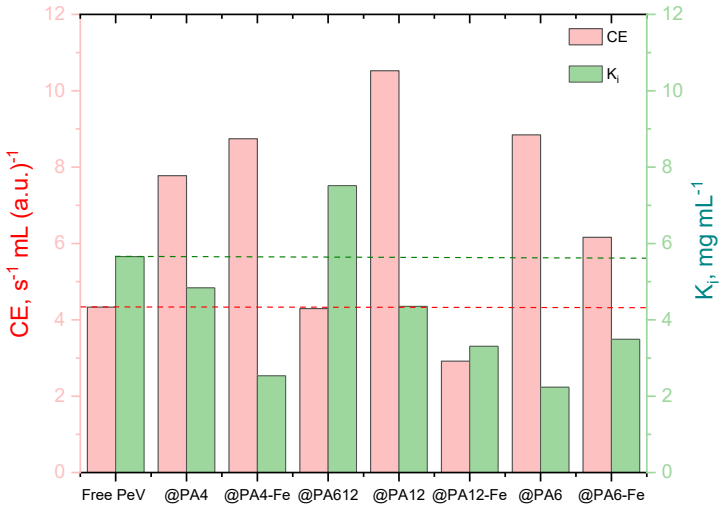


Figure 5.11: Consolidated results from the kinetics studies. CE and K_{k^i}. The dashed lines are guides for the eye highlighting the data of the free enzyme reference. The sample designations are shortened for better visibility.

Considering the importance of CE and K_i values, it can be said that the most suitable complexes for use in larger-scale applications are the catalysts with high CE and K_i, that is, those that combine efficient catalysis with resistance to inhibition at high substrate concentrations. As shown in Figure 5.11, PeV@PA12 is the ideal choice, compared to the free PeV reference, which achieves the highest CE with a sufficiently high K_i. Another promising option is the PeV@PA612 conjugate, featuring the same CE as free PeV but with significantly higher K_i. The next best options

are the PA4-based complexes, PeV@PA4 and PeV@PA4-Fe, followed by the PA6-supported systems, with and without Fe filler. The only system with notably low CE and K_i as compared to the free PeV is PeV@PA12-Fe, where the addition of Fe appears to have compromised both parameters.

In summary, both the morphology and chemical structure of the PA MP support significantly influence the activity and robustness of noncovalently immobilized PeV against the pectin substrate. This insight could guide the design of customized biocatalytic systems for applications in the food industry, particularly for controlling pectin levels.

5.6. Application in rosé must clarification

Based on catalytic performance in terms of activity and kinetics, the PeV@PA complexes were evaluated in the clarification of real rosé must samples containing pectin concentrations of 2.0 mg mL^{-1}. This value is significantly above the threshold concentration of 1.2 mg mL^{-1}, above which inhibitory effects were observed in the kinetic studies. Clarification experiments were carried out at room temperature (23 °C) under gentle agitation, using 0.15 a.u. of either free or immobilized enzyme, achieved by appropriate selection of the mass of the PeV@PA conjugate. The results of all clarification assays are presented in Figures 5.12a and 5.12b. The visual aspect of must during clarification (0, 60, 180 minutes) are presented in Figure 5.13a, and the visual aspect of must after clarification with free and immobilized complexes are presented in Figure 5.13b.

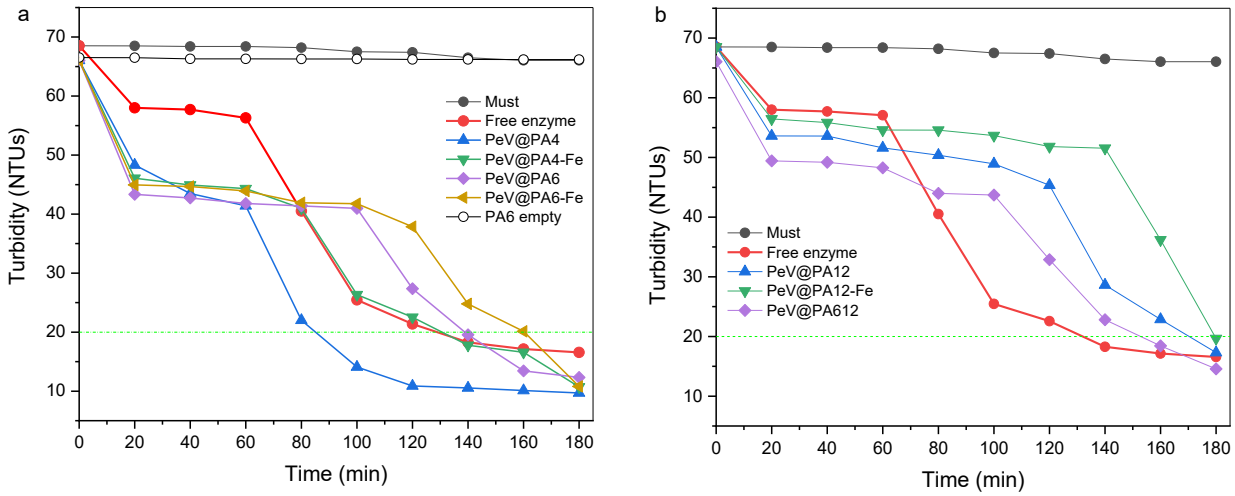


Figure 5.12: Clarification studies with free and immobilized pectinase preparation. a) free PeV compared to PA4 and PA6-based PeV@PA complexes; b) free PeV compared to PA12-based PeV@PA complexes. The dashed lines indicate the level of 20 NTUs, below which the must is considered completely clarified, i.e., not containing pectin.

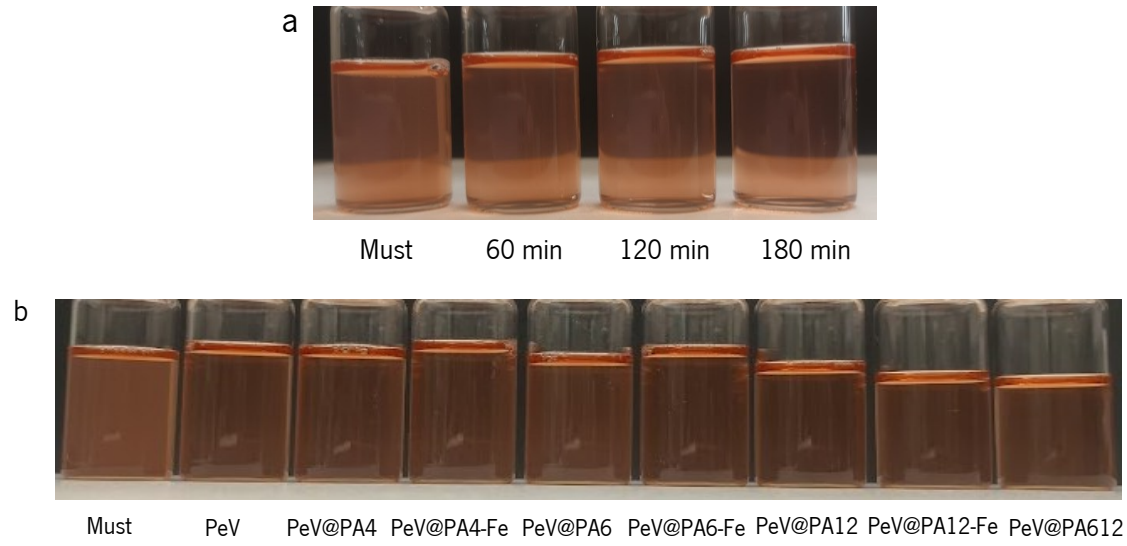


Figure 5.13: Visual aspects of the rosé must during clarification with PeV@PA12 (a). b) Visual aspects of must before and after clarification.

As shown in Figure 5.12a, in the absence of enzymatic treatment, including in the presence of neat PA6 microparticles, the initial turbidity remained constant at approximately 70 NTU throughout the experiment. During the first hour of clarification, all immobilized complexes exhibited faster turbidity reduction than the free PeV, which reached the target turbidity of 20 NTU after approximately 2 hours. The PeV@PA4-Fe complex followed a similar trend, while PeV@PA6 and PeV@PA6-Fe reached 20 NTU after approximately 160 minutes. Notably, the PeV@PA4 complex showed the highest clarification efficiency, reaching the target turbidity in only 80 minutes. Despite its lower enzyme loading, the enzyme exposure on this support likely allows rapid substrate access at the early stages of the reaction. A comparable turbidity reduction profile was observed for PA12-based complexes (Figure 5.12b). All systems reduced turbidity from 70 to 45 NTU within the first 60 minutes, outpacing the free PeV, the most pronounced initial effect observed for the PeV@PA612 complex. Subsequently, the clarification rate of the immobilized systems slowed slightly, achieving the desired clarity between 160 and 180 minutes. Visual monitoring (Figure 5.13a, b) confirms the NTU data, showing a clear transition from turbid to clarified must.

The results presented in Figure 5.12 are consistent with the kinetic data, confirming that PeV@PA4 and PeV@PA12 serve as faster biocatalysts than the free enzyme. However, under real clarification conditions, factors beyond intrinsic kinetics appear to influence performance significantly. The pulverulent catalytic complexes, depending on the polyamide type, density, and molecular weight, behave differently when introduced into the must, showing either surface

flotation, homogeneous suspension, or rapid sedimentation. These physical effects most likely contribute also to the observed differences in clarification rates.

5.6.1. Pectin test

To validate the efficiency of the clarification process, a pectin test was performed on all samples. It is crucial to ensure that the reduction in turbidity corresponds to the actual breakdown of pectin molecules.

Figure 5.14 displays selected images of the tests. It is possible to observe that the unclarified must shows the formation of some aggregates (flocks) on the wall of the recipient, confirming the presence of pectin. In contrast, samples treated with free PeV, PeV@PA4 and PeV@PA4-Fe remain clear, without any observable flocs.

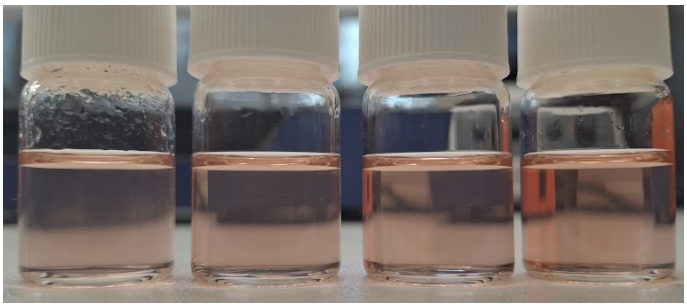


Figure 5.14: Selected images from the pectin test: untreated must, must treated with free enzyme, and PA4-based complexes.

All other samples of must treated with immobilized enzyme remain clear, confirming that turbidity values below 20 NTUs correspond to pectin-free must. That is, all complexes were able to complete the depectinization process under enological conditions.

5.6.2. Color retention of must

The visual aspect of the must is an important factor for its commercialization acceptance, therefore, the color of all samples after clarification was analyzed. Color is typically assessed using three characteristic absorbance bands in the UV/VIS spectrum: 420 nm (yellow), 520 nm (red), and 620 nm (blue) [16,17]. Figure 5.15 presents comparative results for rosé musts treated with the free enzyme and the seven immobilized conjugates.

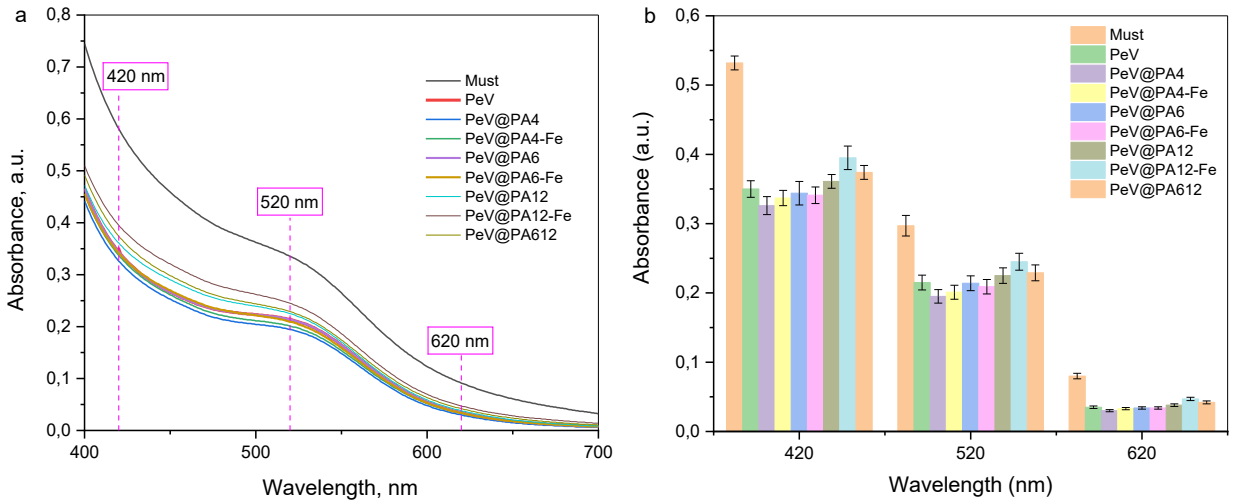


Figure 5.15: Color changes in treated rosé must samples: a) numerical data comparison considering the three spectral intervals at 420, 520 and 620 nm; b) corresponding UV/VIS spectra.

In principle, immobilized enzymes could introduce undesirable color changes, since some compounds might be adsorbed onto the polyamide microparticles. However, Figures 5.15a and 5.15b show that this adsorption did not occur, since the absorbances values at 420 nm, 520 nm, and 620 nm for the immobilized conjugates are statistically comparable to those obtained with the commercially available free enzyme.

Color intensity (I) and hue (T) were calculated using Equations 7 and 8 (Chapter 2), and the results are shown in Figure 5.16. These results confirm that the color variations caused by free PeV are equivalent to those caused by PeV@PA conjugates.

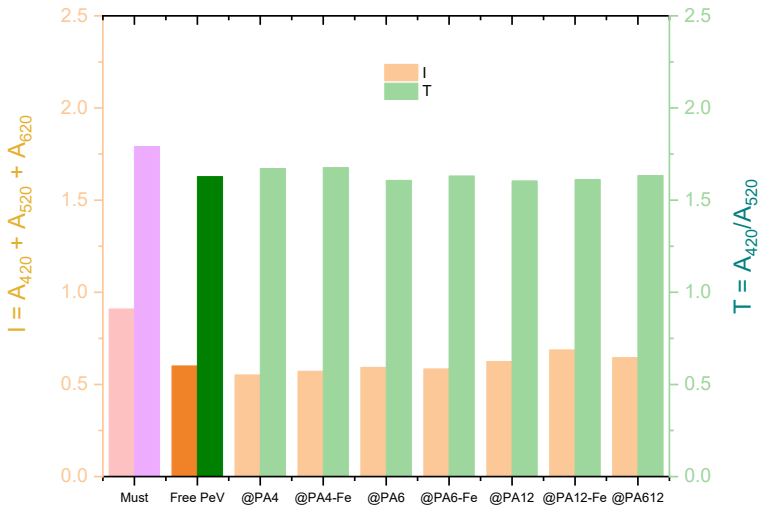


Figure 5.16: Comparison of color intensity (I) and hue (T) parameters of rosé must before and after enzymatic treatment. The sample designations are shortened for better visibility.

In summary, the microparticulate polyamide supports used for non-covalent enzyme immobilization do not induce undesirable color changes in rosé must, demonstrating their suitability for enological clarification applications.

5.7. Multiple use of PeV@PA conjugates

The reusability of PeV@PA complexes was evaluated using two complementary approaches: (i) clarification of rosé must; and (ii) enzymatic activity assays.

The PeV@PA4 and PeV@PA6 complexes, as well as the copolymer PeV@PA612, were reused in three consecutive clarification cycles (Figure 5.17). In all cases, the complexes successfully reduced turbidity to values below 20 NTU. However, the time required to reach that turbidity progressively increased with each reuse cycle: approximately 3 hours in the first cycle (red dots, black squares, and pink triangles in Figure 5.17a and 5.17b), 14 hours in the second cycle (blue and green triangles and brown circles), and 32 hours in the third cycle (yellow triangles and purple diamonds).

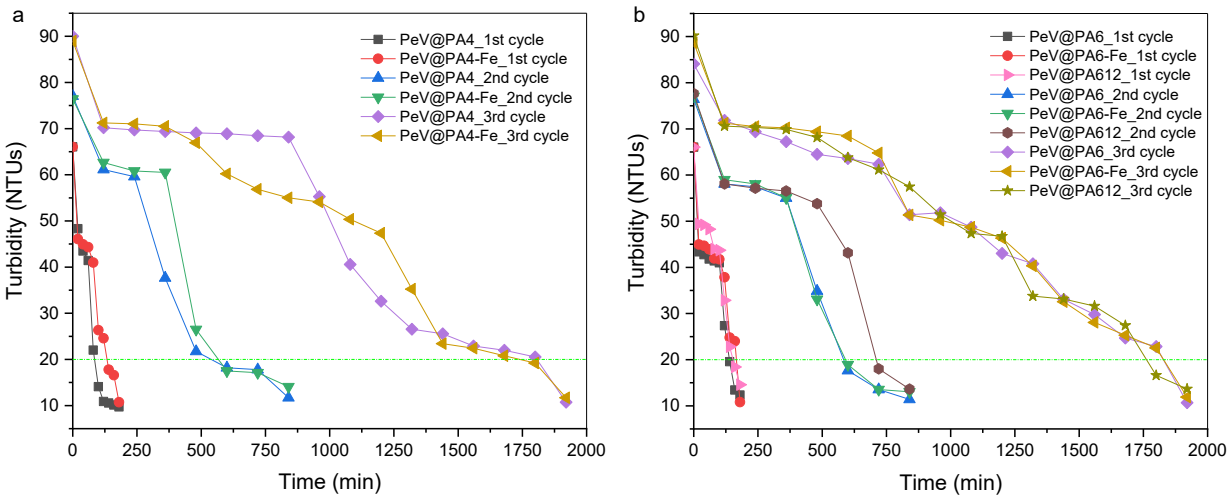


Figure 5.17: Clarification studies of rosé must over multiple reuse cycles: (a) PeV@PA4 and PeV@PA4-Fe; (b) PeV@PA6, PeV@PA6-Fe, and PeV@PA612.

Figure 5.18 presents the reuse of the PeV@PA12 and PeV@PA12-Fe complexes. These systems were successfully applied in two consecutive clarification cycles under the same experimental conditions as the other complexes (first cycle: red dots and black squares; second cycle: yellow triangles and purple rhombuses). As seen in the next Figure 5.18, a third reuse cycle could not be

performed for the PeV@PA12 systems due to their morphology, low density, and lack of magnetic properties, which hindered their effective recovery after the second cycle.

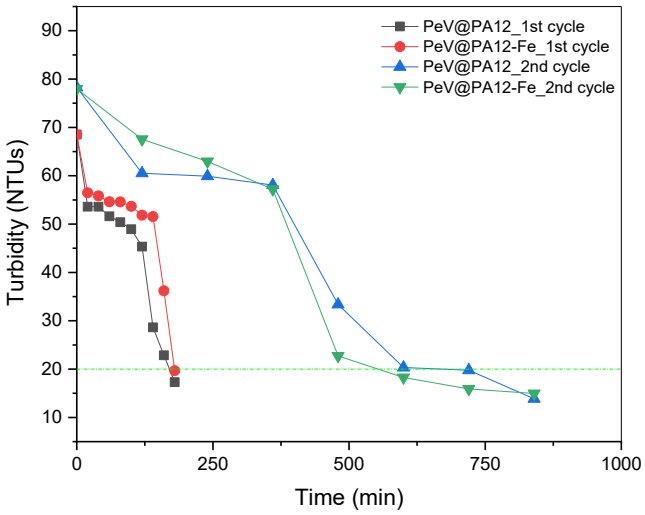


Figure 5.18: Clarification studies of rosé must with Pec@PA12 systems in two different clarification cycles.

The results show that the immobilized enzyme can be used in multiple consecutive clarification cycles of rosé must. The reduced relative activity observed during the second and third clarification cycles most likely results from the adsorption of reaction byproducts on the surface of the catalytic complexes. This surface fouling can hinder substrate diffusion to the enzyme's active sites, thereby prolonging the clarification process. Nevertheless, at the industrial scale, clarification times of 14 or even 32 hours are still considered acceptable.

The reusability of the immobilized enzymes was analyzed by performing consecutive cycles of enzymatic activity, as described in Section 2.10 in Chapter 2. The assays were carried out at 50 °C and pH 3.8 using citric pectin as a substrate. The residual activity after each cycle is presented in Figure 5.19.

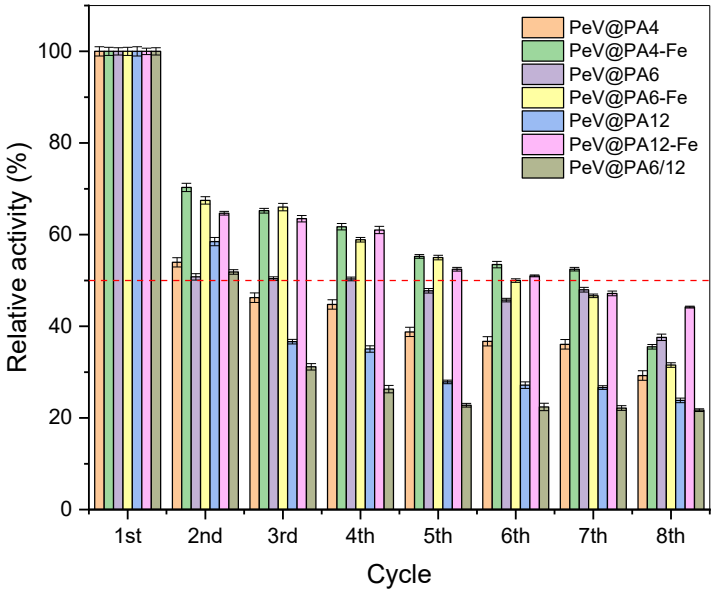


Figure 5.19: Relative activity of immobilized PeV@PA pectinolytic catalysts over eight application cycles. The red dashed line indicates 50% relative activity. The initial activity of each complex was set to 100%.

After the first reuse cycle, the Fe-containing systems (PeV@PA4-Fe, PeV@PA6-Fe, and PeV@PA12-Fe) retained 66–70% of their initial activity, while the non-Fe systems stabilized at approximately 50–55%. This higher activity retention probably results from the easier and more complete removal of the Fe-containing systems using a constant magnet, which minimizes catalyst loss and indirectly supports higher relative activity. The three magnetically susceptible systems maintain activity above or around 50% through the 7th cycle, indicating strong potential for large-scale reuse. Among the non-Fe systems, PeV@PA6 shows the best performance. In all PeV@PA conjugates, possible causes of activity decline may include also enzyme leaching and/or surface contamination of the support particles by pectin degradation products.

After the final reusability cycle, the used PeV@PA particles can be regenerated by boiling in distilled water to remove accumulated contaminants, followed by drying and reuse in a new immobilization process.

5.8. Storage stability of PeV@PA conjugates

The storage stability of PeV@PA complexes was evaluated by monitoring their enzymatic activity over a one-month period at 4°C, as described in Section 2.11, Chapter 2. As shown in Figure 5.20, all immobilized catalysts—except PeV@PA612 and PeV@PA12—exhibited stability comparable to

that of the free enzyme by the end of the study. The lower stability observed for PeV@PA612 and PeV@PA12 may be attributed to weaker enzyme–support interactions or increased enzyme leaching over time, likely due to their porous, sponge-like surface morphology which may not retain the protein as effectively as other supports. Notably, PeV@PA4 and PeV@PA4-Fe showed higher residual activity than the free enzyme up to the third week of storage. This suggests that the higher density of hydrogen bonds characteristic of the PA4 matrix may provide a protective microenvironment, stabilizing the enzyme against gradual deactivation.

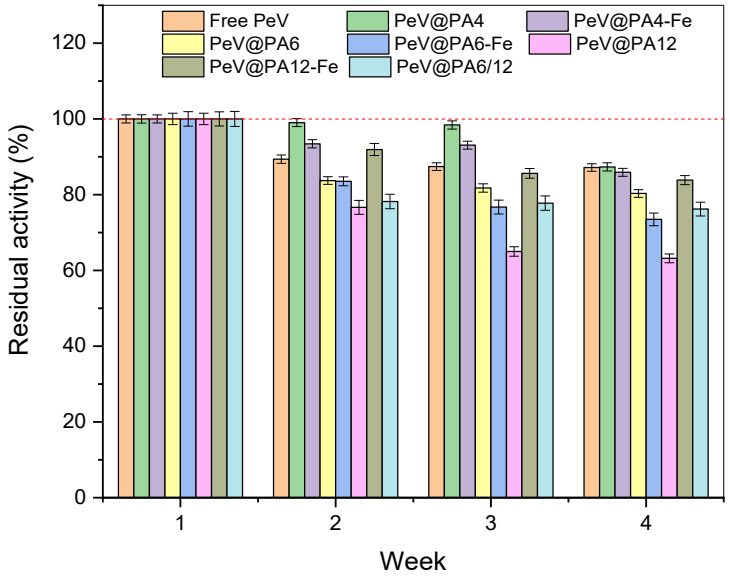


Figure 5.20: Storage stability of immobilized PeV@PA pectinolytic catalysts over four weeks at 4°C. Initial activity is normalized to 100% for each complex. Error bars represent the standard deviation from three independent measurements.

Based on these results, the use of immobilized pectinolytic systems is recommended within 2–3 weeks after immobilization to maximize their performance. This level of stability of the catalytic complexes is not much different from that of the free PeV and considered highly relevant for industrial applications.

5.9. Conclusions

This chapter describes the non-covalent immobilization of a commercial pectinase formulation onto seven distinct polyamide microparticle supports synthesized by AAROP. These supports differ in chemical structure, composition, shape, size, and surface topology. The immobilization strategy

consisted of a simple, one-pot incubation of the supports in buffered aqueous enzyme solutions, without the use of hazardous reagents, rendering the process compatible with food industry requirements.

The results demonstrate a pronounced influence of polyamide type on enzyme immobilization yield and on the catalytic performance of the resulting PeV@PA conjugates. Comparative kinetic analyses revealed that, except for PeV@PA12-Fe, all immobilized systems exhibited higher catalytic efficiency than the free enzyme. This behavior can be attributed to differences in the chemical structure and surface morphology of the polyamide supports.

At the laboratory scale, all polyamide-immobilized pectinase biocatalysts enabled effective clarification of real rosé must within industrially relevant time frames, reaching complete clarification within 80–180 minutes during the first cycle. Most immobilized systems could be reused in second and third consecutive clarification cycles, with clarification times extending to approximately 15 and 30 hours respectively, which remain acceptable for industrial processing. Furthermore, all conjugates sustained up to seven consecutive clarification cycles, with most systems retaining around 50% of their initial activity.

Importantly, all PA MP supports did not induce undesirable color changes in the must, as confirmed by UV/VIS measurements at the characteristic wavelengths for wine color evaluation. In addition, all immobilized systems (except for Pec@PA12), retained up to 75% of their initial activity after four weeks of storage, displaying stability comparable to that of the free pectinase preparation.

Overall, these results highlight the critical role of polyamide structure and morphology in tuning the performance of non-covalently immobilized pectinases, providing clear guidelines for the design of efficient and reusable biocatalysts for enological applications.

5.10. References

[1] Oliveira, S. C.; Araújo, S. M.; Dencheva, N. V.; Denchev, Z. Z. Polyamide microparticles with immobilized enological pectinase as efficient biocatalysts for wine clarification: The role of the polymer support. *Molecules* **2025**, *30*, 114. https://doi.org/10.3390/molecules30010114.

[2] Martín, M. C.; López, O. V.; Ciolino, A. E.; Morata, V. I.; Villar, M. A.; Ninago, M. D. Immobilization of enological pectinase in calcium alginate hydrogels: A potential biocatalyst for winemaking. *Biocatal. Agric. Biotechnol.* **2019**, *18*, 101091. https://doi.org/10.1016/j.bcab.2019.101091.

[3] Ottone, C.; Romero, O.; Aburto, C.; Illanes, A.; Wilson, L. Biocatalysis in the winemaking industry: Challenges and opportunities for immobilized enzymes. *Compr. Rev. Food Sci. Food Saf.* **2020**, *19*, 595–621. https://doi.org/10.1111/1541-4337.12538.

[4] Omelková, J.; Rexová-Benková, L.; Kubánek, V.; Veruovič, B. Endopolygalacturonase immobilized on a porous poly(6-caprolactam). *Biotechnol. Lett.* **1985**, *7*, 99–104. https://doi.org/10.1007/BF01026676.

[5] Rexová-Benková, L.; Omelková, J.; Veruovič, B.; Kubánek, V. Mode of action of endopolygalacturonase immobilized by adsorption and by covalent binding via amino groups. *Biotechnol. Bioeng.* **1989**, *34*, 79–85. https://doi.org/10.1002/bit.260340111.

[6] Shukla, S.; Saxena, S.; Thakur, J.; Gupta, R. Immobilization of polygalacturonase from *Aspergillus niger* onto glutaraldehyde activated Nylon-6 and its application in apple juice clarification. *Acta Aliment.* **2010**, *39*, 277–292. https://doi.org/10.1556/AAlim.39.2010.3.4.

[7] Ben-Othman, S.; Rinken, T. Immobilization of pectinolytic enzymes on nylon 6/6 carriers. *Appl. Sci.* **2021**, *11*, 4591. https://doi.org/10.3390/app11104591.

[8] Lozano, P.; Manjón, A.; Iborra, J. L.; Gálvez, D. M. Characteristics of the immobilized pectin lyase activity from a commercial pectolytic enzyme preparation. *Acta Biotechnol.* **1990**, *10*, 531–539. https://doi.org/10.1002/abio.370100613.

[9] Cappannella, E.; Benucci, I.; Lombardelli, C.; Liburdi, K.; Bavaro, T.; Esti, M. Immobilized lysozyme for the continuous lysis of lactic bacteria in wine: Bench-scale fluidized-bed reactor study. *Food Chem.* **2016**, *210*, 49–55. https://doi.org/10.1016/j.foodchem.2016.04.089.

[10] Diano, N.; Grimaldi, T.; Bianco, M.; Rossi, S.; Gabrovska, K.; Yordanova, G.; et al. Apple juice clarification by immobilized pectolytic enzymes in packed or fluidized bed reactors. *J. Agric. Food Chem.* **2008**, *56*, 11471–11477. https://doi.org/10.1021/jf8019437.

[11] Sattler, R.; Danke, V.; Beiner, M. Long chain polyamides: Influence of methylene sequence length and external forces on structural features. *Macromol. Chem. Phys.* **2023**, *224*, 2200433. https://doi.org/10.1002/macp.202200433.

[12] Zhang, Y.; Wang, M.; Zhang, D.; Wang, Y.; Wang, L.; Qiu, Y.; et al. Crystallization and performance of polyamide blends comprising polyamide 4, polyamide 6, and their copolymers. *Polymers* **2023**, *15*, 3399. https://doi.org/10.3390/polym15163399.

[13] Kohutiar, M.; Kakošová, L.; Krbata, M.; Janík, R.; Fekiač, J. J.; Breznická, A.; et al. Comprehensive review: Technological approaches, properties, and applications of pure and reinforced polyamide 6 (PA6) and polyamide 12 (PA12) composite materials. *Polymers* **2025**, *17*, 442. https://doi.org/10.3390/polym17040442.

[14] Miller, G. L. Use of dinitrosalicylic acid reagent for determination of reducing sugar. *Anal. Chem.* **1959**, *31*, 426–428. https://doi.org/10.1021/ac60147a030.

[15] Gummadi, S. N.; Panda, T. Analysis of kinetic data of pectinases with substrate inhibition. *J. Microbiol. Biotechnol.* **2003**, *13*, 332–337.

[16] Cleland, W. W. Statistical analysis of enzyme kinetic data. *Methods Enzymol.* **1979**, *63*, 103–138. https://doi.org/10.1016/0076-6879(79)63008-2.

[17] International Organization of Vine and Wine (OIV). *Compendium of International Methods of Wine and Must Analysis—Chromatic Characteristics*; OIV: Paris, France, **2022**. Available online: https://www.oiv.int (accessed on 16 October 2024).

CHAPTER 6

PA6-based biocatalyst: Influence of the immobilization strategy

Previous chapters demonstrated that pulverulent synthetic PA MPs are promising supports for the immobilization of industrially relevant pectinolytic enzyme preparations. These porous PA MPs can be synthesized via AAROP of lactams, and the incorporation of Fe into the polyamide matrix imparts magnetic susceptibility to the resulting enzyme conjugates. This feature facilitates their recovery from the reaction medium and enhances reusability, frequently accompanied by improved catalytic performance. So far in this thesis, enzyme immobilization has been carried out exclusively by physical adsorption. This approach was dictated by the intended application of the synthesized polyamide-based biocatalysts for the clarification of industrial wine musts supplied by Sogrape Vinhos Lda., Portugal. The company also provided a specific commercial pectinase preparation for this purpose, the exact composition of which is not fully disclosed.

Accordingly, the objective of this chapter is to compare different enzyme immobilization strategies applied to the same neat and Fe-containing PA6 microparticles. As demonstrated in the previous chapter, these supports combine all the essential properties required for potential industrial application. To ensure a reliable and well-defined basis for comparison, a lyophilized pectinase purchased from Aldrich was used.

6.1. Introduction

As already discussed previously, pectinase is an essential enzyme in wine must clarification, whereby the enological enzymes are mostly used in their free form. This approach, however, impedes enzyme recovery and reuse, leading also to its remaining in the final product [1].

Immobilization offers a robust strategy to overcome these and other imitations of the free enzymes [2]. Polyamides have attracted significant interest as immobilization supports for biomolecules due to their intramolecular –CO-NH– groups and terminal NH_2 and COOH groups, which enable effective H-bond formation or covalent bonding [3]. Physical immobilization by entrapment or adsorption, as well as covalent binding to a support or enzyme crosslinking are the common methods used for the immobilization of pectinase [4].

Specifically, different types of pectinases (e.g., polygalacturonase) have been immobilized onto polyamides via covalent immobilization, using glutaraldehyde (GA) as an activating agent [5-8]. Moreover, GA is also used as a cross-linker for the synthesis of the so-called CLEAs (cross-linked enzyme aggregates) widely used in biotechnology. However, the use of GA is challenging as it is considered a hazardous substance that can undergo multiple molecular transformations in ambient conditions. It is soluble in water, alcohols, organic solvents and has two reactive groups that are

capable of conjugating spontaneously with amine, amide, and thiol groups (Figure 6.1) [9]. GA is also not suitable for direct contact with foods and beverages [10].

It is most commonly employed at pH 7, where the enzyme's amino groups are sufficiently deprotonated to ensure a faster and more efficient reaction [11].

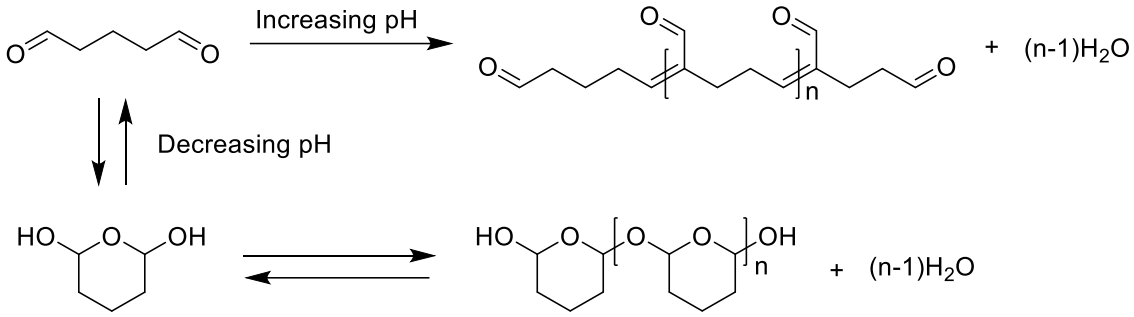


Figure 6.1: Different molecular forms of GA in an aqueous medium. Adapted from [9].

Additionally, physical adsorption is known as a simpler, non-invasive alternative that avoids chemical modifications of the enzyme, potentially preserving its native catalytic activity [12]. The results from the previous Chapter 5 confirmed this general concept in the case of pectinolytic commercial preparations and identified PA6 MP (both neat and Fe-containing) as the most promising supports.

This chapter evaluates comparatively three immobilization strategies: direct cross-linking, covalent bonding, and physical adsorption of commercial pectinolytic preparations on PA6 MPs. The objective is to determine the most effective method balancing immobilization yield, catalytic activity, and reusability of the resulting catalytic conjugates.

6.2. Enzyme immobilization

6.2.1. Covalent immobilization

Polyamide 6 microparticles, with and without Fe (PA6 and PA6-Fe MPs), were synthesized by AAROP according to the procedure described in Section 2.3.1, Chapter 2. The resulting microparticles were used as a support for the covalent immobilization of lyophilized pectinase (PeL) as follows:

- PA6/PA6-Fe MPs (100 mg) were partially hydrolyzed with hydrochloric acid (3 M, 5 mL) for 2 hours, followed by washing with distilled water (1 mL, once) and phosphate buffer

(0.1 M, pH 7; 1 mL, twice) (Figure 6.2a). The purpose was to provide a higher concentration of terminal amino groups that would subsequently react with glutaraldehyde.

- The hydrolyzed MPs were reacted with a glutaraldehyde solution (5 mL, 3% v/v in 0.1 M phosphate buffer, pH 7) for 20, 40, and 60 min. The glutaraldehyde-modified MPs were then washed with phosphate buffer (0.1 M, pH 7; 1 mL, twice) (Figure 6.2b).
- A pectinase solution (5 mL, 1 mg/mL in distilled water) was added to the glutaraldehyde-modified MPs (100 mg) and stirred at room temperature (22°C) for 24 hours (Figure 6.2c).

The chemical reactions that lead to the anchoring of GA to PA6 MP and its bridging with pectinase are presented in Figure 6.2 below.

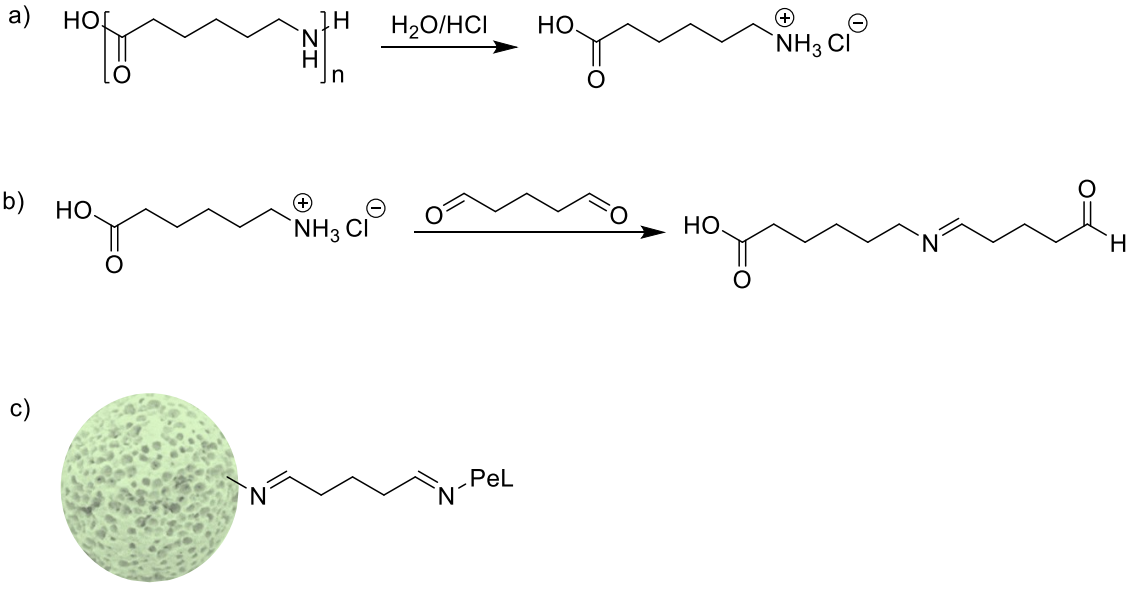


Figure 6.2: Schematic representation of the covalent immobilization steps: a) acid hydrolysis of PA6/PA6-Fe MPs; b) surface activation with glutaraldehyde; c) covalent enzyme attachment.

6.2.2. Adsorption immobilization

PA6 and PA6-Fe MPs were used as supports for the immobilization of lyophilized pectinase by physical adsorption. For this purpose, a pectinase solution (1 mg/mL in distilled water) was added to the MPs (100 mg) and incubated under gentle orbital shaking at room temperature (22°C) for 24 hours (Figure 6.3).

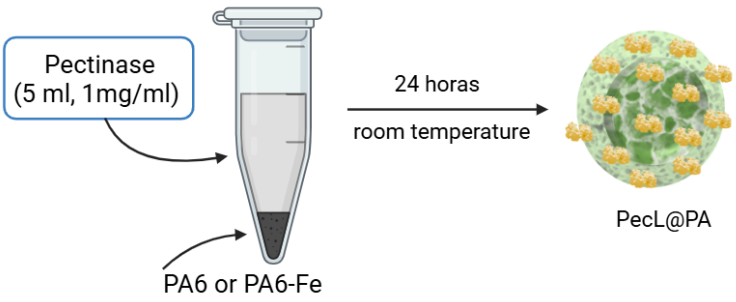


Figure 6.3: Schematic representation of pectinase immobilization by physical adsorption onto PA6/PA6-Fe MPs.

Eight types of immobilizations were performed, 6 covalent and 2 by absorption. Table 6.1 summarizes the designation and composition of the complexes formed.

Table 6.1: Designation of samples obtained by immobilization of lyophilized pectinase.

Sample designation	**Description**
PeL-c-PA6	PeL covalently immobilized on PA6
PeL-c-PA6$_{20}$	PeL covalently immobilized on PA6 (20 min GA activation)
PeL-c-PA6$_{40}$	PeL covalently immobilized on PA6 (40 min GA activation)
PeL-c-PA6$_{60}$	PeL covalently immobilized on PA6 (60 min GA activation)
PeL-c-PA6-Fe$_{20}$	PeL covalently immobilized on PA6-Fe (20 min GA activation)
PeL-c-PA6-Fe$_{40}$	PeL covalently immobilized on PA6-Fe (40 min GA activation)
PeL-c-PA6-Fe$_{60}$	PeL covalently immobilized on PA6-Fe (60 min GA activation)
PeL@PA6	PeL immobilized by physical adsorption on PA6
PeL@PA6-Fe	PeL immobilized by physical adsorption on PA6-Fe

The different activation times (20, 40, and 60 min) were selected to evaluate the influence of glutaraldehyde surface density on the immobilization yield and enzymatic activity.

6.3. Protein estimation

A direct UV/VIS spectrophotometric method was used to determine the amount of immobilized pectinase on PA6 and PA6-Fe MPs. The measurements were performed at 277 nm, corresponding to the absorption of aromatic amino acid residues, such as tryptophan and tyrosine, present in the enzyme. As previously justified, this method provides reliable quantitative data for protein

quantification, with standard deviations between 3–5%, in contrast to indirect assays like Bradford or BCA, which often exhibit higher variability (up to 15%).

The results of the immobilization process, including the spectral changes observed in the supernatants and the calculated immobilization yields, are presented in Figure 6.4.

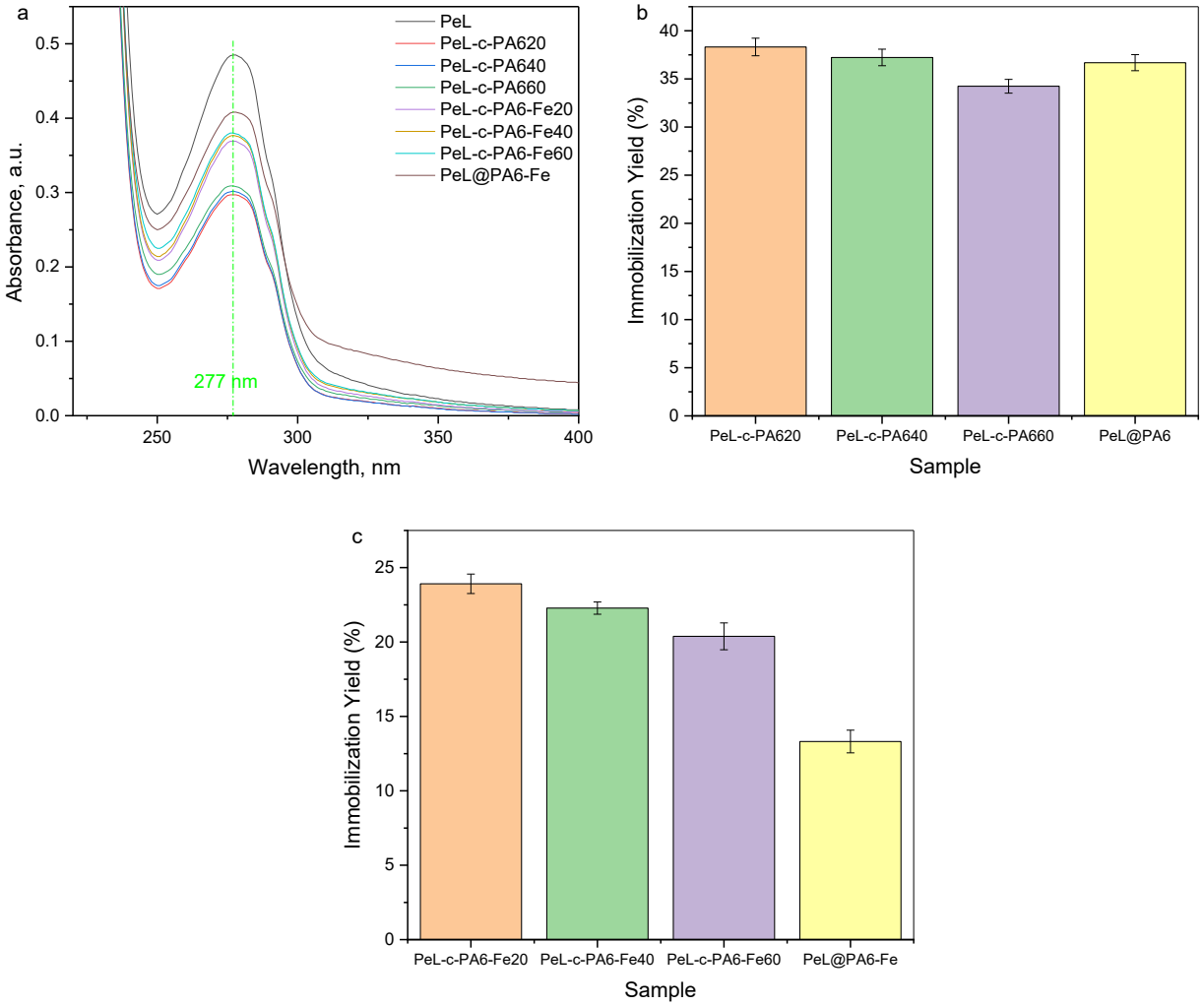


Figure 6.4: Quantification of the Pectinase immobilization: a) UV/VIS spectra of the pectinase solutions before and after immobilization; b) Immobilization efficiency for PeL-c-PA6 and PeL@PA6. c) Immobilization efficiency for PeL-c-PA6-Fe and PeL@PA6-Fe. Standard deviations were calculated from two independent trials.

Based on Figures 6.4b and 6.4c, the covalent immobilization yield ranged between 20–38%, while the adsorption yield was between 13–37%, indicating an insignificant increase in yield for the covalent method. In the case of covalent immobilization, three different activation times (20, 40, and 60 min) were evaluated to determine if the amount of glutaraldehyde influenced the enzyme loading. Figures 6.4b and 6.4c show that the highest immobilization yield was achieved with

microparticles activated for 20 minutes (PeL-c-PA6$_{20}$ and PeL-c-PA6-Fe$_{20}$). Increasing the activation time resulted in a lower amount of immobilized enzyme, suggesting that a higher surface density of glutaraldehyde does not favor immobilization.

Regarding adsorption immobilization, it was observed that PA6-Fe presented a lower immobilization yield. Comparing the two immobilization types, the adsorption yield for PA6 was 37%. This value is approximately equal to that of covalent immobilization with 20 minutes of activation (PeL-c-PA6$_{20}$). Thus, it can be stated that the additional hydrolysis and activation steps do not offer significant improvements in immobilization yield.

For PA6-Fe, covalent immobilization showed an increase of approximately 10% compared to adsorption, which is not considered a significant improvement. As discussed in Chapter 3, PA6 and PA6-Fe microparticles are highly porous, and the Fe is located within the PA6 matrix. These pores are critical for adsorption immobilization because, as demonstrated in Chapter 5, the enzyme enters the pore structure, which provides a high internal surface area for binding. GA is a small compound that easily penetrates these pores. It reacts readily in aqueous solutions, existing in a mixture of various molecular forms [9]. Therefore, the observed decrease in yield with longer activation times suggests that the various molecular forms of glutaraldehyde within the pores may have created a diffusion barrier for pectinase. Furthermore, since Fe is predominantly located within the microparticle matrix, its influence on surface adsorption is limited. However, the slight increase in yield for covalent immobilization on PA6-Fe suggests that the acid hydrolysis step may alter surface accessibility, potentially exposing additional binding sites.

6.4. Determination of pectinase activity

The enzymatic activity of free and immobilized pectinase (via covalent and adsorption immobilization) was determined using the DNS method, as described in detail in Section 2.6.1 (Chapter 2). Figure 6.5 presents the absolute and specific activities of the free enzyme and the resulting complexes.

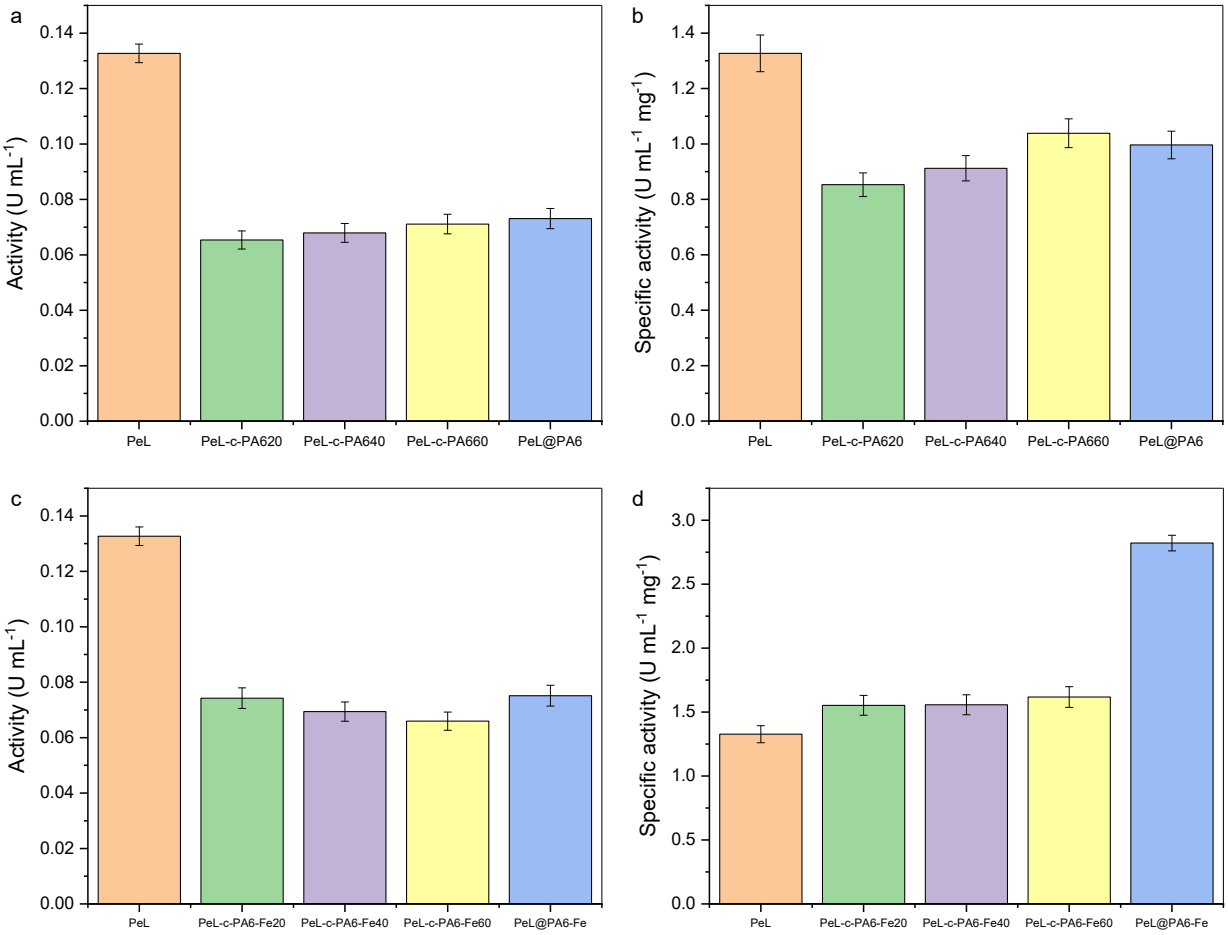


Figure 6.5: Enzymatic activity of PeL-c-PA6 and PeL@PA6 conjugates compared to free PeL: a) absolute activity of PA6-based complexes; b) specific activity of PA6-based complexes; c) absolute activity of PA6-Fe-based complexes; d) specific activity of PA6-Fe-based complexes.

The absolute activity of both PeL-c-PA6 and PeL@PA6 conjugates was approximately half that of the free enzyme. For covalent immobilization on PA6, the activity slightly increased with glutaraldehyde activation time (up to 60 minutes), while adsorption showed slightly higher values. In contrast, PA6-Fe-based complexes followed a different trend, where longer activation times resulted in lower activity. For these supports, the activity achieved by adsorption was similar to that of covalent immobilization with 20 minutes of activation. However, as these differences are not statistically significant, it can be stated that covalent and physical immobilization yielded comparable absolute activities.

When the results are normalized to protein content (specific activity, Figures 6.5b and 6.5d), the immobilized complexes exhibited distinct behaviors. PA6-based complexes showed slightly lower specific activity than the free enzyme, a trend consistent with previous studies on pectinase

covalently immobilized on PA6 [4]. On the other hand, the enzyme covalently immobilized on PA6-Fe demonstrated specific activity similar to the free enzyme. Notably, the enzyme immobilized by adsorption on PA6-Fe exhibited a specific activity up to 3-fold higher than that of the free preparation, highlighting a significant advantage of non-covalent immobilization. This complex exhibits the lowest immobilization yield. This smaller amount of enzyme suggests that the immobilized enzymes are not aggregated; each enzyme remains in its most active conformation with active sites accessible to the substrate. This immobilization method likely preserves the native conformation of pectinase.

These results indicate that physical adsorption onto iron-containing polyamide microparticles is not only the simplest method but also the most effective for preserving the catalytic efficiency of pectinase.

6.5. Reusability of immobilized pectinase

One of the primary advantages of covalent immobilization is the reduction of enzyme leaching into the reaction medium [13]. This stability can be evaluated through reusability assays, as covalent bonds are expected to maintain more stable enzymatic activity over multiple cycles compared to physical adsorption. Figure 6.6 presents the relative activity of the immobilized complexes over four consecutive application cycles.

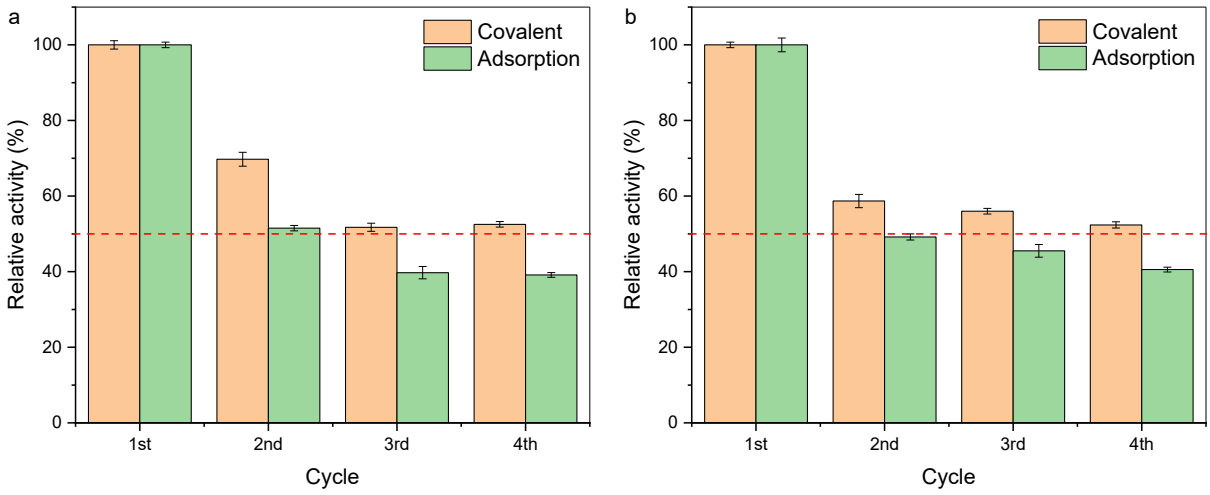


Figure 6.6: Relative activity of immobilized pectinase over four application cycles. a) PeL-c-PA6 and PeL@PA6 b) PeL-c-PA6-Fe and PeL@PA6-Fe. The red dashed line indicates 50% relative activity. The initial activity of each complex was set to 100%.

For the PeL-c-PA6 complex, activity decreased from 100% to 70% after the first reuse, remaining constant at approximately 50% during the third and fourth cycles. In contrast, for PeL@PA6, the activity dropped to 50% after the first reuse and stabilized at 40% in the subsequent cycles. A similar trend was observed for the PA6-Fe-based complexes. For the covalent system (PeL-c-PA6-Fe), activity decreased to approximately 60% after the first cycle and gradually declined to 55% in the final cycle. For PeL@PA6-Fe, the activity dropped to approximately 50% after the first cycle, maintaining 40% of its initial activity by the end of the test. The initial decrease in activity observed from the first to the second cycle in all complexes suggests the leaching of enzyme molecules that were weakly bound to the surface of the microparticles. The stabilization of activity in the remaining cycles (40-55%) indicates that a significant portion of the enzyme remains immobilized on the microparticles (within the porous structure or strongly bound to the support).

These results suggest that some leaching or enzymatic denaturation occurred in both immobilization methods. Although covalent immobilization showed slightly higher residual activity, the difference compared to physical adsorption is not significant. Therefore, considering the complexity of covalent immobilization, physical adsorption continues to have advantages such as its simplicity, lower cost, and reduced preparation time.

The formation of pectinase-based cross-linked enzyme aggregates (CLEAs), i.e., in the absence of a polyamide support, was also investigated using glutaraldehyde as a cross-linking agent at a constant pectinase concentration (0.5 $mg \cdot mL^{-1}$ in H_2O). Different GA concentrations (2.5-10 mM) were tested over a range of pH values; however, no visible precipitation of cross-linked enzyme aggregates was observed under any of the conditions applied.

Enzymatic activity was measured before and after the cross-linking treatment and revealed a pronounced decrease in activity with increasing GA concentration. These results indicate that, in the presence of GA, effective cross-linking of pectinase does not occur. Instead, GA likely induces irreversible conformational changes in the enzyme structure, which negatively affect or block access to the pectinase active site, leading to a loss of catalytic activity.

6.6. Conclusions

This chapter demonstrated that, for the specific pectinase investigated, the formation of CLEA via chemical cross-linking is not feasible, whereas both covalent and physical adsorption immobilization strategies are viable. Covalent immobilization yielded a slightly more stable biocatalyst than physical adsorption, while maintaining a comparable protein loading. Notably, the

PeL@PA6–Fe complex exhibited higher specific activity than the free enzyme and the other immobilized systems, indicating that the enzyme adopts a more stable conformation with active sites readily accessible to the substrate.

With respect to reusability, the covalently immobilized and physically adsorbed biocatalysts displayed very similar stability profiles. Consequently, when differences in processing time, procedural complexity, and cost are taken into account, physical adsorption emerges as the most promising strategy for immobilizing the lyophilized enzyme. This conclusion is further supported by the fact that GA is a hazardous chemical and is not approved for direct use in foods and beverages [9,10].

6.7. References

[1] Martín, M. C.; López, O. V.; Ciolino, A. E.; Morata, V. I.; Villar, M. A.; Ninago, M. D. Immobilization of enological pectinase in calcium alginate hydrogels: a potential biocatalyst for winemaking. *Biocatal. Agric. Biotechnol.* **2019**, *18*, 101091. https://doi.org/10.1016/j.bcab.2019.101091.

[2] Ottone, C.; Romero, O.; Aburto, C.; Illanes, A.; Wilson, L. Biocatalysis in the winemaking industry: challenges and opportunities for immobilized enzymes. *Compr. Rev. Food Sci. Food Saf.* **2020**, *19*, 595–621. https://doi.org/10.1111/1541-4337.12538.

[3] Lehnert, G. Polyamides (PA). *Kunstst. Plast. Eur.* **1998**, *88*, 25–26.

[4] Bié, J.; Sepodes, B.; Fernandes, P. C. B.; Ribeiro, M. H. L. Enzyme immobilization and co-immobilization: main framework, advances and some applications. *Processes* **2022**, *10*, 494. https://doi.org/10.3390/pr10030494.

[5] Shukla, S.; Saxena, S.; Thakur, J.; Gupta, R. Immobilization of polygalacturonase from *Aspergillus niger* onto glutaraldehyde activated Nylon-6 and its application in apple juice clarification. *Acta Aliment.* **2010**, *39*, 277–292. https://doi.org/10.1556/AAlim.39.2010.3.4.

[6] Ben-Othman, S.; Rinken, T. Immobilization of pectinolytic enzymes on nylon 6/6 carriers. *Appl. Sci.* **2021**, *11*, 4591. https://doi.org/10.3390/app11104591.

[7] Pahujani, S.; Kanwar, S. S.; Chauhan, G.; Gupta, R. Glutaraldehyde activation of polymer Nylon-6 for lipase immobilization: enzyme characteristics and stability. *Bioresour. Technol.* **2008**, *99*, 2566–2570. https://doi.org/10.1016/j.biortech.2007.04.042.

[8] Vaillant, F.; Millan, A.; Millan, P.; Dornier, M.; Decloux, M.; Reynes, M. Co-immobilized pectin lyase and endocellulase on chitin and Nylon supports. *Process Biochem.* **2000**, *35*, 989–996. https://doi.org/10.1016/S0032-9592(00)00131-X.

[9] Karunanithy, R.; Holland, T.; Sivakumar, P. Influence of glutaraldehyde's molecular transformations on spectroscopic investigations of its conjugation with amine-modified Fe_3O_4 microparticles. *Langmuir* **2021**, *37*, 5242–5251. https://doi.org/10.1021/acs.langmuir.1c00182.

[10] U.S. Environmental Protection Agency (EPA). Glutaraldehyde: antimicrobials division's risk assessment for issuance of the reregistration eligibility decision (RED) document; EPA: Washington, DC, USA, **2006**. Available online: https://www.regulations.gov/document/EPA-HQ-OPP-2007-0364-0020 (accessed on 12 February 2026).

[11] Fatarella, E.; Spinelli, D.; Ruzzante, M.; Pogni, R. Nylon 6 film and nanofiber carriers: preparation and laccase immobilization performance. *J. Mol. Catal. B Enzym.* **2014**, *102*, 41–47. https://doi.org/10.1016/j.molcatb.2014.01.012.

[12] Nguyen, H. H.; Kim, M. An overview of techniques in enzyme immobilization. *Appl. Sci. Converg. Technol.* **2017**, *26*, 157–163. https://doi.org/10.5757/ASCT.2017.26.6.157.

[13] Smith, S.; Goodge, K.; Delaney, M.; Struzyk, A.; Tansey, N.; Frey, M. A comprehensive review of the covalent immobilization of biomolecules onto electrospun nanofibers. *Nanomaterials* **2020**, *10*, 2142. https://doi.org/10.3390/nano10112142.

CHAPTER 7

Lyophilized pectinase-based biocatalysts: Design, optimization and application for must clarification

From Chapter 6 it became evident that, for the immobilization of pectinase on PA6 MPs, physical adsorption represents the most suitable approach. These studies were carried out using lyophilized purified pectinase from *Aspergillus niger*, whose exact composition and protein content were known, allowing a more rigorous quantitative comparison of immobilization yield, enzymatic activity, and reusability of the resulting catalytic conjugates.

The objective of the present Chapter 7 is to optimize the immobilization conditions of lyophilized pectinase onto PA6 MPs. Immobilization was performed by varying the concentration and pH of the enzymatic solutions in order to evaluate how these parameters influence wine must clarification. Up to this point in the thesis, the developed biocatalysts had been applied exclusively to the clarification of rosé wine must. The research presented in this chapter extends the study to the clarification of white wine must as well. The experimental work was conducted using real industrial white and rosé musts supplied by Sogrape Vinhos Lda.

7.1. Introduction

Wine production involves a series of biochemical and mechanical stages, such as harvesting and fermentation, previously detailed in Chapter 4. However, some production differences are observed for each type of wine (red, rosé, and white), particularly between the musts of white and rosé wines. These differences significantly influence the clarification requirements.

In white wine production, the must is typically separated from the skins immediately after crushing, minimizing the extraction of phenolic compounds and polysaccharides. Conversely, rosé wines are obtained through a limited maceration period. This short contact time with the grape skins, while essential for color and aroma profile, results in higher levels of cell wall-derived polysaccharides and colloidal material. This composition leads to increased turbidity and more complex stabilization challenges compared to white musts [1,2].

Clarification is the process of removing these suspended particles to ensure visual clarity and prevent future sediment formation. The turbidity of the must is mainly caused by pectin. Fresh grapes contain between 0.2% and 1.0% pectin and must contain between 0,2% to 1,0% [3]. While traditionally achieved through fining agents or membrane filtration, the use of exogenous pectinases has become industry standard due to their high efficiency in hydrolyzing the pectic backbone of the grape cell wall [4]. Pectinases can also increase the production and retention of certain volatile substances, thus releasing in wine more of the color- and flavor-determining

compounds contained in grape skin and making more effective the liberation of phenolic compounds [5,6].

Despite their advantages, the industrial application of free pectinases is often limited by low reusability and operational stability [7]. As previously demonstrated, polyamides are excellent supports for pectinase immobilization. In the previous chapter, different immobilization strategies were evaluated. Considering cost, processing time, and potential enzyme structural alterations, the non-covalent immobilization by physical adsorption was identified as the most suitable method for lyophilized pectinase.

In this chapter, two main immobilization parameters were varied. First, at a constant pH of 7, immobilization was performed using two pectinase concentrations, 0.5 mg/mL and 1.0 mg/mL. Subsequently, with the pectinase concentration fixed at 0.5 mg/mL (identified as optimal), the pH of the enzymatic solutions was varied from pH 5 to pH 8. In all cases, the same amount of PA6 MP support was used, and the immobilization was carried out at room temperature (21 ± 2 °C) under gentle shaking for 24 h.

In this manner, four lyophilized pectinase conjugates (PeL@PA6), prepared at pH 5–8, were obtained and subjected to comprehensive characterization. Their morphology, thermal stability, crystallinity, conformational behavior, enzymatic activity, kinetic parameters and storage stability were determined and comparatively analyzed. Finally, the immobilized systems were applied to the clarification of industrial white and rosé wine musts, and their reusability was evaluated.

7.2. Protein estimation

In order to determine the best immobilization conditions, different lyophilized pectinase (PeL) concentrations (1 mg/mL and 0.5 mg/mL) were evaluated at the same pH medium (pH7). The amount of enzyme immobilized after 24 hours of reaction was determined by direct UV/VIS measurement at 277 nm. This wavelength corresponds to the absorption of aromatic amino acid residues, such as tryptophan and tyrosine, present in the enzyme.

The spectra of the different pectinase solutions before and after immobilization, and the graph of the immobilization yield, are shown in Figure 7.1.

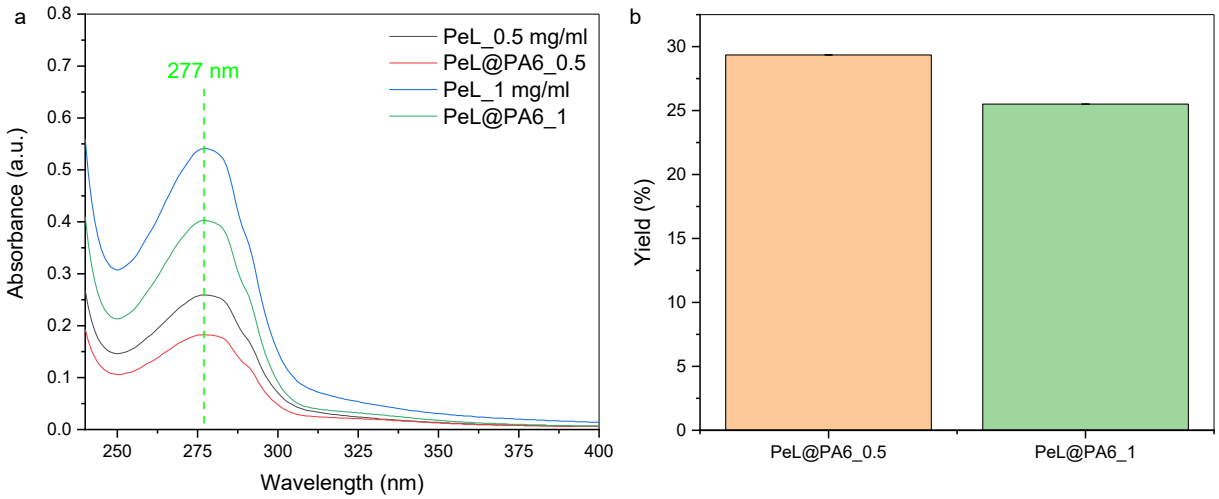


Figure 7.1. Quantification of the Pectinase immobilization: a) UV/VIS spectra of the pectinase solutions before and after immobilization; b) Immobilization efficiency PeL@PA6, where 0.5 corresponds to a pectinase concentration of 0.5 mg/mL and 1 corresponds to a pectinase concentration of 1 mg mL^{-1}. Standard deviations were between 0.4-0.5% and were calculated from two independent trials.

The immobilization yield of the two pectinase concentrations was very similar (Figure 7.1 b). This can be explained by the amount of enzyme that can attach to the microparticle; with both 0.5 mg/mL and 1 mg/mL, the microparticle should not have more capacity to bind to the enzyme. This suggests that the MP surface reached saturation at both concentrations, meaning that increasing the initial enzyme concentration does not result in a higher protein loading. Thus, further optimization of immobilization continued with an enzyme concentration of 0.5 mg/mL. The influence of pH was investigated using buffer solutions with pH in the range of 5 to 8.

The spectra of the different pectinase solutions before (e.g., PeL_pH5) and after immobilization (e.g., SN_PeL@PA6_pH5), and the graph of the immobilization yield, are shown in Figure 7.2.

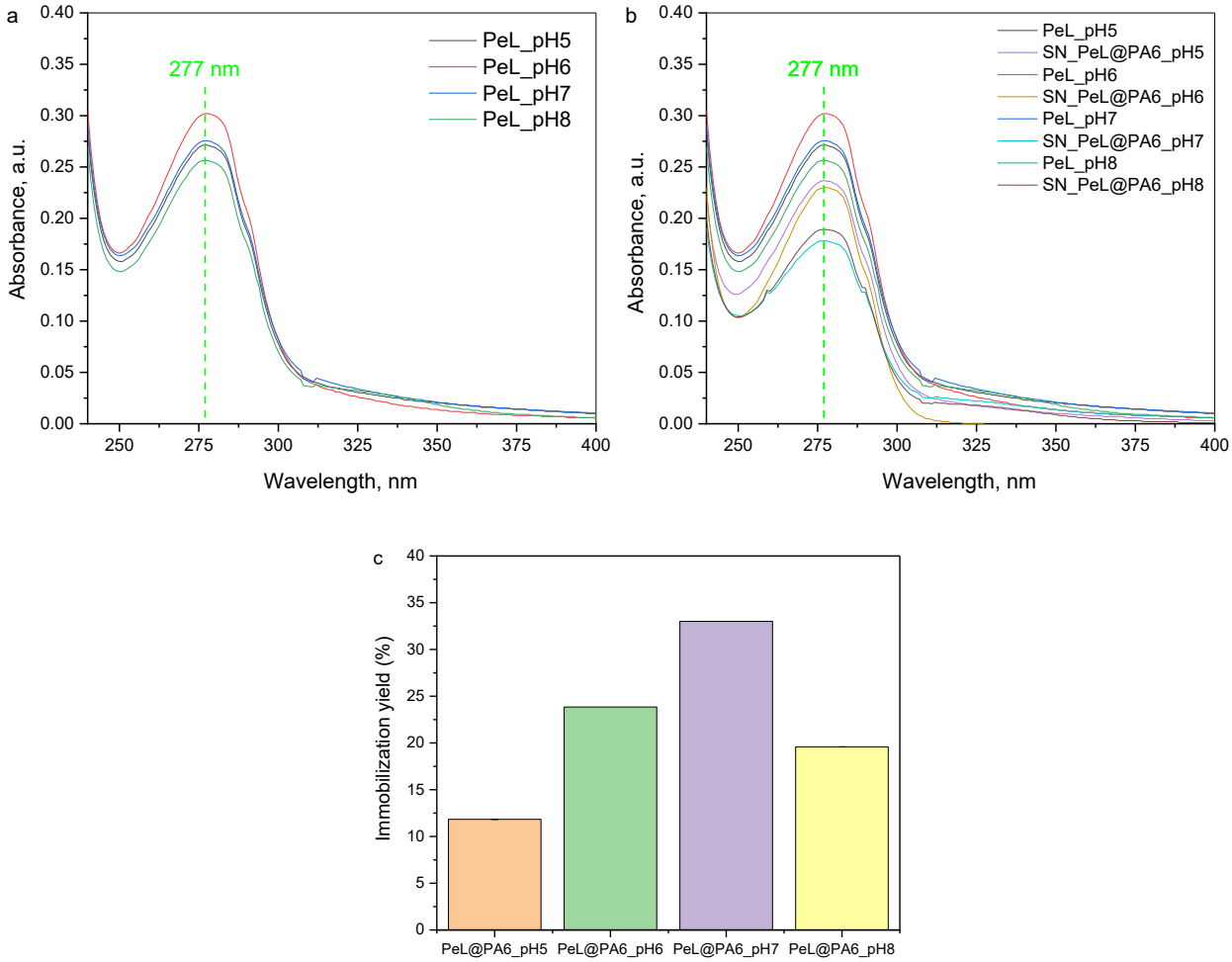


Figure 7.2: Quantification of the Pectinase immobilization: a) UV/VIS spectra of the initial pectinase solutions; b) UV/VIS spectra of the pectinase solutions before and after immobilization c) Immobilization yield of PeL@PA6. Standard deviations were between 0-0.5% and were calculated from two independent trials.

The absorbance of the pectinase solutions (0.5 mg/mL) shows different intensities (Figure 7.2a), indicating that pH influences the structural stability of pectinase, which can be attributed to the complex composition of the commercial pectinase from *Aspergillus niger*. The commercial lyophilized enzyme is a mixture of different pectinases (polygalacturonases, pectin lyases, and pectin methylesterases). The isoelectric point (p*I*) of pectinase enzymes from *Aspergillus niger* is generally acidic, typically ranging from pH 3.5 to 5.5 (polygalacturonases 3.5–5, pectin lyases 3.5–4.5, and pectin methylesterases 3.8–5) [8–10]. At pH 6, the enzyme is probably in a stable conformation, leading to the maximum absorbance (red curve, Figure 7.2a), while at pH 8 (least

intense, blue curve, Figure 7.2a), the enzyme can undergo some changes in its conformation, since this pH is not ideal for enzyme stability.

Regarding immobilization yield, it is observed that at pH 5 the yield is the lowest, while at pH 7 the yield is the highest (Figure 7.2c). These results differ from the pectinase absorption curve, in which the intensities at pH 5 and pH 7 are similar (black and green curves, respectively, Figure 7.2a). This difference can be explained by the charge of the enzyme and PA6. Due to the zeta potential of polyamides, at both pH 7 and pH 5 PA6 is negatively charged (−28.6 mV at pH 7 and −20.9 mV at pH 5) [11]. As to the enzyme, at pH 7 it is negatively charged (pH > p*I*), between pH 4-5 its charge is very close to zero, at pH 8 it is highly negative, and at pH 6 the enzyme has good solubility and stability. The higher immobilization yield observed at pH 7 can be attributed to the superior colloidal stability of both the support and the enzyme at this pH, which prevents aggregation and ensures maximum accessibility to the functional sites of the support. On the other hand, at pH 5, the proximity to the enzyme's p*I* and the reduction in the magnitude of the support's Zeta potential suggest a tendency towards aggregation, justifying the observed decrease in immobilization yield.

It can be concluded that adsorption immobilization of pectinase on PA6 microparticles is not prevented by electrostatic repulsion between the enzyme and the support. Although both the enzyme and the PA6 MPs carry a net negative charge at pH 6–8, hydrogen bonding remains possible because it depends primarily on local functional groups rather than on overall charge. Thus, even if moderate electrostatic repulsion exists, it would not stop hydrogen bonds formation when the two surfaces come into close contact, although the efficiency of this process may be lower than under electrostatic attraction.

PA6 contains a high concentration of surface amide groups (–CONH–), which act as both hydrogen-bond donors and acceptors. Likewise, pectinase presents numerous hydrogen-bonding sites (“patches”) on its surface, including peptide backbone groups and polar amino acid side chains. Consequently, effective adsorption can occur even when net electrostatic attraction is weak or absent, or even when partial repulsion is present. A relevant example is provided by Meissner et al. [12], who reported protein adsorption onto negatively charged silica nanoparticles on both sides of the protein p*I*.

Furthermore, the use of phosphate buffer reduces long-range electrostatic interactions through ionic screening, thereby increasing the relative importance of short-range interfacial hydrogen bonding. The high porosity and large internal surface area of the PA6 microparticles also enhance

enzyme–support contact and residence time within the pores, promoting multivalent interactions. Therefore, in the pH range 5–8, immobilization on PA6 MPs is mainly governed by hydrogen bonding at specific surface regions, with pH controlling the balance between electrostatic repulsion and hydrogen-bond interactions.

7.3. Circular dichroism analysis

The standard UV/VIS spectra of pectinase solutions across different pH values before (Figure 7.2a) and after immobilization on PA6 MPs (Figure 7.2b) revealed distinct absorption intensities, suggesting that the amount of the immobilized pectinase varies with pH. At the same time, it is expected that even the less invasive for the enzyme´s protein matrix non-covalent immobilization will produce some structural changes that can affect enzyme activity. Therefore, comparing the structure of the enzyme before immobilization and that of the enzyme in contact with the polyamide support during immobilization could clarify this issue.

Circular dichroism (CD) spectroscopy in the UV region of 190–250 nm probes electronic transitions of the peptide main chains that are highly sensitive to protein secondary structure. Distinct structural moieties, e.g., α-helix, β-sheet, β-turns, and unordered conformations, produce characteristic spectral signatures, enabling structural discrimination [13].

In the present study, comparative far-UV CD analysis was performed on the pectinase solution prior to immobilization and on the supernatant after immobilization, with pH as the variable parameter. Comparison of these spectra allowed evaluation of pH-induced conformational changes and assessment of possible structural alterations associated with enzyme–support interactions [14]. Quantitative secondary structure content was determined by deconvolution of the experimental spectra using the Contin-LL algorithm (Reference Set 4) [15] within the DichroWeb online server.

The secondary structure percentages are summarized in Table 7.1.

As shown in Table 7.1, no usable CD data were obtained for solutions at pH 5. To meet the instrument's analytical requirements, all solutions needed to be diluted according to the specified method, but after dilution the remaining protein concentration in the solutions at pH 5 was insufficient for reliable analysis.

Table 7.1: Secondary structure estimation of lyophilized pectinase (PeL) before and after immobilization (SN_PeL) at different pH values. The data presented corresponds to average of all matching solutions for enhanced statistical representativeness.

Sample	α-helix (%)	β-sheet (%)	Turns (%)	Unordered (%)
PeL_pH5	–	–	–	–
SN_PeL_pH5	–	–	–	–
PeL_pH6	12.8	37.7	24.8	24.7
SN_PeL_pH6	25.8	11.4	28.2	34.4
PeL_pH7	15.3	33.9	17.1	33.7
SN_PeL_pH7	20.7	20.6	23.4	35.3
PeL_pH8	4.0	33.8	26.5	35.8
SN_PeL_pH8	23.1	12.4	31.8	32.8

Overall, the UV CD data demonstrate systematic changes in the secondary structure of pectinase when comparing the initial enzyme solutions at different pH values with the corresponding supernatants obtained after immobilization. These changes indicate that, during immobilization PA6 microparticles interact with the enzyme (PeL samples in Table 7.1) in a way that alters its secondary structure as captured in the respective supernatants (SN samples).

At all pH values studied, α-helix content increased after immobilization. For example, at pH 6 α-helix roughly doubled, increasing from 12.8 to 25.8% (approximate 100% growth), while at pH 8 the α-helix fraction exhibited an even larger relative increase (≈ 477%). Concurrently, β-sheet content decreased markedly: at pH 6 it dropped by approximately 70% (from 37.7% to 11.4%), and at pH 8 by about 63%. Slighter increases were observed in the fractions of turns and unordered structures, typically rising by about 4–6% and 3–10%, respectively.

The most pronounced trend in the UV CD data is the conversion from β-sheet to α-helix structure upon prolonged contact with the PA6 MPs. Such alterations in the secondary structure are consistent with conformational adaptation upon surface interaction with the PA6 support. α-Helices are generally more compact and thermodynamically stable than extended β-sheets, and a shift toward higher α-helix content can reflect an enzyme adopting a more stable conformation in response to the support surface. In general, α-helices tolerate structural perturbations (including mutation and environmental change) better than β-strands, implying higher conformational robustness [16]. A decrease in β-sheet content accompanied by an increase in α-helix is consistent

with a possible partial reorganization of β-structured segments into more compact conformations upon interaction with the PA6 surface, influenced by interfacial hydrogen bonding and local packing constraints. Similar trends have been reported by Burgos et al. [17] who observed changes in secondary-structure distribution when comparing a free enzyme in buffer with the same enzyme after encapsulation, attributing these differences to confinement effects.

Notably, our UV CD measurements were performed comparing the initial pectinase solutions and the corresponding supernatants after adsorption immobilization. Therefore, the observed β to α redistribution reflects structural differences within the enzyme population remaining in solution and may result from selective adsorption and solution-phase re-equilibration.

The CD results indicate that the pectinase of this study undergoes measurable secondary-structure changes during immobilization depending on both pH and interaction with the PA6 MPs. Such structural variations may influence the catalytic activity and stability of the immobilized PeL@PA6 conjugates, which will be examined in subsequent sections. It should be noted that relatively few far-UV CD studies addressing conformational changes in major pectinase classes are available in the literature, including reports on pectin methylesterase [18], pectate lyases C and E [19], and exo-polygalacturonase [20].

7.4. Characterization of polyamide microparticles

7.4.1. Morphological studies by SEM

Scanning electron microscopy (SEM), combined with energy-dispersive X-ray spectroscopy (EDX), was used to analyze the morphology and composition of PA6 MPs, both neat and after pectinase immobilization (PeL@PA6). SEM analysis was used to evaluate the surface topology (porosity) of the PA6 MPs, as well as to detect any visible changes induced by enzyme immobilization. Additionally, EDX provides localized information on specific elements that confirm the presence of the enzyme in the polymer matrix.

To facilitate a visual comparison of these features, Figure 7.3 presents the micrographs of the PA6 microparticles before and after the immobilization of the lyophilized pectinase.

PA6 MPs exhibit a highly porous, scaffold-like morphology (Figure 7.3a–d). The micropores (Figure 7.3d) appear open, with irregular shapes and different visible depths. The presence of the enzyme did not alter the overall morphology of the microparticles; however, it is possible to observe that the micropores appear filled with enzymes (e.g., Figure 7.3l). The filling of micropores confirms

the success of enzyme immobilization, and the fact that some complexes exhibit a higher number of blocked micropores may indicate a greater presence of immobilized enzyme.

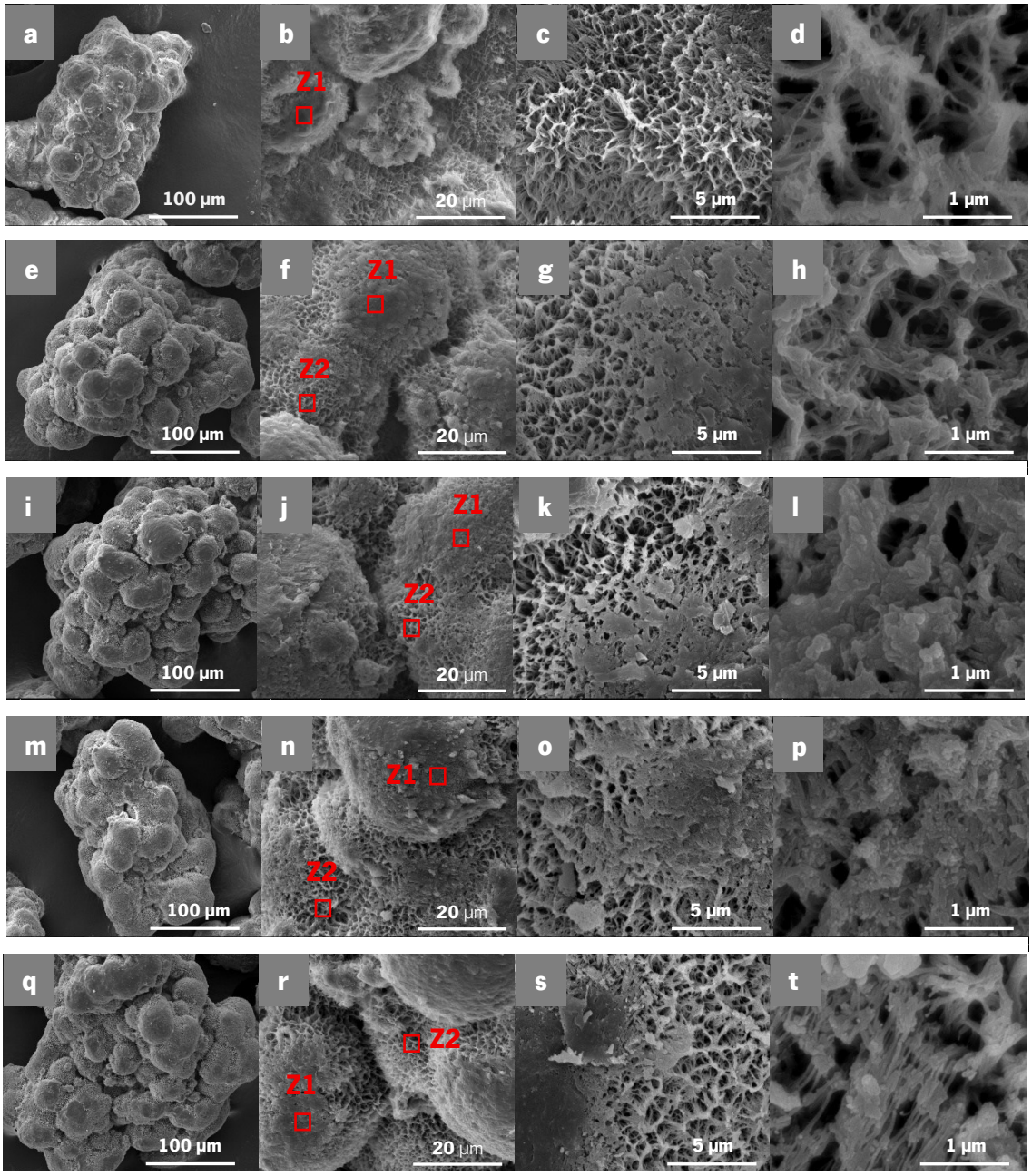


Figure 7.3: SEM micrographs of PA6 (images a–d) and the immobilized complexes formed: PeL@PA6_pH5 (images e–h), PeL@PA6_pH6 (images i–l), PeL@PA6_pH7 (images m–p), and PeL@PA6_pH8 (images q–t). Z1 and Z2 indicate different spots of EDX analysis – on the surface or in the pores of MPs.

EDX results of PMs with and without enzyme are summarized in Table 7.2.

Table 7.2: EDX results. Z1 is analysis on the surface of the microparticle and Z2 is analysis in the micropores of the microparticle.

Sample	Zone	C	N	O	Na	Others*
PA6	Z1	85.71	9.13	5.16	-	-
PeL@PA6_pH5	Z1	61.72	26.51	11.11	0.66	-
	Z2	59.89	25.47	14.64	-	-
PeL@PA6_pH6	Z1	58.61	18.49	17.86	2.26	2.77 (Al, Ca)
	Z2	58.93	24.12	15.91	1.04	-
PeL@PA6_pH7	Z1	60.30	22.97	15.28	0.60	0.85 (Al)
	Z2	58.15	16.95	19.08	2.00	3.82 (Al)
PeL@PA6_pH8	Z1	54.91	18.98	18.48	0.68	6.95 (Al, K)
	Z2	51.66	17.93	21.55	1.51	7.34 (Al, K)

EDX analysis (Table 7.2) reveals a significant increase in the nitrogen and oxygen content in PeL@PA6 samples, as compared to the neat PA6, originating from the immobilized protein. The appearance of elements like Na, Ca, and K is due to the buffer solutions, while the traces of Al most probably belong to the residual DL organo-aluminum initiator remaining in PA6 MP.

Overall, SEM and EDX analyses confirm, although indirectly, enzymatic immobilization both on the surface of the microparticles and within their micropores.

7.4.2. Thermal properties of microparticles

7.4.2.1. By DSC

Differential scanning calorimetry (DSC) was used to study the thermal behavior and crystalline properties of neat PA6 and PeL@PA6 samples.

The DSC thermograms are presented in Figure 7.4, showing the first heating scan (a), followed by the cooling cycle (b) and the second heating scan (c). The main thermal parameters obtained from the DSC analysis are summarized in Table 7.3. For more details on the DSC experiment see the Experimental part (Chapter 2, section 2.13.2.1).

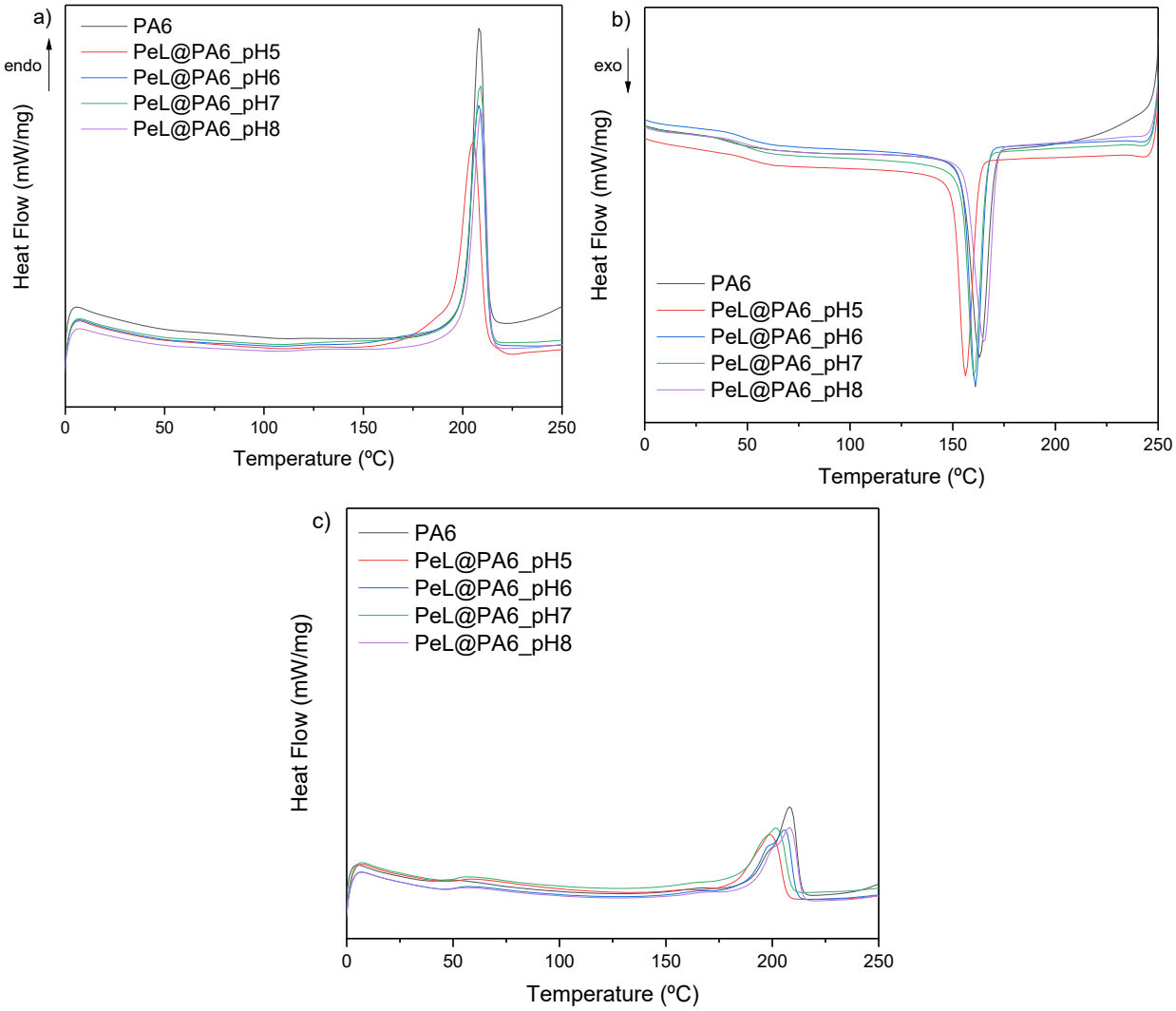


Figure 7.4: DSC curves of PA6 and PeL@PA6 samples: a) first heating scan; b) recrystallization from the melt; c) second heating scan. The scales of y-axes in subfigures a and c are the same to enable comparison.

Table 7.3: DSC data of PA6 MPs and PeL@PA6 samples.

Sample	First heating scan			Cooling scan [a]		Second heating scan			
	$T_m, °C$	$\Delta H, J/g$	$X_C, \%^{b)}$	$T_c, °C$	$-\Delta H, J/g$	$T_m, °C$	$\Delta H, J/g$	T_g, °C	$X_C, \%^{b)}$
PA6	208.5	70.22	36.96	163.1	39.62	208.4	30.18	48.6	15.88
PeL@PA6_pH5	205.2	92.51	48.69	156.3	35.54	199	27.09	58.3	14.26
PeL@PA6_pH6	208.4	77.25	40.66	161	38.14	205.9	28.26	57.3	14.87
PeL@PA6_pH7	208.8	74.74	39.34	160.4	36.3	201.9	26.04	56.5	13.71
PeL@PA6_pH8	209.3	69.53	36.59	165.2	37.91	208.3	29.46	56.3	15.51

a) Performed after first heating scan at 20 deg/min;

b) Determined according to Eq. 19 of Chapter 2;

In the first heating scan (Figure 7.4a and Table 7.3), PA6 exhibited a melting temperature (T_m) of 208.5 °C and an enthalpy of fusion (ΔH_m) 70.22 J g^{-1}, which are typical values for this polymer, corresponding to a degree of crystallinity (X_c) of approximately 37%. The Xc values were calculated using Equation 19 (Chapter 2), considering a polymer weight fraction (w) of 1, even for samples containing enzyme because the amount of enzyme is low and does not significantly affect the comparative analysis between the different immobilized systems. The reference enthalpy ($\Delta H_m{}^0$) for 100% crystalline PA6 was 190 J g^{-1} [21].

As shown in Figure 7.4a and Table 7.3, the first heating scan reveals that both neat PA6 MPs and the PeL@PA6 conjugates prepared at pH 5–8 exhibit 2a single melting endotherm with T_m values in the range of 205–209 °C, characteristic of the predominant α-PA6 polymorph. This indicates that the presence of immobilized pectinase does not alter the crystalline form of the PA6 support, particularly in the first heating cycle.

Nevertheless, variations in the pH used during conjugate preparation influence both the melting temperature and the degree of crystallinity (X_c). The conjugate prepared at pH 5 displays the lowest T_m (205 °C), the highest X_c (≈49%), and the broadest melting endotherm. Conjugates obtained at pH 6 and 7 exhibit X_c values around 40%, slightly higher than that of the neat PA6 support, while maintaining nearly constant T_m values and comparable peak widths. The observed melting behavior does not directly indicate the presence of the immobilized enzyme, since no additional thermal transitions attributable to the protein are detected. A plausible explanation is that during immobilization in aqueous media at pH 5–7, water absorption plasticizes the amorphous regions of PA6, effectively enhancing chain mobility. Theoretically, this may promote secondary crystallization or interfacial ordering even at room temperature, leading to increased crystallinity without significant changes in T_m. At pH 8, this effect appears less pronounced.

The PeL@PA6 conjugate prepared at pH 5 deserves special attention. It shows a particularly high X_c and a slight reduction in T_m (≈3 °C relative to neat PA6). The broad melting endotherm suggests a wider distribution of lamellar thicknesses or less uniform crystalline organization. This behavior may reflect additional interfacial effects associated with enzyme adsorption, such as conformational rearrangements of the protein, densification within the porous support, or enhanced heterogeneous nucleation of PA6 chains at the enzyme–polymer interface. As indicated by the data of Mayans et al. [22], protein crystallization under these conditions cannot be entirely excluded.

Overall, the DSC data from the first heating scan data suggest that immobilization conditions, particularly pH, influence the crystalline organization of the PA6 support primarily through interfacial and plasticization phenomena rather than through changes in polymorphic structure.

Upon cooling from 250 °C to 0 °C at 20 °C/min, the PeL@PA6 conjugates prepared at pH 5–7 exhibited crystallization temperatures (T_c) in the range of 156.3–161.0 °C, all of which are lower than that of neat PA6 microparticles (163.1 °C). In contrast, the conjugate obtained at pH 8 displayed the highest T_c (165.2 °C), exceeding that of the unmodified support. These results indicate that the crystallization behavior of PA6 supports is influenced by the immobilization conditions. The PeL@PA6_pH5 sample, showing the lowest T_c, appears to recrystallize with greater difficulty, suggesting either reduced chain mobility during cooling or a lower effective nucleation density. The conjugates prepared at pH 6 and 7 exhibit intermediate behavior, with T_c values around 161 °C. At the other extreme, the PeL@PA6_pH8 conjugate crystallizes at the highest temperature, implying facilitated nucleation.

The most probable explanation of the DSC data in cooling mode is that the crystallization behavior correlates with the amount and/or distribution of immobilized pectinase. If a higher enzyme loading is achieved under certain pH, the protein (denaturated and/or partially carbonized at this stage) may act as a heterogeneous nucleating agent, promoting earlier recrystallization i.e., higher T_c. Conversely, lower enzyme loading or its less favorable interfacial organization may reduce nucleation efficiency, shifting T_c to lower values. Therefore, the observed trend in T_c likely reflects a balance between heterogeneous nucleation effects induced by the immobilized protein and possible restrictions in chain mobility arising from enzyme–polymer interactions.

In the second heating scan, the glass transition temperature (T_g) of all samples is clearly detectable in the range of 50–52 °C, which is typical for PA6. The X_c of the PeL@PA6 conjugates is relatively low (13.7–14.5%), slightly below that of the neat PA6 support ($X_c \approx 16\%$). This decrease is consistent with the relatively fast cooling rate (20 °C/min) applied during the preceding crystallization step, which limits crystal growth and favors the formation of smaller and less perfect crystallites.

Compared to the first heating ramp (Figure 7.4a), the melting endotherms in the second heating scan (Figure 7.4c) are broader and less intense for all samples. The peak broadening, together with the appearance of shoulders, suggests the coexistence of α- and γ-PA6 polymorphs. The lower melting enthalpies and reduced peak intensities indicate the formation of thinner and less perfect lamellae during the controlled cooling step.

It can be concluded that while the differences detected in the first DSC heating scan likely originate from interfacial effects and structural rearrangements occurring during immobilization in aqueous media at different pH, the second heating reflects predominantly the melting behavior of the PA6 support.

Summarizing, DSC analysis demonstrates that pectinase immobilization induces measurable, pH-dependent modifications in the thermal behavior of PA6 microparticles. These effects are most pronounced in the initial crystalline structure (first heating) and in the crystallization step, while the fundamental thermal transitions of PA6 (T_g and T_m range) remain largely unchanged during the second heating. Additional insight into PA6–pectinase interactions was obtained by thermogravimetric analysis (TGA).

7.4.2.1. By TGA

To verify whether the thermal stability of the microparticles was affected by the presence of the enzyme, TGA of the microparticles with and without immobilized enzyme was performed.

The thermogravimetric curves, in both integral and differential forms, are presented in Figure 7.5, and the corresponding numerical values are summarized in Table 7.4.

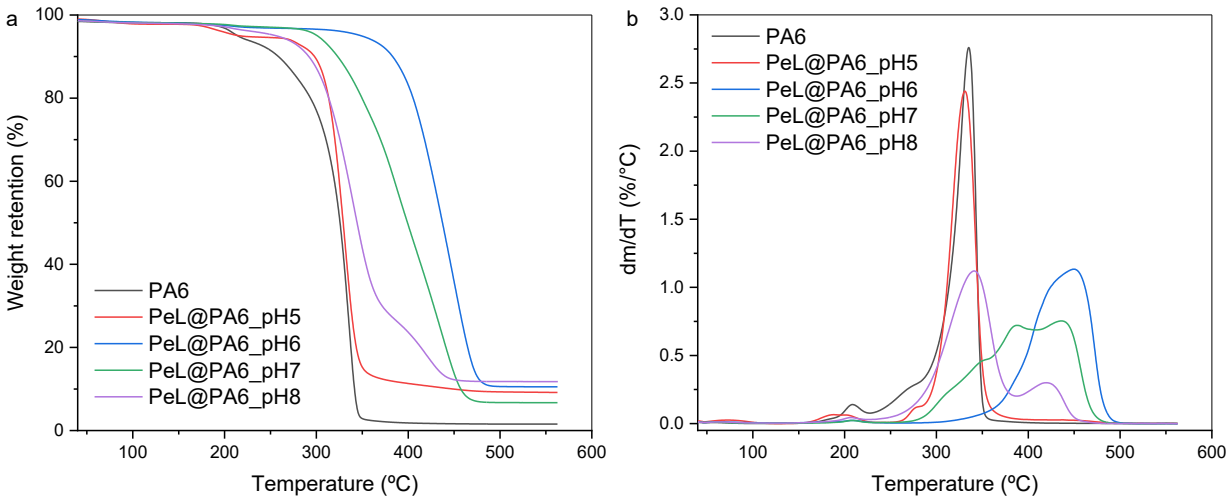


Figure 7.5: TGA curves of MP: a) Integral weight loss curves; b) First derivative curves.

Table 7.4: TGA analysis of polyamide microparticles.

Sample	T_{in}, °C[a)]	$T_{max,}$°C[b)]			V_{max}, %/ºC			Residue at 600 °C, %
		I	II	III	I	II	III	
PA6	266.95	335.38	-	-	2.76	-	-	1.546
PeL@PA6_pH5	311.36	330.96	-	-	2.44	-	-	9.161
PeL@PA6_pH6	396.69	450.28	-	-	1.133	-	-	10.53
PeL@PA6_pH7	333.65	346.72	387.57	436.21	0.4466	0.7211	0.7536	6.708
PeL@PA6_pH8	305.41	340.60	423.47	-	1.12	0.296	-	11.77

a) T_{in} = Temperature of initial degradation obtained from integral TGA curves;

b) T_{max} = Maximum degradation temperature obtained from the peak of the 1st derivative of the TGA curves;

c) V_{max} = Maximum degradation rate at T_{max} obtained from the first derivative of the TGA curves.

The thermal behavior of the samples, as shown in the thermogravimetric curves in Figures 7.5a and 7.5b, reveals clear differences between pure PA6 MPs and immobilized samples PeL@PA6. This finding confirms that the immobilized pectinase modifies the thermal stability of the PA6 support. The thermal behavior of neat PA6 MPs is characteristic of this thermoplastic polymer, displaying a single major degradation event with $T_{in} \approx 267\ ºC$, a maximum degradation temperature T_{max} of 335.38 °C, a maximum degradation rate $V_{max} = 2.76\ \%/min$, and a low final residue of 1.546% (Table 7.4). The enzymatic complexes exhibit higher initial thermal resistance than PA6 MPs, as evidenced by their higher T_{in} values. Among them, PeL@PA6_pH6 shows the greatest increase in thermal stability, with a T_{in} of 396.69 °C. These results suggest that the immobilized enzyme contributes to the thermal stabilization of the microparticles and that the immobilization pH influences the enzyme–support interactions.

Multiple thermal degradation stages are observed in the differential TGA curves of immobilized systems (Figure 7.5 b). They can be attributed to the decomposition of the enzyme superimposed to that of the polymer matrix. Furthermore, the V_{max} values of the complexes are lower than that of pure PA6, indicating a more gradual degradation process. An increase in residual mass at 600°C is also observed for all enzyme-containing samples (ranging from 6.7–11.8%), compared to PA6 MPs (1.546%). This increase of the carbonized residue reflects the presence of immobilized pectinase; however, it cannot be quantitatively correlated with the enzyme content. Most probably, pectinase, like all enzymes, contains sulfur and nitrogen atoms in its protein matrix, which are widely considered effective flame-retardant elements for polymers, including polyamides [23,24]. Flame- retardant compounds act through various mechanisms, most frequently involving controlled

dehydration and the formation of highly cross-linked structures or stable insulating char layers that protect the polymer against ignition, pyrolysis or other forms of thermal degradation. With these considerations in mind, the increase in the high-temperature residue reported in Table 7.4 results from both enzyme carbonization and non-degraded, char-protected PA6.

Overall, the TGA results confirm successful enzyme immobilization through the presence of additional mass loss events above 270°C, corresponding to protein-related decomposition. Pectinase immobilization significantly alters the thermal behavior of PA6 MPs, leading to enhanced thermal stability and a more complex degradation profile that shows some dependence on the pH of the pectinase solution used during the immobilization.

The described improved thermal behavior is not an isolated observation. Similar increases of thermal stability have also been observed upon immobilization of other proteins or enzymes on polyamide MPs, namely bovine serum albumin [25] and laccase [11].

7.5. Determination of pectinase activity and related parameters

The DNS method was used for the determination of the activity of free and immobilized pectinase, as described in detail in Section 2.6.1 (Chapter 2). All activity assays were performed under the same conditions (pectin as substrate in citrate buffer (50 mM, pH 3.8), 50 °C,), allowing direct comparison between free and immobilized systems. The results of pectinase activity and specific activity are presented in Figure 7.6.

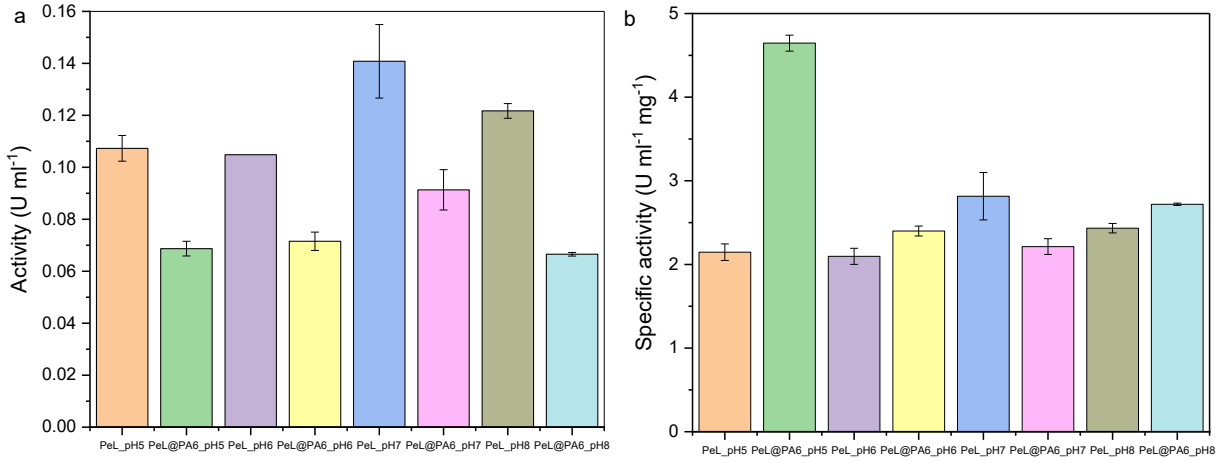


Figure 7.6: Studies of the activity of free pectinase solution and its immobilized complexes: a) activity in units per milliliter (U/mL), where 1 U is defined as the amount of enzyme required to release 1 µmol of galacturonic acid per minute under the assay conditions; b) specific activity, representing the activity units per milligram of protein (U mL^{-1} mg^{-1}). Standard deviation values were obtained based on two independent assays for each sample.

The PeL and PeL@PA6 samples obtained at different immobilization pH values are presented together for comparison (Figure 7.6a). The activity of PeL_pH 7 is the highest, followed by PeL_pH8. The activities of PeL_pH5 and PeL_pH6 are similar. The immobilized complex PeL@PA6_pH7 exhibits the highest activity, while the remaining complexes show similar activities, slightly lower than those of the corresponding free enzymes.

When the activity values are normalized by the protein content (Figure 7.6b), the PeL@PA6_pH5 complex exhibits a specific activity approximately twice as high as that of the corresponding free enzyme (PeL_pH5). The complexes PeL@PA6_pH6 and PeL@PA6_pH7 also display specific activities that are statistically higher than those of their respective free enzyme samples. Only at pH 7 the specific activity of the free PeL is slightly higher than that of the immobilized complex. These results indicate that, in most cases, the fraction of PeL attached to the PA6 support remains highly active after immobilization.

In addition to immobilization yield and activity, two more important parameters related to enzyme immobilization were determined, namely: immobilization efficiency $(IE, \%)$ (Equation 3, Section 2.6.2, Chapter 2) and activity recovery $(AR, \%)$ (Equation 4, Section 2.6.2, Chapter 2).

The evolution of AR and IE as a function of pH during immobilization on PA6 MPs are shown in Figure 7.7.

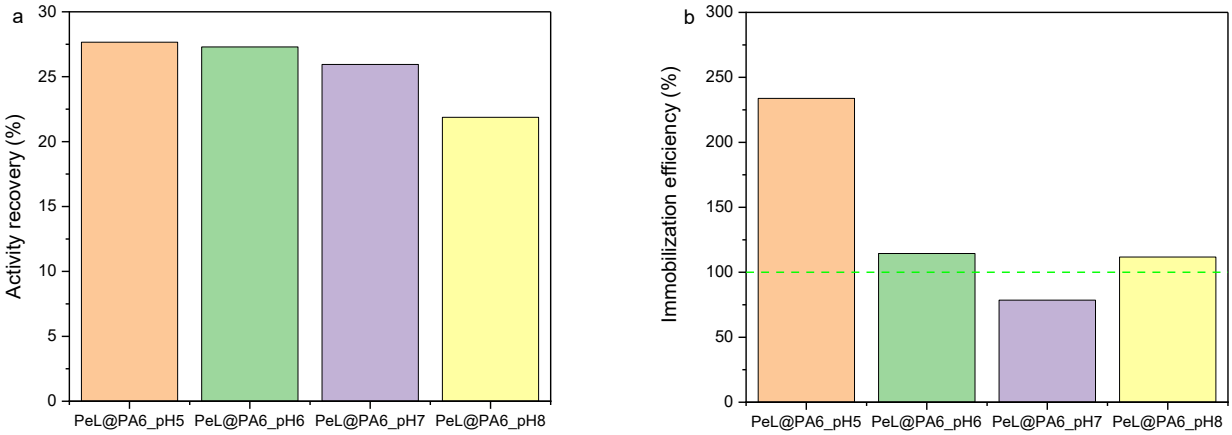


Figure 7.7: Studies of the activity recovery (a) and efficiency of immobilized pectinase (b). Standard deviations were between 1-1.6% and were calculated from two independent trials. The dashed line in Figure 7.7.b indicates the level of IE = 100%.

Table 7.5 summarizes the immobilization parameters of all PeL@PA6 complexes at pH values between 5 and 8.

Table 7.5: Activity parameters of free and immobilized lyophilized pectinase as a function of pH.

Sample designation	**Protein content (mg)**	**Immobilization Yield** (IY* (%))	**Specific activity (U/mg protein)**	**Immobilization Efficiency** (IE (%))	**Activity recovery** (AR (%))
PeL_pH5	2.500	–	2.146	–	–
PeL@PA6_pH5	0.296	11.8	4.646	233.8	27.6
PeL_pH6	2.500	–	2.097	–	–
PeL@PA6_pH6	0.596	23.8	2.400	114.6	27.3
PeL_pH7	2.500	–	2.816	–	–
PeL@PA6_pH7	0.825	33.0	2.213	78.6	25.9
PeL_pH8	2.500	–	2.434	–	–
PeL@PA6_pH8	0.489	19.6	2.719	111.7	21.9

* See also Figure 7.2c.

The activity results in Figures 7.6., 7.7. and the consolidated numerical data in Table 7.5 demonstrate a clear dependence of the immobilization behavior and catalytic performance of the resulting PeL@PA6 conjugates on the pH of the enzyme solution.

The IY increases from 11.8% at pH 5 to a maximum of 33.0% at pH 7, followed by a decrease to 19.6% at pH 8. Evidently, enzyme adsorption immobilization onto the PA6 MPs becomes more favorable as the pH approaches neutral conditions, perhaps due to favorable balance between electrostatic interactions, hydrogen bonding, and hydrophobic contacts between at the PeL/PA6 interface. At higher pH values, however, increased electrostatic repulsion between protein molecules and the support surface (both negatively charged) may partially suppress adsorption decreasing the IY observed at pH 8.

The catalytic properties of the immobilized systems show a different trend. The IE reaches its highest value at pH 5 (233.8%), which indicates hyperactivation. This effect can arise from several factors, including favorable enzyme orientation on the support surface, improved accessibility of the catalytic cleft, or stabilization of catalytically competent conformations of the enzyme upon PA6 support. At pH 6 and pH 8, the immobilization efficiency remains slightly above 100% (114.6% and 111.7%, respectively), suggesting that the immobilization process still provides some stabilization or activation of the enzyme. In contrast, the conjugate prepared at pH 7 exhibits the lowest IE value (78.6%). Interestingly, this sample corresponds to the highest immobilization yield (see also Figure 7.2c). This indicates that a considerable fraction of the enzyme immobilized at pH7 may

adopt less favorable orientations or experience steric constraints partially limiting catalytic accessibility. Such effects are typical for systems with higher enzyme loading, where crowding on the support surface or within pores increases steric and diffusional constraints, lowering the fraction of catalytically accessible enzyme molecules [26].

The AR values remain relatively similar for the conjugates obtained at pH 5–7 (25.9–27.6%), while a somewhat lower value is observed at pH 8 (21.9%). These moderate AR values indicate that only part of the initial enzymatic activity is retained after immobilization, which is common for adsorption-based immobilization systems [27].

Overall, all these results reveal a clear trade-off between immobilization yield and catalytic efficiency: although pH 7 provides the highest PeL loading, the most catalytically efficient conjugate is obtained at pH 5, where the lowest amount of immobilized enzyme exhibits clear hyperactivation.

7.5.1. Influence of glucose and ethanol in enzyme activity

In this work, pectinase activity was determined under standard conditions—pectin substrate in citrate buffer, 50 mM, pH 3.8 and 50 °C. Pectinases are applied in the clarification of different beverages, such as must and juice. The literature shows that the effectiveness of these enzymes in activity determination and in clarification applications differs, generally being higher in activity assays. Even when applied to the clarification of the same type of must, enzymes have shown variable effectiveness [28].

These differences can be explained by the conditions under which they are applied, such as the presence of sugars and possibly ethanol. Grape must and wine contain high concentrations of sugars (mainly glucose and fructose) and increasing levels of ethanol during fermentation [29]. Naturally, must contains approximately 110 g/L (10% w/v) of glucose before fermentation [30], and the amount of ethanol varies between 10-15% v/v [30,31].

To simulate conditions similar to those used in must clarification, pectinase activity was evaluated in the presence of 5–15% (w/v) glucose and 5–15% (v/v) ethanol, as described in section 2.6.2 of Chapter 2. The results of activity and specific activity are presented in Figure 7.8 and Figure 7.9.

As shown in Figure 7.8, glucose exerts a clear inhibitory effect on pectinase activity in both the free enzyme (Figure 7.8a and c) and the immobilized systems (Figure 7.8b and d), confirming previous observations reported by Radoi et al. [32]. In the absence of glucose, the activities of all samples (PeL and PeL@PA6) reach their maximum at pH 6-7 (Figure 7.8a and b). Upon addition

of 5% w/v glucose, the activity decreases by approximately 20–30% for all systems. Further increasing the glucose concentration to 10–15% results only in minor fluctuations of the measured activities, remaining within the limits of experimental error.

When the activities are normalized by protein content (Figure 7.8c and d), the dependence remains basically the same.

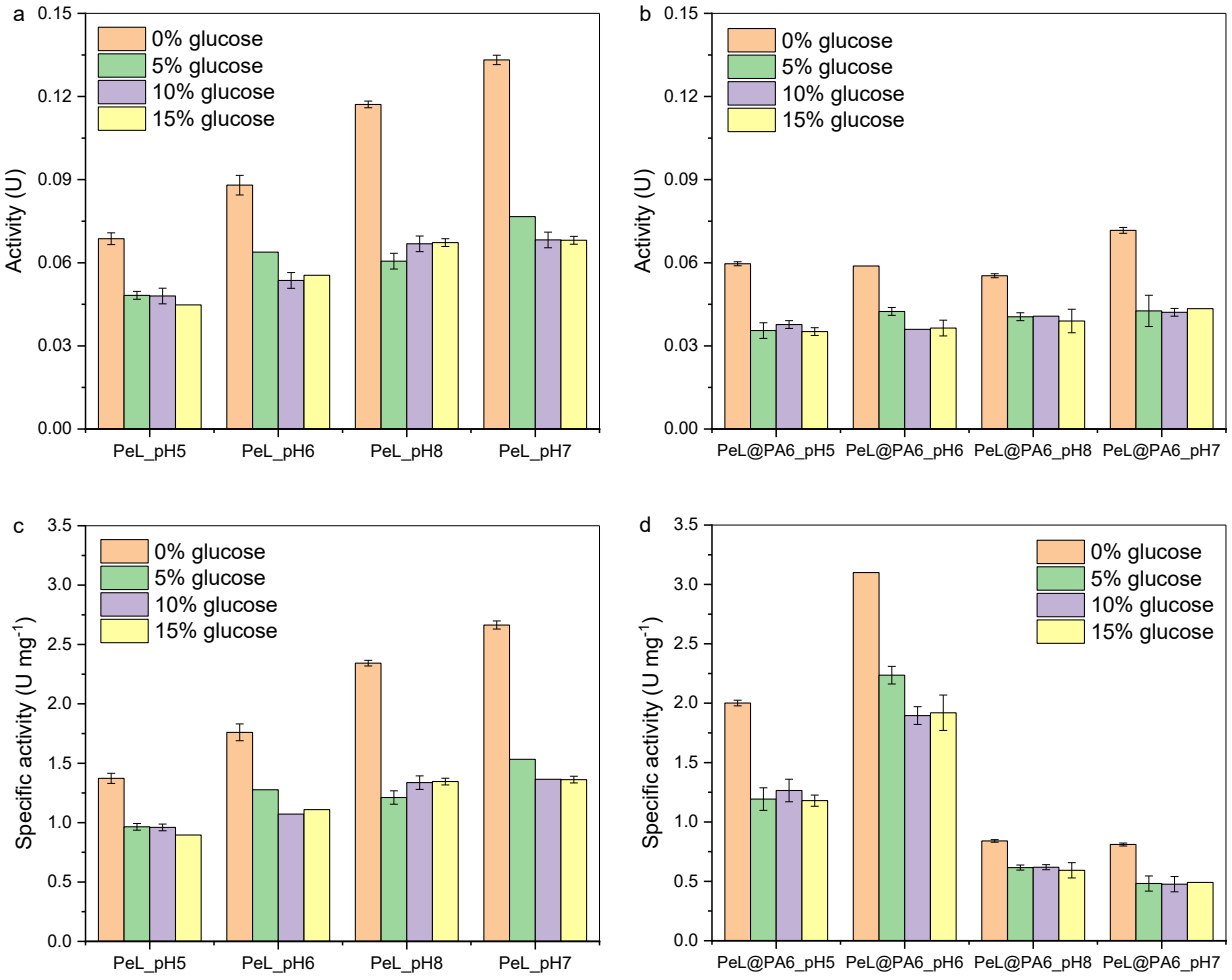


Figure 7.8: Effect of glucose concentration on enzymatic activity. a) free enzyme absolute activity; b) immobilized enzyme absolute activity; c) free enzyme specific activity; d) immobilized enzyme specific activity.

The inhibitory effect of glucose can be attributed to changes in the microenvironment of the enzyme and possible conformational adjustments that reduce the accessibility of the catalytic cleft to the pectin substrate. High concentrations of glucose may also modify the hydration structure of the solution and increase medium viscosity, both of which can hinder substrate diffusion toward

the active site. The absence of a strong additional decrease in activity between 10 and 15% glucose suggests that the enzyme approaches a limiting functional state under these conditions.

Overall, these observations are consistent with a partial non-competitive inhibition mechanism, in which glucose does not compete directly with the substrate for the catalytic site but reduces the apparent catalytic capacity of the enzyme [33].

The effect of ethanol added on the activity of free PeL (Figure 7.9a and b) and PeL@PA6 conjugates (Figure 7.9c and d) did not produce the inhibitory behavior commonly reported for organic solvents acting on enzymatic proteins [29,31].

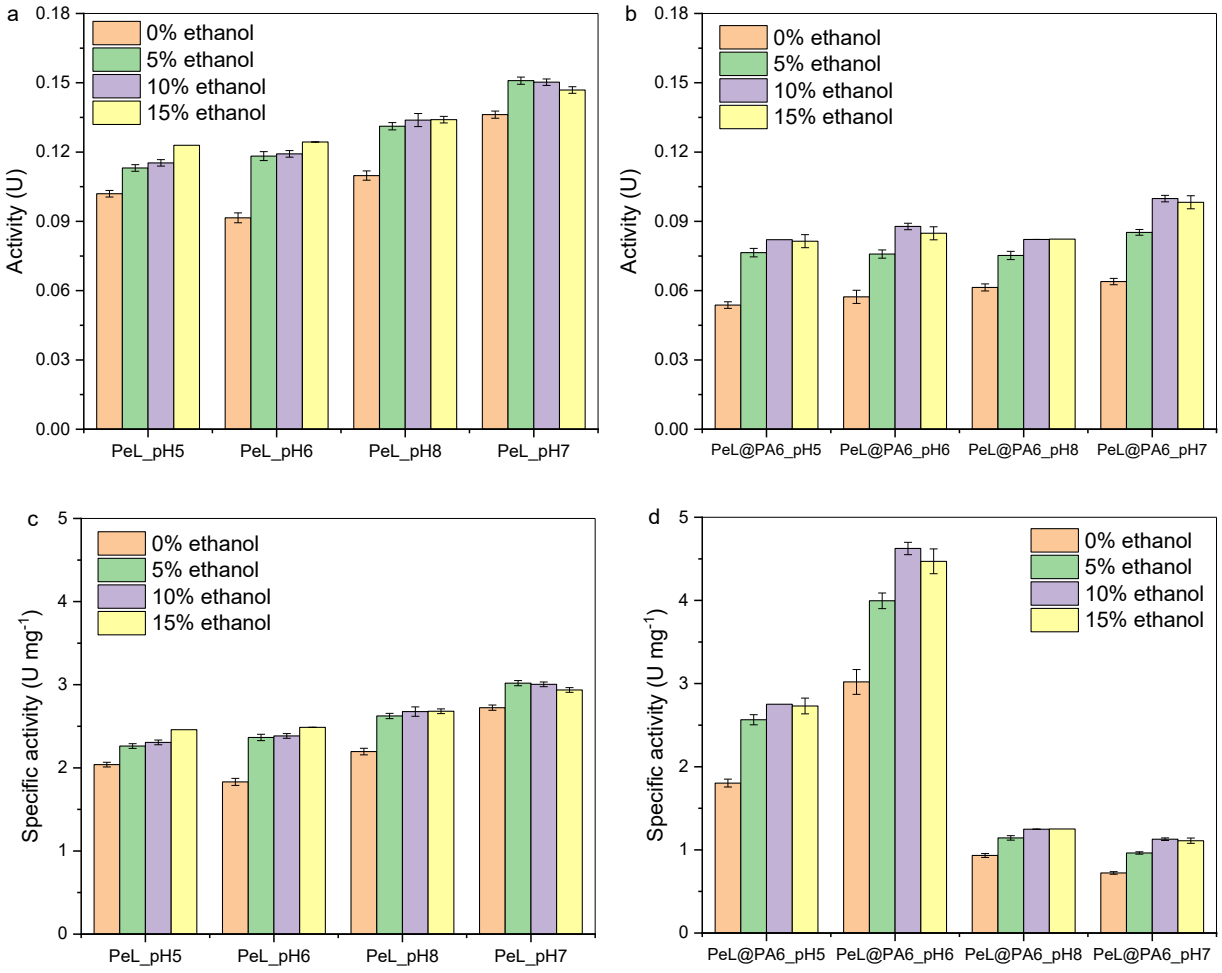


Figure 7.9: Effect of ethanol content on enzymatic activity. a) free enzyme absolute activity; b) immobilized enzyme absolute activity; c) free enzyme specific activity; d) immobilized enzyme specific activity.

In contrast, in the present study the addition of ethanol (5–15% v/v) led to an increase in the catalytic activity (absolute and specific) of both free and immobilized pectinase. The pectinase

activity displayed a non-linear dependence on ethanol concentration. At 5% ethanol, a significant increase in activity was observed (approximately 10–45% higher than the control without ethanol), suggesting a solvent-induced activation effect. At higher ethanol concentrations (10 and 15%), the activity decreased compared with that at 5%, although it remained above the control level. Such activation of pectinolytic activity in the presence of ethanol has also been reported in the literature. For example, at 15% (v/v) ethanol the pectinolytic activity of *Aureobasidium pullulans* GM-PN-22 increased by 24%, while in *Saccharomyces cerevisiae* B-17 an increase of 99% was observed [29].

In summary, the results indicate that glucose exerts an inhibitory effect on the enzymatic activity of lyophilized pectinase, both in the free and immobilized forms, whereas ethanol promotes pectin degradation within the studied concentration range. This behavior demonstrates that the enzyme exhibits good tolerance to ethanol. Consequently, the enzyme, whether free or non-covalently immobilized on PA6 microparticles, may operate more efficiently under the conditions typical of wine clarification than in the earlier stages of must processing.

7.6. Kinetic parameters

Kinetic studies are essential to evaluate the practical feasibility of immobilized enzymes in industrial bioprocesses. The kinetic parameters V_{max} (i.e., the maximum reaction rate attained at substrate saturation) and K_m (the apparent Michaelis constant reflecting the effective affinity of the enzyme for the substrate) of free and immobilized pectinases were determined by measuring the initial reaction rates for each enzymatic system using pectin concentrations ranging from 0.045 to 3.15 mg mL^{-1} in citrate buffer (50 mM) at constant pH (3.8) and temperature (50 °C), as described in Section 2.7.2, Chapter 2.

Figure 7.10 a-b illustrates the kinetic analysis performed by plotting the specific activity per unit of protein (V_{spec}) as a function of substrate concentration (S) following the Michaelis–Menten model. Figure 7.10 c-d illustrates the Lineweaver–Burk double-reciprocal linearization.

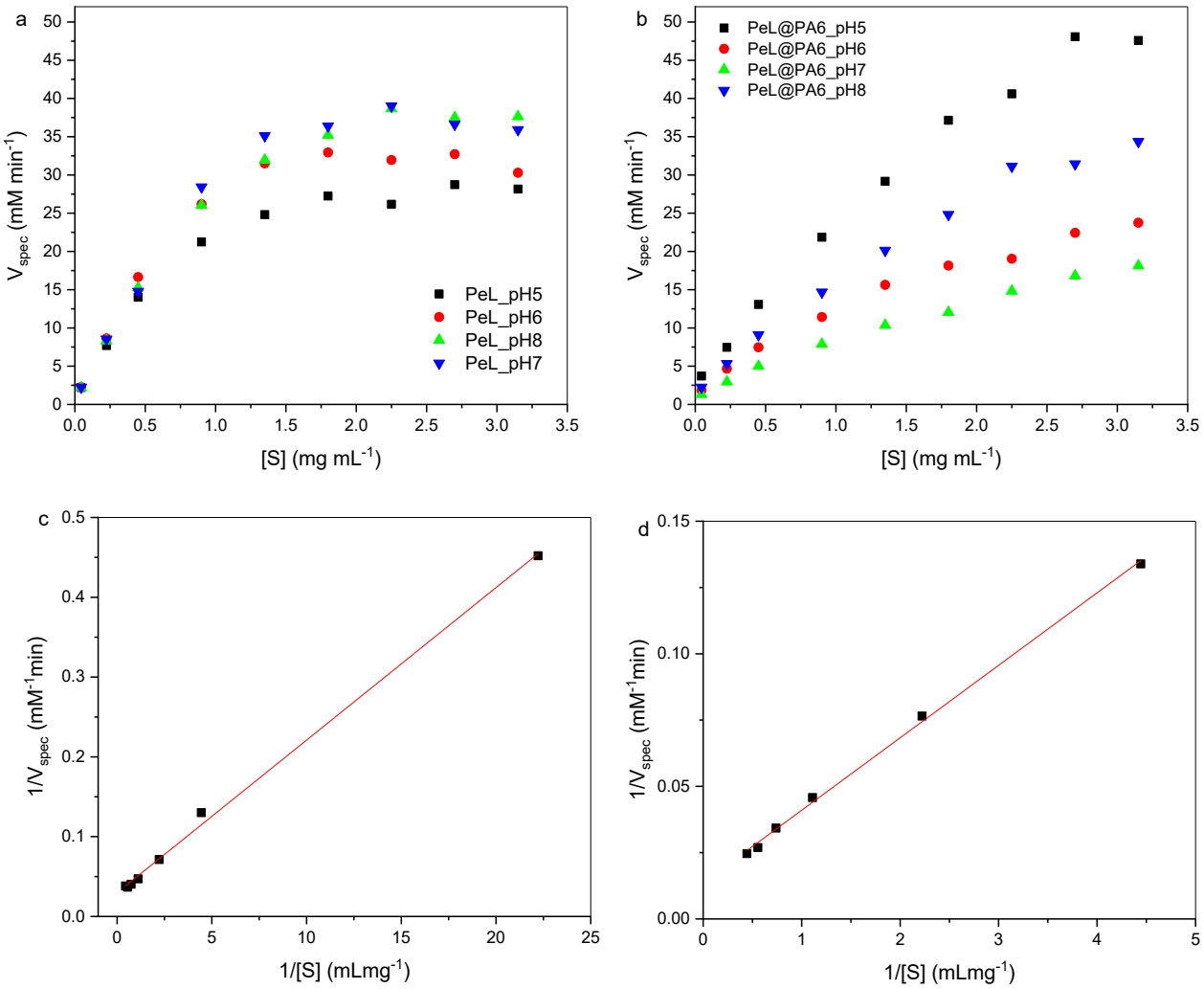


Figure 7.10: Selected experimental kinetic curves of free (a) and immobilized pectinases (b). Selected experimental Lineweaver-Burke plot of PeL_pH5 (c) and PeL@PA6_pH5 (d).

The kinetic curves presented in Figure 7.10a for the free PeL at different pH values clearly demonstrate that, unlike the enological pectinase previously investigated (Section 4.4, Chapter 4 and Section 5.6, Chapter 5), the lyophilized pectinase PeL follows classical Michaelis–Menten kinetics, showing a well-defined saturation plateau at substrate concentrations above 2 mg mL^{-1}. In contrast, for the immobilized enzyme systems (Figure 7.10b), complete saturation was not reached within the substrate concentration range studied, with (V_{sepc}) still increasing slightly around substrate concentrations of 3.0–3.15 mg mL^{-1}.

Therefore, the kinetic parameters V_{max} and K_m were estimated by nonlinear regression using the Michaelis–Menten equation (Equation 5, Section 2.7.1, Chapter 2, abbreviated as MM) and compared to the same parameters obtained using the Lineweaver–Burk double-reciprocal

linearization (Equation 8, Section 2.7.2, Chapter 2, abbreviated as LB; Figures 7.10c and 7.10d). The resulting values are summarized in Table 7.6.

For discussion, the kinetic parameters obtained from nonlinear Michaelis–Menten fitting were prioritized due to their higher statistical reliability. As noted by Robinson [34], reciprocal linearization methods amplify experimental errors at low substrate concentrations and distort the statistical weighting of the data, which can lead to biased estimates of kinetic parameters, particularly K_m.

Table 7.6: Kinetic parameters of free and immobilized pectinase.

Sample	Parameters*	Equation 5 (MM)	Equation 8 (LB)
PeL_pH5	$V_{max}(mM\ min^{-1}mg^{-1})$	35.327±1.399	33.478± 3.746
	$K_m(mg\ mL^{-1})$	0.654±0.086	0.398±0.044
	$Adj.R^2$	0.988	0.998
PeL@PA6_pH5	$V_{max}(mM\ min^{-1}mg^{-1})$	93.061±9.136	73.368±6.243
	$K_m(mg\ mL^{-1})$	2.814±0.484	2.006±0.179
	$Adj.R^2$	0.992	0.998
PeL_pH6	$V_{max}(mM\ min^{-1}mg^{-1})$	40.159±2.870	47.801±5.670
	$K_m(mg\ mL^{-1})$	0.563±0.143	0.906±0.110
	$Adj.R^2$	0.955	0.999
PeL@PA6_pH6	$V_{max}(mM\ min^{-1}mg^{-1})$	37.456±2.712	27.420±2.482
	$K_m(mg\ mL^{-1})$	1.916±0.283	1.119±0.111
	$Adj.R^2$	0.991	0.992
PeL_pH7	$V_{max}(mM\ min^{-1}mg^{-1})$	49.707±4.462	52.301±8.483
	$K_m(mg\ mL^{-1})$	0.789±0.215	1.015±0.169
	$Adj.R^2$	0.955	0.998
PeL@PA6_pH7	$V_{max}(mM\ min^{-1}mg^{-1})$	36.806±4.386	21.386±1.815
	$K_m(mg\ mL^{-1})$	3.325±0.655	1.416±0.129
	$Adj.R^2$	0.990	0.996
PeL_pH8	$V_{max}(mM\ min^{-1}mg^{-1})$	52.068±2.969	50.050±7.184
	$K_m(mg\ mL^{-1})$	0.950±0.151	0.988±0.144
	$Adj.R^2$	0.985	0.998
PeL@PA6_pH8	$V_{max}(mM\ min^{-1}mg^{-1})$	69.480±7.691	48.123±6.647
	$K_m(mg\ mL^{-1})$	3.150±0.587	1.836±0.260
	$Adj.R^2$	0.991	0.994

Note: * V_{max} normalized by the weight of the protein in fact represents the catalytic turnover K_{cat}. It represents the number of substrate molecules converted into product per milligram enzyme for per minute, when the enzyme is saturated with substrate.

The results summarized in Table 7.6 show that immobilization at pH 5 and pH 8 produced enzyme–support complexes exhibiting higher V_{max} values than the corresponding free enzymes. In particular, at pH 5 the immobilized enzyme displays a V_{max} value of 93.061 mM min^{-1} mg^{-1}, which is more than twice that of the free enzyme (35.327 mM min^{-1} mg^{-1}), corresponding to an efficiency of approximately 223% and indicating a clear hyperactivation effect. In contrast, the complexes obtained at pH 6 and pH 7 exhibit V_{max} values comparable to those of the corresponding free enzymes.

For all samples studied, however, a substantial increase in K_m was observed. For example, at pH 5 the K_m value increases from 0.654 (PeL) to 2.814 mg mL^{-1} after immobilization (PeL@PA6_pH5). Such increases in K_m are frequently reported for immobilized enzyme systems and are generally attributed to mass-transfer limitations and diffusional restrictions rather than intrinsic changes in the enzyme–substrate interaction. Although the PA6 microparticles possess a highly porous morphology and large internal surface area, as demonstrated by SEM analysis, the diffusion of pectin molecules through the pore network toward the immobilized enzyme molecules may still be partially hindered. As a result, the effective substrate concentration at the catalytic sites decreases, leading to an increased apparent K_m. In other words, there is a weaker affinity of the enzyme for its substrate, but once the active site is reached, a rapid reaction follows, being much faster than that with the free enzyme. This is evidenced by the high values of the specific activity and K_m.

The overall catalytic performance of the systems was evaluated through the catalytic efficiency (CE), defined as the ratio V_{max}/K_m (Equation 22, Section 5.6, Chapter 5), as presented in Figure 7.11.

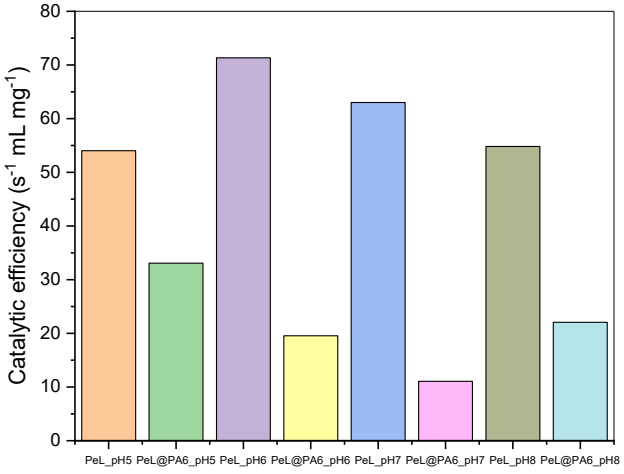


Figure 7.11: Catalytic efficiency of free and immobilized pectinases.

As shown in Figure 7.11, the catalytic efficiency of the free enzyme is generally higher than that of the immobilized systems. Although V_{max} increases significantly in some cases, particularly for the conjugate prepared at pH 5, the concurrent increase in K_m ultimately reduces the overall catalytic efficiency of the immobilized enzyme. This behavior can be attributed primarily to limited substrate accessibility, as a fraction of the immobilized enzyme molecules may reside within internal pores of the PA6 MPs where substrate diffusion is restricted. Additionally, adsorption of the enzyme onto the polyamide surface may impose steric constraints that partially limit substrate access to the catalytic cleft, further contributing to increased apparent K_m values and lower CE.

In summary, both the morphology and chemical nature of the PA6 MP support play an important role in determining the catalytic behavior of the immobilized pectinase. Although diffusion-related limitations influence the apparent kinetic parameters, the possibility of efficient biocatalyst recovery and reuse, together with the hyperactivation observed under specific immobilization conditions, are expected to favor the practical relevance of this immobilization strategy for potential industrial applications.

7.7. Application in must clarification

To evaluate the potential industrial applicability of the immobilized enzymes, they were applied to the clarification of rosé and white must. In addition to differences in their production processes, these musts differ in composition, particularly regarding polysaccharide and monosaccharide content, which can influence enzyme performance during clarification [35,36].

Rosé and white must, with pH 3.44 and 3.19 respectively, containing 2.0 mg mL^{-1} of pectin were clarified using 180 µL of pectinase solution containing 0.1 mg of free pectinase (pH 5-8) and the corresponding amount of immobilized enzyme (prepared at pH 5–8) at room temperature (23 °C ± 2 °C), as described in Chapter 2, Section 2.7.1.

The results of clarification studies and the visual aspect of the must after and before clarification are presented in Figure 7.12.

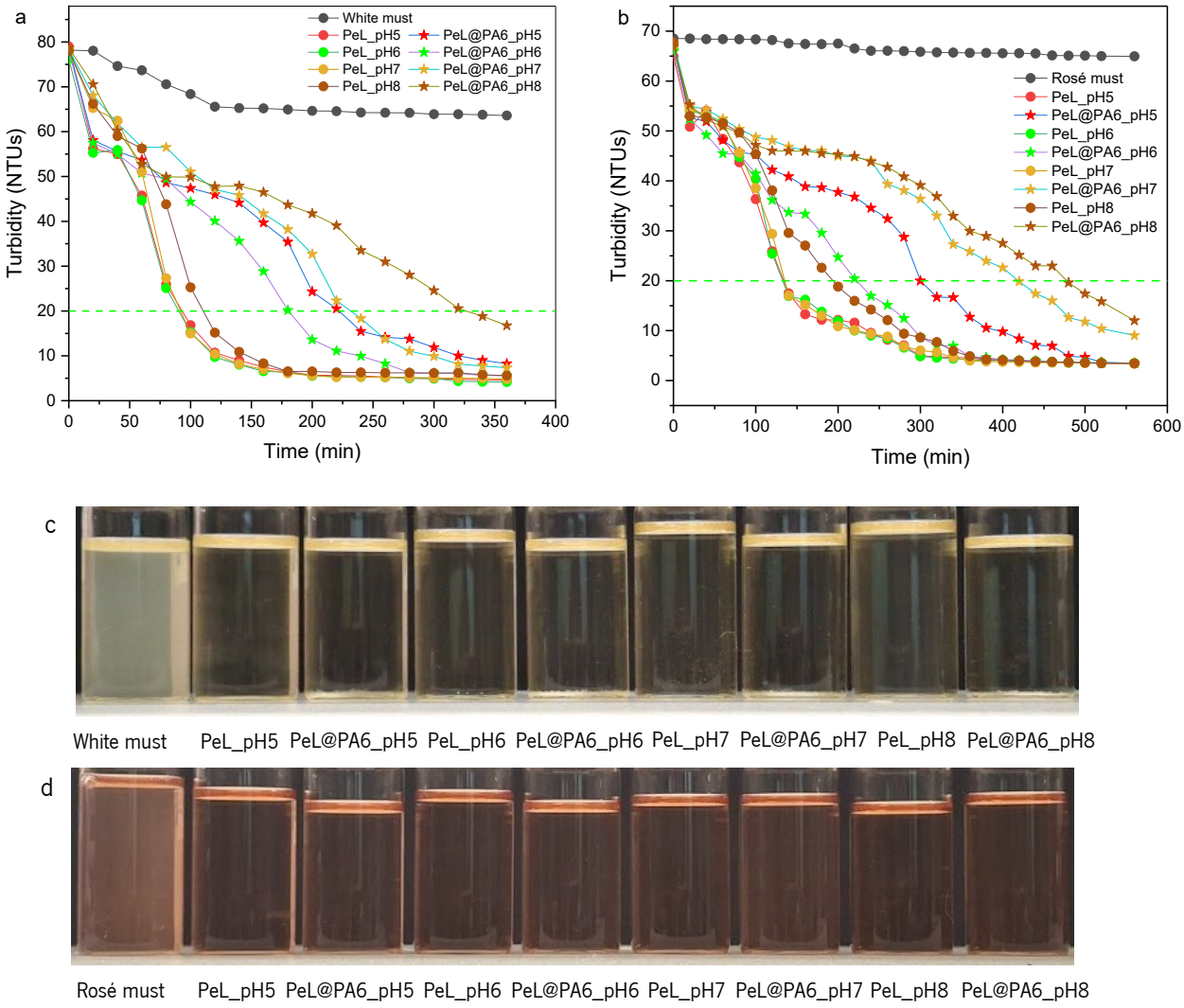


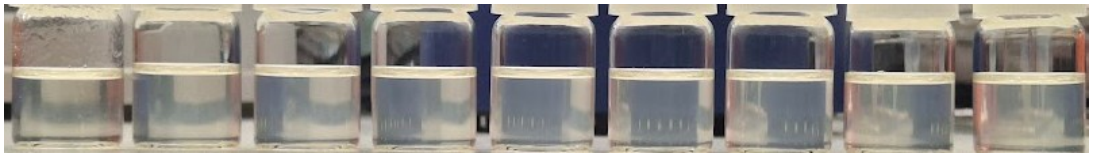
Figure 7.12: Clarification studies of white (a) and rosé must (b) with free and immobilized pectinase preparation. Images of the white (c) and rosé (d) must after clarification.

The graphs shown in Figure 7.12 reveal distinct clarification behaviors and clarification times (defined as turbidity values below 20 NTU, Sections 4.5, Chapter 4 and 5.7, Chapter 5) for the two types of must. In untreated white must (Figure 7.12a), turbidity initially measured approximately 80 NTU and stabilized at around 65 NTU after 120 minutes. Enzymatic treatment began immediately upon enzyme addition, and after 20 minutes all systems exhibited turbidity values of approximately 55 NTU, which are lower than the stabilization level of the untreated must. Among the enzymatic systems, both free and immobilized enzymes samples at pH 5 and pH 6 showed the fastest clarification, whereas those at pH 8 were slightly slower. After 100 minutes, all free enzyme samples achieved turbidity below 20 NTU. The same turbidity level was reached by the

immobilized complex at pH 6 after 200 minutes, while the complexes at pH 5, pH 7, and pH 8 required 240, 240, and 340 minutes, respectively, to reach the desired turbidity. Visual differences in clarified white must samples are shown in Figure 7.12c. In the case of rosé must (Figures 7.12b and 7.6d), the turbidity of the untreated sample remained nearly constant at approximately 70 NTU throughout the clarification period. As expected, due to the higher concentration of cell wall-derived components [34], this turbidity is slightly higher than that observed for white must. The enzymatic treatments followed a similar trend to that observed for white must, with free enzymes clarifying the must more rapidly. However, in this case, clarification required approximately 40 additional minutes for enzymes immobilized at pH 5, pH 6, and pH 7, and more than twice as long for the enzyme at pH 8. Among the immobilized systems, the pH 6 complex was the fastest, reaching turbidity values below 20 NTU after 240 minutes (4 hours), followed by the pH 5 complex, which required 320 minutes. The slowest system was the pH 8 complex, which required 480 minutes (8 hours) to achieve the target turbidity. These results are consistent with kinetic studies, as complexes with higher Km values exhibited slower clarification rates, reflecting lower apparent substrate affinity. The results are also in agreement with the catalytic efficiency data, as the free enzyme consistently displayed faster clarification performance than the immobilized systems.

7.7.1. Pectin test

A residual pectin test was performed on all samples after the clarification process (as described in Section 2.8.3, Chapter 2) to evaluate the presence of pectin in the must. This qualitative test, based on the precipitation of pectin in the presence of acidified ethanol, is essential to confirm the effective degradation of the pectin during clarification process. The results are presented in Figure 7.13 and Figure 7.14.



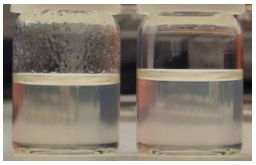
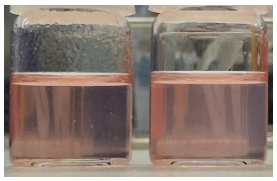


Figure 7.13: Pectin test results of white must samples.



Rosé must PeL_pH5 PeL@PA6_pH5 PeL_pH6 PeL@PA6_pH6 PeL_pH7 PeL@PA6_pH7 PeL_pH8 PeL@PA6_pH8



Rosé must PeL_pH5

Figure 7.14: Pectin test results of rosé must samples.

Visible aggregates (gelatinous floccules) were observed exclusively in the untreated must samples (control), all samples treated with either free or immobilized pectinase remained clear. As can be seen in Figure 7.13 and 7.14 some aggregates are visible in the untreated must sample, confirming that pectin was not hydrolyzed in the absence of enzymatic treatment.

These results indicate that both free and immobilized pectinase successfully complete the depectinization process under enological conditions. This confirms that the turbidity values achieved (lower than 20 NTUs) effectively correspond to pectin-free must. From an industrial standpoint, complete pectin removal is a critical quality parameter to ensure the colloidal stability of the must, preventing the formation of "pectin haze" and facilitating subsequent filtration and winemaking processes.

7.7.2. pH determination

To evaluate whether the clarification process affected must acidity, the pH of the samples was measured after clarification.

The pH of the must acts as an essential regulatory parameter that ensures food safety and microbiological stability by optimizing the precipitation of undesirable microorganisms, simultaneously influencing color preservation and the activity of exogenous enzymes. Ideally, it should be maintained between 3.0 and 3.8 to maximize the effectiveness of clarification and stabilization processes [3,37].

The pH values of must after clarification are summarized in Table 7.7.

Table 7.7: pH of must after clarification time.

Must	White must	Rosé must
Untreated Must	3.19	3.44
PeL_pH5	3.14	3.41
PeL@PA6_pH5	3.13	3.39
PeL_pH6	3.12	3.38
PeL@PA6_pH6	3.13	3.40
PeL_pH7	3.10	3.39
PeL@PA6_pH7	3.11	3.44
PeL_pH8	3.14	3.41
PeL@PA6_pH8	3.12	3.41

White must was slightly more acidic (pH 3.19, Table 7.7) than rosé must (pH 3.44, Table 7.7), and the clarification process did not significantly alter the pH in either case. This confirms that neither the immobilization support nor the clarification process interferes with the chemical stability of the must. These results demonstrate that the PA6 support is chemically inert, ensuring that the organoleptic properties and the natural acid-base balance of the must are preserved throughout the enzymatic treatment.

7.7.3. Must color analysis

The color of the must/wine is a primary attribute determining consumer preference and a critical quality parameter subject to rigorous control. It is influenced by both the must's pH and the action of enzymes during the winemaking process [3,37,38].

The color of the must after clarification with free and immobilized enzymes was performed by acquiring UV/VIS absorption spectra, as described in Section 2.9.1 of Chapter 2. The color of the must was evaluated at three specific wavelengths: 420 nm (yellow component), 520 nm (red component), and 620 nm (blue component) [39].

The results of the color analysis are presented in Figure 7.15.

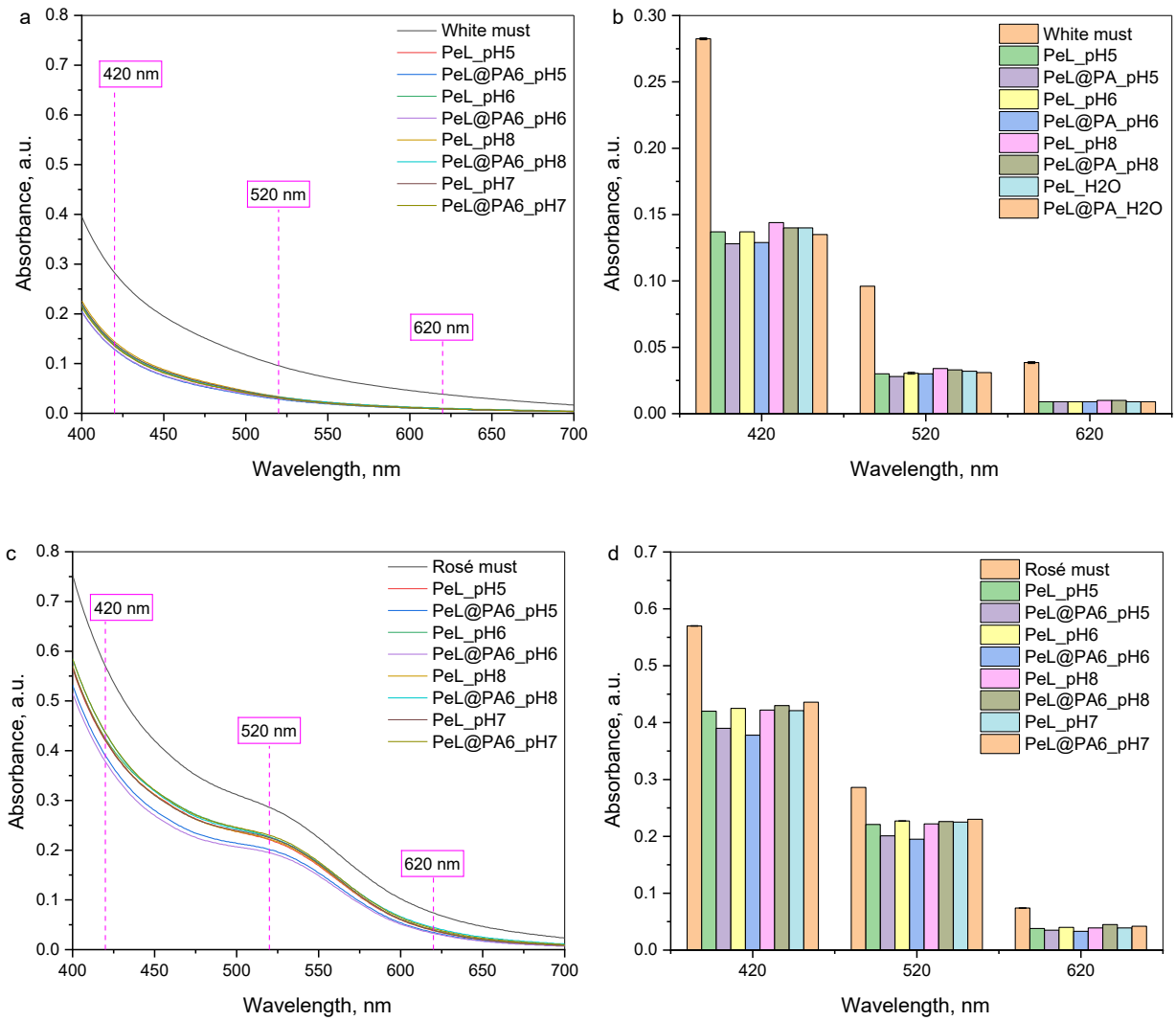


Figure 7.15: Analysis of must color changes after clarification. (a,c) Comparison of UV/VIS absorption spectra in three characteristic regions (420, 520, and 620 nm) for white and rosé must, respectively; (b,d) comparison of numerical color parameters for white and rosé must, respectively.

The UV/VIS spectra shown in Figures 7.15a and 7.15c, together with the bar graphs presented in Figures 7.15b and 7.15d, indicate that must treated with immobilized enzymes exhibits absorbance values at 420, 520, and 620 nm comparable to those obtained with the corresponding free enzymes. The use of porous polymeric supports, such as polyamides, may potentially affect must color due to the adsorption of certain compounds onto the microparticles. However, the results demonstrate that the polyamide microparticulate supports employed in this study do not induce undesirable color changes in the must.

For a more detailed evaluation of must color and composition before and after clarification, several additional parameters were determined, including color intensity (I), which provides an

objective quantitative assessment of must/wine color; the relative contribution of each absorption component to the overall color intensity ($\%\ Yellow\ (Y), \%\ Red\ (R), and\ \%\ Blue\ (B)$); hue ($T$), which reflects the chromatic characteristics of the must; browning index (BI), associated with oxidation reactions that lead to brown coloration and changes in brightness; total polyphenolic index (TPI), which estimates the overall phenolic content; hydroxycinnamic acids (HCA); and flavanols ($FLAV$). All parameters were measured or calculated as described in Section 2.9.1 of Chapter 2. The results are summarized in Tables 7.8 and 7.9.

Table 7.8: Estimated white must color and composition measures after clarification with free and immobilized pectinases. Two tests were performed for each sample.

White must	$\boldsymbol{BI}$ $(\boldsymbol{a.u.})$	$\boldsymbol{I}$ $(\boldsymbol{a.u.})$	$\boldsymbol{T}$ $(\boldsymbol{a.u.})$	$\boldsymbol{Y}$ (%)	$\boldsymbol{R}$ (%)	$\boldsymbol{B}$ (%)	$\boldsymbol{TPI}$ $(\boldsymbol{a.u.})$	$\boldsymbol{HCA}$ $(\boldsymbol{a.u.})$	$\boldsymbol{FLAV}$ $(\boldsymbol{a.u.})$
Untreated Must	0.2825	0.417	2.94	67.75	23.02	9.23	8.88	4.305	1.005
PeL_pH5	0.137	0.176	4.57	77.84	17.05	5.11	8.04	3.86	0.73
PeL@PA6_pH5	0.128	0.165	4.57	77.58	16.97	5.45	8.03	3.89	0.745
PeL_pH6	0.137	0.1765	4.49	77.62	17.28	5.10	7.85	3.77	0.715
PeL@PA6_pH6	0.129	0.168	4.30	76.79	17.86	5.36	7.215	3.51	0.685
PeL_pH8	0.144	0.188	4.24	76.60	18.09	5.32	7.66	3.69	0.72
PeL@PA6_pH8	0.14	0.183	4.24	76.50	18.03	5.46	7.65	3.705	0.72
PeL_pH7	0.14	0.181	4.38	77.35	17.68	4.97	9.11	4.395	0.85
PeL@PA6_pH7	0.135	0.175	4.35	77.14	17.71	5.14	8.305	4.01	0.76

Table 7.8 presents the color and compositional parameters of white must after clarification. The BI value of untreated must is higher than that of treated samples, suggesting that both free and immobilized pectinases are effective in limiting oxidation phenomena. The I of white must decreased significantly after clarification, from 0.417 to approximately 0.17, indicating a high degree of clarification. The increase in T reflects the removal of suspended solids and unstable pigments, resulting in a characteristic straw-yellow hue and improved color stability. The TPI, HCA, and $FLAV$ values remained relatively constant after treatment, indicating that neither free nor immobilized enzymes promote the removal of important phenolic compounds.

Table 7.9: Estimated rosé must color and composition measures after clarification with free and immobilized pectinases. Two tests were performed for each sample.

Rosé must	BI $(a.u.)$	I $(a.u.)$	T $(a.u.)$	Y (%)	R (%)	B (%)	TPI $(a.u.)$	HCA $(a.u.)$	$FLAV$ $(a.u.)$
Untreated Must	0.5705	0.93	1.99	61.29	30.75	7.96	15.24	7.835	1.65
PeL_pH5	0.42	0.679	1.90	61.86	32.55	5.60	16.05	8.135	1.495
PeL@PA6_pH5	0.39	0.626	1.94	62.30	32.11	5.59	15.16	7.84	1.425
PeL_pH6	0.425	0.692	1.86	61.42	32.80	5.78	15.475	7.865	1.45
PeL@PA6_pH6	0.378	0.606	1.94	62.38	32.18	5.45	14.975	7.665	1.41
PeL_pH8	0.422	0.683	1.90	61.79	32.50	5.71	15.48	7.895	1.45
PeL@PA6_pH8	0.436	0.701	1.93	61.34	32.24	6.42	15.025	7.665	1.44
PeL_pH7	0.421	0.685	1.87	61.46	32.85	5.69	15.96	8.08	1.465
PeL@PA6_pH7	0.436	0.708	1.90	61.58	32.49	5.93	15.33	7.885	1.45

Table 7.9 summarizes the corresponding results for rosé must. In this case, BI values were also lower after enzymatic treatment, indicating reduced oxidative effects. The I decreased from 0.93 in untreated must values between 0.6 and 0.7 after clarification, suggesting partial removal of unstable colored polymers and improved color stabilization. Since rosé must contain anthocyanins, which may potentially be adsorbed by polymeric supports, the similarity in tonality values between musts treated with free and immobilized enzymes indicates that the polyamide microparticles do not significantly adsorb these pigments. As observed for white must, the TPI, HCA, and $FLAV$ values remained essentially unchanged, confirming that the polyamide 6 microparticles do not remove relevant phenolic fractions from rosé must.

In summary, the microparticulate polyamide supports used for non-covalent enzyme immobilization do not induce undesirable changes in the color or phenolic composition of either white or rosé must, demonstrating their suitability for enological clarification applications.

7.8. Reusability of immobilized pectinase

The possibility of reusing enzymes is an important advantage of enzyme immobilization [40]. In this work, reuse was evaluated both in must clarification and in enzymatic activity assays.

The PeL@PA6 complexes were used in two consecutive clarification cycles, as described in Section 2.10.2.2, Chapter 2, and the results are presented in Figure 7.16.

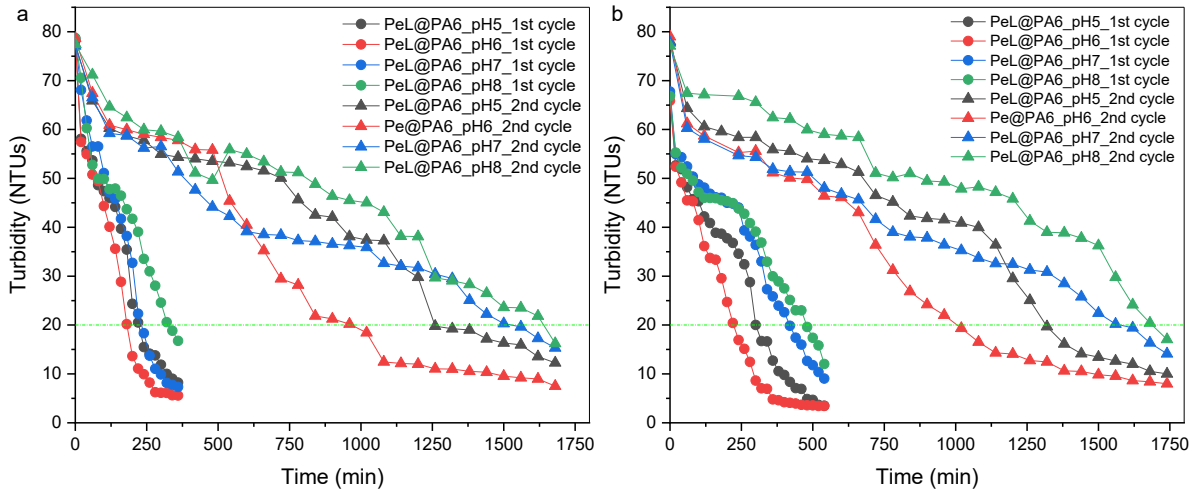


Figure 7.16: Reuse of immobilized enzyme in the clarification of white (a) and rosé (b) must.

The complexes successfully reduced turbidity to values below 20 NTU in both clarification cycles: in the first cycle, 6 hours for white must (Figure 7.16a) and 9 hours for rosé must (Figure 7.16b); in the second cycle, 28 hours for white must (Figure 7.16a) and 29 hours for rosé must (Figure 7.16b). PeL@PA6_pH6 was the fastest system in clarifying both musts, which was expected based on the kinetic results, as this immobilized system exhibited the lowest K_m value. Despite the longer clarification time in the second cycle, it is important to highlight that all systems achieved the desired turbidity (< 20 NTU), proving that catalytic integrity remains sufficient for industrial standards. The increased time required for must clarification in the second cycle is likely due to the adsorption of byproducts generated during pectin hydrolysis onto the microparticles. These byproducts may hinder substrate access to the enzyme's active site. It can therefore be stated that these complexes can be used industrially for at least two consecutive cycles; the increase in clarification time from 6/9 to 28/29 hours is still acceptable in an industrial context. Typically, the clarification process under industrial conditions can take 24 hours or more.

The complexes were also used for five consecutive cycles of enzymatic activity testing, using pectin as a substrate at pH 3.8 and 50 °C, as described in Section 2.10.1, Chapter 2. The results of the enzymatic activity reuse tests are summarized in Figure 7.17.

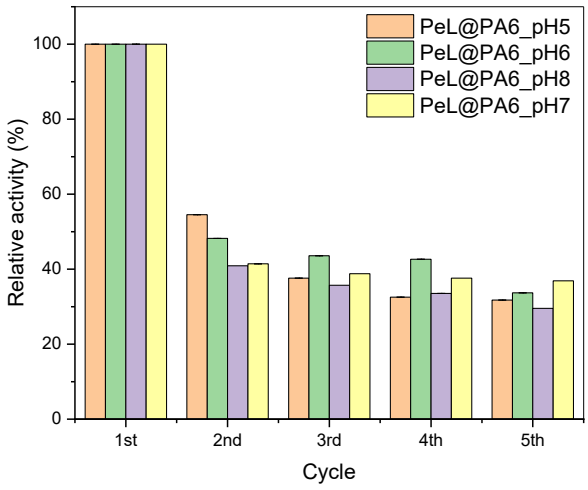


Figure 7.17: Reuse of immobilized enzymes over five activity test cycles. Two tests were performed for each sample, with standard deviations ranging from 0 to 0.003%.

After the first reuse cycle, the PeL@PA6_pH5 and PeL@PA6_pH6 systems retained 55–48% of their initial activity, while the remaining systems retained approximately 40%. In subsequent cycles, the activity remained between 30–40% of the initial activity. The best-performing system was PeL@PA6_pH7, which retained approximately 35% of its initial activity at the end of the fifth reuse cycle. Overall, the activity decreased significantly after the first cycle and then remained relatively stable up to the fifth reuse cycle. The loss of activity is likely due to partial enzyme desorption from the microparticles, leaving only the more strongly bound enzyme fraction. However, the stabilization of residual activity between the second and fifth cycles suggests a robust interaction between the enzyme and the microparticles, which prevents further leaching under the tested conditions.

From a practical standpoint, the immobilized systems can be reused in consecutive cycles of must clarification and enzymatic activity, demonstrating a clear advantage of immobilization and an industrial benefit by enabling enzyme reuse. The reuse results obtained in clarification and activity assays are not directly comparable, as must is a much more complex medium (e.g. polyphenols) than the substrate solution used in activity tests, which explains the differences observed between the two reuse studies.

7.9. Storage stability

Stability during storage is one of the most important characteristics of enzymes, as it directly affects their applicability in industrial processes. Evaluating storage stability allows the assessment of biocatalyst performance under defined storage conditions. In this study, free and immobilized pectinases were stored at 4 °C, and their activities were periodically determined over four months using the DNS method as described in Section 2.11.2, Chapter 2. Figure 7.18 shows the residual activity profiles of the free and immobilized enzymes during the evaluated period.

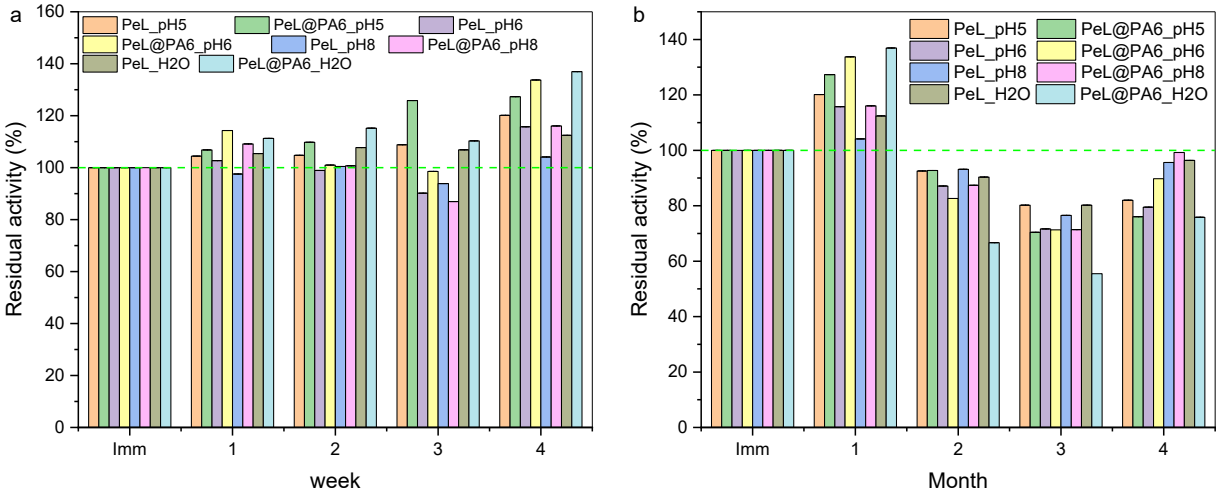


Figure 7.18: Storage stability profile at 4 °C of free and immobilized pectinases: a) stability over 4 weeks; b) stability over 4 months. The dashed green line corresponds to 100% activity. Standard deviation values were obtained from two independent assays for each sample and ranged between 0.002 and 0.005%.

The initial activity was considered 100%. During the first month of evaluation (Figure 7.18a), enzymatic activities increased in almost all cases. In the third week, PeL at pH 6 and pH 8, as well as PeL@PA6 complexes at pH 6 and pH 8, exhibited activities below 100%. However, these values increased again in the fourth week. Consequently, after four weeks of storage, both the free enzyme and the immobilized complexes showed activities higher than their initial values. In all cases, immobilized enzymes exhibited higher activity than their respective free enzymes, with PeL@PA6_pH7 showing the highest activity.

When storage stability was evaluated over a period of four months (Figure 7.18b), a different behavior was observed. In this case, all enzymatic activities were lower than their respective initial activities. Activity decreased during the first three months, followed by a slight increase in the fourth month of storage. Overall, the activity of the immobilized complexes was lower than that of the

corresponding free enzyme, except for the PeL@PA6_pH6 and PeL@PA6_pH8 systems, which exhibited slightly higher activity than their respective free enzymes. This trend suggests that while the PA6 support provides initial stabilization, long-term storage may lead to some enzyme leaching or slow protein denaturation within the porous structure of the microparticles.

These results suggest that both free and immobilized biocatalysts exhibit hyperactivation, as evidenced by residual activities higher than 100% after four weeks of storage. The hyperactivation of pectinases has been previously reported by Bustamante-Vargas et al., who observed a residual activity of 198% after 229 days for an immobilized pectinolytic system [41]. In the present study, this phenomenon may be associated with the presence of the polyamide support, which can provide external protection to the enzyme and create a favorable microenvironment. This microenvironment may enhance pectinolytic activity by protecting the enzyme from adverse temperature effects and by mimicking confinement and aggregation effects similar to those observed in living cells [42]. Furthermore, the gradual hydration of the polyamide matrix over time may improve the accessibility of the substrate to the enzyme's active sites, while the synergistic action between the different enzymes in the commercial cocktail (e.g., pectin methylesterases and polygalacturonases) may be optimized during the initial storage period, leading to the observed hyperactivation. Additionally, conformational rearrangements of the enzyme during storage may contribute to maintaining the enzyme in a more active state.

In summary, PeL@PA6 pectinolytic systems are recommended to be used within 2 to 3 weeks after immobilization in order to preserve their enhanced activity compared to free PeL. This storage behavior allows flexibility in enzymatic preparation, enabling them to be prepared and stored before application, a significant advantage for an industrial application.

7.10. Conclusions

Lyophilized pectinase PeL was successfully immobilized on PA6 MPs through a simple adsorption-based procedure. Among the immobilization conditions examined, an enzyme concentration of 0.5 mg mL^{-1} was identified as optimal for preparing stable and catalytically active conjugates. SEM–EDX analysis confirmed the presence of the enzyme on the surface and within the pore structure of the microparticles. Thermal characterization by DSC and TGA demonstrated that the immobilization process did not compromise the thermal stability of the PA6 support. On the contrary, TGA profiles indicated that the presence of the protein modified the degradation behavior of some of the complexes, producing a more gradual thermal decomposition.

UV-CD analysis revealed that the secondary structure of pectinase is strongly influenced by pH, with the enzyme displaying the greatest conformational stability in the pH range 6–7. In most of the cases, the immobilized enzyme retained significant catalytic competence, as reflected by higher specific activities and immobilization efficiencies, as well as the occurrence of hyperactivation effects under certain conditions.

The catalytic performance of both free and immobilized enzymes was affected by components relevant to enological environments. Glucose acted as an inhibitor of pectinase activity, whereas ethanol promoted moderate activation within the tested concentration range, indicating that the enzyme exhibits good tolerance to ethanol-rich media. These results suggest that the immobilized enzyme is well suited for applications in wine-processing environments.

Kinetic analysis showed that immobilization generally resulted in higher apparent K_m values while V_{max} remained comparable to, or even higher than that of the free enzyme in some cases. These changes are consistent with diffusional limitations and restricted substrate accessibility associated with the porous structure of the PA6 support rather than intrinsic alterations of the catalytic mechanism.

Application tests using industrial white and rosé wine musts demonstrated the practical relevance of the immobilized system. Although clarification required slightly longer times than with the free enzyme, the immobilized pectinase preserved the color and phenolic integrity of the musts, maintaining product quality. Importantly, the immobilized biocatalysts showed good operational stability, displayed retained activity of 40% up to five consecutive cycles. The reusability of the complexes in real wine musts proved industrially viable in two consecutive cycles. After four months of storage, the immobilized complexes displayed higher remaining activities than the respective free enzymes.

Overall, the results demonstrate that PA6 MPs constitute robust and effective supports for pectinase immobilization, enabling stabilization of enzymatic activity while maintaining catalytic functionality under conditions relevant to enological processing. The combination of structural stability, catalytic performance, and operational durability highlights the potential of this immobilization strategy for practical applications in wine clarification and related biotechnological processes related with pectin elimination.

7.11. References

[1] Ottone, C.; Romero, O.; Aburto, C.; Illanes, A.; Wilson, L. Biocatalysis in the winemaking industry: challenges and opportunities for immobilized enzymes. *Compr. Rev. Food Sci. Food Saf.* **2020**, *19*, 595–621. https://doi.org/10.1111/1541-4337.12538.

[2] La Placa, L.; Tsitsigiannis, D.; Camardo Leggieri, M.; Battilani, P. From grapes to wine: impact of the vinification process on ochratoxin A contamination. *Foods* **2023**, *12*, 260. https://doi.org/10.3390/foods12020260.

[3] Kashyap, D. R.; Vohra, P. K.; Chopra, S.; Tewari, R. Applications of pectinases in the commercial sector: a review. *Bioresour. Technol.* **2001**, *77*, 215–227. https://doi.org/10.1016/S0960-8524(00)00118-8.

[4] Hosseini, S. S.; Khodaiyan, F.; Mousavi, S. M.; Azimi, S. Z. Continuous clarification of barberry juice with pectinase immobilised by oxidised polysaccharides. *Food Technol. Biotechnol.* **2021**, *59*, 174–184. https://doi.org/10.17113/ftb.59.02.21.6976.

[5] Martín, M. C.; Morata de Ambrosini, V. I. Effect of a cold-active pectinolytic system on colour development of Malbec red wines elaborated at low temperature. *Int. J. Food Sci. Technol.* **2014**, *49*, 1893–1901. https://doi.org/10.1111/ijfs.12498.

[6] Belda, I.; Conchillo, L. B.; Ruiz, J.; Navascués, E.; Marquina, D.; Santos, A. Selection and use of pectinolytic yeasts for improving clarification and phenolic extraction in winemaking. *Int. J. Food Microbiol.* **2016**, *223*, 1–8. https://doi.org/10.1016/j.ijfoodmicro.2016.02.003.

[7] Deng, Z.; Wang, F.; Zhou, B.; Li, J.; Li, B.; Liang, H. Immobilization of pectinases into calcium alginate microspheres for fruit juice application. *Food Hydrocolloids* **2019**, *89*, 691–699. https://doi.org/10.1016/j.foodhyd.2018.11.031.

[8] Delincée, H. Irradiation of industrial enzyme preparations II. Characterization of fungal pectinase by thin-layer isoelectric focusing and gel filtration. *J. Food Biochem.* **1978**, *2*, 71–85. https://doi.org/10.1111/j.1745-4514.1978.tb00604.x.

[9] Kester, H. C. M.; Visser, J. Purification and characterization of polygalacturonases produced by the hyphal fungus *Aspergillus niger*. *Biotechnol. Appl. Biochem.* **1990**, *12*, 150–160. https://doi.org/10.1111/j.1470-8744.1990.tb00088.x.

[10] Kester, H. C. M.; Visser, J. Purification and characterization of pectin lyase B, a novel pectinolytic enzyme from *Aspergillus niger*. *FEMS Microbiol. Lett.* **1994**, *120*, 63–68. https://doi.org/10.1111/j.1574-6968.1994.tb07008.x.

[11] Dencheva, N.; Oliveira, S.; Braz, J.; Getya, D.; Malfois, M.; Denchev, Z.; et al. Magnetically responsive PA6 microparticles with immobilized laccase show high catalytic efficiency in the enzymatic treatment of catechol. *Catalysts* **2021**, *11*, 239. https://doi.org/10.3390/catal11020239.

[12] Meissner, J.; Prause, A.; Bharti, B.; Findenegg, G. H. Characterization of protein adsorption onto silica nanoparticles: influence of pH and ionic strength. *Colloid Polym. Sci.* **2015**, *293*, 3381–3391. https://doi.org/10.1007/s00396-015-3754-x.

[13] Miles, A. J.; Janes, R. W.; Wallace, B. A. Tools and methods for circular dichroism spectroscopy of proteins: a tutorial review. *Chem. Soc. Rev.* **2021**, *50*, 8400–8413. https://doi.org/10.1039/d0cs00558d.

[14] Whitmore, L.; Wallace, B. A. DICHROWEB, an online server for protein secondary structure analyses from circular dichroism spectroscopic data. *Nucleic Acids Res.* **2004**, *32*, W668–W673. https://doi.org/10.1093/nar/gkh371.

[15] Sreerama, N.; Woody, R. W. Estimation of protein secondary structure from circular dichroism spectra. *Anal. Biochem.* **2000**, *287*, 252–260. https://doi.org/10.1006/abio.2000.4880.

[16] Abrusán, G.; Marsh, J. A. Alpha helices are more robust to mutations than beta strands. *PLoS Comput. Biol.* **2016**, *12*, e1005242. https://doi.org/10.1371/journal.pcbi.1005242.

[17] Burgos, M. I.; Ochoa, A.; Perillo, M. A. β-Sheet to α-helix conversion and thermal stability of β-galactosidase encapsulated in a nanoporous silica gel. *Biochem. Biophys. Res. Commun.* **2019**, *508*, 270–274. https://doi.org/10.1016/j.bbrc.2018.11.077.

[18] Pellicer, J. A.; Navarro, P.; Gómez-López, V. M. Pectin methylesterase inactivation by pulsed light. *Innov. Food Sci. Emerg. Technol.* **2020**, *62*, 102366. https://doi.org/10.1016/j.ifset.2020.102366.

[19] Sieber, V.; Jurnak, F.; Moe, G. R. Circular dichroism of the parallel β helical proteins pectate lyase C and E. *Proteins Struct. Funct. Bioinform.* **1995**, *23*, 32–37. https://doi.org/10.1002/prot.340230105.

[20] Sharma, D. C.; Satyanarayana, T. Thermostable and alkalistable exopolygalacturonase of *Bacillus pumilus*. *Int. J. Biol. Macromol.* **2020**, *164*, 3340–3348. https://doi.org/10.1016/j.ijbiomac.2020.08.204.

[21] Shan, G. F.; Yang, W.; Yang, M. B.; Xie, B. H.; Feng, J. M.; Fu, Q. Effect of temperature and strain rate on the tensile deformation of polyamide 6. *Polymer* **2007**, *48*, 2958–2968. https://doi.org/10.1016/j.polymer.2007.03.013.

[22] Mayans, O.; Scott, M.; Connerton, I.; Gravesen, T.; Benen, J.; Visser, J.; et al. Two crystal structures of pectin lyase A from *Aspergillus* reveal a pH driven conformational change. *Structure* **1997**, *5*, 677–689. https://doi.org/10.1016/S0969-2126(97)00222-0.

[23] Duran Garzon, C.; Habrylo, O.; Lemaire, A.; Guillaume, A.; Carré, Y.; Millet, C.; et al. Characterization of a novel strain of *Aspergillus aculeatinus*. *Carbohydr. Polym.* **2021**, *262*, 117943. https://doi.org/10.1016/j.carbpol.2021.117943.

[24] Dowbysz, A.; Samsonowicz, M.; Kukfisz, B. Modification of glass/polyester laminates with flame retardants. *Materials* **2021**, *14*, 7901. https://doi.org/10.3390/ma14247901.

[25] Dencheva, N. V.; Oliveira, F. D.; Braz, J. F.; Denchev, Z. Z. Bovine serum albumin-imprinted magnetic microparticles. *Eur. Polym. J.* **2020**, *122*, 109375. https://doi.org/10.1016/j.eurpolymj.2019.109375.

[26] Rios, N. S.; Arana-Peña, S.; Mendez-Sanchez, C.; Lokha, Y.; Cortes-Corberan, V.; Gonçalves, L. R. B.; et al. Increasing the enzyme loading capacity of porous supports. *Catalysts* **2019**, *9*, 576. https://doi.org/10.3390/catal9070576.

[27] Datta, S.; Christena, L. R.; Rajaram, Y. R. S. Enzyme immobilization: an overview. *3 Biotech* **2013**, *3*, 1–9. https://doi.org/10.1007/s13205-012-0071-7.

[28] Solís-Oviedo, R.; Pech-Canul, Á., Eds. *Frontiers and New Trends in the Science of Fermented Food and Beverages*; IntechOpen: London, UK, **2019**. https://doi.org/10.5772/intechopen.73404.

[29] Merín, M. G.; Morata de Ambrosini, V. I. Highly cold-active pectinases under wine-like conditions. *Lett. Appl. Microbiol.* **2015**, *60*, 467–474. https://doi.org/10.1111/lam.12390.

[30] Berthels, N.; Cordero-Otero, R.; Bauer, F.; Thevelein, J.; Pretorius, I. Discrepancy in glucose and fructose utilisation. *FEMS Yeast Res.* **2004**, *4*, 683–689. https://doi.org/10.1016/j.femsyr.2004.02.005.

[31] Reynolds, A.; Knox, A.; Di Profio, F. Evaluation of macerating pectinase enzyme activity. *Beverages* **2018**, *4*, 10. https://doi.org/10.3390/beverages4010010.

[32] Radoi, F.; Kishida, M.; Kawasaki, H. Endo-polygalacturonase in wine yeasts. *FEMS Yeast Res.* **2005**, *5*, 663–668. https://doi.org/10.1016/j.femsyr.2004.09.006.

[33] Masson, P.; Mukhametgalieva, A. R. Partial reversible inhibition of enzymes and its metabolic and pharmaco-toxicological implications. *Int. J. Mol. Sci.* **2023**, *24*, 12973. https://doi.org/10.3390/ijms241612973.

[34] Robinson, P. K. Enzymes: principles and biotechnological applications. *Essays Biochem.* **2015**, *59*, 1–41. https://doi.org/10.1042/bse0590001.

[35] Martínez-Lapuente, L.; Guadalupe, Z.; Higueras, M.; Ayestarán, B.; Pérez-Porras, P.; Bautista-Ortín, A. B.; et al. Effect of pre-fermentative treatments. *J. Agric. Food Chem.* **2024**, *72*, 1928–1937. https://doi.org/10.1021/acs.jafc.2c08976.

[36] Aleixandre-Tudo, J. L.; du Toit, W. The role of UV-visible spectroscopy for phenolic compounds quantification. In *Frontiers and New Trends in the Science of Fermented Food and Beverages*; IntechOpen: London, UK, **2019**. https://doi.org/10.5772/intechopen.79550.

[37] Baca-Bocanegra, B.; Gonçalves, S.; Nogales-Bueno, J.; Mansinhos, I.; Heredia, F. J.; Hernández-Hierro, J. M.; et al. Influence of wine pH and ethanol content. *Foods* **2022**, *11*, 1688. https://doi.org/10.3390/foods11121688.

[38] Tapre, A. R.; Jain, R. K. Pectinases: enzymes for fruit processing industry. *Int. Food Res. J.* **2014**, *21*, 447–453.

[39] Faragó, P.; Gălătuş, R.; Hintea, S.; Boşca, A. B.; Feurdean, C. N.; Ilea, A. Intra-oral optical sensor for wine intake. *Sensors* **2019**, *19*, 4719. https://doi.org/10.3390/s19214719.

[40] Homaei, A. A.; Sariri, R.; Vianello, F.; Stevanato, R. Enzyme immobilization: an update. *J. Chem. Biol.* **2013**, *6*, 185–205. https://doi.org/10.1007/s12154-013-0102-9.

[41] Bustamante-Vargas, C. E.; De Oliveira, D.; Nyari, N. L. D.; Valduga, E.; Soares, M. B. A.; Backes, G. T.; et al. In situ immobilization of commercial pectinase. *J. Mol. Catal. B Enzym.* **2015**, *122*, 199–206. https://doi.org/10.1016/j.molcatb.2015.08.009.

[42] Zhang, L.; Jiang, Y.; Shi, J.; Sun, X.; Li, J.; Jiang, Z. Biomimetic polymer-inorganic hybrid microcapsules. *React. Funct. Polym.* **2008**, *68*, 1486–1493. https://doi.org/10.1016/j.reactfunctpolym.2008.08.007.

CHAPTER 8

PA6-based biocatalysts for enzymatic clarification of apple juice

It is known that, in addition to its use in must clarification, pectinases can also be applied to the clarification of fruit juices, such as apple juice. Unlike grape must, apple juice presents a more challenging matrix due to its high pectin content, complex colloidal system, and susceptibility to browning reactions, which can significantly affect clarification efficiency. Notably, the reuse of immobilized enzymes is particularly attractive for juice processing, contributing to cost reduction and process sustainability.

Therefore, this chapter explores the performance of pectinase immobilized on PA6 in the clarification of fresh apple juice, evaluating its potential as a versatile tool for the beverage industry.

8.1. Introduction

Fruit juices are among the most common food groups in the daily diet due to their pleasant taste and positive health effects, such as the effective prevention of cardiovascular diseases [1,2].

The fruit juice production process can be divided into eight main stages. First, the fruits are collected, washed, and selected. The selected fruits are then pressed, and the pulp is separated from the juice. At this stage, the juice is not yet ready to be delivered to the consumer; it must be centrifuged, clarified, and filtered, resulting in a clear liquid with an appealing appearance [1]. Clarification of fruit juice is a fundamental step in the production process, being directly related to its quality, sensory characteristics, and stability during storage. Similar to must clarification, this process can be achieved using enzymes, primarily pectinases [1,3,4].

The industrial application of free enzymes, such as in wine production, presents several disadvantages, including operational instability and low reusability. These enzymes remain in the final product, potentially altering the quality of the juice. In addition, most juices are acidic, and enzyme activity may be affected by pH, reducing their performance and considerably limiting their applications [1]. Immobilization is the process of converting the biocatalysts from a homogeneous (free enzyme) to a heterogeneous (immobilized enzyme) system. As mentioned earlier, immobilized enzymes are more resistant to industrial conditions and can be reused multiple times [1,5].

Apple juice is among the most consumed fruit juices worldwide, appreciated for its characteristic and distinct flavor [4]. Apples possess a high carbohydrate content (approximately 13.8%), which includes both soluble sugars and structural polysaccharides such as starch, pectin, and cellulose, often present as insoluble particles in suspension (pulp). The high pectin content poses a significant challenge in apple juice processing due to the formation of a stable cloud. While suspended pulp particles can be partially removed by mechanical filtration, the presence of pectin significantly

hinders this process by increasing viscosity and stabilizing the suspension. Consequently, the juice must undergo enzymatic clarification, using pectinases to degrade these macromolecules and obtain a clear product [3,4,6–8]. Apple juice also contains various sugars, primarily fructose (5–7%), sucrose (3–4%), and glucose (0.7–1.6%). Although it was demonstrated in the previous chapter that high glucose concentrations (5–15%) can inhibit enzymatic activity, the relatively low levels of glucose naturally present in apple juice suggest that such inhibition may be negligible in this specific matrix *(9)*. Pectinase has been used in several studies to reduce the turbidity of apple juice, [10,11] for example pectinase from *Aspergillus aculeatus* was immobilized on alginate beads and coupled to a continuous reactor for the clarification of apple juice. The resulting juice had a clarification rate of 97% meaning that the pectic substances causing turbidity were almost completely eliminated [12].

Another factor influencing juice appearance is darkening, which is a critical quality parameter, as changes in the original color of the juice can indicate degradation and negatively affect consumer acceptance. This phenomenon generally occurs due to the oxidation of phenolic compounds and, in apple juice, can be either enzymatic or non-enzymatic. One way to prevent this process is the addition of lemon juice (ascorbic acid), which inhibits the oxidation of phenolic compounds [4,13–15]. Furthermore, enzymatic clarification has been reported to assist in color stabilization by promoting the removal of suspended solids that can participate in browning reactions [4,15].

Following the successful development and application of PeL@PA6 biocatalysts in winemaking (Chapters 7), this chapter explores their versatility in a different food matrix: apple juice. The influence of enzymatic clarification on typical juice properties, such as color, is also assessed.

8.2. Juice clarification

The PeL@PA6 complexes obtained by adsorption immobilization at different pH were applied to the clarification of apple juice in order to evaluate the potential industrial applicability of the immobilized enzymes. The apple juice was produced as described in Section 2.8.2 (Chapter 2). Briefly, after washing and cutting the apples into cubes, the apple pieces were crushed and the resulting thick liquid was filtered, yielding raw apple juice with an extraction yield of 69.3%. Unlike the white and rosé musts, which were supplemented with 2 mg/mL of commercial pectin, apple juice contains significant amounts of endogenous pectin (0.5% to 1.6% w/v). This natural pectin is characterized by a high degree of esterification (91-92%) and is composed of homogalacturonan (HG) and rhamnogalacturonan (RG-I and RG-II) domains. Due to its high methylation, this matrix is

particularly susceptible to clarification by specific pectinases, such as pectin lyase (PL), one of the key enzymatic activities present in the lyophilized pectinase preparation used in this study [15–17].

Clarification experiments were performed at room temperature (23 °C) under gentle agitation, using 0.1 mg of either free pectinase or the corresponding immobilized enzyme. The results of all clarification assays are presented in Figure 8.1.

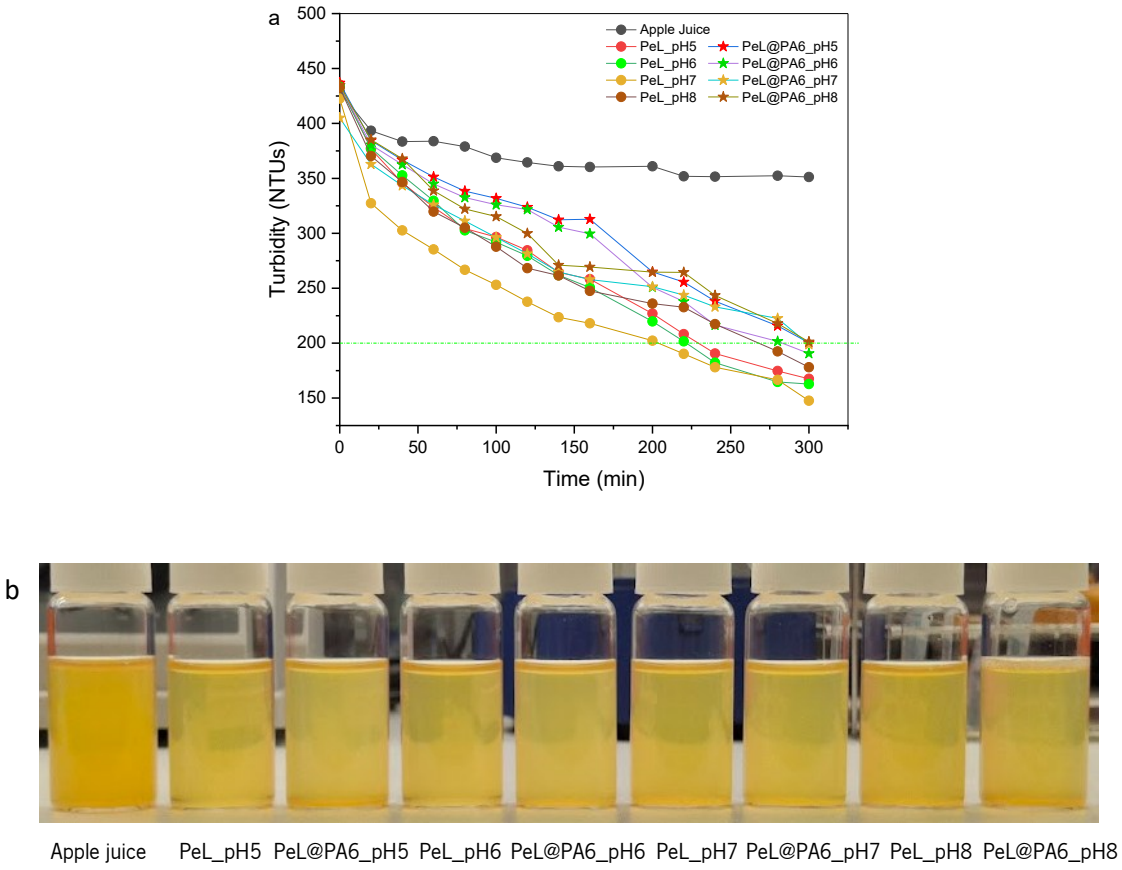


Figure 8.1: Clarification studies with free and immobilized pectinases: a) clarification of apple juice, the dashed line indicates the level of 200 NTUs below which the apple juice is considered completely clarified.; b) visual appearance of the juice before and after clarification.

As shown in Figure 8.1a, the initial turbidity of the apple juice (430 Nephelometric Turbidity Units (NTU)) was significantly higher than that observed for grape must (60–80 NTU), which was expected, since the juice did not undergo any pre-treatment prior to enzymatic clarification. Filtration was the only step applied before enzyme addition; nevertheless, residual pulp components may have remained in the juice, contributing to its high turbidity. After 20 minutes, a decrease in turbidity was observed for all samples. In the control sample (without enzyme), turbidity

decreased from 430 NTU to approximately 390 NTU, while in the samples treated with enzymes it decreased to around 375 NTU, indicating the onset of enzymatic clarification. After 100 minutes, the turbidity of the untreated juice stabilized at approximately 375 NTU. According to C. Çesko et al. [15] apple juice can be considered clarified when turbidity values fall below 200 NTU. Higher clarification rates can be achieved using different clarification methods, such as ultrafiltration [4]. Oliveira et al. [12] obtained a clarification rate of 97% by combining the efficiency of a continuous reactor with immobilized pectinase.

In the present study, this threshold was reached after 4 hours for free enzymes and after 5 hours for immobilized enzymes. Among the free enzymes, the fastest clarification was observed for the PeL_pH7 sample (Figure 8.1a). The remaining free enzyme systems exhibited similar behavior, although PeL_pH8 showed the slowest clarification rate, as also observed during must clarification in the previous chapter.

For the immobilized enzymes, the clarification profiles were similar to those of the free enzymes during the first 160 minutes. The PeL@PA6_pH7 complex showed the fastest initial decrease in turbidity. However, the complex immobilized at pH 6 reached the target turbidity (<200 NTU) in the shortest overall time. The longer clarification time observed for immobilized enzymes can be attributed to diffusional limitations and reduced substrate accessibility to the active sites, which may be partially hindered by immobilization within or on the surface of the microparticles.

Figure 8.1b illustrates the visual appearance of the juice before and after clarification. As expected, the untreated juice appears significantly cloudier than the enzymatically treated samples.

Generally, all systems were able to reach the desired turbidity level. Although the immobilized enzymes required a slightly longer clarification time, they demonstrated clear applicability for apple juice clarification. In the literature, similar turbidity values are typically achieved after approximately 2 hours of treatment at elevated temperatures (40–50 °C) [15]. In contrast, in the present study clarification was achieved at room temperature, albeit requiring approximately 3 additional hours, which represents an important advantage in terms of energy savings and process sustainability.

Turbidity measurements allowed monitoring of the clarification process but did not unequivocally demonstrate effective pectin degradation. For this reason, a pectin test was performed on all apple juice samples.

8.2.1. Pectin test

The depectinization of apple juice was confirmed using the pectin test, as described in Section 2.8.3.2 (Chapter 2). Pectin is composed mainly of galacturonic acid and, in the presence of ethanol, it precipitates, forming insoluble flakes or a gel-like structure. Figure 8.2 shows the visual appearance of apple juice samples after the addition of ethanol.

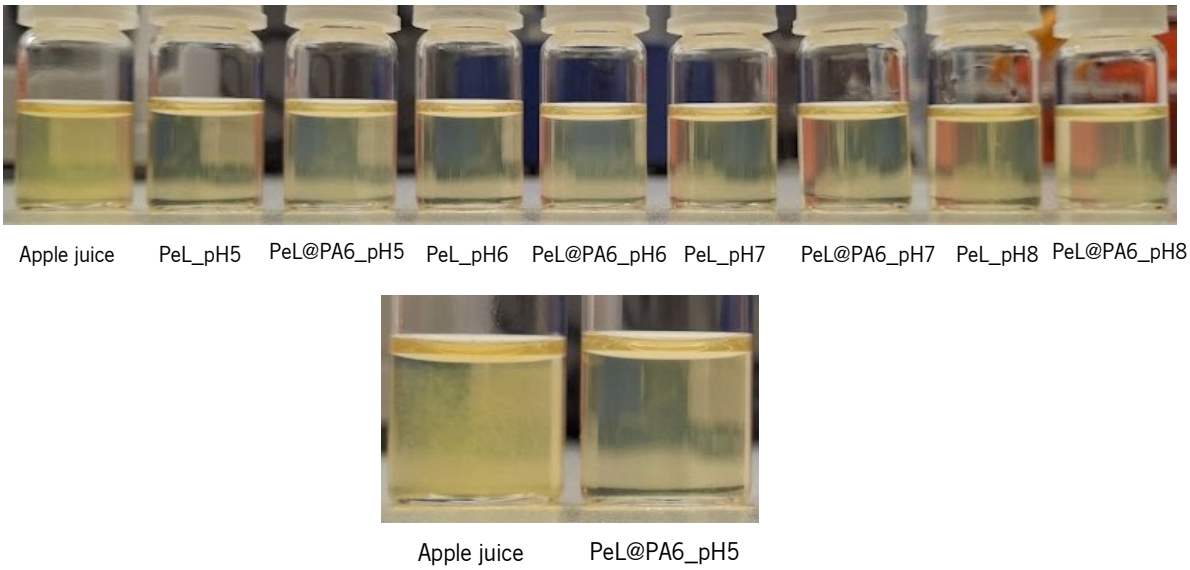


Figure 8.2: Pectin test results of apple juice samples.

When the results are examined, it is possible to see that unclarified apple juice presents visible aggregates, confirming the presence of pectin. In contrast, apple juice treated with enzyme did not show sediment formation, indicating that the pectin was completely degraded by both free and immobilized pectinase. According to the pectin test results, both PeL and PeL@PA6 were able to completely depectinize the apple juice under the tested conditions. These results confirm that turbidity values below 200 NTU correspond to pectin-free juice, validating the clarification data discussed in the previous section. Residual turbidity remained 200 NTU suggests that the remaining turbidity is likely composed of protein-polyphenol (tannin) complexes or other colloidal particles that were not completely sedimented by the centrifugation parameters employed. These results are consistent with the literature, which identifies enzymes as a necessary step to reduce viscosity and facilitate subsequent filtration or ultrafiltration, which are ultimately required to achieve complete industrial transparency [15].

8.2.2. pH determination

The pH of apple juice is a critical regulatory parameter for both quality and safety; by modulating the zeta potential and electrostatic repulsion of cloud particles, it optimizes the precipitation of undesirable microorganisms and enhances the performance of pectolytic enzymes (active at pH 3–4). Maintaining pH levels between 2.5 and 4.5 is essential to ensure microbiological stability and chromatic preservation through more effective clarification and stabilization processes [15,17–19]. The previously produced apple juice had a pH of 3.93. To assess whether clarification affects the acidity of the juice, its pH was determined, and the results are presented in Table 8.1.

Table 8.1: pH of samples after enzymatic clarification.

Sample	**pH**	**Sample**	**pH**
Untreated juice	3.93		
PeL_pH5	4.06	PeL@PA6_pH5	4.07
PeL_pH6	4.01	PeL@PA6_pH6	4.05
PeL_pH7	3.99	PeL@PA6_pH7	3.95
PeL_pH8	4.01	PeL@PA6_pH8	3.98

The pH of the samples after clarification is slightly higher than the pH before the addition of enzymes (Table 8.1). This increase is not significant and may be due to the addition of enzymatic solutions. The small variations observed are within the typical pH range of apple juice. The results indicate that enzyme clarification does not compromise the acidity of the juice. Maintaining the pH is important for the microbiological stability and sensory profile of apple juice.

8.2.3. Optical properties of apple juice

Apple juice, with and without enzymatic treatment, was analyzed by Ultraviolet-Visible (UV/VIS) spectroscopy, as described in Section 2.9.2 (Chapter 2). The parameters determined were clarity and browning index (BI). Clarity, an essential parameter for clarified juices, was determined at 660 nm, where light scattering by suspended particles is the dominant factor, providing an estimate of the juice's transparency and homogeneity. Thus, higher clarity values correspond to lower turbidity [4,15]. Browning refers to the darkening of the juice's color, a phenomenon that generally occurs due to the oxidation of phenolic compounds. It is a critical quality parameter, as changes in the

original color of the juice may indicate degradation and negatively affect consumer acceptance. BI was determined at 420 nm, a wavelength characteristic of the absorption of oxidized phenolic compounds, corresponding to chemical changes in color [3,13,15,20]. The results are shown in Figure 8.3 and Table 8.2.

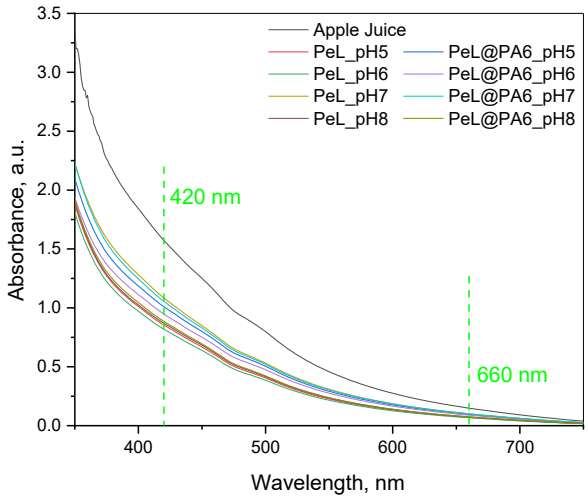


Figure 8.3: UV/VIS spectrum of apple juice before and after clarification. Dashed green lines correspond to the wavelengths used to determine the clarity and browning index.

Table 8.2: Results of the clarity and browning index for all juice samples.

Sample	**Clarity (%)**	**BI (a.u.)**	**Decrease in browning index (%)**
Apple juice	0	1.573	0
PeL_pH5	52.35	0.855	45.65
PeL@PA6_pH5	39.60	1.011	35.73
PeL_pH6	53.02	0.819	47.93
PeL@PA6_pH6	39.60	0.949	39.67
PeL_pH7	32.21	1.085	31.02
PeL@PA6_pH7	32.21	1.056	32.87
PeL_pH8	49.66	0.87	44.69
PeL@PA6_pH8	49.66	0.886	43.67

The results show that both free and immobilized enzymes significantly improved the optical properties of apple juice.

The clarity of apple juice before clarification was 0% and increased to 32 to 52% in juices treated with enzymes. Clarification with free enzymes at pH 5 and pH 6 resulted in juices with higher clarity than those treated with the respective immobilized enzymes; conversely, at pH 7 and pH 8, the clarity values were identical for free and immobilized enzymes. The clarity results obtained show significant agreement with the data from Maryani et al., who reported a 42.6% increase in the clarity of apple juice when using free pectinases produced by Bacillus sp. under optimal conditions of 40 °C and pH 5.0 [21].

BI of the juice decreased significantly after enzymatic treatment, indicating the effectiveness of pectinase in reducing oxidized polyphenolic compounds and pigments, which resulted in a juice with enhanced color stability. This phenomenon is attributed to the co-precipitation of oxidized polyphenolic aggregates along with the hydrolyzed pectin molecules; once the pectin network is degraded, these complexes are destabilized and can be removed, improving the visual characteristics of the final product [22]. A strong correlation was observed between juice clarity and BI reduction, with samples showing greater transparency also exhibiting the lowest browning values. Furthermore, the reduction achieved (up to 47.93%) is consistent with reduction levels (48–86%) reported in the literature for natural agents, such as green tea extracts, and for other enzymatic stabilization systems in apple juice, namely immobilized laccases [13,22].

In summary, treatment of apple juice with both free and immobilized enzymes resulted in clearer and more visually appealing products. Immobilization of the enzyme on PA6 microparticles successfully preserves the enzyme's ability to clarify and decolorize complex fruit matrices.

8.3. Reuse of immobilized pectinase in consecutive clarification cycles

In the previous chapter, the complexes were reused in two consecutive cycles of must clarification and in five consecutive cycles of enzymatic activity. These results demonstrated that the complexes can be reused multiple times. In this section, the same complexes were applied in multiple cycles of apple juice clarification, as described in Section 2.10.2.2 (Chapter 2). The results are presented in Figure 8.4.

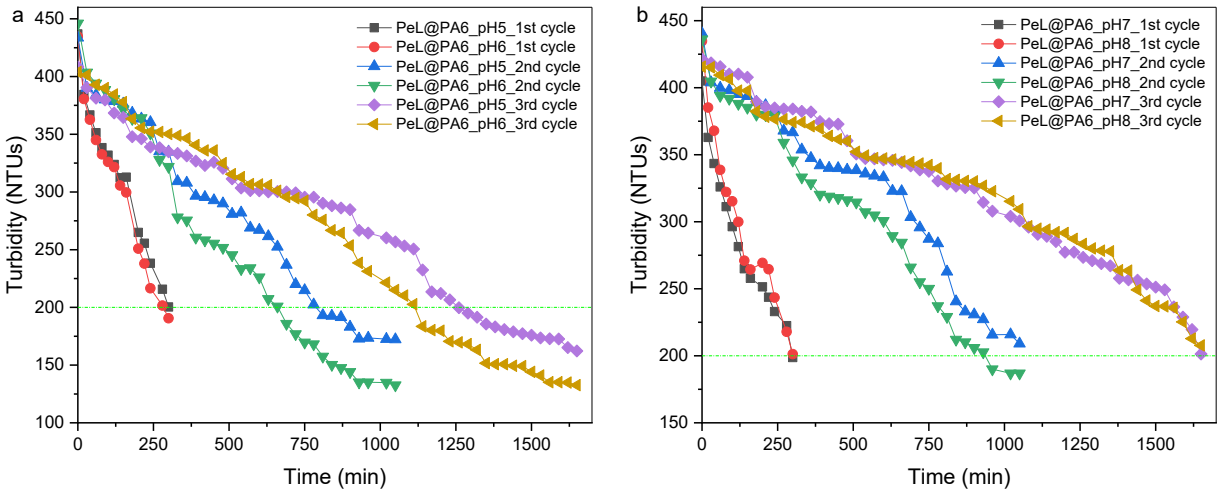


Figure 8.4: Reuse of immobilized enzyme in three consecutive cycles of clarification of apple juice. a) PeL@PA6_pH5 and PeL@PA6_pH6; b) PeL@PA6_pH7 and PeL@PA6_pH8.

Analysis of Figure 8.4 shows that apple juice clarification can be performed using the same immobilized enzyme for at least three consecutive cycles. The clarification time increased with each cycle. The first cycle required approximately 5 hours (red dots and black squares), the second cycle required 18 hours (green and blue triangles), and the third cycle was the longest, lasting 28 hours (yellow triangles and purple diamonds). The increase in clarification time can be explained by the increased difficulty of substrate access to the enzyme's active site, possibly due to the adsorption of byproducts generated during pectin hydrolysis onto the microparticles and juice components (such as polyphenols or proteins).

In conclusion, the immobilized enzyme can be reused for at least three consecutive clarification cycles, representing a significant advantage at the industrial level.

8.4. Conclusions

In this chapter, the versatility of the PeL@PA6 complexes obtained at various pH was demonstrated by extending their application from white and rosé must clarification to apple juice processing. The juice was produced at a laboratory scale with a yield of 69%, and enzymatic clarification was achieved at room temperature within approximately 5 hours. This process reached a clarification rate of approximately 56% for both free and immobilized systems, effectively bringing the turbidity below the industrial threshold of 200 NTU. While this rate is lower than the 97% reported by Oliveira et al.[12], it is important to note that their study employed a continuous reactor

and higher operating temperatures. In contrast, the PeL@PA6 systems achieved successful depectinization at room temperature (23 °C), which represents a significant advantage for preserving the juice's sensory profile and reducing energy consumption.

Although the immobilized systems required slightly longer processing times compared to the free enzyme, complete depectinization was achieved, as confirmed by the pectin test. Optical analyses revealed a significant improvement in juice clarity and a marked reduction in the browning index, resulting in a more visually appealing product without compromising essential physicochemical properties, such as pH. Notably, the clarity increase (32–53%) and browning reduction (up to 47.93%) obtained in this study are superior to results reported for other stabilization methods, such as the use of *Bacillus sp.* pectinases (42.6% clarity) [21] or green tea extracts for browning prevention [13].

Furthermore, the immobilized pectinase was successfully reused for at least three consecutive clarification cycles, highlighting a major advantage of this system in terms of operational stability. Overall, these results demonstrate that PA6-immobilized pectinase is a robust and versatile biocatalyst, capable of efficiently clarifying and decolorizing complex fruit-based matrices, reinforcing its potential applicability across different beverage processing sectors.

8.5. References

[1] Wang, F.; Xu, H.; Wang, M.; Yu, X.; Cui, Y.; Xu, L.; et al. Application of immobilized enzymes in juice clarification. *Foods* **2023**, *12*, 4258. https://doi.org/10.3390/foods12234258.

[2] Bartoszek, M.; Polak, J. A comparison of antioxidative capacities of fruit juices, drinks and nectars, as determined by EPR and UV/VIS spectroscopies. *Spectrochim. Acta Part A Mol. Biomol. Spectrosc.* **2016**, *153*, 546–549. https://doi.org/10.1016/j.saa.2015.09.022.

[3] Uzuner, S. Effect of crude pectinase on apple juice quality characteristics by desirability approach. *Gıda* **2018**, *43*, 558–568. https://doi.org/10.15237/gida.GD18024.

[4] Nehmé, L.; El Tekle, M.; Barakat, N.; El Khoury, A.; Azzi-Achkouty, S.; El Rayess, Y. Alternative processes for apple juice stabilization and clarification: a bibliometric and comprehensive review. *Processes* **2024**, *12*, 296. https://doi.org/10.3390/pr12020296.

[5] Homaei, A. A.; Sariri, R.; Vianello, F.; Stevanato, R. Enzyme immobilization: an update. *J. Chem. Biol.* **2013**, *6*, 185–205. https://doi.org/10.1007/s12154-013-0102-9.

[6] Ribeiro, D. S.; Henrique, S. M. B.; Oliveira, L. S.; Macedo, G. A.; Fleuri, L. F. Enzymes in juice processing: a review. *Int. J. Food Sci. Technol.* **2010**, *45*, 635–641. https://doi.org/10.1111/j.1365-2621.2010.02177.x.

[7] Ceci, L.; Lozano, J. Determination of enzymatic activities of commercial pectinases for the clarification of apple juice. *Food Chem.* **1998**, *61*, 237–241. https://doi.org/10.1016/S0308-8146(97)00088-5.

[8] Sandri, I. G.; Fontana, R. C.; Barfknecht, D. M.; da Silveira, M. M. Clarification of fruit juices by fungal pectinases. *LWT-Food Sci. Technol.* **2011**, *44*, 2217–2222. https://doi.org/10.1016/j.lwt.2011.02.008.

[9] Lee, C. Y.; Shallenberger, R. S.; Vittum, M. T. Free sugars in fruits and vegetables. *N. Y. Food Life Sci. Bull.* **1970**, *1*, 1–12.

[10] McLellan, M. R.; Kime, R. W.; Lind, L. R. Apple juice clarification with the use of honey and pectinase. *J. Food Sci.* **1985**, *50*, 206–208. https://doi.org/10.1111/j.1365-2621.1985.tb13310.x.

[11] Singh, S.; Gupta, R. Apple juice clarification using fungal pectinolytic enzyme and gelatin. *Indian J. Biotechnol.* **2004**, *3*, 573–576.

[12] de Oliveira, R. L.; Dias, J. L.; da Silva, O. S.; Porto, T. S. Immobilization of pectinase from *Aspergillus aculeatus* in alginate beads and clarification of apple and umbu juices in a packed bed reactor. *Food Bioprod. Process.* **2018**, *109*, 9–18. https://doi.org/10.1016/j.fbp.2018.02.005.

[13] Klimczak, I.; Gliszczyńska-Świgło, A. Green tea extract as an anti-browning agent for cloudy apple juice. *J. Sci. Food Agric.* **2017**, *97*, 1420–1426. https://doi.org/10.1002/jsfa.7880.

[14] Zhu, D.; Ji, B.; Eum, H. L.; Zude, M. Evaluation of the non-enzymatic browning in thermally processed apple juice by front-face fluorescence spectroscopy. *Food Chem.* **2009**, *113*, 272–279. https://doi.org/10.1016/j.foodchem.2008.07.009.

[15] Çesko, C.; Veseli, J.; Paluzar, H.; Sfishta, A.; Koraqi, H.; Durmishi, N.; et al. Investigation of the effect of pectinase and amyloglucosidase enzyme mixture on clarification of apple juice. *Food Sci. Technol.* **2024**, *12*, 159–169. https://doi.org/10.13189/fst.2024.120301.

[16] Tapre, A. R.; Jain, R. K. Pectinases: enzymes for fruit processing industry. *Int. Food Res. J.* **2014**, *21*, 447–453.

[17] Kashyap, D. R.; Vohra, P. K.; Chopra, S.; Tewari, R. Applications of pectinases in the commercial sector: a review. *Bioresour. Technol.* **2001**, *77*, 215–227. https://doi.org/10.1016/S0960-8524(00)00118-8.

[18] Liu, D.; Liu, X.; Liu, J.; Bi, J.; Schols, H. A. Characterization of pectic polysaccharides and apple juice properties for 13 apple varieties. *Int. J. Biol. Macromol.* **2025**, *321*, 146216. https://doi.org/10.1016/j.ijbiomac.2025.146216.

[19] Baca-Bocanegra, B.; Gonçalves, S.; Nogales-Bueno, J.; Mansinhos, I.; Heredia, F. J.; Hernández-Hierro, J. M.; et al. Influence of wine pH and ethanol content on the fining efficacy of proteins from winemaking by-products. *Foods* **2022**, *11*, 1688. https://doi.org/10.3390/foods11121688.

[20] Selen Burdurlu, H.; Karadeniz, F. Effect of storage on nonenzymatic browning of apple juice concentrates. *Food Chem.* **2003**, *80*, 91–97. https://doi.org/10.1016/S0308-8146(02)00245-5.

[21] Berutu, C. A. M.; Fahrurrozi, F.; Meryandini, A. Pectinase production and clarification treatments of apple (Malus domestica) juice. *Ann. Bogor* **2017**, *21*, 63–68. https://doi.org/10.14203/ann.bogor.2017.v21.n2.63-68.

[22] Shirvani, A.; Mirzaaghaei, M.; Goli, S. A. H. Application of natural fining agents to clarify fruit juices. *Compr. Rev. Food Sci. Food Saf.* **2023**, *22*, 4190–4216. https://doi.org/10.1111/1541-4337.13207.

CHAPTER 9

Final conclusions and future perspectives

9.1. Final conclusions

The present PhD thesis addressed the development of polyamide-based immobilized biocatalysts, with and without magnetic responsiveness, for applications in beverage processing, focusing particularly on the clarification of wine musts and fruit juices through immobilized pectinase systems.

The work combined polymer synthesis and characterization with enzymology and elements of applied food biotechnology, aiming to design efficient, reusable, and industrially compatible polymer-supported biocatalytic systems. The results obtained demonstrate that polyamide microparticles (PAMP) synthesized via activated anionic ring-opening polymerization (AAROP) constitute versatile and robust supports for enzyme immobilization and represent promising platforms for sustainable biocatalytic processes in the food industry.

9.1.1. Development of polyamide microparticle supports

Porous polyamide microparticles based on PA4, PA6, PA12 and PA612 copolymer systems, both with and without incorporation of Fe payloads, were successfully synthesized using AAROP of lactam monomers. Polymerization yields ranged from 42 to 77%, confirming the suitability of this synthetic route for producing pulverulent polyamide materials.

Comprehensive characterization using FTIR spectroscopy, optical microscopy, SEM, DSC and TGA demonstrated that the incorporation of 3–5 wt.% Fe particles does not significantly affect the intrinsic structural and thermal properties of the polymer matrix. Instead, the Fe particles provide magnetic responsiveness while also acting as heteronucleating agents. Importantly, the variation of lactam monomers and the presence or absence of Fe produced microparticles with distinct morphologies, particle sizes, surface topologies and pore structures. These structural characteristics proved to be key parameters governing enzyme immobilization efficiency and catalytic performance.

9.1.2. Immobilization of pectinolytic enzymes

Both a commercial enological pectinase preparation (Viazym® Extrem, PeV) and a purified lyophilized pectinase (PeL) were immobilized onto the synthesized polyamide microparticles.

Among the immobilization approaches investigated, physical adsorption emerged as the most practical and efficient strategy. Compared with covalent immobilization, adsorption offers clear

advantages in terms of operational simplicity, lower cost, and compatibility with food-processing regulations, as it avoids the use of potentially hazardous reagents such as glutaraldehyde.

Although the immobilization yield per cycle was relatively moderate (approximately 15%), the enzyme solutions could be reused multiple times during immobilization, ensuring efficient use of the enzymatic preparation and minimizing waste without impairing the activity of the enzyme complexes. The initial amount of enzyme has almost no influence on the immobilization process, the pH of the medium, on the contrary, strongly influences the immobilization yield being the highest at pH6-7.

9.1.3. Catalytic performance and kinetic behavior

The catalytic properties of the immobilized systems were evaluated through enzymatic activity measurements and kinetic analysis.

Most immobilized systems displayed equal or superior catalytic efficiencies compared with the free enzyme, with specific activities reaching values up to 2.5 times higher in certain cases. This behavior indicates a hyperactivation effect, likely associated with favorable enzyme orientation and stabilization at the polymer–enzyme interface.

Kinetic analysis demonstrated that immobilization generally results in comparable or slightly increased V_{max} values, and higher apparent K_m values. The increase in K_m is primarily attributed to substrate diffusion limitations within the porous polymer structure, rather than to intrinsic changes in the catalytic mechanism. Interestingly, while the PeV and its immobilized conjugates (PeV@PA) display a clear substrate inhibition effect during the pectin degradation, PeL and PeL@PA obey the Michaelis-Menten kinetic model.

These results demonstrate that the chemical structure, morphology and surface topology of the polyamide supports strongly influence the catalytic behavior of the immobilized enzymes, highlighting the importance of support design in immobilized biocatalysis.

9.1.4. Stability and environmental effects

The immobilized enzymes exhibited excellent storage stability, maintaining significant catalytic activity after prolonged storage at 4 °C. Systems prepared with the commercial enzyme retained approximately 75% of their initial activity after one month, whereas immobilized systems based on the purified enzyme remained active for up to four months.

The influence of environmental factors relevant to winemaking was also investigated. The results showed that glucose acts as an inhibitor of pectinase activity and that moderate ethanol concentrations may induce certain activation of enzymatic activity.

9.1.5. Validation of enzymatic action in real beverages

The developed biocatalysts were successfully validated using real industrial matrices, including white and rosé wine musts supplied by Sogrape Vinhos Lda. and fresh apple juice produced at laboratory scale.

Immobilized enzymes achieved complete clarification of rosé wine musts (≤20 NTU) within 3–9 hours, depending on the polyamide support and immobilization pH used. Similarly, the immobilized purified enzyme enabled complete clarification of white wine must within approximately 6 hours. Importantly, the clarification process did not alter the color or odor characteristics of the must, initially confirming the compatibility of the polyamide supports with enological applications.

The versatility of the developed biocatalysts was further demonstrated through apple-juice clarification, where the immobilized enzyme achieved complete depectinization within less than 5 hours, improvements in juice clarity of 32–53%, and reductions in browning index of 31–46%. These results were obtained without compromising the physicochemical or sensory properties of the juice.

9.1.6. Reusability and process sustainability

One of the most significant advantages of the developed systems is their reusability. The immobilized biocatalysts of this thesis could be reused for at least three consecutive clarification cycles in both wine must and fruit juice processing. In enzymatic activity assays, the commercial enzyme system maintained approximately 50% of its initial activity after seven reuse cycles, while the purified enzyme system retained significant activity after five cycles.

These results demonstrate that the developed immobilized enzyme systems provide clear operational and economic advantages over free enzymes, contributing to more sustainable and efficient beverage-processing technologies.

9.1.7. Major scientific contribution

The results of this thesis demonstrate that polyamide microparticles synthesized via AAROP represent efficient and versatile supports for enzyme immobilization. Among the investigated materials, PA6-based microparticles, with and without Fe incorporation, emerged as the most suitable supports for pectinase immobilization.

The developed immobilized biocatalysts combine high catalytic activity, structural stability, operational reusability, compatibility with real beverages. These characteristics confirm their strong potential for industrial application in wine and fruit-juice clarification processes.

The scientific studies presented in this thesis complement and harmoniously expand the range of applications of porous polyamide particles as effective enzyme carriers, a role that has already been demonstrated in the immobilization of other enzymes from the oxidoreductase group, including laccases, as well as in their use as carriers for enzyme cascades.

9.2. Future perspectives

The potential of immobilized pectinases for the clarification of apple juice and white and rosé wine must was demonstrated in this thesis at laboratory scale. Nevertheless, several relevant aspects remain unexplored and represent promising directions for future research.

Sensory evaluation of must clarified using the developed biocatalysts, particularly through triangular sensory tests, would allow a systematic assessment of their impact on sensory attributes such as aroma, flavor, and overall sensory quality. Such analyses are essential to confirm consumer acceptance and to ensure that the enzymatic treatment does not introduce perceptible differences when compared with conventional clarification processes.

Furthermore, detailed profiling of volatile compounds by gas chromatography–mass spectrometry would provide valuable information on whether polyamide microparticles may selectively adsorb key varietal aroma compounds, thereby ensuring that the full aromatic complexity of the wines is preserved.

In addition, validation of the developed biocatalysts at semi-industrial scale, involving clarification of larger volumes of must, would provide important information regarding process efficiency, operational handling, hydrodynamics, and mass-transfer limitations. Such studies would also enable future evaluation of the recovery and reuse of the biocatalyst under conditions even closer to industrial practice.

Another important challenge currently faced by both the wine industry and consumers is the production of wines with reduced alcohol content. This objective could potentially be addressed through the co-immobilization or sequential immobilization of multiple enzymes on polyamide supports, particularly systems based on glucose oxidase. The integration of clarification and partial sugar conversion within a single or combined biocatalytic platform represents an attractive strategy for process intensification, potentially enabling simultaneous control of turbidity and fermentable sugar content.

Finally, further optimization of polyamide supports, e.g., through surface functionalization and better control of pore architecture aimed at improving enzyme retention, orientation, and long-term stability, may enhance the performance and durability of the immobilized systems. Such developments could also contribute to improved resistance to fouling and enhanced catalytic lifetime during repeated processing cycles.

These future developments may enable the design of multifunctional, reusable, and industrially viable biocatalysts, reinforcing the potential of polyamide-based systems as versatile tools for the sustainable processing and clarification of beverages.

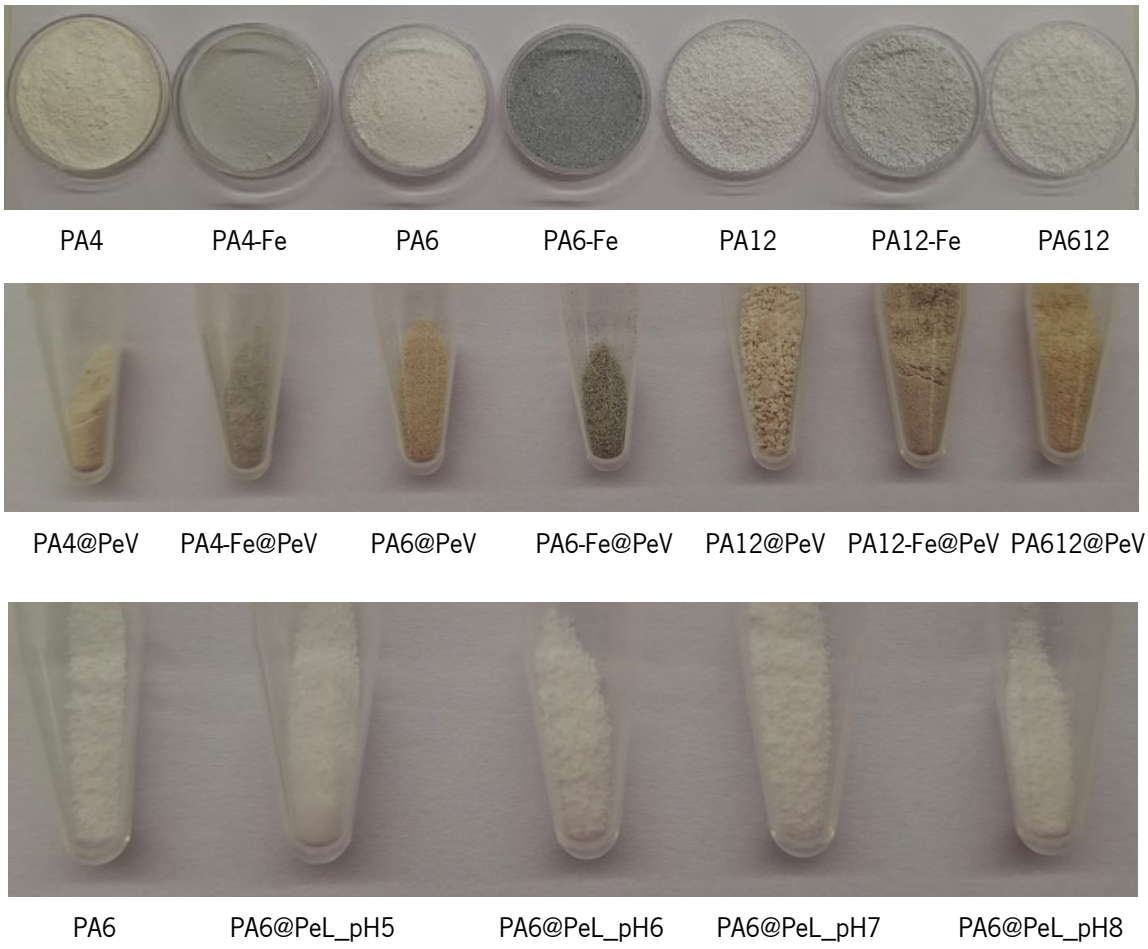
APPENDIX

A.1. Photographic Record of Experimental Work



PeV PeL

Figure A.1: Visual comparison of enzyme preparations.



PA4 PA4-Fe PA6 PA6-Fe PA12 PA12-Fe PA612

PA4@PeV PA4-Fe@PeV PA6@PeV PA6-Fe@PeV PA12@PeV PA12-Fe@PeV PA612@PeV

PA6 PA6@PeL_pH5 PA6@PeL_pH6 PA6@PeL_pH7 PA6@PeL_pH8

Figure A.2: Visual comparison of PA microparticles before and after immobilization.

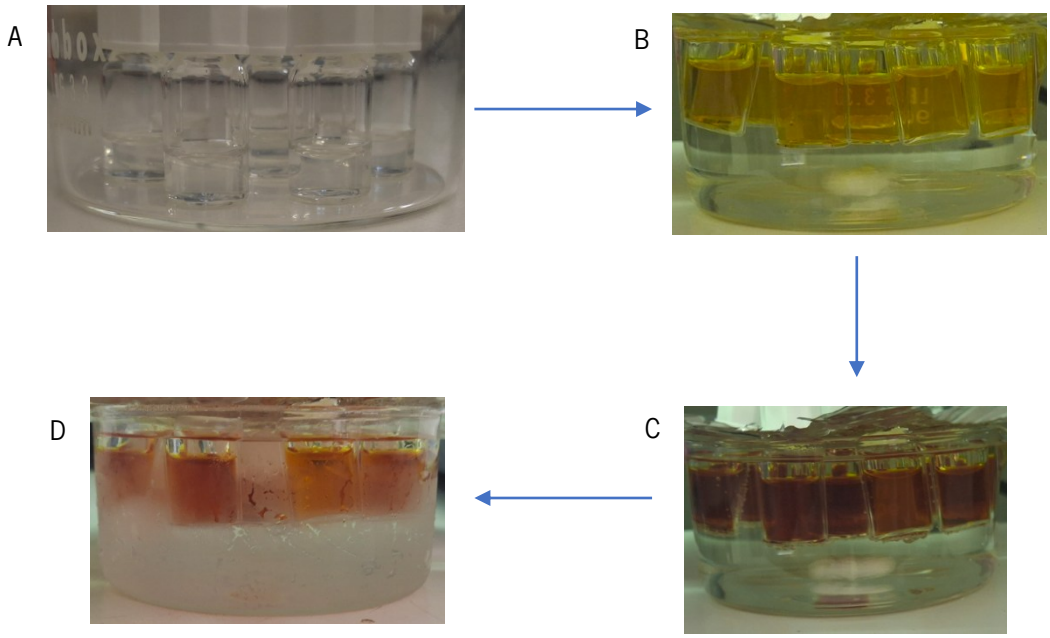


Figure A.3: DNS Method: A) Enzyme + substrate; B) Add DNS; C) 90°C water bath; D) Ice water bath.

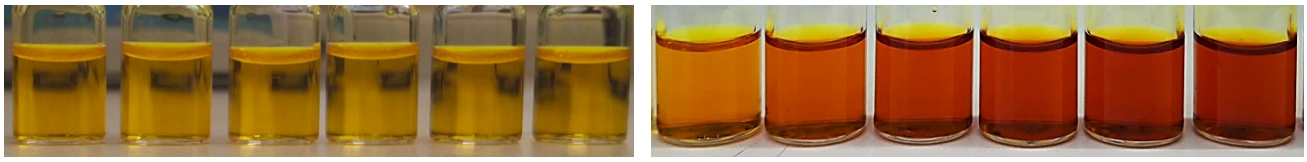


Figure A.4: Visual comparison of Calibration curve (0.14 - 2.83 µmol/mL) (before and after adding DNS and heating to 90°C).

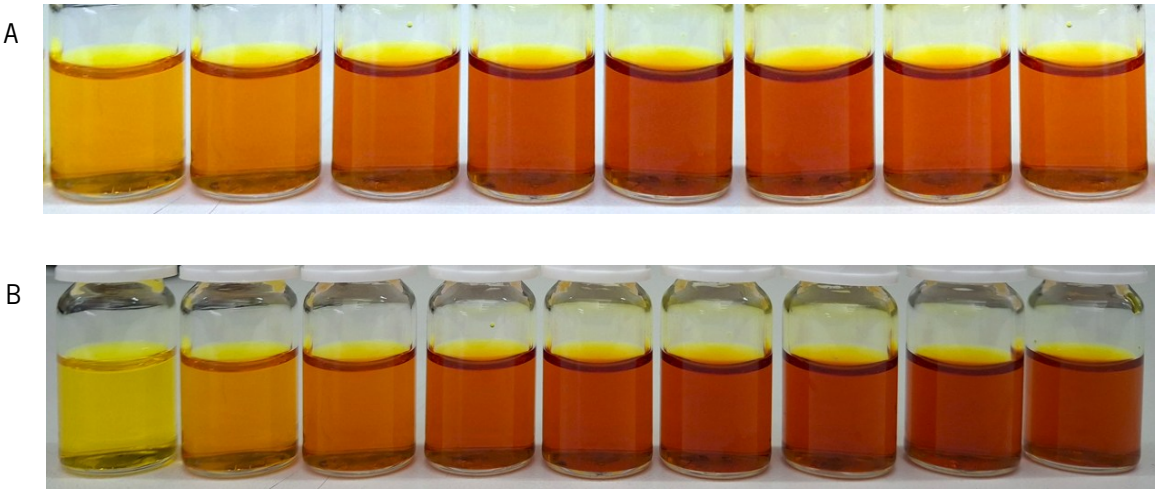


Figure A.5: Visual comparison of kinetic: A) PeV; B) PeL.

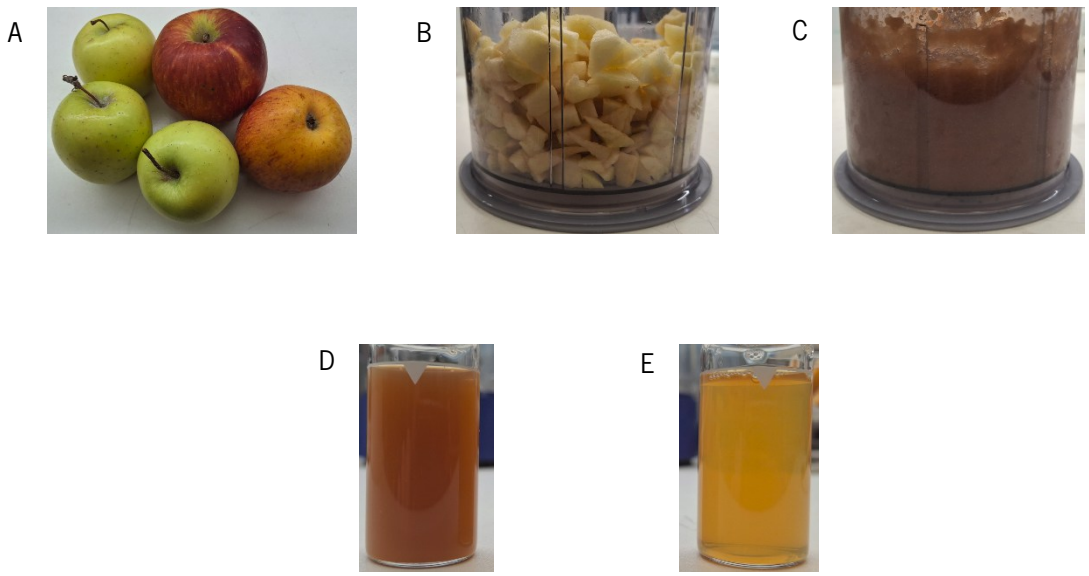


Figure A.6: Apple juice production (visual flowchart: A) Apples B) Sliced apples -> C) Blending -> D) Filtration/Centrifugation -> E) Raw juice).

A.2. Spectroscopic

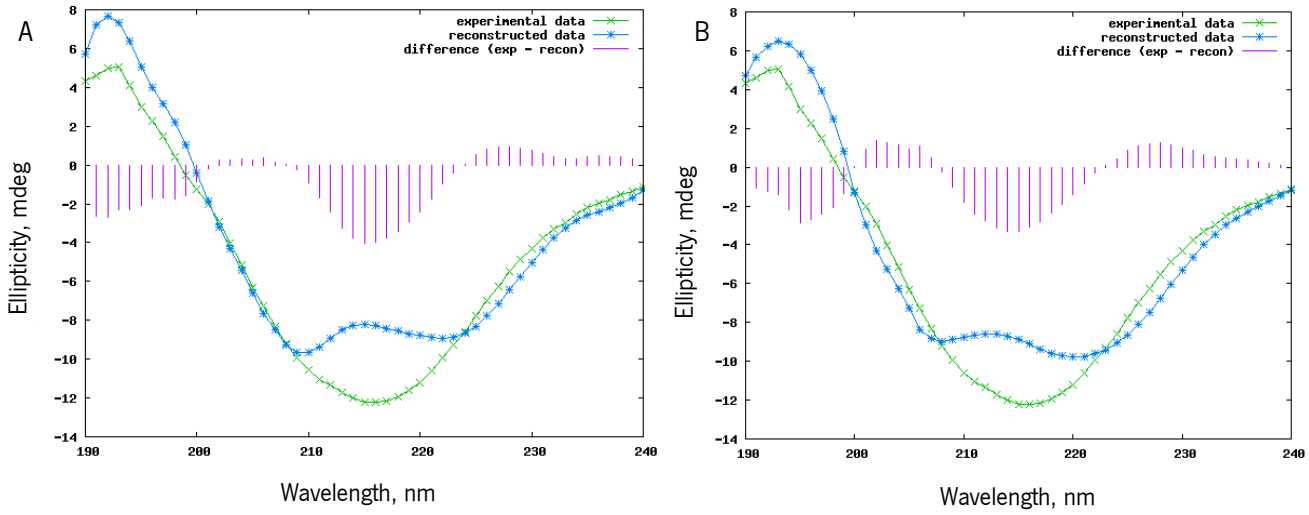


Figure A.7: Graphs of pectinase CD at pH 6: A) free enzyme, B) supernatants after immobilization.

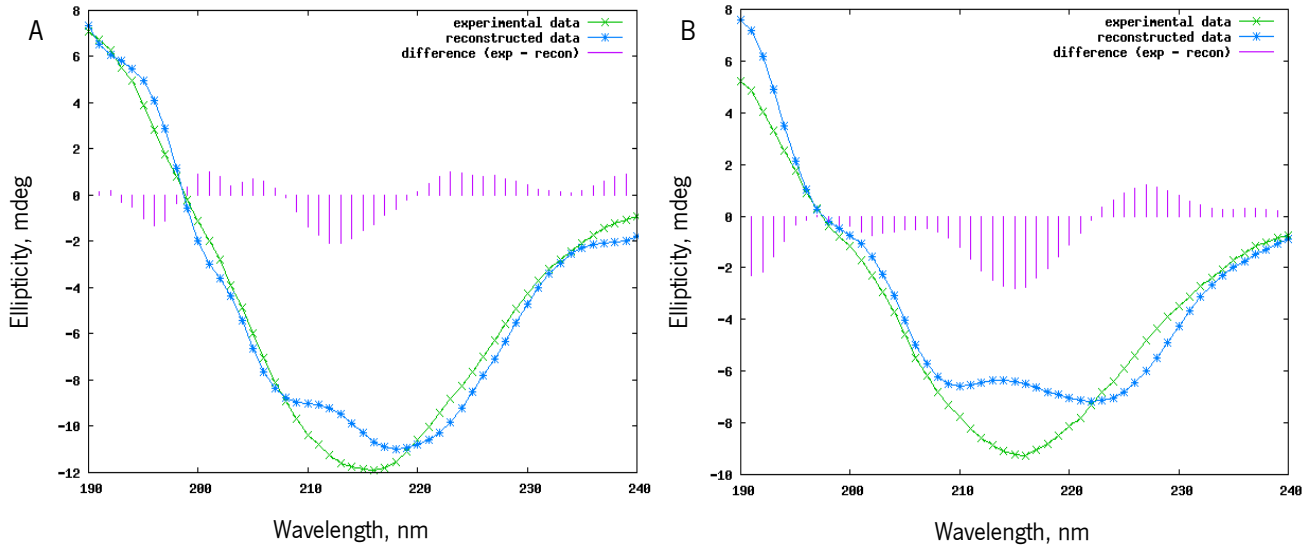


Figure A.8: Graphs of pectinase CD at pH 7: A) free enzyme, B) supernatants after immobilization.

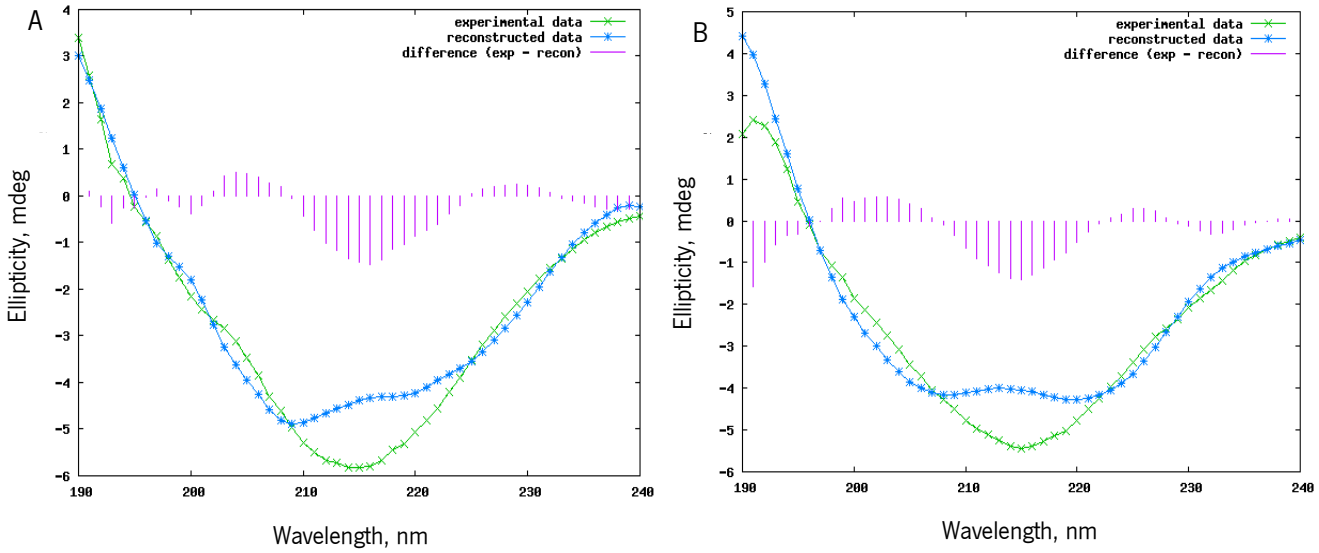


Figure A.9: Graphs of pectinase CD at pH 8: A) free enzyme, B) supernatants after immobilization.